

# This is to certify that the dissertation entitled

# THE INTERACTIONS OF S-ADENOSYLMETHIONINE AND PYRUVATE FORMATE-LYASE- ACTIVATING ENZYME: A RADICAL ACTIVATION

presented by

#### **DANILO OCTAVIANO ORTILLO**

has been accepted towards fulfillment of the requirements for the

Doctoral	degree in	CHEMISTRY
Doctora	acgioc iii	Of IEIMIO I I I

Major Professor's Signature

Date

MSU is an Affirmative Action/Equal Opportunity Institution







# LIBRARY Michigan State University

PLACE IN RETURN BOX to remove this checkout from your record.

TO AVOID FINES return on or before date due.

MAY BE RECALLED with earlier due date if requested.

DATE DUE	DATE DUE	DATE DUE

2/05 p:/CIRC/DateDue.indd-p.1

# THE INTERACTIONS OF S-ADENOSYLMETHIONINE AND PYRUVATE FORMATE-LYASE- ACTIVATING ENZYME: A RADICAL ACTIVATION

Ву

Danilo Octaviano Ortillo

#### A DISSERTATION

Submitted to
Michigan State University
in partial fulfillment of the requirements
for the degree of

**DOCTOR OF PHILOSOPHY** 

**Chemistry Department** 

2006

#### ABSTRACT

# THE INTERACTIONS OF S-ADENOSYLMETHIONINE AND PYRUVATE FORMATE-LYASE- ACTIVATING ENZYME: A RADICAL ACTIVATION

By

#### **Danilo Octaviano Ortillo**

Pyruvate formate-lyase activating enzyme (PFL-AE) belongs to the "radical SAM" protein superfamily. Enzymes in this superfamily catalyze diverse reactions, which include unusual methylation, isomerization, sulfur insertion, ring formation, anaerobic oxidation and protein radical formation reactions. PFL-AE, which activates pyruvate formate-lyase (PFL) utilizes an Fe-S cluster and S-adenosylmethionine (AdoMet) to generate catalytically essential radicals. During generation of a glycyl radical on PFL, AdoMet is converted stoichiometrically to methionine and 5'-deoxyadenosine. An AdoMet-derived adenosyl radical has been implicated as the intermediate responsible for abstraction of the pro-S hydrogen atom of PFL Gly734.

In order to probe the mechanism by which the Fe-S cluster interacts with AdoMet to generate an adenosyl radical intermediate, we have undertaken an investigation of the interaction of PFL-AE with isotopically labeled AdoMets and AdoMet analogues. AdoMets labeled with <sup>15</sup>N, <sup>13</sup>C, <sup>2</sup>H, and <sup>17</sup>O at specific sites were employed to probe its interaction with the Fe-S cluster of PFL-AE. AdoMet

analogues will give us additional insight on the formation of the adenosyl radical. Syntheses and characterization of the labeled AdoMets and AdoMet analogues will be presented, along with the results of the EPR and ENDOR spectroscopic studies aimed at probing the interaction of AdoMet with the [4Fe-4S] cluster of PFL-AE.

Copyright by DANILO OCTAVIANO ORTILLO 2006

To my beloved Mom, Lagrimas, and my Dad, Ariston.

#### **ACKNOWLEDGEMENTS**

To my adviser, Dr. Joan B. Broderick, my gratitude and respect knows no bounds. Thank you for inspiring me and for believing in me. To my committee members: Dr. James McCusker, Dr. John McCracken and Dr. David Weliky, I appreciate your guidance and assistance in my graduate work. To Dr. Brian Hoffman, Dr. Roman Davydov, Dr. Nick Lees and Dr. Charles Walsby, for a productive collaboration. To Dr. Muthukumaran Rajendra-Bose, thank you for your patience and perseverance in training me how to operate the EPR machine. To Dr. Will Broderick, for being available not just for me but for the whole group as well if we need some help. Dr. Jennifer Cheek and Dr. Magdalena Makowska-Grzyska, the two most helpful post-docs I've come to work with. Thanks for all the training and for sharing your baking experiences with me. To Wei, for showing me the ropes when I first joined the group, I learned a great deal as I was working with a friend. To Jeff, for always challenging me to go further and for keeping me grounded at the same time. It was great having you as a colleague. To Shujuan and Zhen Wei, for being there for me through the good and the bad. To Sophia, my little sis in the group, I will miss our little chats. Wish you and Yi Duo all the best. To Meng, Thalia, Egis, Cliff, Washington and Yi, it was great fun working with all of you. To the former members of the group, Tim, Mbako, and Silvana and the undergrads, Kelly, Dan, Mike, Brian, Emily, Waleed, and Ryan, it

was great working with all of you. To Lisa Dillingham, the best graduate secretary ever, thank you for taking the time to help me out with all the paperwork and for having faith in me. To the Dooley lab at Montana State University especially to Doreen, Greg, Eric and Dalia, it was great having known all of you. To Eric Brecht, it was fun running those EPR samples at Utah. To Jennifer, Chris and Sherry, many, many thanks. To the new members of the lab, Tilak, Kaitlin, Sunshine, Rachel and Avery, good luck.

To my friends Celeste, Rovelyn, Jenny, Jennifer and Roner, and Mara and James, thank you for putting up with me all these years. To Rica, it is a privilege to have you as my friend. You are the sister I never had. Thank you for the support and for just being you. To Janice, Stephanie, Jessette and Eric, many, many thanks. Anthony and Cecilia, all my gratitude. To Nanay Mercy and Tatay Delfin and the rest of the family, the Ortillos and the Octavianos, I hope that I have made all of you proud.

## **TABLE OF CONTENTS**

LIST OF TABLES	xi
LIST OF FIGURES	xii
CHAPTER 1	
INTRODUCTION	1
Radical S-Adenosyl-L-Methionine (AdoMet/SAM) Superfamily	1
AdoMet-dependent Fe-S Enzymes	3
Pyruvate Formate-Lyase	
Pyruvate Formate-Lyase Activating Enzyme (PFL-AE)	20
S-Adenosylmethionine and the Fe-S Cluster of PFL-AE	
in Radical Generation	24
References	
CHAPTER 2	
OVEREXPRESSION AND CHARACTERIZATION OF PYRUVATE	
FORMATE-LYASE AND PYRUVATE FORMATE-LYASE	
ACTIVATING ENZYME	35
Introduction	
ExperimentalMethods	
Materials	40
Growth and Expression of PFL	40
Purification of PFL	
Growth and Expression of PFL-AE	
Purification of PFL-AE	
Protein Assays	
Iron Assays	
Sulfide Assays	
EPR Spectroscopy	46
Results and Discussion	
Expression and Purification of PFL	
Expression and Purification of PFL-AE	
Characterization of Purified PFL-AE	
Conclusion	
References	

CHAPTER 3	
SYNTHESES AND CHARACTERIZATION OF ISOTOPICALLY	
LABELED S-ADENOSYL-L-METHIONINES	
Introduction	
Experimental Methods	64
Materials	
Growth and Purification of SAM Synthetase	
Synthesis of Carboxy- <sup>17</sup> O-L-Methionine	
Synthesis and Purification of Isotopically Labeled SAM	
NMR Spectroscopy	69
Mass Spectrometry	69
Results and Discussion	
Growth and Purification of SAM Synthetase	
Syntheses and Purification of Isotopically Labeled SAM	71
Conclusion	
References	81
CHAPTER 4	
INVESTIGATING THE INTERACTION OF SAM WITH PFL-AE USING	
EPR AND ENDOR SPECTROSCOPY	83
Introduction	83
Experimental Methods	88
Synthesis and Purification of CD <sub>3</sub> -AdoMet, <sup>13</sup> CH <sub>3</sub> -AdoMet, <sup>15</sup> NH <sub>2</sub> -	
AdoMet, <sup>13</sup> COO-AdoMet, CO <sup>17</sup> O-AdoMet, and α-D-AdoMet	88
[1+ / AdoMet] Sample Preparation	
[2+ / AdoMet] Sample Preparation	90
[2+ / AdoMet] <sub>red</sub> Sample Preparation	90
EPR Spectroscopy	90
ENDOR Spectroscopy	91
Results and Discussion	93
EPR Spectroscopy	
ENDOR Spectroscopic Evidence for a Close Interaction Between	
AdoMet and the [4Fe-4S] Cluster of PFL-AE	95
Coordination of S-Adenosylmethionine to the Unique Iron Site	113
Conclusion	
References	
CHAPTER 5	
SYNTHESES AND CHARACTERIZATION OF S-ADENOSYL-	
L-METHIONINE ANALOGS	137
Introduction	137
Experimental Methods	141
Materials	
NMR Spectroscopy	
Radiochemical Assay of Adenosine Kinase	142

Synthesis of S-Vinylhomocysteine	142
Synthesis of S-Allylhomocysteine	143
Synthesis of 3',4'- Anhydroadenosine Triphosphate (anATP)	144
Synthesis of SAM Analogues	147
Results and Discussions	
Radiochemical Assay of Adenosine Kinase	
Synthesis of S-Vinylhomocysteine	
Synthesis of S-Allylhomocysteine	
Synthesis of 3',4'-Anhydroadenosine Triphosphate (anATP)	
Synthesis of SAM Analogues	
Conclusions	
References	
CHAPTER 6	
INVESTIGATING THE INTERACTION OF SAM WITH PFL-AE	
USING EPR SPECTROSCOPY	171
Introduction	171
Experimental Methods	184
Materials	184
NMR Spectroscopy	185
Mass Spectrometry	185
Synthesis of 5-Deazariboflavin	
Single Turnover Experiment with PFL-AE and Allyl-AdoMet	
EPR Spectroscopy	
Results and Discussions.	
Synthesis of 5-Deazariboflavin	
Single Turnover Experiment with PFL-AE and Allyl-AdoMet	
Conclusions	
References	
CHAPTER 7	
CONCLUSIONS	
References	219

# LIST OF TABLES

Table I.1	Radical SAM Superfamily	2
Table II.1	Ratio of absorbances at 426 nm and 280 nm of PFL-AE fractions off the 2nd run of the gel filtration column	53
Table IV.1	Photoreduction data of PFL-AE in the presence of isotopically labeled AdoMet	95
Table IV.2	T values derived from the dipolar interpretation of the <sup>2</sup> H ENDOR data	110
Table V.1	Percent yield of pivalyl reaction products at various reflux times	. 154

## LIST OF FIGURES

Figure I.1	Interconversion of L-lysine to L-β-lysine	4
Figure I.2	Structural comparison of adenosylcobalamin with S-adenosylmethionine	6
Figure I.3	Proposed mechanism of thymine dimer repair by spore photoproduct lyase	7
Figure I.4	Minimal mechanism for biotin synthase	9
Figure I.5	Reaction catalyzed by lipoate synthase (LipA)	.12
Figure I.6	Reaction catalyzed by anaerobic ribonucleotide reductase	.14
Figure I.7	Formation of benzylsuccinate from the addition of toluene to fumarate	.16
Figure I.8	The cleavage of pyruvate by coenzyme A (CoA)	. 17
Figure I.9	The activation / deactivation of PFL by generation or quenching of the glycyl radical on PFL	.18
Figure I.10	Resonance structures for the captodative stabilization of glycyl radicals	.20
Figure I.11	Activation of PFL, catalyzed by the action of PFL-activase (PFL-AE)	21
Figure I.12	Electron transfer from the [4Fe-4S] <sup>+</sup> center to SAM	. 25
Figure II.1	The phosphoroclastic reaction of pyruvate	.35
Figure II.2	The thioclastic reaction of pyruvate	. 36
Figure II.3	Activation of PFL by hydrogen abstraction from Gly 734 catalyzed by PFL-AE	37

Figure II.4	Chromatogram of purification of PFL. Elution profile for the Accell Plus QMA Anion Exchange column (Quaternary Methylamine, 300 Å, Waters Corp., 5 x 30 cm), gradient from Buffer A (20 mM Hepes, pH 7.2, 1 mM DTT) to Buffer B (20 mM Hepes, pH 7.2, 500 mM NaCl, 1 mM DTT) over 900 mL, flow rate 5 mL/min. PFL eluted at approximately 240 mM NaCl, and was dialyzed against Buffer C (40 mM Hepes, pH 7.2, 1 M ammonium sulfate, 1mM DTT)
Figure II.5	Chromatogram of purification of PFL. Elution profile for the Phenyl-Sepharose column (Pharmacia 16/10), gradient from Buffer C to Buffer A over 50 mL, followed by a wash with 50 mL of Buffer A, flow rate 1mL/min. PFL was eluted through last half of the gradient
Figure II.6	SDS-PAGE analysis of PFL fractions off the Accell Plus QMA anion-exchange column. Upper panel, Lanes 1-10 from left, 12, 14, molecular marker (kDa), 16, 18, 20, 23, 26, 29, 32; Lower panel, Lanes 1-10 from left, 35, 38, 41, molecular marker (kDa), 44, 47, 50, 53, 56, 59. Fractions 23-41 were pooled50
Figure II.7	SDS-PAGE analysis of PFL fractions off the Phenyl-Sepharose hydrophobic column. Lanes 1-10 from left, molecular marker (kDa), fractions 3,5,6,9,11,13,15,17, and 19. Fractions 15, 17, 19, 21 (not shown) were pooled
Figure II.8	SDS-PAGE analysis of overexpression of PFL-AE in <i>E. coli</i> cells. A: Lane 1, molecular marker (kDa); lanes 2 and 3, pre-induced cells; B: Lane 1, molecular marker (kDa); lanes 2 and 3, post-induced cells
Figure II.9	Purification of PFL-AE by gel-filtration chromatography (Superdex 75 column, 5 x 60 cm). The protein was eluted with 50 mM Tris-sulfate, pH 7.5, 200 mM NaCl, 1 mM DTT at 3 mL/min. PFL-AE eluted from the column in a relatively sharp peak at approximately 680 mL after injection
Figure II.10	SDS-PAGE analysis of PFL-AE fractions off the 2nd run of the gel filtration column. Lane 1, molecular marker (kDa); lane 2-8, fractions 17, 18, 19, 20, 22, 24, 26. Fractions 19-25 were pooled
Figure II.11	X-band EPR spectrum of PFL-AE [3Fe-4S] <sup>+</sup> of as-isolated protein; 7.41 % (based on 97.9 $\mu$ M spin for 1321 $\mu$ M protein with 3.70 mol Fe/ mol PFL-AE); g = 2.17, Conditions of measurement:

	$T = 12$ K; microwave power, 20 $\mu$ W; microwave frequency = 9.49 GHz; modulation amplitude, 10.084 G; single scan55
Figure III.1	Reversible production of 5'-deoxyadenosyl radical from SAM
Figure III.2	Reductive cleavage of AdoMet by PFL-AE in PFL activation
Figure III.3	Proposed proximity of SAM and the Fe-S cluster of PFL-AE during radical generation
Figure III.4	Enzymatic synthesis of S-adenosyl-L-methionine63
Figure III.5	SDS-PAGE analysis of SAM synthetase. Overexpression of AdoMet synthetase in <i>E. coli</i> cells (no induction is required). Lane 8, molecular marker (kDa); Lanes 1-4, duplicate samples of whole cells; Lanes 5-7, crude extract
Figure III.6	SDS-PAGE analysis of SAM synthetase fractions off the Phenyl-Sepharose column. Lane 1, molecular marker (kDa); Lanes 2-10, fractions 32-40. Fractions 33-38 were pooled71
Figure III.7	Chromatogram of isolation of CD <sub>3</sub> -AdoMet by SOURCE 15S cation exchange chromatography (Pharmacia, 8 mL), gradient from 0-1 M HCl, flow rate, 1 mL/min. CD <sub>3</sub> -SAM eluted as a distinct peak from 38 – 56 % Buffer B
Figure III.8	Chromatogram of isolation of <sup>13</sup> CH <sub>3</sub> -AdoMet by SOURCE 15S cation exchange chromatography (Pharmacia, 8 mL), gradient from 0-1 M HCl, flow rate, 1 mL/min. <sup>13</sup> CH <sub>3</sub> -SAM eluted as a distinct peak from 38 – 56 % Buffer B
Figure III.9	Chromatogram of isolation of <sup>15</sup> NH <sub>2</sub> -SAM by SOURCE 15S cation exchange chromatography (Pharmacia, 8 mL), gradient from 0-1 M HCl, flow rate, 1 mL/min. <sup>15</sup> NH <sub>2</sub> -SAM eluted as a distinct peak from 38 – 56 % Buffer B
Figure III.10	Chromatogram of isolation of COO <sup>17</sup> -AdoMet by SOURCE 15S cation exchange chromatography (Pharmacia, 8 mL), gradient from 0-1 M HCl, flow rate, 1 mL/min. COO <sup>17</sup> -SAM eluted as a distinct peak from 38 – 56 % Buffer B
Figure III.11	Chromatogram of isolation of <sup>13</sup> COO-AdoMet by SOURCE 15S cation exchange chromatography (Pharmacia, 8 mL), gradient from

	0-1 M HCl, flow rate, 1 mL/min. <sup>13</sup> COO-SAM eluted as a distinct peak from 38 –56 % Buffer B
Figure III.12	Chromatogram of isolation of $\alpha$ -CD-AdoMet by SOURCE 15S cation exchange chromatography (Pharmacia, 8 mL), gradient from 0-1 M HCl, flow rate, 1 mL/min. $\alpha$ -CD-AdoMet eluted as a distinct peak from 38 –56 % Buffer B
Figure IV.1	Reaction catalyzed by pyruvate formate-lyase activating enzyme
Figure IV.2	9.5 GHz CW EPR spectra of PFL-AE photoreduced with deazariboflavin as described in the text. (A) PFL-AE (0.7 mM) photoreduced for 1 h. The signal accounts for 197 $\mu$ M [4Fe-4S] <sup>+</sup> based on EPR spin quantitation, and has been multiplied by 3 for comparison purposes. (B) PFL-AE (0.78 mM) photoreduced for 1 h, followed by addition of two molar equivalents of AdoMet. The signal accounts for 416 $\mu$ M [4Fe-4S] <sup>+</sup> based on EPR spin quantitation. Conditions: $T = 12$ K, power = 20 $\mu$ W, gain = 2 x 10 <sup>4</sup> , frequency = 9.483 (A) or 9.476 (B), modulation amplitude = 8.231 (A) or 9.571 (B)
Figure IV.3	X-band EPR spectrum of PFL-AE [4Fe-4S] $^{\dagger}$ in the presence of CD <sub>3</sub> - AdoMet. The sample contained 910 $\mu$ M PFL-AE, 1 equivalent of Na <sub>2</sub> S <sub>2</sub> O <sub>4</sub> , 200 $\mu$ M 5-deazariboflavin, and 2 equivalents of CD <sub>3</sub> - AdoMet; 38.0 % reduction (based on 324 $\mu$ M spin for 910 $\mu$ M protein with 3.75 mol Fe/ mol PFL-AE); g = 2.005, 1.949, 1.883. Conditions of measurement: $T$ = 12 K; microwave power, 20 $\mu$ W; microwave frequency, 9.47 GHz; modulation amplitude, 10.053 G; single scan.
Figure IV.4	X-band EPR spectrum of PFL-AE [4Fe-4S] <sup><math>^+</math></sup> in the presence of $^{13}$ CH <sub>3</sub> -AdoMet. The sample contained 777 $\mu$ M PFL-AE, 1 equivalent of Na <sub>2</sub> S <sub>2</sub> O <sub>4</sub> , 200 $\mu$ M 5-deazariboflavin, and 2 equivalents of $^{13}$ CH <sub>3</sub> -AdoMet; 68.9 % reduction (based on 404 $\mu$ M spin for 777 $\mu$ M protein with 3.02 mol Fe/ mol PFL-AE); g = 2.011, 1.948, 1.880. Conditions of measurement: $T$ = 12 K; microwave power, 20 $\mu$ W; microwave frequency, 9.49 GHz; modulation amplitude, 9.571 G; single scan
Figure IV.5	X-band EPR spectrum of PFL-AE [4Fe-4S] <sup>1+</sup> in the presence of $^{15}$ NH <sub>2</sub> -AdoMet. The sample contained 650 $\mu$ M PFL-AE, 1 equivalent of Na <sub>2</sub> S <sub>2</sub> O <sub>4</sub> , 200 $\mu$ M 5-deazariboflavin, and 2 equivalents of $^{15}$ NH <sub>2</sub> -AdoMet; 42.1 % reduction (based on 224 $\mu$ M spin for 567 $\mu$ M protein with 3.75 mol Fe/ mol PFL-AE); g = 2.018, 1.948,

	1.883. Conditions of measurement: <i>T</i> = 12 K; microwave power, 20 μW; microwave frequency, 9.49 GHz; modulation amplitude, 9.571 G; single scan98
Figure IV.6	X-band EPR spectrum of PFL-AE [4Fe-4S] <sup>+</sup> in the presence of $^{13}$ COO-AdoMet. The sample contained 650 $\mu$ M PFL-AE, 1 equivalent of Na <sub>2</sub> S <sub>2</sub> O <sub>4</sub> , 200 $\mu$ M 5-deazariboflavin, and 2 equivalents of $^{13}$ COO-AdoMet; 21.7 % reduction (based on 141 $\mu$ M spin for 650 $\mu$ M protein with 3.75 mol Fe/ mol PFL-AE); g = 2.01, 1.948, 1.889. Conditions of measurement: $T$ = 12 K; microwave power, 20 $\mu$ W; microwave frequency, 9.49 GHz; modulation amplitude, 9.571 G; single scan
Figure IV.7	X-band EPR spectrum of PFL-AE [4Fe-4S] <sup>+</sup> in the presence of CO <sup>17</sup> O-AdoMet. The sample contained 521 $\mu$ M PFL-AE, 1 equivalent of Na <sub>2</sub> S <sub>2</sub> O <sub>4</sub> , 200 $\mu$ M 5-deazariboflavin, and 2 equivalents of CO <sup>17</sup> O -AdoMet; 68.9 % reduction (based on 156 $\mu$ M spin for 521 $\mu$ M protein with 3.75 mol Fe/ mol PFL-AE); g = 2.01, 1.948, 1.883. Conditions of measurement: $T$ = 12 K; microwave power, 20 $\mu$ W; microwave frequency, 9.49 GHz; modulation amplitude, 9.571 G; single scan
Figure IV.8	X-band EPR spectrum of PFL-AE [4Fe-4S] $^+$ in the presence of $\alpha$ -D-AdoMet. The sample contained 650 $\mu$ M PFL-AE, 1 equivalent of Na <sub>2</sub> S <sub>2</sub> O <sub>4</sub> , 200 $\mu$ M 5-deazariboflavin, and 2 equivalents of $\alpha$ -D - AdoMet; 14.9 % reduction (based on 97.1 $\mu$ M spin for 650 $\mu$ M protein with 3.75 mol Fe/ mol PFL-AE); g = 2.01, 1.948, 1.889. Conditions of measurement: $T$ = 12 K; microwave power, 20 $\mu$ W; microwave frequency, 9.49 GHz; modulation amplitude, 9.571 G; single scan
Figure IV.9	35 GHz Mims pulsed-ENDOR spectra of PFL-AE with methyl-D <sub>3</sub> -AdoMet; (a) and (d) photoreduced sample; (b) cryoreduced sample. The spectra at $\mathbf{g}_{\perp}$ have been scaled to the height of the natural abundance <sup>57</sup> Fe peaks visible to higher frequency of the <sup>13</sup> C signals. Conditions: $T = 2$ K, $v_{MW} = 34.8$ GHz, MW pulse lengths = 80 nS, $\tau = 456$ ns, RF pulse length = 60 $\mu$ s, repetition rate = 30 Hz. Each spectrum consists of 256 pointswith each point an average of 240-300 transients. (c) and (e) Simulations (dashed lines) with dipolar A tensors. Closest <sup>2</sup> H: $T = 0.6$ MHz (corresponding to $R = 3.1$ Å for $K = 1.0$ ), $\alpha = \beta = 30^{\circ}$ , $\gamma = 0^{\circ}$ ; $P = 0.1$ MHz, $\alpha = \beta = \gamma = 0^{\circ}$ . More distant methyl deuterons: $r(Fe_k-D) = 4.7$ Å, representative value of $K = 1.6$ , angles tetrahedrally disposed, orientations: $\alpha = 19^{\circ}$ , $\beta = 20^{\circ}$ , $\gamma = 0$ and $\alpha = 30^{\circ}$ , $\beta = 54^{\circ}$ , $\gamma = 0$ , quadrupole as above. Mims suppression effects included

Figure IV.10	35 GHz Mims pulsed-ENDOR spectra of PFLAE (a) with methyl- $^{13}$ C-AdoMet, photoreduced, at $\mathbf{g}_{\perp}$ , (b) with methyl- $^{13}$ C-AdoMet, (d) with methyl- $^{13}$ C-AdoMet, photoreduced, at $\mathbf{g}_{\parallel}$ . Irradiated at 77 K, at $\mathbf{g}_{\perp}$ (c) with natural abundance $^{13}$ C-AdoMet at $\mathbf{g}_{\parallel}$ . Experimental conditions as for Figure IV.9 except that $\tau$ = 600 nS and number of transients = 600
Figure IV.11	Field dependence data with conditions as above (full line) and simulation (dashed line). Simulation parameters: $\mathbf{A} = [-0.6, 0.4, -0.5], \ \alpha = \beta = 30^{\circ}, \ \gamma = 0^{\circ}; \ \text{EPR line width} = 170 \ \text{MHz}, \ \text{ENDOR}$ line width = 0.2 MHz; $\tau$ = 600 ns, Mims suppression effects included
Figure IV.12.	35-GHz pulsed ENDOR spectra of PFL-AE with (a) $^{17}$ O and (b) $^{13}$ C carboxylato-labeled and (c) $^{15}$ N-amino-labeled AdoMet compared with data from an unlabeled sample, at $g_{\perp}$ Conditions: $T$ = 2 K. (a) $^{17}$ O labeled, Davies ENDOR. $v_{MW}$ = 34.9 MHz; microwave pulse lengths = 80, 40, 80 ns; RF pulse length ) 60 ms. Number of averaged transients at each point: $^{17}$ O, 288; unlabeled, 200. (b) $^{13}$ C-labeled, Mims ENDOR. $v_{MW}$ = 34.8 MHz, microwave pulse lengths = 80 ns, $\tau$ = 552 ns, RF pulse length = 60 ms. Number of averaged transients: $^{13}$ C-labeled, 144; unlabeled, 600. (c) $^{15}$ N-labeled, Davies ENDOR. $v_{MW}$ = 34.9 MHz; microwave pulse lengths = 80, 40, 80 ns; RF pulse length = 60 ms. Number of average transients: $^{15}$ N-labeled, 80; unlabeled, 624
Figure IV.13.	Field dependence data (s) and simulations () from 35-GHz Mims pulsed ENDOR of PFL-AE with carboxy- $^{13}$ C-SAM, with conditions as in Figure IV.12. Simulation parameters: <b>A</b> = [1.1, -0.95, -0.82], $\alpha$ = 30, $\beta$ = $\gamma$ = 90, EPR line width = 120 MHz, ENDOR line width = 0.1 MHz, $\tau$ = 562 ns. Mims suppression effects are included
Figure IV.14	35-GHz Davies ENDOR spectra of PFL-AE <sup>+</sup> with unlabeled SAM and with <sup>17</sup> O-carboxyl SAM. Left: Comparison of ENDOR from <sup>17</sup> O-labeled and unlabeled SAM. Right: <sup>17</sup> O ENDOR and simulations. Experimental conditions: $T=2$ K; Davies pulse sequence; microwave pulse lengths = 80, 40, 80 ns; repetition rate = 100 Hz; RF pulse length = 60 ms. <sup>17</sup> O Simulation parameters: Program GENDOR, $A = [8.6, 14.4, 8.2]$ , $\alpha = 30$ , $\beta = \gamma = 0$ , $P = [-0.05, 0.1, -0.05]$ , $\alpha = 30$ , $\beta = \gamma = 0$ , ENDOR line width = 0.5 MHz, EPR line width = 100 Hz

Figure IV.15.	35-GHz Davies ENDOR of PFL-AE <sup>+</sup> with unlabeled SAM and with <sup>15</sup> N-amino SAM. Left: Comparison of <sup>14</sup> N and <sup>15</sup> N ENDOR. Right: <sup>15</sup> N ENDOR and simulations. Experimental conditions: $T = 2$ K; Davies pulse sequence; microwave pulse lengths = 80, 40, 80 ns; repetition rate = 100 Hz; RF pulse length = 60 ms. <sup>15</sup> N Simulation parameters: Program ENDORSIM, <b>A</b> = [9.7, 6, 3.5], $\alpha = 0$ , $\beta = 30$ , $\gamma = 0$ , ENDOR line width = 0.8 MHz, EPR line width = 300 MHz
Figure IV.16	Model for the interaction of AdoMet with the [4Fe-4S] of PFL-AE
Figure IV.17	AdoMet forms a classical N/O chelate with the unique iron site of the [4Fe-4S] cluster of PFL-AE128
Figure IV.18	Proposed mechanism for iron-sulfur cluster and SAM-mediated radical generation catalyzed by PFL-AE
Figure V.1	Synthesis of S-adenosyl-L-methionine as catalyzed by SAM synthetase
Figure V.2	Methionine analogues: (I) S-vinylhomocysteine, (II) S-allylhomocysteine, (III) S-(methanethio)cysteine, (IV) S-(methanethio)homocysteine, and (V) S-cyanohomocysteine
Figure V.3	Allylic delocalization of anSAM during reductive cleavage
Figure V.4	Reaction mechanism for the synthesis of S-vinylhomocysteine
Figure V.5	Reaction mechanism for the synthesis of <i>S</i> -allylhomocysteine
Figure V.6	Reaction scheme for the protection of adenosine
Figure V.7	Reaction of 2'3'-O-methoxyethylideneadenosine with sodium iodide and pivalyl chloride in pyridine153
Figure V.8	Reaction with AgOAc of the crude product from the 2'3'-O- methoxy-ethylideneadenosine reaction with sodium iodide and pivalyl chloride
Figure V.9	Deprotection of 3'-deoxyadenosine in NaOMe

Figure V.10	Elution time of anAdo loaded into a Spherisorb S5 SAX column. The buffer used was 100 mM NaH <sub>2</sub> PO <sub>4</sub> pH = 3.0 for pump A and 100 mM NaH <sub>2</sub> PO <sub>4</sub> /1 M NaCl pH = 3.0 for pump B. AnAdo eluted as a distinct peak at 3-4 minutes and 0% buffer B
Figure V.11	Elution time of anATP (6 hours) loaded into a Spherisorb S5 SAX column. The buffer used was 100 mM NaH $_2$ PO $_4$ pH = 3.0 for pump A and 100 mM NaH $_2$ PO $_4$ /1 M NaCl pH = 3.0 for pump B. AnAdo eluted as a distinct peak at 13-14 minutes and 29-37% buffer B
Figure V.12	Elution time of anATP (15 hours) loaded into a Spherisorb S5 SAX column. The buffer used was 100 mM NaH <sub>2</sub> PO <sub>4</sub> pH = 3.0 for pump A and 100 mM NaH <sub>2</sub> PO <sub>4</sub> /1 M NaCl pH = 3.0 for pump B. AnAdo eluted as a distinct peak at 13-14 minutes and 28-40% buffer B
Figure V.13	Elution time of anATP (24 hours) loaded into a Spherisorb S5 SAX column. The buffer used was 100 mM NaH <sub>2</sub> PO <sub>4</sub> pH = 3.0 for pump A and 100 mM NaH <sub>2</sub> PO <sub>4</sub> /1 M NaCl pH = 3.0 for pump B. AnAdo eluted as a distinct peak at 13-14 minutes and 29-38% buffer B
Figure V.14	Elution time of anATP (42 hours) loaded into a Spherisorb S5 SAX column. The buffer used was 100 mM NaH <sub>2</sub> PO <sub>4</sub> pH = 3.0 for pump A and 100 mM NaH <sub>2</sub> PO <sub>4</sub> /1 M NaCl pH = 3.0 for pump B. AnAdo eluted as a distinct peak at 13-14 minutes and 29-38% buffer B
Figure V. 15	Absorbance readings of the anATP fractions collected
Figure V.16	Enzymatic synthesis of adenosyl-S-allyl-L-homocysteine 163
Figure V. 17	Chromatogram of isolation of allyISAM by SOURCE 15S cation exchange chromatography(Pharmacia, 8 mL), gradient from 0-1 M HCI, flow rate = 1 mL/min. AllyISAM eluted as a distinct peak from 38 – 56 % Buffer B
Figure V.18	Enzymatic synthesis of 3', 4'-anhydro-S-adenosyl-L-methionine
Figure V.19	Chromatogram of isolation of anSAM by SOURCE 15S cation exchange chromatography(Pharmacia, 8 mL), gradient from 0-1 M HCl, flow rate = 1 mL/min. AnSAM eluted as a distinct peak from 38 – 56 % Ruffer B

Figure VI.1	Assay of PFL-AE activity using EPR spectroscopy. (A) EPR spectra recorded at 10, 20, 40, and 80 min (bottom to top) during PFL activation. (B) Plots of the glycyl radical spin quantitation as a function of time for PFL-AE at 6.25 ug/mL (•) and 25 ug/mL (•); higher concentrations of AE provide a higher rate of activation, as expected. EPR parameters: <i>T</i> , 60 K; microwave power, 20 μW; microwave frequency, 9.48 GHz; modulation amplitude, 5.054 G	
Figure VI.2	EPR-detected single-turnover experiments to define the catalytically active iron-sulfur cluster in PFL-AE. (A) EPR spectra of samples containing PFL-AE, SAM, and 5-deazariboflavin as a function of illumination (reduction) time in minutes. (B) EPR spectra of samples as in A to which PFL has been added prior to freezing for EPR. (C) EPR spin quantitation of the [4Fe-4S]+ and glycyl radical signals shows a 1:1 correspondence	1
Figure VI.3	Reaction catalyzed by pyruvate formate-lyase activating enzyme	<u>}</u>
Figure VI.4	Proposed mechanism for iron-sulfur cluster and SAM-mediated radical generation catalyzed by PFL-AE184	•
Figure VI.5	Reaction mechanism for the synthesis of 6-[N-(D-ribityl)-3,4-xylidino]uracil189	•
Figure VI.6	Reaction mechanism for the synthesis of 6-[N-2',3',4',5'-tetra-O-acetyl-(D-ribityl)-3,4-xylidino]uracil19	1
Figure VI.7	Reaction mechanism for the synthesis of 2',3',4',5'- tetra-O-acetyl-5-deazariboflavin	2
Figure VI.8	Reaction mechanism of the synthesis of 5-deazariboflavin19	3
Figure VI.9.a	X-band EPR spectrum of PFL-AE [4Fe-4S] <sup>+</sup> in the presence of allyl-AdoMet after 1 minute of illumination. The sample contained 200 $\mu$ M PFL-AE, 1 equivalent of Na <sub>2</sub> S <sub>2</sub> O <sub>4</sub> , 100 $\mu$ M 5-deazariboflavin, and 2 equivalents of allyl-AdoMet; 9.23 % reduction (based on 68.3 $\mu$ M spin for 200 $\mu$ M protein with 3.70 mol Fe/ mol PFL-AE); g = 2.011, 1.948, 1.880. Conditions of measurement: $T$ = 12 K; microwave power, 20 $\mu$ W; microwave frequency, 9.49 GHz; modulation amplitude, 10.084 G; single	

Figure VI.9.b	X-band EPR spectrum of PFL-AE [4Fe-4S] <sup>+</sup> in the presence of allyl-AdoMet after 2 minutes of illumination. The sample contained 200 $\mu$ M PFL-AE, 1 equivalent of Na <sub>2</sub> S <sub>2</sub> O <sub>4</sub> , 100 $\mu$ M 5-deazariboflavin, and 2 equivalents of allyl-AdoMet; 9.84 % reduction (based on 72.8 $\mu$ M spin for 200 $\mu$ M protein with 3.70 mol Fe/ mol PFL-AE); g = 2.011, 1.948, 1.880. Conditions of measurement: $T$ = 12 K; microwave power, 20 $\mu$ W; microwave frequency, 9.49 GHz; modulation amplitude, 10.084 G; single scan
Figure VI.9.c	X-band EPR spectrum of PFL-AE [4Fe-4S] $^+$ in the presence of allyl-AdoMet after 5 minutes of illumination. The sample contained 200 $\mu$ M PFL-AE, 1 equivalent of Na <sub>2</sub> S <sub>2</sub> O <sub>4</sub> , 100 $\mu$ M 5-deazariboflavin, and 2 equivalents of allyl-AdoMet; 14.7 % reduction (based on 108.7 $\mu$ M spin for 200 $\mu$ M protein with 3.70 mol Fe/ mol PFL-AE); g = 2.011, 1.948, 1.880. Conditions of measurement: $T$ = 12 K; microwave power, 20 $\mu$ W; microwave frequency, 9.49 GHz; modulation amplitude, 10.084 G; single scan
Figure VI.9.d	X-band EPR spectrum of PFL-AE [4Fe-4S] $^{+}$ in the presence of allyl-AdoMet after 10 minutes of illumination. The sample contained 200 $\mu$ M PFL-AE, 1 equivalent of Na <sub>2</sub> S <sub>2</sub> O <sub>4</sub> , 100 $\mu$ M 5-deazariboflavin, and 2 equivalents of allyl-AdoMet; 16.1 % reduction (based on 118.8 $\mu$ M spin for 200 $\mu$ M protein with 3.70 mol Fe/ mol PFL-AE); g = 2.011, 1.948, 1.880. Conditions of measurement: $T$ = 12 K; microwave power, 20 $\mu$ W; microwave frequency, 9.49 GHz; modulation amplitude, 10.084 G; single scan
Figure VI.9.e	X-band EPR spectrum of PFL-AE [4Fe-4S] <sup>+</sup> in the presence of allyl-AdoMet after 30 minutes of illumination. The sample contained 200 μM PFL-AE, 1 equivalent of Na <sub>2</sub> S <sub>2</sub> O <sub>4</sub> , 100 μM 5-deazariboflavin, and 2 equivalents of allyl-AdoMet;15.9 % reduction (based on 117.3 μM spin for 200 μM protein with 3.70 mol Fe/ mol PFL-AE); $g = 2.011$ , 1.948, 1.880. Conditions of measurement: $T = 12$ K; microwave power, 20 μW; microwave frequency, 9.49 GHz; modulation amplitude, 10.084 G; single scan
Figure VI.9.f	X-band EPR spectrum of PFL-AE [4Fe-4S] <sup>+</sup> in the presence of allyl-AdoMet after 60 minutes of illumination. The sample contained 200 μM PFL-AE, 1equivalent of Na <sub>2</sub> S <sub>2</sub> O <sub>4</sub> , 100 μM 5-deazariboflavin, and 2 equivalents of allyl-AdoMet;16.6 %

	reduction (based on 123.3 $\mu$ M spin for 200 $\mu$ M protein with 3.70 m Fe/ mol PFL-AE); g = 2.011, 1.948, 1.880. Conditions of measurement: $T$ = 12 K; microwave power, 20 $\mu$ W; microwave frequency, 9.49 GHz; modulation amplitude, 10.084 G; single scan	
Figure VI.10	Spin quantitation of the EPR spectra shown in Figure VI.9 (a-f) [4Fe-4S] <sup>1+</sup> as a function of illumination time	200
Figure VI.11	a X-band EPR spectrum of PFL-AE [3Fe-4S] <sup>+</sup> in the presence of allyl-AdoMet after 1 minute of illumination. The sample contained 200 μM PFL-AE, 200 μM PFL, 1 equivalent of Na <sub>2</sub> S <sub>2</sub> O 100 μM 5-deazariboflavin, and 2 equivalents of allyl-AdoMet; 2.45 % (based on 18.1 μM spin for 200 μM protein with 3.70 mol Fe/ mol PFL-AE); g = 2.017. Conditions of measurement: $T = 12$ microwave power, 20 μW; microwave frequency, 9.49 GHz; modulation amplitude, 10.084 G; single scan	
Figure VI.11	.b X-band EPR spectrum of PFL-AE [3Fe-4S] <sup>+</sup> in the presence of allyl-AdoMet after 2 minutes of illumination. The sample contained 200 $\mu$ M PFL-AE, 200 $\mu$ M PFL, 1 equivalent of Na <sub>2</sub> S <sub>2</sub> O 100 $\mu$ M 5-deazariboflavin, and 2 equivalents of allyl-AdoMet; 1.53 % (based on 11.4 $\mu$ M spin for 200 $\mu$ M protein with 3.70 mol Fe/ mol PFL-AE); g = 2.017. Conditions of measurement: $T$ = 12 microwave power, 20 $\mu$ W; microwave frequency, 9.49 GHz; modulation amplitude, 10.084 G; single scan	K;
Figure VI.11	.c X-band EPR spectrum of PFL-AE [3Fe-4S] $^{+}$ in the presence of allyl-AdoMet after 5 minutes of illumination. The sample contained 200 $\mu$ M PFL-AE, 200 $\mu$ M PFL, 1 equivalent of Na <sub>2</sub> S <sub>2</sub> O 100 $\mu$ M 5-deazariboflavin, and 2 equivalents of allyl-AdoMet; 1.30 % (based on 9.6 $\mu$ M spin for 200 $\mu$ M protein with 3.70 mol Fe/ mol PFL-AE); g = 2.017. Conditions of measurement: $T$ = 12 microwave power, 20 $\mu$ W; microwave frequency, 9.49 GHz; modulation amplitude, 10.084 G; single scan	K;
Figure VI.11	.d X-band EPR spectrum of PFL-AE [3Fe-4S] <sup>+</sup> in the presence of allyl-AdoMet after 10 minutes of illumination. The sample contained 200 $\mu$ M PFL-AE, 200 $\mu$ M PFL, 1 equivalent of Na <sub>2</sub> S <sub>2</sub> O 100 $\mu$ M 5-deazariboflavin, and 2 equivalents of allyl-AdoMet; 0.50 % (based on 3.7 $\mu$ M spin for 200 $\mu$ M protein with 3.70 mol Fe/ mol PFL-AE); g = 2.017. Conditions of measurement: $T = 12$ microwave power, 20 $\mu$ W; microwave frequency, 9.49 GHz; modulation amplitude, 10 084 G: single scan	

Figure VI.11.	e X-band EPR spectrum of PFL-AE [ $3Fe-4S$ ] <sup>+</sup> in the presence of allyl-AdoMet after 30 minutes illumination. The sample contained 200 $\mu$ M PFL-AE, 200 $\mu$ M PFL, 1 equivalent of Na <sub>2</sub> S <sub>2</sub> O <sub>4</sub> , 100 $\mu$ M 5-deazariboflavin, and 2 equivalents of allyl-AdoMet; 1.48 % (based on 11.0 $\mu$ M spin for 200 $\mu$ M protein with 3.70 mol Fe/ mol PFL-AE); g = 2.017. Conditions of measurement: $T$ = 12 K; microwave power, 20 $\mu$ W; microwave frequency, 9.49 GHz; modulation amplitude, 10.084 G; single scan
Figure VI.11.	f X-band EPR spectrum of PFL-AE [3Fe-4S] <sup>+</sup> in the presence of allyl-AdoMet after 60 minutes of illumination. The sample contained 200 $\mu$ M PFL-AE, 200 $\mu$ M PFL, 1 equivalent of Na <sub>2</sub> S <sub>2</sub> O <sub>4</sub> , 100 $\mu$ M 5-deazariboflavin, and 2 equivalents of allyl-AdoMet; 0.85 % (based on 6.26 $\mu$ M spin for 200 $\mu$ M protein with 3.70 mol Fe/ mol PFL-AE); g = 2.017. Conditions of measurement: $T$ = 12 K; microwave power, 20 $\mu$ W; microwave frequency, 9.49 GHz; modulation amplitude, 10.084 G; single scan
Figure VI.12	X-band EPR spectrum of PFL-AE [3Fe-4S] $^{+}$ of as-isolated protein (based on 97.9 $\mu$ M spin for 1321 $\mu$ M protein with 3.70 mol Fe/ mol PFL-AE); g = 2.017. Conditions of measurement: $T$ = 12 K; microwave power, 20 $\mu$ W; microwave frequency, 9.49 GHz; modulation amplitude, 10.084 G; single scan207
Figure VII.1	Interaction of AdoMet With the [4Fe-4S] cluster of PFL-AE, as deduced from <sup>2</sup> H and <sup>13</sup> C pulsed Q-band ENDOR spectroscopy
Figure VII.2	Representation of the proposed interactions of AdoMet with the [4Fe-4S] cluster of PFL-AE, as derived from ENDOR spectroscopy of the atoms: <sup>2</sup> H, <sup>13</sup> C, <sup>14,15</sup> N, and <sup>17</sup> O

## **KEY TO SYMBOLS AND ABBREVIATIONS**

SAM	S-Adenosyl-L-methionine
DNA	Deoxyribonucleic acid
AdoMet	S-Adenosyl-L-methionine
EPR	Electron Paramagnetic Spectroscopy
UV-vis	Ultraviolet – visible
kDa	kiloDalton
DTT	Dithiothreitol
BioB	Biotin synthase
LipA	Lipoate synthase
ARR	Anaerobic ribonucleotide reductase
NADPH	. Nicotinamide adenine dinucleotide phosphate
BssD	Benzyl succinate synthase
PFL	Pyruvate formate-lyase
PFL-AE	Pyruvate formate-lyase activating enzyme
ENDOR	Electron-Nuclear Double Resonance
RNA	Ribonucleic acid
OD	Optical density
LAM	Lysine aminomutase
NADH	Nicotinamide adenine dinucleotide

SPL	Spore photoproduct lyase
D <sub>2</sub> O	Deuterium oxide
BDE	Bond dissociation energy
PMSF	Phenylmethylsulfonyl fluoride
SDS-PAGE	Sodium dodecyl sulfate-polyacrylamide gel electrophoresis
EDTA	Ethylenediaminetetraacetic acid
<i>β</i> -ME	β-mercaptoethanol
NMR	Nuclear Magnetic Resonance
ppm	parts-per-million
TRIS	Tris(hydroxymethyl)aminomethane
HEPES	N-(2-Hydroxyethyl)piperazine-N'-2-ethanesulfonic acid
BSA	Bovine serum albumin
DMSO	Dimethylsulfoxide
HPLC	High pressure liquid chromatography
ESEEM	Electron Spin Echo Envelope Modulation
FAB-MS	Fast atom bombardment-mass spectrometry

#### **CHAPTER 1**

#### INTRODUCTION

I.1 Radical S-Adenosyl-L-Methionine (AdoMet/SAM) Superfamily

Radical SAM proteins catalyze diverse reactions, including unusual methylations, isomerization, sulfur insertion, ring formations, anaerobic oxidation and protein radical formation. They function in DNA precursor, vitamin, cofactor, antibiotic and herbicide biosynthesis and in biodegradation pathways. In 2001, over 600 members of the radical SAM superfamily were discovered by iterative profile searches and analysis using bioinformatics and information visualization methods. Evidence exists that these proteins generate a radical species by reductive cleavage of SAM through an unusual Fe-S center.<sup>2-9</sup> The superfamily also provides evidence that radical-based catalysis is important in a number of previously well studied but unresolved biochemical pathways and reflects an ancient conserved mechanistic approach to difficult chemistries. Exploratory statistical methods were used to analyze the sequence similarity relationships and integrate these results with other data types (motif, domain, operon, structure, biochemical pathway and the biomedical literature) for discovery efforts on previously uncharacterized sequences.<sup>1</sup>

The organized view of the radical SAM proteins show 30 distinct groups associated with some kind of biochemical data as shown in Table I.1.

PROTEIN	FUNCTION
NifB	Nitrogenase cofactor (FeMoCo)
MiaB	Methylthiolation of tRNA
Nclk-binding	Cdk5 activator binding
BioB	Sulfur Transfer to dethiobiotin
LipA	Sulfur transfer to octanoate
HemN	Coproporphyrinogen III oxidase
HemN-like	Coproporphyrinogen III oxidase
PhuW	Associated with virulence
MoaA	Pterin formation in Molybdopterin
PfIA	Pyruvate formate-lyase activation
BchE	Bacteriochlorophyll
Best5	Eukaryotic interferon-inducible
PqqE	Pyrroloquinoline quinone
ThiH	Thiazole ring formation in thiamine
SpIB	Spore photoproduct lyase
Desll	Desosamine moiety in antibiotics
AtsB	Formylglycine in sulfatases
Cmo	Putative cofactor modification
Nirj	Heme dl biosynthesis
BssD	Benzylsuccinate Synthase
ExsD	Succinoglycan production
NrdG	Anaerobic ribonucleotide reductase
SpcY	Spertinomycin biosynthesis
AlbA	Subtilosin biosynthesis
SanA	Nikkomycin biosynthesis
P-methylase	Bialaphos biosynthesis
MitD	Mitomycin C biosynthesis
MmcD	Mitomycin C biosynthesis
OxsB	Oxetanocin biosynthesis
Methylases	Fortimicin, fosfomycin
LAM	Lysine 2,3-aminomutase

Table I.1. Radical SAM Superfamily.

Interestingly, the most distantly related members belonging to the same cluster (diverging first in the hierarchical tree) seem to share an involvement with sulfur atom transfer. These include the proteins NifB, MiaB, BioB and LipA. 4-6,10-13 A mechanism for sulfur transfer from the Fe-S cluster of BioB has been proposed and like BioB, the NifB proteins act as reagents and not as catalysts in existing *in vitro* assays. 4,11 Likewise, ThiH of thiamine biosynthesis and MoaA of molybdopterin biosynthesis are found in pathways involving sulfur transfer but most likely do not act directly in this role. 10,14

The proteins HemN and BchE are examples of radical SAM proteins that provide an anaerobic or oxygen independent mechanism that is found as an aerobic reaction with other proteins. <sup>15,16</sup> HemN catalyzes the oxygen-independent oxidation in anaerobic heme biosynthesis and has been shown to require NADH in addition to either SAM or ATP and methionine for *in vitro* activity. <sup>17</sup> Ring-forming reactions are also associated with several members of the superfamily as well as involvement in secondary metabolic pathways such as antibiotic and herbicide biosynthesis. <sup>1</sup> Biodegradation is represented by BssD in toluene catabolism and DNA repair by spore photoproduct lyase (SPL). <sup>18,19</sup>

### I.2 AdoMet-dependent Fe-S Enzymes

Five defining members not previously recognized as homologous sequences are lysine 2,3-aminomutase, biotin synthase, lipoic acid synthase and the activating enzymes for pyruvate formate-lyase and anaerobic ribonucleotide reductase. These deoxy-adenosyl radical enzymes have been the focus of

detailed experimental work, which includes UV-vis, EPR, Mössbauer, resonance Raman, variable temperature magnetic circular dichroism and mutagenesis experiments.<sup>2-9</sup> Although a characteristic cysteine motif has been noted for these proteins, bioinformatics methods detected distant sequence similarity between these five proteins which is evidence for a shared ancestor and supports the prediction of a common fold for the core domain.<sup>1</sup>

H.A. Barker studied the metabolism of lysine by *Clostridium* species in the late 1960s and early 1970s and discovered a novel enzyme, lysine 2,3-aminomutase.<sup>20</sup> The enzyme catalyzes the first step in the metabolism of lysine to acetate.<sup>21,22</sup> The reaction in Figure I.1, which shows the interconversion of L-lysine and L- $\beta$ -lysine, was novel.

$$+H_3N$$
 $+H_3N$ 
 $+H_3$ 

**Figure I.1.** Interconversion of L-lysine to L- $\beta$ -lysine.

Another novel aspect was that the enzyme activity required coenzymes that had never before been associated with enzyme catalysis of an isomerization reaction. The interconversion of  $\alpha$ - and  $\beta$ - lysine was analogous to coenzyme B<sub>12</sub>- dependent enzymes but did not require adenosylcobalamin or any other corrinoid for activity. Lysine 2,3-aminomuatase displayed activity only under anaerobic conditions and addition of ferrous ions and pyridoxal-5'-phosphate (PLP)

increased its activity. The addition of SAM was also required to catalyze the reaction.<sup>23</sup>

The reaction catalyzed is similar to adenosylcobalamin-dependent enzymatic reactions and it proceeds as a 1,2-migration of an unreactive hydrogen atom concomitant with the reverse migration of a group on the adjacent carbon, which in this case is the 2-amino group. The hydrogen and the amino group do not exchange positions because their migration proceeds with an inversion of configuration.<sup>24</sup> The movement of hydrogen from C2 to C3 also proceeds without exchange with the protons of the solvent water, so hydrogen in the substrate is retained in the product.<sup>25</sup>

However, the absence of the adenosylcobalamin in the action of lysine 2,3-aminomutase led to a search for another coenzyme that would mediate the hydrogen transfer. SAM has an adenosyl moiety, which is something it has in common with adenosylcobalamin (Figure I.2), although it has little else in common in terms of chemical properties. Experiments carried out using [adenosyl-5'-³H]SAM resulted in the appearance of tritium in both L-lysine and L-β-lysine at equilibrium. Tritium associated with enzyme-bound [adenosyl-5'-³H]SAM was transferred to the substrate and product. Excess SAM in the solution was also observed not to participate in the hydrogen exchange. This result proves that the adenosyl moiety of SAM mediates hydrogen transfer in the lysine 2,3-aminomutase reaction, similar to that for adenosyl-cobalamin in coenzyme B<sub>12</sub>-dependent enzymatic processes.

**Figure I.2** Structural comparison of adenosylcobalamin with *S*-adenosylmethionine.

Spore photoproduct lyase (SPL) from *Bacillus subtilis* is a 41 kDa ironsulfur protein, that repairs methylene-bridged thymine dimers in DNA. <sup>1,19</sup> The reaction, unlike that of DNA photolyase, proceeds in the dark. Experiments have shown that SPL contains a [4Fe-4S] center and it also requires SAM for activity, cleaving SAM into 5'-deoxyadenosine and methionine in the course of repairing the dimers. <sup>28</sup>

The repair of spore photoproduct labeled at C-6 with tritium led to tritium incoporation in SAM, while spore photoproduct repair using [5'-³H] SAM led to tritiated thymine.<sup>29</sup> The evidence thus points to the elegant repair mechanism of methylene-bridged thymine dimers by SPL shown in Figure I.3. The reversible cleavage of SAM by reaction with the [4Fe-4S]<sup>1+</sup> center produces the 5'-deoxy-adenosyl radical, which abstracts the C6 hydrogen from the thymine dimer to form the dimer radical and 5'-deoxyadenosine. Radical fragmentation generates one thymine and the thymine monomer radical, which abstracts a hydrogen from 5'-deoxyadenosine to form the second thymine and regenerate the 5'-deoxy-adenosyl radical.<sup>29</sup>

**Figure I.3** Proposed mechanism of thymine dimer repair by spore photoproduct lyase.

Biotin is an essential vitamin for humans that is only produced by plants and certain microorganisms. Present in very small amounts in mammalian cells, biotin functions as a coenzyme in various carboxylation reactions, which is of utmost importance especially in gluconeogenesis. The genes involved in the biosynthetic pathway of biotin have been described in many organisms including *E. coli*, <sup>30</sup> *B. Subtilis*, <sup>31</sup> *B. spaericus*, <sup>32</sup> *Saccharomyces cerevisiae*, <sup>33</sup> and higher plants. <sup>34</sup> In *E. coli*, an operon that consists of five genes, *bio*ABFCD, encodes for enzymes that catalyze the last four steps in the pathway. Only *bio*C appears to function in an earlier step of biotin biosynthesis. The four steps from pimeloyl CoA to biotin appear to be common for most bacteria and plants. The last step in this pathway is catalyzed by the BioB protein, which is a product of the bioB gene, and involves insertion of a sulfur adjacent to the ureido ring of dethiobiotin (DTB). <sup>35-37</sup>

BioB is a homodimer with a native molecular mass of 78 kDa. The reported requirements for biotin synthase activity have varied somewhat between laboratories but the requirement for SAM and DTB has remained unrefuted.

Biotin formation in cell free extracts of *E. coli* was first measured in 1992. 23 Microbiological assays have shown that enzyme activity required SAM, dethiobiotin, NADPH, 1,6-biphosphate, Fe<sup>2+</sup>, and KCI. 38 The role of SAM as a hydrogen carrier between the substrate and cofactor was firmly established by experiments using tritium-labeled SAM and BioB from either *E. coli* or *B. sphaericus*. 39 It was shown that methionine and 5'-deoxyadenosine were formed in a 1:1 ratio while both compounds were formed in a 3:1 ratio with respect to

biotin.<sup>39</sup> A minimal mechanism for biotin synthase is given by the reaction in Figure I.4 where DTB is converted into a sulfur-containing intermediate with the concomitant cleavage of SAM into methionine and 5'-deoxyadenosine. The second step involves another molecule of SAM, another H abstraction, and another S-C bond formation, to yield biotin.

Figure I.4. Minimal mechanism for biotin synthase.

The first purified preparations of biotin synthase from *E. coli* and *B. sphaericus* were reported to contain Fe-S clusters.<sup>40,41</sup> The preparations and purification scheme developed have always been performed under aerobic conditions followed by anaerobic reconstitution of the enzyme. This results in purified protein containing a non-functional form of the Fe-S cluster. The first detailed spectroscopic characterization of BioB established the presence of a

9

diamagnetic S = 0 [2Fe-2S]<sup>2+</sup> cluster in each dimer subunit of the as-purified protein.<sup>4</sup> Incubation with dithionite in 60% ethylene glycol resulted in a nearly stoichiometric conversion to an S = 0, [4Fe-4S]<sup>2+</sup> cluster. However, prolonged incubation with excess dithionite produced a paramagnetic [4Fe-4S]<sup>+</sup> cluster.<sup>4,42</sup>

More recent work has demonstrated the formation of two [4Fe-4S]<sup>2+</sup> clusters per mole of BioB upon incubation with iron, sulfide, and DTT and complete reduction of these clusters by dithionite.<sup>43</sup> Exclusion of 60% ethylene glycol from the samples resulted exclusively in the formation of [4Fe-4S]<sup>+</sup> clusters upon reduction. Reversibility between the 1+/2+ redox pair was established suggesting that this form is the redox-active form of BioB under anaerobic conditions.<sup>43</sup> The conserved cysteine motif, which is thought to provide the ligands for the [4Fe-4S] cluster of the protein in BioB, includes the residues Cys53, Cys57, and Cys60. The roles of these and other less conserved cysteines have been probed by site directed mutagenesis studies.<sup>44-47</sup> Single Cys-Ala mutations of all eight cysteine residues in BioB showed that only the C276A and C288A displayed behavior similar to the wild-type protein. The remaining Cys-Ala mutations rendered the enzyme inactive but able to assemble the [Fe-S] cluster under highly reducing conditions.<sup>47</sup>

The origin of the sulfur in biotin has been a matter of controversy. It has been described that in *in vivo*<sup>48</sup> and in crude extracts, <sup>49,50</sup> cysteine is the most likely source. However, incorporation of sulfur from cysteine does not occur with the purified enzyme. Reconstitution of apoprotein from either *E. coli* or *B. sphaericus* with FeCl<sub>3</sub>, Na<sub>2</sub>[<sup>34</sup>S], and DTT yields <sup>34</sup>S-labeled biotin with ~65%

incorporation.<sup>51</sup> Another study corro-borated biosynthetic incorporation of sulfur into BioB by growth in the presence of [<sup>35</sup>S]cysteine and [<sup>35</sup>S]sulfide and showed significant transfer of radioactivity into biotin.<sup>52</sup> These experiments imply that BioB acts as a reagent in the reaction and not simply as a catalyst. This also suggests that the sulfur donor in biotin synthase is the Fe-S cluster of the protein itself.

This idea of the Fe-S cluster serving both as a redox catalyst providing an electron for the cleavage of SAM, and as a source of sulfur in biotin was probed using careful iron, sulfide and spectrophotometric analysis. <sup>53</sup> The results showed that anaerobically purified BioB contains two apparently distinct [2Fe-2S]<sup>2+</sup> cluster per monomer. These clusters can be converted to the [4Fe-4S] form in the presence of excess iron, sulfide, and a strong reducing agent. Conversion of one of the [2Fe-2S]<sup>2+</sup> to the [4Fe-4S]<sup>2+</sup> cluster has a midpoint potential of –140mV. <sup>53</sup> Further reduction to the 1+ oxidation state occurs at a potential of –450 mV. <sup>53</sup> This cluster was proposed to serve as the reducing agent for SAM. The other cluster has a much lower potential and is converted directly to the [4Fe-4S]<sup>1+</sup> form at –505mV. <sup>53</sup> This cluster in its [2Fe-2S]<sup>2+</sup> form is proposed to be the source of sulfur during biotin formation. <sup>53</sup>

Genetic and biochemical work have indicated that the insertion of two sulfur atoms into octanoate to produce lipoic acid, might be catalyzed by the product of the *lipA* gene.<sup>54-56</sup> The *lipA* gene encodes for a 321-amino-acid-protein with an estimated molecular mass of 36 kDa. Significant similarities with BioB were noted including the CX<sub>3</sub>CX<sub>2</sub>C motif, which led to the proposal that LipA would contain an Fe-S cluster.<sup>55,57</sup> The protein is purified mainly in dimeric form

and characterization by UV-vis and resonance Raman spectroscopies showed that it contains one [4Fe-4S]<sup>2+</sup> cluster.<sup>58</sup> Purification of the enzyme from insoluble inclusion bodies followed by reconstitution under strict anaerobic conditions in the presence of iron, sulfide, and DTT, shows that each subunit binds one [4Fe-4S]<sup>2+</sup> cluster as determined by iron and sulfide analysis and UV-vis and Mössbauer spectroscopies.<sup>59</sup> Reduction by dithionite or 5-deazariboflavin leads to partial reduction to the [4Fe-4S]<sup>+</sup> form and exposure to O<sub>2</sub> results in degradation to the [2Fe-2S]<sup>2+</sup> form.<sup>53</sup>

The formation of lipoic acid involves the insertion of two sulfur atoms into carbons 6 and 8 of octanoic acid respectively as shown in Figure I.5. Early *in vivo* labeling studies in *E. coli* showed that sulfur insertion is most likely to proceed at C8 than at C6, because [8-<sup>2</sup>H<sub>2</sub>]-thiooctanoic acid could serve as a better precursor for lipoic acid. <sup>60</sup> Experiments have provided evidence that the true substrate in the LipA reaction might be the acylated form of octanoic acid covalently attached to an acyl-carrier protein (ACP). <sup>61</sup> This hypothesis has been tested, by devising an assay using octanoyl-ACP as a substrate and relying on

**Figure I.5.** Reaction catalyzed by lipoate synthase (LipA).

the transfer of lipoyl-ACP to apo-pyruvate dehydrogenase complex (apo-PDC) via the action of LipB.<sup>6</sup> Spectrophotometric detection of the product was accomplished through the reduction of 3-acetylpyridine adenine dinucleotide by PDC. However, only 0.32 mol of lipoyl-ACP per mole of LipA could be generated in the assay, demonstrating that additional components are lacking to yield a sustainable catalytic system. The assay also showed SAM dependence with a 10-fold increase in activity in the presence of SAM and that cluster reduction to the [4Fe-4S]<sup>+</sup> state was required.<sup>6</sup>

Ribonucleotide reductases catalyze the essential formation of deoxynucleotides. They are ubiquitous in nature and provide the only pathway for the de novo production of DNA precursors. The ribonucleotide reductases fall into three categories based on cofactor requirements of the enzymes although the mechanism is believed to be the same for all classes. Class I enzymes are the most abundant and contain a binuclear iron center and a tyrosyl radical cofactor. Class III ribonucleotide reductases uses adenosyl-cobalamin as a cofactor. Class III ribonucleotide reductases are found in anaerobically grown *E. coli*, and are often referred to as anaerobic ribonucleotide reductase (ARR). All of these enzymes are thought to use a thiyl radical derived from a cysteine residue of the protein to initiate the reduction process by abstraction of the 3'-hydrogen atom of the ribonucleotide substrates. However, the strategy to generate the thiyl radical differs between the classes. Cass

ARR, which is encoded by the nrdD gene, is a 160 kDa  $\alpha_2$ -homodimer. Sequence analysis has shown that ARR has some similarity to PFL especially

around the glycine radical site.<sup>64</sup> EPR experiments have confirmed the presence of an organic radical located on Gly681 in ARR.<sup>65</sup> The role of the glycyl radical is to serve as an initiator of catalysis by generating the thiyl radical at the active site; this role is similar to that of the tyrosyl radical in the class I enzymes.

However, unlike the tyrosyl radical, which is 35Å from the active-site thiyl radical residue, the Gly681 in ARR is reasonably close to the active-site cysteine, allowing for direct H-atom transfer.<sup>66,67</sup> ARR uses formate as an external reductant as shown by the overall stoichiometry of the reaction in Figure I.6. The use of formate by ARR provides an important link between ARR and PFL in the anaerobic metabolism of E. coli because formate is one of the products in the reaction catalyzed by PFL.

Figure I.6. Reaction catalyzed by anaerobic ribonucleotide reductase.

ARR is purified in an inactive dimeric form and requires activation under anaerobic conditions in the presence of SAM, NADPH, flavodoxin, flavodoxin reductase, DTT,  $K^+$ , and a protein component named  $\beta$ . <sup>68-70</sup> The  $\beta$ -protein is a dimer encoded by the nrdG gene with a subunit molecular mass of 17.5 kDa. <sup>70</sup> It has been shown that one equivalent of  $\beta_2$  is capable of activating several

equivalent of  $\alpha_2$ , demonstrating that the  $\beta$ -protein is in fact a true activating enzyme.<sup>71</sup>

The presence of an Fe-S cluster or clusters in the ARR  $\alpha_2\beta_2$  complex was noted early on.<sup>65</sup> However, the ARR activase ( $\beta_2$ ) isolated from an over-expression system under aerobic conditions is devoid of iron and sulfide. Anaerobic reconstitution in the presence of iron and sulfide showed an uptake of two equivalents of Fe and S for every polypeptide. Under highly reducing conditions, a [4Fe-4S]<sup>+</sup> cluster was detected by EPR.<sup>72</sup> A combination of various spectroscopic techniques showed that the reconstituted cluster was a [2Fe-2S]<sup>2+</sup> that was converted to the [4Fe-4S]<sup>+</sup> state upon reduction by 5-deazariboflavin and light or dithionite.<sup>7</sup> The importance of only three cysteine ligands in ARR-activase was confirmed by site-directed mutagenesis. The protein contains five cysteine residues and only the variants in the CX<sub>2</sub>CX<sub>3</sub>C motif (C26A, C30A, C33A) were inactive.<sup>73</sup>

Benzylsuccinate synthase (BSS) catalyzes the addition of toluene to fumarate to yield benzylsuccinate as shown in Figure I.7. The reaction is novel in biological systems because C-C bond formation occurs via carbon addition to a C=C double bond instead of a C=O double bond or to CO<sub>2</sub>. The reaction is the first step in the anaerobic catabolism of toluene in several denitrifying and sulfate reducing bacteria. The enzyme, which has been partially purified from T. aromatica and Azoarcus sp. strain T, is a heterohexamer  $\alpha_2\beta_2\gamma_2$  with subunit molecular masses of 98, 8.6, and 6.6 kDa for the  $\alpha$ ,  $\beta$ , and  $\gamma$  subunits, respectively. The amino acid sequence of BSS shares homology with PFL and

**Figure I.7.** Formation of benzylsuccinate from the addition of toluene to fumarate.

ARR,especially around the glycyl radical site, and it contains a conserved active-site cysteine residue. Recently, a stable free radical in BSS from *Azoarcus* sp. strain has been demonstrated. The radical is a doublet (A  $\approx$  15G) and has all the characteristics of a glycyl radical. The doublet EPR signal becomes a singlet upon incubation in D<sub>2</sub>O, which is consistent with a H/D exchange of the strongly coupled hydrogen atom.

Very little is known about the activase involved in glycyl radical generation in BSS; thus far, it has not been purified. Genetic analyses of *T. aromatica* have shown that the gene encoding for the putative activase is in the first operon with the structural genes of BSS.<sup>70</sup> The predicted sequence of the activase gene encodes for a protein of 36 kDa and contains the characteristic Cys motif close to the N-terminus.<sup>23</sup>

# I.3 Pyruvate Formate-Lyase

Pyruvate formate-lyase (acetyl-CoA:formate *C*-acetyltransferase, EC 2.3.1.54; PFL) catalyzes the reaction of coenzyme A with pyruvate to produce acetyl-CoA and formate as shown in Figure I.8. The reaction is the first committed step in anaerobic glucose metabolism in *E. coli* cells. The reaction is fully reversible with turnover numbers of 770 s<sup>-1</sup> for the forward reaction

Figure I.8. The cleavage of pyruvate by coenzyme A (CoA).

and 260 s<sup>-1</sup> for the reverse reaction at 30°C. 82 Purified from *E. coli*, PFL is a homodimer with a molecular mass of 170 kDa and contains no metals or cofactors. 83,84 The enzyme is catalytically inactive when isolated under aerobic conditions. Activation is accomplished only under anaerobic conditions by the action of another enzyme, the pyruvate formate-lyase activating enzyme, (PFL-AE). 82,85 Knappe and co-workers have shown that activation of PFL entails the generation of a stable free radical on the enzyme, which is equivalent to one radical spin per dimer. The radical is however highly susceptible to oxygen and displays a half-life of only 10s in air-saturated buffer at room temperature. 9,86

The enzyme can exist in an active form (PFL<sub>a</sub>), which contains one glycyl radical per dimer, and an inactive form (PFL<sub>i</sub>) in which the glycyl radical is reduced. The catalytically essential glycyl radical of PFL is post-translationally generated under anaerobic conditions by the stereospecific abstraction of the pro-S hydrogen atom of the Gly734 methylene group. <sup>83</sup> The interconversion of PFL between its inactive and active forms requires the pyruvate formate-lyase-activating enzyme (PFL-AE), *S*-adenosyl-L-methionine (AdoMet), flavodoxin, and flavodoxin reductase as shown in Figure I.9. <sup>55</sup> In addition, it has been suggested

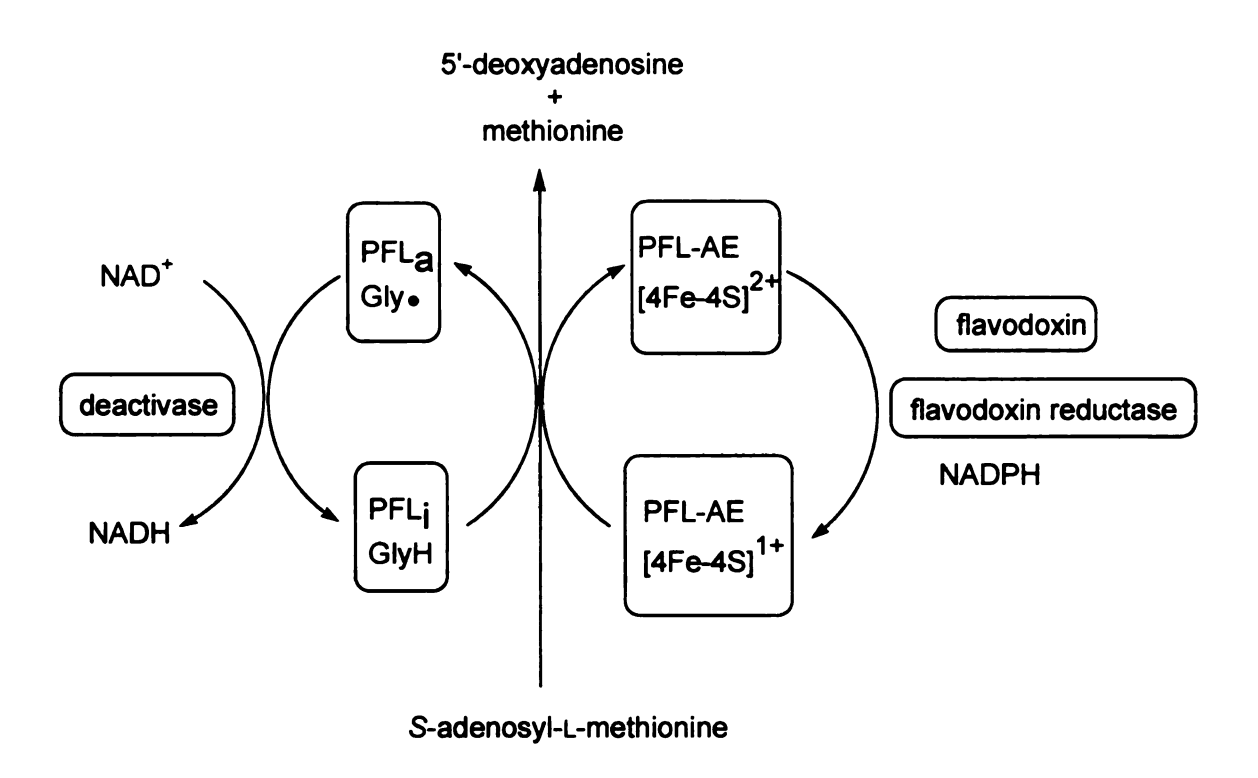


**Figure I.9** The activation / deactivation of PFL by generation or quenching of the glycyl radical on PFL.

that a "deactivase" reduces the glycyl radical of PFL to glycine, preventing its destruction by O<sub>2</sub>.87,88

The nature of the stable radical in PFL was established by performing EPR experiments with isotopically labeled forms of PFL and by examining the  $O_2$  cleavage products by mass spectrometry and amino acid sequencing. The radical was assigned to the  $\alpha$ -carbon of Gly734 and this discovery was the first proven case of a protein-derived glycyl radical involved in enzymatic catalysis. The EPR spectrum of the glycyl radical displayed a prominent doublet ( $A_{iso} = 15$  G) centered at g = 2.0037, which was attributed to a hyperfine coupling to the remaining  $\alpha$ -hydrogen. <sup>89</sup> An intriguing property of the glycyl radical in PFL is that the  $\alpha$ -hydrogen of Gly734 exchanges with solvent. This is apparent from EPR experiments done in  $D_2O$  buffer, which resulted in the disappearance of the 15-G doublet splitting. The exchange process is relatively rapid with a half-life of ~5 min at  $0^{\circ}C$ . Site directed mutagenesis studies have shown that this exchange occurs through the active-site cysteine residues.

The stability of the glycyl radical in the absence of dioxygen can be attributed to the summation of the effects of resonance electron withdrawal by the glycyl-carbonyl group and resonance electron donation by the adjacent amide nitrogen through its lone electron pair. This effect is shown by the resonance structures shown in Figure I.10. Gly734 does not directly participate in catalysis, but rather serves as the source of an unpaired electron that can be relayed to the active site in the form of a cysteinyl-thiyl unpaired electron that can be relayed to the active site in the form of a cysteinyl-thiyl radical, which is

**Figure I.10** Resonance structures for the captodative stabilization of glycyl radicals.

directly involved in homolytic cleavage of the pyruvate C-C bond. 90,91 Based on steric relationships among the amino acid residues, the Gly734 radical was proposed to abstract a hydrogen atom from Cys419, and the Cys419 thiyl radical in turn relays the radical center to Cys418, which is in the pyruvate binding site. 92

# 1.4 Pyruvate Formate-Lyase Activating Enzyme (PFL-AE)

The formation of the glycyl radical of PFL is catalyzed by PFL-activating enzyme, a 28 kDa monomeric protein. The reaction is dependent on AdoMet, pyruvate and an external electron source, which can be supplied either by NADPH via the flavodoxin/flavodoxin reductase system or by chemical reductants, such as dithionite or 5-deazariboflavin. Early experiments showed the catalytic activity of PFL-AE to be completely dependent on the presence of exogenous iron in the assay, which was the first indication of the role of iron in glycyl radical generation. <sup>83,85</sup> The reaction requires one equivalent of AdoMet, which is cleaved to yield 5-deozyadenosine and methionine as shown in Figure 1.11. <sup>9,83</sup> AdoMet is used as a cosubstrate in the reaction, which differs from its

role in the case of LAM and SPL where it acts as a coenzyme. Using [2-²H]-Gly-labeled PFL, Knappe and co-workers demonstrated the stoichiometric incorporation of deuterium into 5'-deoxyadenosine, thereby providing a direct link between the cleavage of SAM and H-atom transfer from Gly734 via the 5'-deoxyadenosyl radical. <sup>93</sup> The use of short peptides that mimicked the Gly radical site in the protein showed that the reaction proceeds by stereospecific abstraction of the pro-S hydrogen of Gly734. <sup>93</sup> The hydrogen atom abstracted from Gly734 of PFL has been shown to be incorporated into the

Figure I.11 Activation of PFL, catalyzed by the action of PFL-activase (PFL-AE).

5'-deoxyadenosine product by isotopic labeling, suggesting that the role of AdoMet is to produce an adenosyl radical intermediate as the immediate

hydrogen atom abstractor. Using an octapeptide analogous to the Gly734 site of PFL, but with a dehydroalanyl residue in the glycyl position, Wagner and coworkers have trapped the adenosyl radical intermediate by *C*-adenosylation of the dehydroalanyl residue.<sup>94</sup>

PFL-AE was initially isolated aerobically from non-overexpressing *E.coli* cells with a broad absorbance from 310 to 550 nm suggesting the presence of a covalently bound cofactor.<sup>83</sup> The first overexpression of PFL-AE in *E. coli* was reported by Kozarich and co-workers, but solubility problems made it necessary to purify and then refold the denatured protein.<sup>95</sup> The refolded protein was able to bind stoichiometric quantities of Fe as well as other divalent metals such as Cu(II) and Co(II), but it was found to have enzymatic activity only in the presence of Fe(II) and DTT. A cysteinal coordination sphere for the iron center of PFL-AE was suggested because thiophilic metals such as Cu(II), Zn(II), Hg(II) and Cd(II) were found to be inhibitors of PFL-AE activity.<sup>95</sup>

The first isolation of PFL-AE in its native state under strictly anaerobic conditions and identification of the presence of an iron-sulfur cluster in PFL-AE were achieved by Broderick and co-workers. PFL-AE with an intact Fe-S cluster has been purified and a high specific activity (95 U/mg in the absence of added iron) was obtained containing 2.65 Fe per protein. When purified under anaerobic conditions in the absence of DTT, PFL-AE was shown to contain primarily a [3Fe-4S]<sup>+</sup> cluster by a combination of UV-vis, EPR and resonance Raman spectroscopic methods. A complete description of the states of the cluster present in the enzyme was provided by Mössbauer spectroscopy.

major component was confirmed to be the cuboidal [3Fe-4S]<sup>+</sup> cluster, accounting for 66 % of the total iron. Minor contributions from [2Fe-2S]<sup>2+</sup> (12 % of the total Fe), [4Fe-4S]<sup>2+</sup> (8 % of the total Fe) and linear [3Fe-4S]<sup>+</sup> (~10 % of the total Fe) were also found in the Mössbauer spectrum of the as-isolated PFL-AE. When PFL-AE was anaerobically reduced with dithionite, complete conversion of all cluster types to [4Fe-4S]<sup>2+/+</sup> clusters was observed by Mössbauer spectroscopy.<sup>98</sup>

The above work has clearly demonstrated that the Fe-S cluster of PFL-AE is required for enzymatic activity, and that no ferrous iron is required for activity when an intact cluster is present. 97-99 Among the mixture of Fe-S clusters present in PFL-AE, the [4Fe-4S] cluster was considered to be the catalytically relevant cluster, as PFL-AE activity is observed in vitro only under anaerobic reducing conditions. 83 A definite assignment of the [4Fe-4S] of PFL-AE as the catalytically active cluster was achieved in a "single turnover" experiment. 100 Deazariboflavin-mediated photoreduction afforded quantitative reduction of PFL-AE to the [4Fe-4S] tate. After the excess reductant was removed by placing the sample in the dark, either AdoMet alone, or AdoMet plus PFL (equimolar to PFL-AE) was added to the reduced PFL-AE. Spin quantitation of the resulting EPR spectra, taken as a function of illumination time, show a 1:1 correspondence between the amount of PFL glycyl radical generated and the amount of [4Fe-4S]<sup>+</sup> cluster present in the PFL-AE prior to addition of PFL. The

[4Fe-4S]<sup>+</sup> was converted to an EPR silent state concomitant with glycyl radical formation, and preliminary data suggest that the final cluster state is [4Fe-4S]<sup>2+</sup>. This is the first direct quantitative spectroscopic evidence that the [4Fe-4S]<sup>+</sup> of PFL-AE is the catalytically relevant cluster, and this cluster provides the electron necessary for AdoMet-dependent glycyl radical generation.<sup>100</sup>

Site-directed mutagenesis studies have identified Cys29, Cys33, Cys36 as the cluster ligands in PFL-AE.<sup>99</sup> In general, a similar cluster-binding motif comprised of only three cysteines (CX<sub>3</sub>CX<sub>2</sub>C) is common to all of the Fe-S/AdoMet-dependent enzymes for which the gene sequence is known.<sup>30,55,70,84,101,102</sup> Considering that the [4Fe-4S] cluster of PFL-AE is the catalytically relevant cluster, the fourth ligand to the [4Fe-4S] cluster is presumably non-cysteine, therefore, resulting in a unique iron site, which may be important in binding / interacting with AdoMet.

# I.5 S-Adenosylmethionine and the Fe-S cluster of PFL-AE in RadicalGeneration

The mechanism by which SAM is reductively cleaved in its reversible reaction with [4Fe-4S]<sup>+</sup> is of considerable interest. Unlike the weak Co-C5' bond in adenosylcobalamin, which generates the 5'-deoxyadenosyl radical, the C-S bonds in SAM are strong (~60kcal mol<sup>-1</sup> BDE), and the bond linking the adenosyl moiety to sulfur cannot be cleaved homolytically simply by binding to the enzyme. Electron transfer from the [4Fe-4S]<sup>+</sup> center to SAM must somehow be involved.

The process of the electron transfer may be described by Figure I.12 which specifies the bond cleavage in SAM and change in oxidation state of the [4Fe-4S] center although without describing the mechanism of the reaction.<sup>23</sup>

$$[4Fe-4S]^{+1}$$
 +  $S^{+}$   $C$  Ado  $[4Fe-4S]^{+2}$  +  $H_{2}$   $C$  Ado  $H_{2}$ 

Figure I.12 Electron transfer from the [4Fe-4S]<sup>1+</sup> center to SAM.

Mechanisms that have been considered for SAM-dependent radical enzymes include the following: (1) Outer-sphere electron transfer from the [4Fe-4S]<sup>+</sup> center to SAM to form a SAM-radical, which then undergoes fragmentation to the 5'-deoxyadenosyl radical and methionine. (2) Adenosylation of a thiolate ligand or sulfide in [4Fe-4S]<sup>+</sup> to form methionine and an S-adenosyl iron-sulfur center, followed by fragmentation of this center to the 5'-deoxyadenosyl radical and [4Fe-4S]<sup>2+</sup>. (3) Adenosylation of iron in the [4Fe-4S]<sup>+</sup> to form methionine and an Fe-adenosyl iron-sulfur center, followed by fragmentation of this center to the 5-deoxyadenosyl radical and [4Fe-4S]<sup>2+</sup>. (4) Inner-sphere electron transfer from the [4Fe-4S]<sup>+</sup> center to the sulfonium center of SAM, accompanied by ligation of iron to sulfur of methionine and concomitant cleavage of the S-C5' bond of SAM and formation of the 5'-deoxyadenosyl radical.

It has been shown for LAM,<sup>106</sup> PFL-AE,<sup>100</sup> and aRNR-AE<sup>103</sup> that the [4Fe-4S]<sup>+</sup> is the cluster that interacts with AdoMet to initiate radical chemistry,

and one-electron oxidation of the cluster appears to accompany radical generation. The presence of AdoMet has been shown to dramatically affect the EPR signal of the PFL-AE [4Fe-4S]<sup>+</sup>, suggesting the possibility of a direct interaction between AdoMet and Fe-S cluster of PFL-AE. 98,100 The central and most intriguing mechanistic step involves the reduced cluster donating an electron to convert AdoMet to methionine and 5'-deoxyadenosyl radical intermediate. Label-transfer from the glycine residue of PFL to 5'-deoxyadenosyl product has provided indirect evidence for an adenosyl radical intermediate, but direct spectroscopic evidence for the existence of the adenosyl radical intermediate is not available due to the instability of this radical intermediate. However, an allylic analog of the 5'-deoxyadenosyl radical has been detected in the LAM catalyzed reaction.

The key question regarding the mechanism by which the Fe-S cluster interacts with *S*-adenosylmethionine to generate an adenosyl radical intermediate remains to be answered. As the sulfur-5'-deoxyadenosyl carbon bond is reductively cleaved during the radical generation, the sulfonium center of AdoMet is likely to be positioned close to the Fe-S cluster. In this, the putative interaction between AdoMet and the Fe-S cluster was probed. The sulfonium center of AdoMet was synthetically modified, and used along with a variety of spectroscopic methods to investigate the interaction between AdoMet and the Fe-S cluster of PFL-AE. Specifically, the methyl group of AdoMet was labeled with <sup>2</sup>H and <sup>13</sup>C, and the sulfur was replaced by selenium to take advantage of the natural abundance of <sup>77</sup>Se (7.50 %). Additional studies were conducted

using the nuclei <sup>17</sup>O, and <sup>13</sup>C at the carboxy group, <sup>15</sup>N at the amino group, and a <sup>2</sup>H label at the α-carbon of the methionine end of AdoMet. All of these nuclei have non-zero nuclear spins, and therefore, are effective probes in spectroscopic studies, such as electron paramagnetic resonance (EPR) and electron-nuclear double resonance (ENDOR) spectroscopy, to demonstrate the interaction between AdoMet and the unique iron site of the Fe-S cluster of PFL-AE.

Analogues of SAM were also used to probe the formation of the putative 5'-deoxyadenosyl radical prior to the generation of the glycyl radical in pyruvate formate-lyase.

#### I.6 References

- (1) Sofia, H. J.; Chen, G.; Hetzler, B. G.; Reyes-Spindola, J. F.; Miller, N. E. *Nucleic Acids Research* **2001**, *29*, 1097-1106.
- (2) Wu, W.; Booker, S.; Lieder, K. W.; Bandarian, V.; Reed, G. H.; Frey, P. A. *Biochemistry* **2000**, *39*, 9561-9570.
- (3) Frey, P. A.; Moss, M. L. Cold Spring Harbor Symp. Quant. Biol. **1987**, *52*, 571-577.
- (4) Duin, E. C.; Lafferty, M. E.; Crouse, B. R.; Allen, R. M.; Sanyal, I.; Flint, D. H.; Johnson, M. K. *Biochemistry* **1997**, *36*, 11811-11820.
- (5) Ollagnier-de Choudens, S.; Sanakis, Y.; Hewitson, K. S.; Roach, P.; Baldwin, J. E.; Münck, E.; Fontecave, M. *Biochemistry* **2000**, *39*, 4165-4173.
- (6) Miller, J. R.; Busby, R. W.; Jordan, S. W.; Cheek, J.; Henshaw, T. F.; Ashley, G. W.; Broderick, J. B.; Cronan, J. E., Jr.;; Marletta, M. A. *Biochemistry* **2000**, *39*, 15166-15178.
- (7) Ollagnier, S.; Meier, C.; Mulliez, E.; Gaillard, J.; Schuenemann, V.; Trautwein, A.; Mattioli, T.; Lutz, M.; Fontecave, M. *J. Am. Chem. Soc.* **1999**, *121*, 6344.
- (8) Külzer, R.; Pils, T.; Kappl, R.; Hüttermann, J.; Knappe, J. *J. Biol. Chem.* **1998**, *273*, 4897-4903.
- (9) Knappe, J.; Neugebauer, F. A.; Blaschkowski, H. P.; Ganzler, M. *Proc. Natl. Acad. Sci. USA* **1984**, *81*, 1332-1335.
- (10) Begley, T. P.; Xi, J.; Kinsland, C.; Taylor, S.; McLafferty, F. *Curr. Opin. Chem. Biol.* **1999**, *3*, 623-629.
- (11) Allen, R. M.; Chatterjee, R.; Ludden, P. W.; Shah, V. K. *J. Biol. Chem.* **1995**, *270*, 26890-26896.
- (12) Esberg, B.; Leung, H.-C. E.; Tsui, H.-C. T.; Björk, G. R.; Winkler, M. E. *J. Bacteriol.* **1999**, *181*, 7256.
- (13) Reed, K. E.; Morris, T. W.; Cronan, J. E., Jr.; *Proc. Natl. Acad. Sci. USA* **1994**, *91*, 3720.
- (14) Rieder, C.; Eisenreich, W.; O'Brien, J.; Richter, G.; Götze, E.;

- Boyle, P.; Blanchard, S.; Bacher, A.; Simon, H. Eur. J. Biochem. 1998, 255, 24.
- (15) Akhtar, M. Ciba Found. Symp. 1994, 180, 131-155.
- (16) Suzuki, J. Y.; Bollivar, D. W.; Bauer, C. E. *Annu. Rev. Genet.* **1997**, 31.
- (17) Tait, G. H. Biochem. J. 1972, 128, 1159-1169.
- (18) Heider, J.; Spormann, A. M.; Beller, H. R.; Widdel, F. *FEMS Microbiol. Rev.* **1999**, *22*, 459-473.
- (19) Rebeil, R.; Sun, Y.; Chooback, L.; Pedreza-Reyes, M.; Kinsland, C.; Begley, T. P.; Nicholson, W. L. *J. Bacteriol.* **1998**, *180*, 4879-4885.
- (20) Chirpich, T. P.; Zappia, V.; Costilow, R. N.; Barker, H. A. *J. Biol. Chem.* **1970**, *245*, 1778.
- (21) Stadtman, T. C. Adv. Enzymol. Relat. Areas Mol. Biol. 1973, 38, 413.
- (22) Baker, J. J.; Stadtman, T. C., Eds. *Aminomutases. In B12: Biochemistry and Medecine*; Wiley-Interscience: New York, 1982;
  Vol. 2.
- (23) Frey, P. A.; Magnusson, O. T. Chem. Rev. 2003, 103, 2129-2148.
- (24) Aberhart, D. J.; Gould, S. J.; Lin, H.-J.; Thiuruvengadam, T. K.; Weiller, B. H. *J. Am. Chem. Soc.* **1983**, *105*, 5461.
- (25) Baraniak, J.; Moss, M. L.; Frey, P. A. J. Biol. Chem. **1989**, 264, 413.
- (26) Frey, P. A.; Essenberg, M. K.; Abeles, R. H. *J. Biol. Chem.* **1967**, 242, 5369.
- (27) Moss, M. L.; Frey, P. A. J. Biol. Chem. 1987, 1987, 1332.
- (28) Rebeil, R.; Nicholson, W. L. *Proc. Natl. Acad. Sci. USA* **2001**, *98*, 9038.
- (29) Cheek, J.; Broderick, J. B. J. Am. Chem. Soc. 2002, 124, 2860.
- (30) Otsuka, A. J.; Buoncristiani, M. R.; Howard, P. K.; Flamm, J.;

- Johnson, C.; Yamamoto, R.; Uchida, K.; Cook, C.; Ruppert, J.; Matsuzaki, J. *J. Biol. Chem.* **1988**, *263*, 19577.
- (31) Bower, S.; Perkins, J. B.; Yocum, R. R.; Howitt, C. L.; Rahaim, P.; Pero, J. *J. Bacteriol.* **1996**, *178*, 4122.
- (32) Gloeckler, R.; Ohsawa, I.; Speck, D.; Ledoux, C.; Bernard, S.; Zinsius, M.; Villeval, D.; Kisou, T.; Kamogawa, K.; Lemoine, Y. *Gene* **1990**, *87*, 63.
- (33) Phalip, V.; Kuhn, I.; Lemoine, Y.; Jeltsch, J.-M. *Gene* **1999**, *232*, 43.
- (34) Baldet, P.; Gerbling, H.; Axiotis, S.; Douce, R. *Eur. J. Biochem.* **1993**, *217*, 479.
- (35) Parry, R. J.; Kunitani, M. G. Methods Enzymol. 1979, 217, 479.
- (36) Trainor, D. A.; Parry, R. J.; Gitterman, A. J. Am. Chem. Soc. 1980, 102, 1467.
- (37) Frappier, F.; Jouany, M.; Marquet, A.; Olesker, A.; Tabet, J. C. *J. Org. Chem.* **1982**, *47*, 2257.
- (38) Ifuku, O.; Tse Sum Bui, B.; Florentin, D.; Begley, T. P., Ed.; Academic Press: San Diego, 2001; Vol. 61, p 51.
- (39) Guianvarch, D.; Florentin, D.; Bui, B. T. S.; Nunzi, F.; Marquet, A. *Biochem. Biophys. Res. Commun.* **1997**, *236*, 402.
- (40) Sanyal, I.; Cohen, G.; Flint, D. H. Biochemistry 1994, 33, 3625.
- (41) Méjean, A.; Tse Sum Bui, B.; Florentin, D.; Ploux, O.; Izumi, Y.; Marquet, A. *Biochem. Biophys. Res. Commun.* **1995**, *217*, 1231.
- (42) Brereton, P. S.; Duderstadt, R. E.; Staples, C. R.; Johnson, M. K.; Adams, M. W. *Biochemistry* **1999**, *39*, 5206.
- (43) Ugulava, N. B.; Gibney, B. R.; Jarrett, J. P. *Biochemistry* **2000**, *39*, 5206.
- (44) McIver, L.; Baxter, R. L.; Campopiano, D. J. *J. Biol. Chem.* **2000**, 275, 13888.
- (45) Hewitson, K. S.; Baldwin, J. E.; Shaw, N. M.; Roach, P. L. *FEBS Letters* **2000**, *466*, 372.

- (46) Ollagnier-de Choudens, S.; Sanakis, Y.; Hewitson, K.; Roach, P.; Münck, E.; Fontecave, M. J. Biol. Chem. 2002, 277, 13449.
- (47) Hewitson, K. S.; Ollagnier-de Choudens, S.; Sanakis, Y.; Shaw, N. M.; Baldwin, J. E.; Münck, E.; Roach, P.; Fontecave, M. *J. Biol. Inorg. Chem.* **2002**, *7*, 83.
- (48) DeMoll, E.; Shive, W. *Biochem. Biophys. Res. Commun.* **1983**, *110*, 243.
- (49) Ifuku, O.; Kishimoto, J.; Haze, S.; Yanagi, M.; Fukushima, S. *Biosci. Biothecnol. Biochem* **1992**, *56*, 1780.
- (50) Florentin, D.; Tse Sum Bui, B.; Marquet, A.; Oshiro, T.; Izumi, Y. C. *R. Acad. Sci. Ser.* **1994**, *317*, 485.
- (51) Tse Sum Bui, B.; Florentin, D.; Fournier, F.; Ploux, O.; Mejean, A.; Marquet, A. *FEBS Lett.* **1998**, *440*, 226.
- (52) Gibson, K. J.; Pelletier, D. A.; Turner, S. I. M. *Biochem. Biophys. Res. Commun.* **1999**, *254*, 632.
- (53) Ugulava, N. B.; Gibney, B. R.; Jarrett, J. P. *Biochemistry* **2001**, *40*, 8343.
- (54) Van den Boom, T. J.; Reed, K. E.; Cronan, J. E., Jr. *J. Bacteriol.* **1991**, *173*, 6411.
- (55) Hayden, M. A.; Huang, I.; Bussiere, D. E.; Ashley, G. W. *J. Biol. Chem.* **1992**, *267*, 9512.
- (56) Hayden, M. A.; Huang, I.; Iliopoulos, G.; Orozco, M.; Ashley, G. W. *Biochemistry* **1993**, *32*, 3778.
- (57) Reed, K. E.; Cronan, J. E., Jr. J. Bacteriol. 1993, 175, 1325.
- (58) Busby, R. W.; Schelvis, J. P. M.; Yu, D.; Babcock, G. T.; Marletta, M. A. *J. Am. Chem. Soc.* **1999**, *121*, 4706.
- (59) Ollagnier-de Choudens, S.; Fontecave, M. FEBS Lett. 1999, 453, 25.
- (60) Parry, R. J. Tetrahedron 1983, 39, 1215.
- (61) Jordan, S. W.; Cronan, J. E., Jr. J. Biol. Chem. 1997, 272, 17903.

- (62) Stubbe, J.; van der Donk, W. A. Chem. Rev. 1998, 98, 705.
- (63) Jordan, A.; Reichard, P. Annu. Rev. Biochem. 1998, 67, 71.
- (64) Sun, X.; Harder, J.; Krook, M.; Jörnvall, H.; Sjöberg, B.-M.; Reichard, P. *Proc. Natl. Acad. Sci. USA* **1993**, *90*, 577.
- (65) Mulliez, E.; Fontecave, M.; Gaillard, J.; Reichard, P. *J. Biol. Chem.* **1993**, *268*, 2296.
- (66) Logan, D. T.; Andersson, J.; Sjöberg, B.-M.; Nordlund, P. *Science* **1999**, *283*, 1499.
- (67) Uhlin, U.; Eklund, H. Nature 1994, 370, 533.
- (68) Harder, J.; Eliasson, R.; Pontis, E.; Ballinger, M. D.; Reichard, P. *J. Biol. Chem.* **1992**, *267*, 25548.
- (69) Bianchi, V.; Eliasson, R.; Fontecave, M.; Mulliez, E.; Hoover, D. M.; Matthews, R. G.; Reichard, P. *Biochem. Biophys. Res. Commun.* **1995**, *197*, 792.
- (70) Sun, X.; Eliasson, R.; Pontis, E.; Andersson, J.; Buist, G.; Sjöberg, B.-M.; Reichard, P. *J. Biol. Chem.* **1995**, *270*, 2443.
- (71) Tamarit, J.; Mulliez, E.; Meier, C.; Trautwein, A.; Fontecave, M. *J. Biol. Chem.* **1999**, *274*, 31291.
- (72) Ollagnier, S.; Mulliez, E.; Gaillard, J.; Eliasson, R.; Fontecave, M.; Reichard, P. *J. Biol. Chem.* **1996**, *271*, 9410.
- (73) Tamarit, J.; Gerez, C.; Meier, C.; Mulliez, E.; Trautwein, A.; Fontecave, M. *J. Biol. Chem.* **2000**, *275*, 15669.
- (74) Biegert, T.; Fuchs, G.; Heider, J. Eur. J. Biochem. 1996, 238.
- (75) Beller, H. R.; Spormann, A. M. J. Bacteriol. 1997, 179, 670.
- (76) Coschigano, P. W.; Wehrman, T. S.; Young, L. Y. *Appl. Environ. Microbiol.* **1998**, *64*, 1650.
- (77) Beller, H. R.; Spormann, A. M. *Appl. Environ. Microbiol.* **1997**, *63*, 3729.
- (78) Rabus, R.; Heider, J. Arch. Microbiol. 1998, 170, 377.

- (79) Leuthner, B.; Leutwein, C.; Schulz, H.; Hörch, P.; Haehnel, W.; Schiltz, E.; Schägger, H.; Heider, J. *Mol. Microbiol.* **1998**, *28*, 615.
- (80) Beller, H. R.; Spormann, A. M. *FEMS Microbiol. Lett.* **1999**, *178*, 147.
- (81) Krieger, C. J.; Roseboom, W.; Albracht, S. P. J. *J. Biol. Chem.* **2001**, *276*, 12924.
- (82) Knappe, J.; Blaschkowski, H. P.; Gröbner, P.; Schmitt, T. *Eur. J. Biochem.* **1974**, *50*, 523.
- (83) Conradt, H.; Hohmann-Berger, M.; Hohmann, H. P.; Blaschowski, H. P.; Knappe, J. *Arch. Biochem. Biophys.* **1984**, *228*, 133.
- (84) Rödel, W.; Plaga, W.; Frank, R.; Knappe, J. *Eur. J. Biochem.* **1988**, 177, 153.
- (85) Knappe, J.; Schnacht, J.; Möckel, W.; Höpner, T.; Vetter, H., Jr.;; Edenharder, R. Eur. J. Biochem. 1969, 11, 316.
- (86) Unkrig, V.; Neugebauer, F. A.; Knappe, J. *Eur. J. Biochem.* **1989**, *184*, 723.
- (87) Kessler, D.; Leibrecht, I.; Knappe, J. *FEBS Lett.* **1991**, *281*, 59.
- (88) Kessler, D.; Herth, W.; Knappe, J. J. Biol. Chem. 1992, 267, 18073.
- (89) Wagner, A. F. V.; Frey, M.; Neugenbauer, F. A.; Schafer, W.; Knappe, J. *Proc. Natl. Acad. Sci. USA* **1992**, *89*, 996.
- (90) Reddy, S. G.; Wong, K. K.; Parast, C. V.; Peisach, J.; Magliozzo, R. S.; Kozarich, J. W. *Biochemistry* **1998**, *37*, 558.
- (91) Parast, C. V.; Wong, K. K.; Lewisch, S. A.; Kozarich, J. W. *Biochemistry* **1995**, *34*, 2393.
- (92) Becker, A.; Fritz-Wolf, K.; Kabsch, W.; Knappe, J.; Schultz, S.; Wagner, A. F. V. *Nat. Struc. Biol.* **1999**, *6*, 969.
- (93) Frey, M.; Rothe, M.; Wagner, A. F. V.; Knappe, J. *J. Biol. Chem.* **1994**, *269*, 12432.
- (94) Wagner, A. F. V.; Demand, J.; Schilling, G.; Pils, T.; Knappe, J. *Biochem. Biophys. Res. Commun.* **1999**, *254*, 306.

- (95) Wong, K. K.; Murray, B. W.; Lewisch, S. A.; Baxter, M. K.; Ridky, T. W.; Ulissi-Demario, L.; Kozarich, J. W. *Biochemistry* **1993**, *32*, 14102.
- (96) Broderick, J. B.; Duderstadt, R. E.; Fernandez, D. C.; Wojtuszewski, K.; Henshaw, T. F.; Johnson, M. K. *J. Am. Chem. Soc.* **1997**, *119*, 7396.
- (97) Broderick, J. B.; Henshaw, T. F.; Cheek, J.; Wojtuszewski, K.; Smith, S. R.; Trojan, M. R.; McGhan, R. M.; Kopf, A.; Kibbey, M.; Broderick, W. E. *Biochem. Biophys. Res. Commun.* **2000**, *269*, 451.
- (98) Krebs, C.; Henshaw, T. F.; Cheek, J.; Huynh, B. H.; Broderick, J. B. *J. Am. Chem. Soc.* **2000**, *122*, 12497.
- (99) Külzer, R.; Pils, T.; Kappl, R.; Hüttermann, J.; Knappe, J. *J. Biol. Chem.* **1998**, *273*, 4897.
- (100) Henshaw, T. F.; Cheek, J.; Broderick, J. B. *J. Am. Chem. Soc.* **2000**, *122*, 8331.
- (101) Fajardo-Cavazos, P.; Salazar, C.; Nicholson, W. L. *J. Bacteriol.* **1993**, *175*, 1735.
- (102) Ruzicka, F. J.; Lieder, K. W.; Frey, P. A. *J. Bacteriol.* **2000**, *184*, 469.
- (103) Ollagnier, S.; Mulliez, E.; Schmidt, P. P.; Eliasson, R.; Gaillard, J.; Deronzier, C.; Bergman, T.; Gräslund, A.; Reichard, P.; Fontecave, M. J. Biol. Chem. 1997, 272, 24216.
- (104) Frey, P. A.; Reed, G. H. Adv. Enzymol. Relat. Areas Mol. Biol. **1992**, *66*, 1.
- (105) Frey, P. A.; Booker, S. Adv. Free Radical Chem. 1999, 2, 1.
- (106) Lieder, K. W.; Booker, S.; Ruzicka, F. J.; Beinert, H.; Reed, G. H.; Frey, P. A. *Biochemistry* **1998**, *37*, 2578.

#### **CHAPTER II**

# OVEREXPRESSION AND CHARACTERIZATION OF PYRUVATE FORMATE-LYASE AND PYRUVATE FORMATE-LYASE ACTIVATING ENZYME

#### II.1 Introduction

In the late 1960s and early 1970s, research on the metabolism of pyruvate led to the recognition of "clastic" reactions. The phosphoroclastic reaction of pyruvate required phosphate and led to acetyl phosphate, hydrogen peroxide, and carbon dioxide as shown in Figure II.1. The enzyme is pyruvate oxidase [pyruvate:oxygen 2-oxidoreductase (phosphorylating) EC 1.2.3.3], a flavoprotein

$$H_3C$$
 +  $HPO_4^{2-}$  +  $H^+$  +  $H_3C$  +  $CO_2$  +  $H_2O_2$  +  $H_2O_2$ 

**Figure II.1** The phosphoroclastic reaction of pyruvate.

that requires thiamine pyrophosphate (TPP), as a coenzyme. In a distinct process, known as the "thioclastic" reaction, pyruvate was cleaved by coenzyme A (CoA) to form acetyl-CoA and formate as shown in Figure II.2.<sup>2</sup> This enzyme was difficult to assay and characterize. In cellular extracts, it seemed to be

activated by TPP and AdoMet. Because the carboxyl group was removed from pyruvate, it seemed natural that TPP would be required, as it was for pyruvate, carboxylase, pyruvate dehydrogenase, and many pyruvate oxidoreductases.

Figure II.2 The thioclastic reaction of pyruvate.

However, purification studies have shown that the effect of TPP was on another protein that seemed to increase the activity of the enzyme catalyzing the thioclastic reaction. This effect could be replaced by the imposition of strict anaerobic conditions and the addition of Co<sup>2+</sup> and a reducing agent.<sup>1</sup> Thus, the effect of TPP appeared to be to bring about anaerobic conditions through the action of a TPP-dependent enzyme in the extract. The purified enzyme catalyzing the thioclastic reaction was named pyruvate-formate-lyase [EC 2.3.1.54], and its activation required a second protein, AdoMet, ferrous ion, and a reducing agent. The second protein was eventually found to be an AdoMet-dependent activase that introduced a radical site into pyruvate formate-lyase.<sup>3</sup>

Pyruvate formate-lyase (PFL) from *E. coli* is a dimeric enzyme of 170 kDa composed of identical units. The newly synthesized inactive enzyme is activated by posttranslational modification, to contain a glycyl radical at position 734.<sup>4,5</sup> The glycyl- 734 radical in the sequence <sub>731</sub>RVSGY<sub>735</sub> of PFL has been characterized

by EPR spectroscopy.<sup>4</sup> Abstraction of the pro-S hydrogen from C-2 of Gly734 is catalyzed by PFL activase (PFL-AE) and proceeds with concomitant cleavage of AdoMet into methionine and 5'-deoxyadenosine. AdoMet does not function catalytically in this process, but rather as a substrate in an irreversible reaction.<sup>6</sup>

A radical SAM enzyme, PFL-AE catalyzes the reaction in Figure II.3. PFL-AE from *E. coli*, with a molecular mass of 28 kDa, contains an iron-sulfur center and catalyzes the transient cleavage of SAM, presumably into methionine and 5'-deoxyadenosyl radical. The cosubstrate is inactive PFL, and the products are active PFL, methionine and 5'-deoxyadenosine.<sup>6</sup>

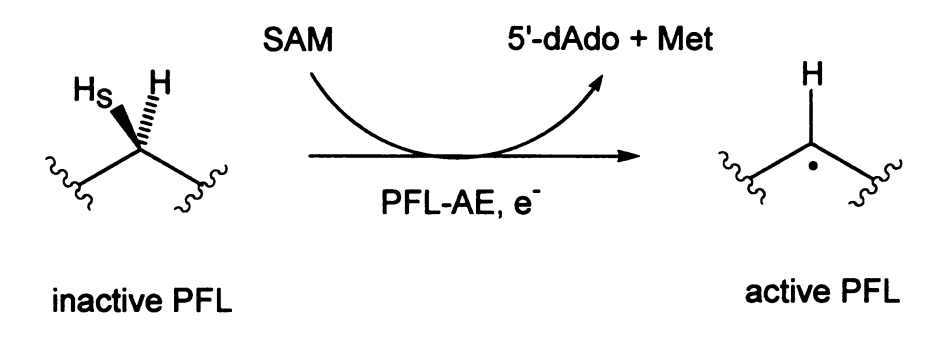


**Figure II.3** Activation of PFL by hydrogen abstraction from Gly 734 catalyzed by PFL-AE.

PFL-AE was initially isolated aerobically from non-overexpressing *E. coli* cells with an absorption spectrum indicating the presence of a covalently bound cofactor.<sup>7</sup> The catalytic activity of PFL-AE was found to be totally dependent on the presence of exogenous iron in the assay. This was the first indication of the role of iron in the glycyl radical generation.<sup>8</sup> The first reported purification and

characterization of PFL-AE from overexpressing *E. coli* cells detailed the necessity of purifying under denaturing conditions due to solubility problems. The protein was refolded, which afforded an apo-enzyme that did not contain the covalent chromophore. The refolded protein was able to bind stoichiometric quantities of iron as well as other divalent metals such as Cu(II) and Co(II) and was found to have enzymatic activity in the presence of Fe(II) and DTT, but the specific activity was low (1.9 U/mg) relative to the wild-type protein (25 U/mg). A cysteinal coordination sphere for the iron center of PFL-AE was suggested because thiophilic metals such as Cu(II), Zn(II), Hg(II) and Cd(II) were found to be inhibitors of the enzyme. <sup>7,8</sup>

Isolation of large quantities of native PFL-AE, without resorting to denaturation and artificial reconstitution, is critical to understanding the nature of the iron center in PFL-AE and its role in radical generation. The first isolation of PFL-AE in its native state under strictly anaerobic conditions and identification of the presence of an iron-sulfur cluster in PFL-AE were achieved when the protein was purified under anaerobic conditions in the absence of DTT. PFL-AE was shown to contain primarily a [3Fe-4S]<sup>+</sup> cluster by a combination of UV-visible, EPR and resonance Raman spectroscopic methods. A complete description of the states of the cluster present in the enzyme was provided by Mössbauer spectroscopy, a method that can detect and quantify all iron species in the samples. Detailed analysis of the Mössbauer data indicates a mixture of Fe-S clusters with the cuboidal [3Fe-4S]<sup>+</sup> cluster as the primary cluster form, accounting for 66 % of the total iron. Also present are [2Fe-2S]<sup>2+</sup> (12 % of the

total Fe), [4Fe-4S]<sup>2+</sup> (8 % of the total Fe) and linear [3Fe-4S]<sup>+</sup> (~10 % of the total Fe). The isolated native enzyme has nearly a full complement of Fe-S cluster with approximately 3 irons and 3 sulfides per protein molecule. It exhibits a high specific activity (95 U/mg) in the absence of added iron, while the apo-enzyme exhibits no such activity, indicating the cluster present in native enzyme is essential and sufficient for enzymatic activity. 9

In the dithionite-reduced form of PFL-AE, all cluster types were converted into the [4Fe-4S] form. 11 The [4Fe-4S] cluster was expected to be the catalytically relevant cluster, which is generated under the reducing conditions present in the activity assay. 11 Henshaw and co-workers have demonstrated that the [4Fe-4S] is indeed the catalytically active cluster of PFL-AE and that it donates the electron required for reductive cleavage of AdoMet. 12 The purification of PFL-AE containing primarily [3Fe-4S] clusters implies a labile fourth iron site, and is consistent with the observation that only three cysteines have been implicated in cluster coordination. 13 These three cysteines exist in a CX<sub>3</sub>CX<sub>2</sub>C motif that is common to all of the AdoMet dependent Fe-S enzymes for which a sequence has been determined. The identity of the fourth ligand to the [4Fe-4S] cluster in PFL-AE and these related enzymes is currently unknown. However, by analogy to aconitase, in which substrate coordinates to the unique iron site 14-16 and solvent binds in the absence of substrate or product. 14 it is reasonable to propose that exogenous ligands such as water or substrate may bind to the unique labile iron site in PFL-AE.

Currently, PFL-AE is purified under anaerobic reducing conditions in the presence of DTT to yield essentially EPR-silent clusters, presumably in the [4Fe-4S]<sup>2+</sup> state, which can be readily reduced to [4Fe-4S]<sup>+</sup>, the cluster that is responsible for providing the electron necessary for AdoMet dependent glycyl radical generation on PFL.

# II.2 Experimental Methods

#### II.2.1 Materials

The plasmids pMG-AE and pKK-PFL were obtained as generous gifts from John Kozarich (Merck). The *Escherichia coli* BL21(DE3)pLysS strain and pCAL-n-EK expression vector were obtained from Stratagene. 5-Deazariboflavin was synthesized in our laboratory according to published procedures, and characterized using NMR spectroscopy and Mass spectrometry. All other chemicals were of highest purity, obtained commercially and used as received.

## II.2.2 Growth and Expression of PFL

pKK-PFL was used to transform BL21(DE3)pLysS. A single colony of transformed cells was used to inoculate 50 mL LB media containing  $50\mu g/mL$  ampicillin (LB/Amp). This culture was grown for 16 h to saturation and then used to inoculate LB/Amp in a 9 L bench-top fermentor (New Brunswick). The 9 L culture was grown at 37 °C with continuous air purge and vigorous agitation to early log phase (OD<sub>600</sub> ~ 0.6-0.8), and then induced by addition of 1 mM isopropyl-β-D-thiogalactopyranoside (IPTG). The culture was grown for 2 more

hours before harvesting by centrifugation at 10,816 × g (8,000 rpm, Sorvall GS3 rotor). The supernatant was decanted and the cells stored at -80 °C.

#### II.2.3 Purification of PFL

PFL was purified from the BL21(DE3)pLysS/pKK-PFL cells. Cell paste (typically approximately 10 g) was suspended in enzymatic lysis buffer (5 mL per gram of cell paste) containing 20 mM Hepes, pH 7.2, 1% (w/v) Triton X-100, 5 % (w/v) glycerol, 10 mM MgCl<sub>2</sub>, 8 mg lysozyme, 1 mM PMSF, and trace amounts (approximately 0.1 mg each) RNase A and DNase I. The suspension was agitated and then incubated at ambient temperature for 1 hour. The lysed cells were centrifuged at 26,892 x g (15,000 rpm, SS34) for 20 min at 4°C. The crude extract (typically approximately 50 mL) was decanted and loaded onto an Accell Plus QMA Anion Exchange column (Quaternary Methylamine, 300 Å, Waters Corp., 5 x 30 cm) equilibrated with Buffer A (20 mM Hepes, pH 7.2, 1 mM DTT). The column was washed with 300 mL of the same buffer prior to running a gradient from Buffer A to Buffer B (20 mM Hepes, pH 7.2, 500 mM NaCl, 1 mM DTT) over 900 mL. PFL eluted at approximately 240 mM NaCl. Fractions containing > 75 % pure PFL (as judged by SDS-PAGE on a 5% - 20% Tris-HCl gel) were combined, flash frozen and stored at - 80 °C. Another 50 mL of crude extract was run through the same procedure, and the > 75% pure fractions from both runs were combined, dialyzed against Buffer C (40 mM Hepes, pH 7.2, 1 M ammonium sulfate, 1 mM DTT), and centrifuged to remove precipitated protein. The supernatant was loaded onto a Phenyl-Sepharose column (Pharmacia

16/10) equilibrated with Buffer C. The column was washed with 50 mL of Buffer C prior to running a gradient from Buffer C to Buffer A over 50 mL, followed by a wash with 50 mL of Buffer A. PFL was eluted through the last half of the gradient. Fractions containing ≥ 95% pure PFL (as judged by SDS-PAGE) were combined, dialyzed against Buffer A, concentrated, flash-frozen and stored at − 80 °C.

## II.2.4 Growth and Expression of PFL-AE

A single colony of transformed BL21(DE3)pLysS/pCALnAE3 was used to inoculate 50 mL LB/Amp. This culture was grown for 16 h to saturation at 37 °C and then used to inoculate 9 L of defined MOPS medium based on one previously described. 17 The media was modified to include (per 9 L) 75.6 a MOPS, 99 g casamino acid, 7.2 g tricine, 26.3 g NaCl, 14.4 g KOH, 4.6 g NH, Cl, 200 mL of 20 % glucose, 20 mL of "O" solution, 20 mL of 1 M KH<sub>2</sub>PO<sub>4</sub>, 10 mL of 276 mM K<sub>2</sub>SO<sub>4</sub>, and 50 mL of 0.1 M CaCl<sub>2</sub> The "O" solution consists of 0.1 g FeCl<sub>2</sub>·4H<sub>2</sub>O in 10 mL concentrated HCl, 1 mL of "T" solution which includes 8 mL concentrated HCl, 18.4 mg of CaCl<sub>2</sub>·2H<sub>2</sub>O, 64 mg H<sub>3</sub>BO<sub>3</sub>, 40 mg MnCl<sub>2</sub>·4H<sub>2</sub>O, 18 mg CoCl<sub>2</sub>·6H<sub>2</sub>O, 4 mg CuCl<sub>2</sub>·2H<sub>2</sub>O, 340 mg ZnCl<sub>2</sub>, 605 mg Na<sub>2</sub>MoO<sub>4</sub>·2H<sub>2</sub>O, and 2.68 g MgCl<sub>2</sub>·6H<sub>2</sub>O. Ampicillin (9 mL of 50 mg/mL) and 10 mg each of riboflavin, thioctic acid, vitamin B12, niacinamide, pantothenic acid, piridoxine, biotin and folic acid were added to the 9 L culture right before the inoculation. The 9 L culture was grown at 37 °C in a bench-top fermentor (New Brunswick) with a continuous air purge and vigorous agitation to early log phase (OD<sub>600</sub> ~0.5), and then induced by addition of IPTG to 1 mM. At this time the medium was

supplemented with 750 mg Fe( $NH_4$ )<sub>2</sub>( $SO_4$ )<sub>2</sub>. The culture was allowed to grow for an additional 2 h, purging with air before cooling down and purging with nitrogen for 20 min. The medium was then supplemented with another 750 mg Fe( $NH_4$ )<sub>2</sub>( $SO_4$ )<sub>2</sub>. When the temperature was reduced to 20°C, the culture was incubated for 14-17 hours at 4°C under argon. The cells were harvested by centrifugation at 10,816 x g (8,000 rpm, GS3) under anaerobic conditions. The harvested cells were stored under nitrogen at -80°C until used for purification.

#### II.2.5 Purification of PFL-AE

PFL-AE was purified from E.coli BL21(DE3)pLysS transformed with pCAL-n-AE3, prepared as described above. All steps in the purification were performed in a single day under strictly anaerobic conditions in a Coy anaerobic chamber (Coy Laboratories, Grass Lake, MI) at ambient temperature except where noted. Solutions and buffers used in the purification were thoroughly degassed or purged with nitrogen prior to bringing them into the Coy chamber. Cell paste was suspended in enzymatic lysis buffer (2 mL per gram of cells) containing 50 mM Tris-sulfate, pH 7.5, 200 mM NaCl, 1% Triton X-100, 5% glycerol, 10 mM MgCl<sub>2</sub>, 1 mM DTT, 8 mg lysozyme, 1 mM PMSF and trace amounts (approximately 0.1 mg each) of RNase A and DNase I. The suspension was agitated with a 10 mL syringe and then incubated at ambient temperature for 1h. The suspension was centrifuged at 38,724 x g (18,000 rpm, SS34) for 30 min at 4°C. The extract was decanted and used directly in purification. Up to 30 mL of the crude extract was loaded onto a Superdex 75 column (5 x 60 cm) equilibrated with 50 mM Tris-

buffer at 5 mL/min. PFL-AE eluted from the column in a relatively sharp peak at approximately 680 mL after injection. The fractions that had fairly dark red/brown color were pooled and concentrated down to less than 10 mL using an Amicon concentrator with YM10 filter membranes. Another aliquot of crude extract was run through the same procedure. Fractions pooled from both runs were combined, concentrated to less than 20 mL, and re-run on the same column as above. The final fractions were checked by the ratio of UV absorbance at 426 nm and 280 nm. Fractions that have the highest ratio (greater than 0.15, but fractions with a blue-shifted 280 nm peak, indicating nucleic acid contaminants, were

avoided) were pooled, concentrated, flash-frozen, and stored at – 80°C.

sulfate, pH 7.5, 200 mM NaCl, 1 mM DTT. The protein was eluted with this same

## II.2.6 Protein Assays

Routine determinations of protein concentrations were done by the method of Bradford, <sup>18</sup> using a kit purchased from Bio-Rad, and bovine serum albumin as a standard. Calibration of the results from the Bradford assays of PFL-AE was obtained by amino acid hydrolysis of the purified enzymes, performed at the MCB Core Facility, University of Massachusetts, Amherst. Actual protein concentrations could then be determined by applying a correction factor of 0.65 to the Bradford assays.

#### II.2.7 Iron Assays

Iron assays were carried out using the method of Beinert. 19 A standard solution of Fe was obtained by diluting a sample of an Fe standard used for atomic absorption spectroscopy (1015 ug/mL) to 10.15 ug/mL in 0.1 M H<sub>2</sub>SO<sub>4</sub>. In 15 mL Falcon tubes (USA scientific), aliquots of the Fe standard was added from  $0 \mu L$  to 200  $\mu L$  in 40  $\mu L$  increments. The volume was made up to 1000  $\mu L$  with MQ water. In the same manner, aliquots of a 10-fold diluted protein sample of the purified and concentrated PFL-AE lysate were prepared using 25, 50, 100, 150, and 200  $\mu$ L volume amounts and the volume was made up to 1000  $\mu$ L by the addition of MQ water. Reagent A (45% w/v KMnO<sub>4</sub>/1.2 N HCl; 1:1) was added (0.5 mL) to both the standard and the protein samples. The Falcon tubes were capped tight and incubated in a water bath for 2 h at 65°C. After the incubation period, 100 µL of Reagent B (8.8 g Ascorbic Acid, 9.7 g (NH<sub>4</sub>)OAc, 80 mg ferrozine, and 80 mg neucuproine, dissolved in MQ water to a final volume of 25 mL) was added to each tube and allowed to stand at room temperature for 30 minutes before reading the absorbance at 562 nm. The Fe number is obtained by extrapolating the data obtained for the protein samples based on the standard curve generated using the Fe standard samples.

#### II.2.8 Sulfide Assays

Sulfide assays were carried out with a modification of the method of Beinert. 19,20 The use of siliconized Eppendorf tubes was found to yield more reproducible results, perhaps due to the minimized head space for loss of sulfide

as H<sub>2</sub>S. The tubes were kept tightly capped except when adding reagents. Rather than using stir bars, the tubes were closed and vortexed when mixing was called for. The procedure used was as follows. The sample volumes were brought to 100 μL with MQ H<sub>2</sub>O, pH 8.1. One at a time, each tube was opened, 300 μL 1% ZnOAc and 15 μL 12% NaOH were added simultaneously, the tube was closed tightly and vortexed. When all tubes had been treated in this way, they were allowed to sit for 12 to 15 h before addition (again, one tube processed at a time) of 75 μL DMPD (0.1% in 5 M HCl) and 2 μL FeCl<sub>3</sub> (23 mM in 1.2 M HCl). Na<sub>2</sub>S·9H<sub>2</sub>O was used as standard and prepared as follows: a small-to-medium chunk of Na<sub>2</sub>S·9H<sub>2</sub>O was rinsed with MQ H<sub>2</sub>O, pH 8.1, dried by gently patting with Kim-wipe, weighed to 4 decimal places, and dissolved in 100 mL deoxygenated 0.1 M NaOH solution to make a standard solution of concentration between 1.2 to 2.7 mM. The standard solution was sealed with septum, purged thoroughly with nitrogen, and was good for at least a month.

## II.2.9 EPR Spectroscopy

EPR first-derivative spectra were obtained at X-band on a Bruker
ESP300E spectrometer equipped with a liquid He cryostat and a temperature
controller from Oxford Instruments. Spectra were recorded at 12 K for [3Fe-4S]<sup>+</sup>
and [4Fe-4S]<sup>+</sup>, and at 60 K, to detect the glycyl radical. Spin quantifications were
done as described previously.<sup>21</sup> The double integrals of the EPR signals were
evaluated by using a computer on-line with the spectrometer. Spin
concentrations in the protein samples were determined by calibrating double

integrals of the EPR spectra recorded under nonsaturating conditions (i) with a standard sample of 0.1 mM Cu(II) and 1 mM EDTA solution for the cluster signals, or (ii) with a 1.04 mM  $K_2(SO_3)_2NO$  solution for the glycyl radical signals. The concentration of the  $K_2(SO_3)_2NO$  standard was determined using the optical extinction coefficient. <sup>22</sup>

#### II.3 Results and Discussion

#### II.3.1 Expression and Purification of PFL

PFL was purified from BL21(DE3)pLysS cells harboring the pKK-PFL plasmid. The cells were lysed by an enzymatic procedure and two portions of partially purified PFL from the first ion-exchange column (see Fig. II.4 for chromatogram; see Figure II.6 for SDS-PAGE gel) were combined, dialyzed, and run on an hydrophobic column to yield  $\geq$  95% pure PFL (see Fig. II.5 for chromatogram; see Figure II.7 for SDS-PAGE gel). Yield was approximately 50 mg of purified PFL per liter of bacterial culture.

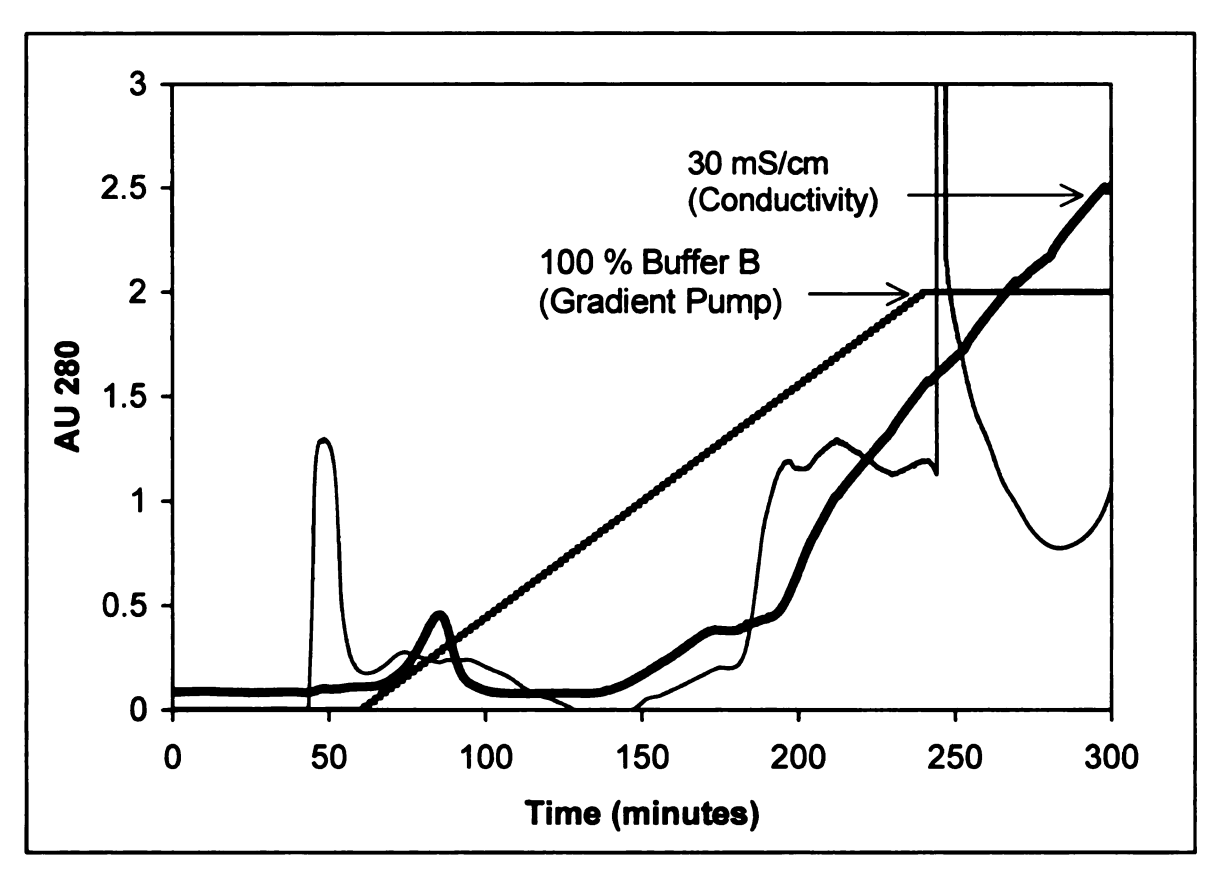


**Figure II.4** Chromatogram of purification of PFL. Elution profile for the Accell Plus QMA Anion Exchange column (Quaternary Methylamine, 300 Å, Waters Corp., 5 x 30 cm), gradient from Buffer A (20 mM Hepes, pH 7.2, 1 mM DTT) to Buffer B (20 mM Hepes, pH 7.2, 500 mM NaCl, 1 mM DTT) over 900 mL, flow rate 5 mL/min. PFL eluted at approximately 240 mM NaCl, and was dialyzed against Buffer C (40 mM Hepes, pH 7.2, 1 M ammonium sulfate, 1mM DTT).

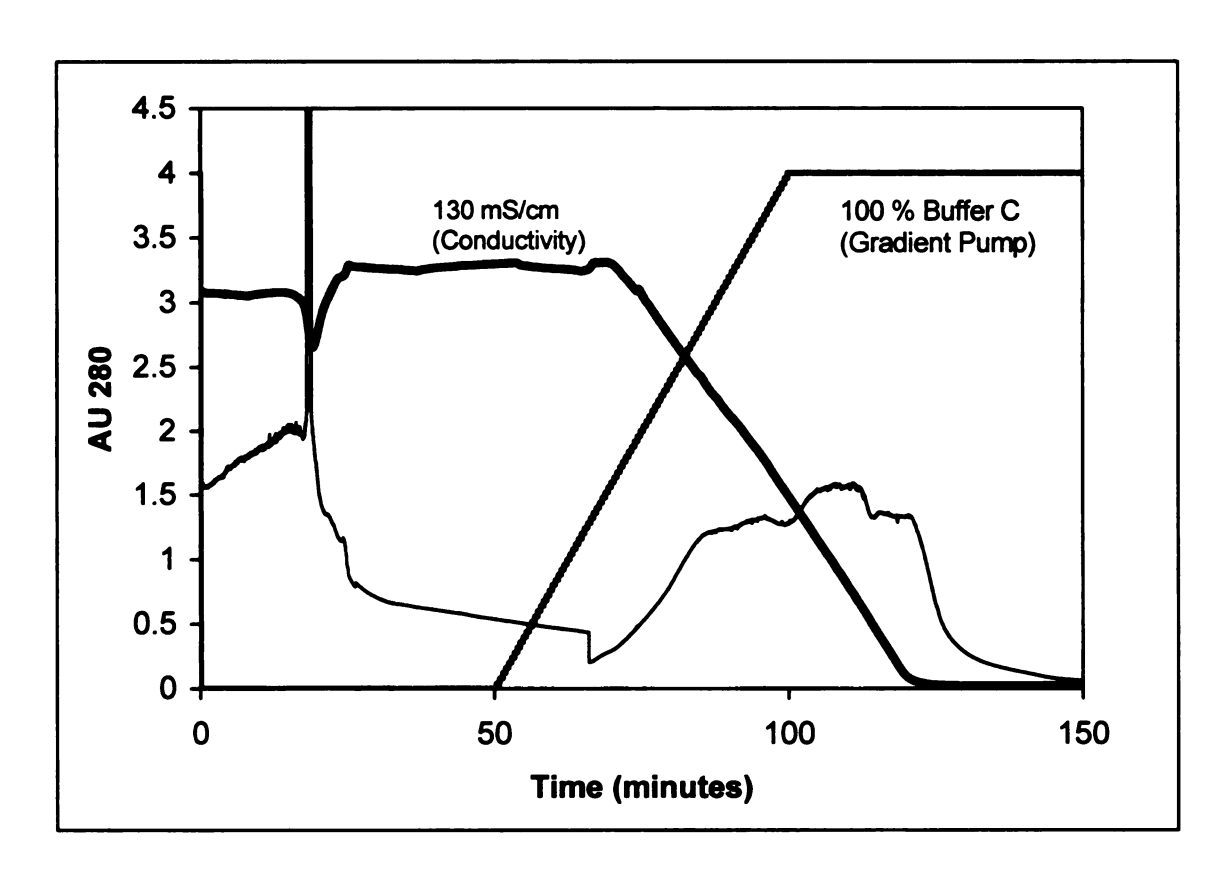


**Figure II.5** Chromatogram of purification of PFL. Elution profile for the Phenyl-Sepharose column (Pharmacia 16/10), gradient from Buffer C to Buffer A over 50 mL, followed by a wash with 50 mL of Buffer A, flow rate 1 mL/min. PFL was eluted through last half of the gradient.

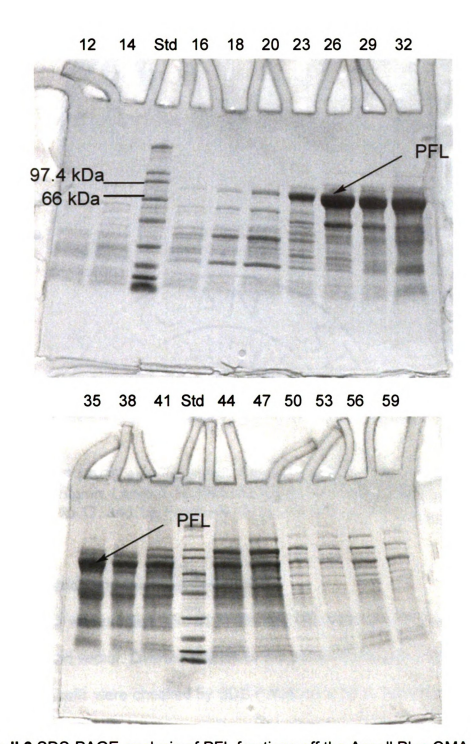


Figure II.6 SDS-PAGE analysis of PFL fractions off the Accell Plus QMA anion-exchange column. Upper panel: Lanes 1-10 from left, 12,14, molecular marker (kDa), 16, 18, 20, 23, 26, 29, 32; Lower panel: Lanes 1-10 from left, 35, 38, 41, molecular marker (kDa), 44, 47, 50, 53, 56, 59. Fractions 23-41 were pooled.

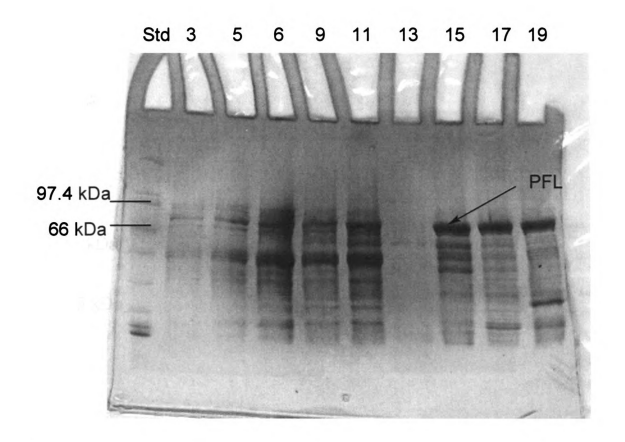


Figure II.7 SDS-PAGE analysis of PFL fractions off the Phenyl-Sepharose hydrophobic column. Lanes 1-10 from left, molecular marker (kDa), fractions 3,5.6,9.11,13,15.17, and 19. Fractions 15, 17, 19, 21(not shown) were pooled.

#### II.3.2 Expression and Purification of PFL-AE

PFL-AE was purified from BL21(DE3)pLysS cells harboring the pCAL-n-AE3 expression vector. Overexpression of the protein in the pre-induced and post-induced cells were checked by SDS-PAGE on a 12 % Tris-HCl gel (Figure II.8). The cells were lysed by an enzymatic procedure, and PFL-AE was purified from this crude extract by two passages through a preparative gel filtration column (Figure II.9). The enzyme eluted as a reddish brown peak, and pure fractions from the final run of the column were identified by the highest ratio

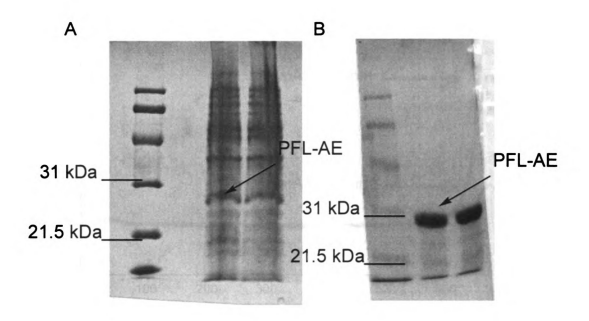
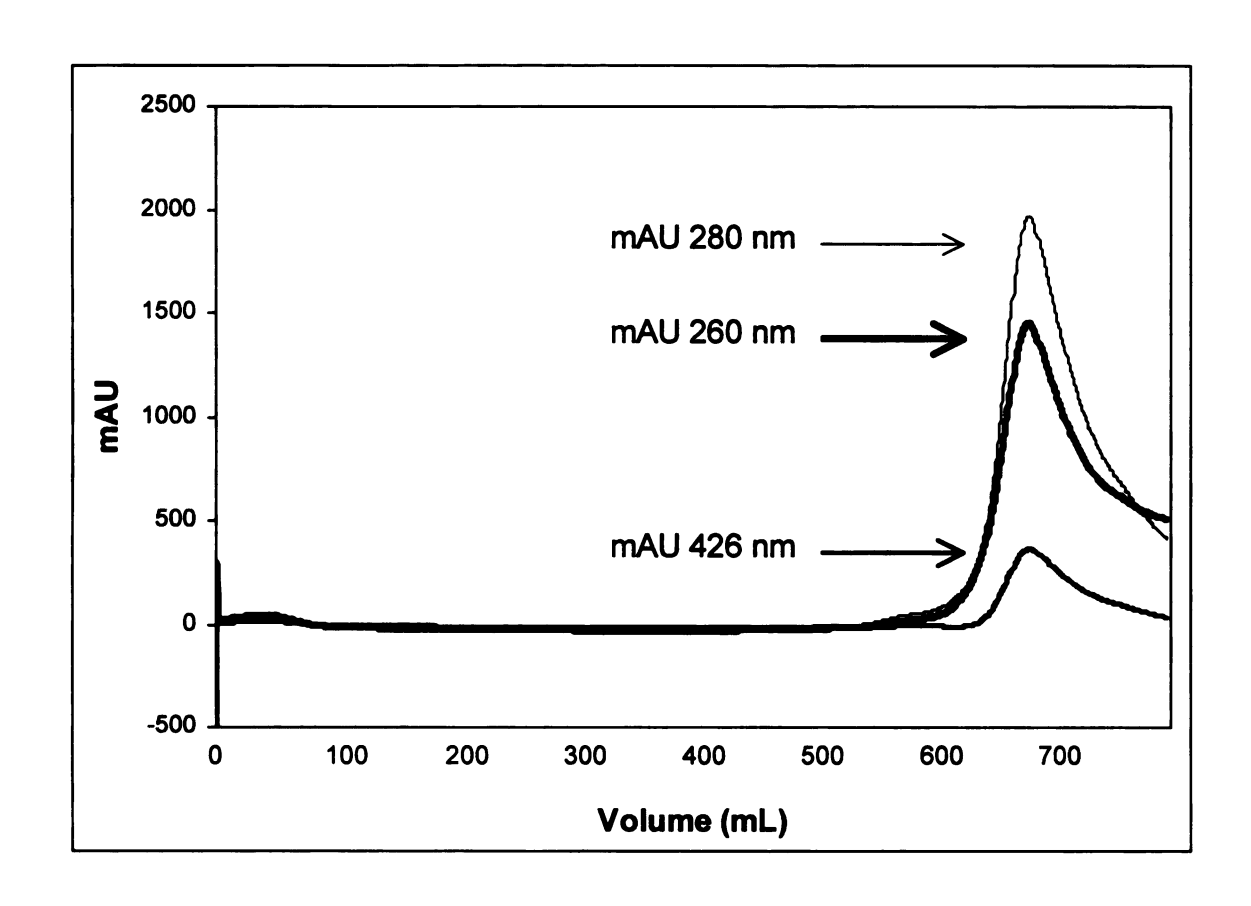


Figure II.8 SDS-PAGE analysis of overexpression of PFL-AE in *E. coli* cells. A: Lane 1, molecular marker (k(Da); lanes 2 and 3, pre-induced cells; B: Lane 1, molecular marker (k(Da); lanes 2 and 3, post-induced cells.

of absorbance at 426 nm and 280 nm. Both [3Fe-4S]<sup>+</sup> and [4Fe-4S]<sup>2+</sup>, the major cluster forms found in purified PFL-AE, have significant absorbance at 426 nm. All proteins have maximal absorbance at 280 nm. The high iron content in the enzyme, thus, is indicated by the high ratio of the absorbance values (Table II.1). Fraction purity was confirmed by SDS-PAGE (Figure II.10), and the purest fractions were combined, concentrated, and stored under nitrogen in small aliquots at -80 °C. Yield was typically 40-50 mg of purified PFL-AE per liter of bacterial culture.



**Figure II.9** Purification of PFL-AE by gel-filtration chromatography (Superdex 75 column, 5 x 60 cm). The protein was eluted with 50 mM Tris-sulfate, pH 7.5, 200 mM NaCl, 1 mM DTT at 3 mL/min. PFL-AE eluted from the column in a relatively sharp peak at approximately 680 mL after injection.

Fraction	Ratio: 426nm/280 nm	Abs 426 nm	Abs 280 nm
17	0.085	0.022	0.255
18	0.128	0.046	0.359
19	0.154	0.067	0.435
21	0.184	0.069	0.378
23	0.213	0.046	0.216
25	0.153	0.019	0.125
27	0.101	0.009	0.091
28	0.095	0.008	0.080

**Table II.1** Ratio of absorbances at 426 nm and 280 nm of PFL-AE fractions off the 2nd run of the gel filtration column.

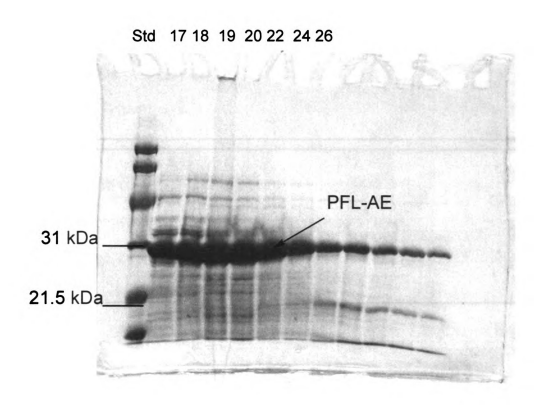


**Figure II.10** SDS-PAGE analysis of PFL-AE fractions off the 2nd run of the gel filtration column. Lane 1, molecular marker (kDa); lane 2-8, fractions 17, 18, 19, 20, 22, 24, 26. Fractions 19-25 were pooled.

#### II.3.3 Characterization of Purified PFL-AE

PFL-AE purified under anaerobic reducing conditions in the presence of 1mM DTT was essentially EPR-silent, presumably in the [4Fe-4S]<sup>2+</sup> state, containing approximately 7.4 % [3Fe-4S]<sup>+</sup> as indicated by EPR spectroscopy (Figure II.11). The protein was found to contain 3.7 mol Fe/mol protein.

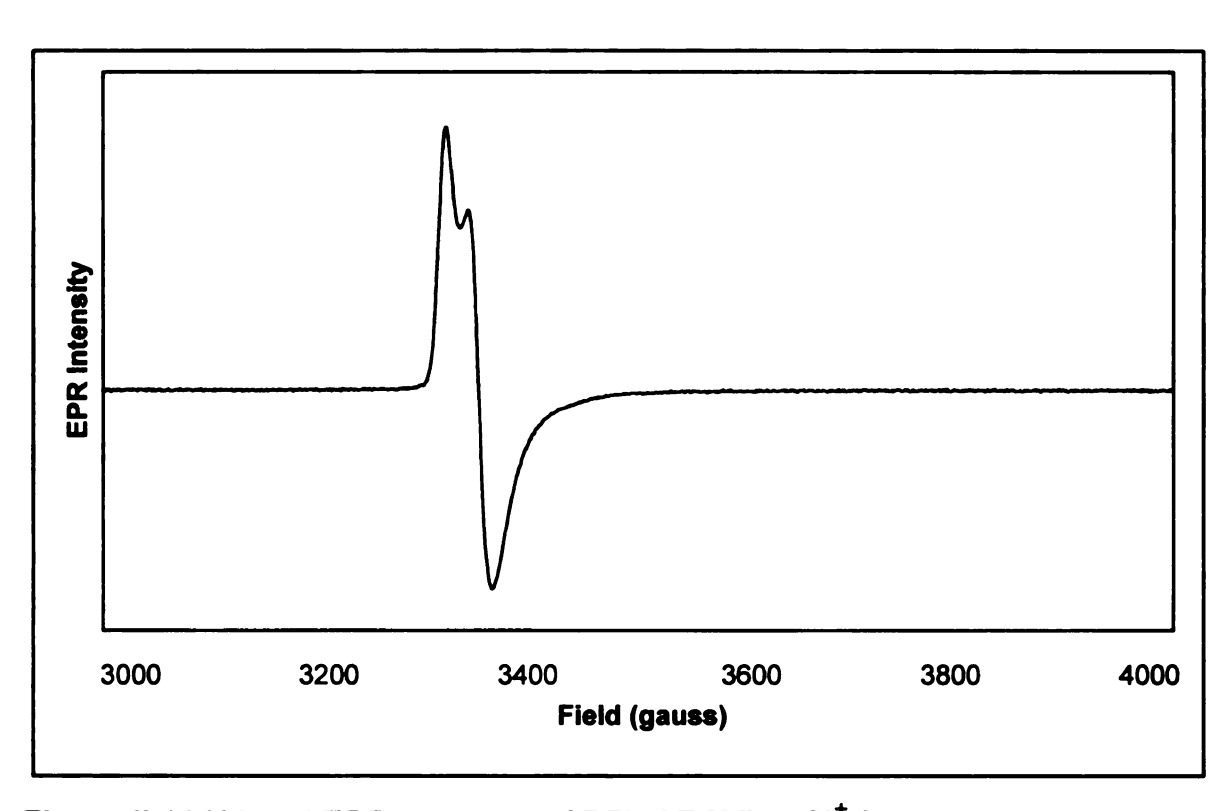


**Figure II.11** X-band EPR spectrum of PFL-AE [3Fe-4S]<sup>+</sup> from as-isolated protein; 7.41 % (based on 97.9  $\mu$ M spin for 1321  $\mu$ M protein with 3.70 mol Fe/ mol PFL-AE); g = 2.17, Conditions of measurement: T = 12 K; microwave power, 20  $\mu$ W; microwave frequency = 9.49 GHz; modulation amplitude, 10.084 G; single scan.

#### II.4 Conclusion

The optimization of the growth and purification conditions for PFL-AE has been a long and evolving process in our laboratory. Inducing at an earlier log phase (OD<sub>600</sub> ~ 0.5 vs. ~0.8) and supplementing iron to the medium after making the culture anaerobic contributed to better overexpression and iron inclusion of PFL-AE. The component of the holoenzyme in the isolated native enzyme that contains full complement of iron was also improved in the purification procedure. The enzyme was purified by passing through the gel filtration column twice under strictly anaerobic conditions in the presence of 1 mM DTT, and pooling fractions based not only on SDS-PAGE analysis but also on the UV absorbance ratio at 426 nm and 280 nm. In summary, under current growth and purification conditions, approximately 400 mg of purified PFL-AE was obtained from a 9 L bacteria culture; this represents a 2-3-fold improvement over earlier procedures. The PFL-AE contains 2.5 – 3.8 mol Fe/ mol protein and a stoichiometric amount of acid-labile sulfide. The F-S clusters in the isolated protein are essentially EPRsilent, presumably in the [4Fe-4S]<sup>2+</sup> form, with about 7.4 % of [3Fe-4S]<sup>+</sup> cluster and containing 3.7 mol Fe/ mol protein.

#### II.5 References

- (1) Knappe, J. S., J.; Möckel, W.; Höpner, Th.; Vetter, H., Jr.; Edenharder, R. *Eur. J. Biochem.* **1969**, *11*, 316.
- (2) Knappe, J. Adv. Protein Chem. 2001, 58, 277.
- (3) Knappe, J. N., F.A.; Blaschkowski, H.P.; Ganzler, M. *Proc. Natl. Acad. Sci. U.S.A.* **1984**, *81*, 1332.
- (4) Volker Wagner, A. F. F., M.; Neugebauer, F.A.; Schäfer, W.; Knappe, J. *Proc. Natl. Acad. Sci. U.S.A.* **1992**, *89*, 996.
- (5) Knappe, J. E., S.; frey, M.; Volkner Wagner, A.F. *Biochem. Soc. Trans.* **1993**, *21*, 731.
- (6) Frey, P. A. Annu. Rev. Biochem. 2001, 70, 121.
- (7) Conradt, H. H.-B., M.; Hohmann, H.P.; Blaschkowski, H.P.; Knappe, J. *Arch. Biochem. Biophys.* **1984**, *228*, 133.
- (8) Wong, K. K. M., B.W.; Lewisch, S.A.; Baxter, M.K.; Ridky, T.W.; Ulissi-DeMario, L.; Kozarich, J.W. *Biochemistry* **1993**, *32*, 14102.
- (9) Broderick, J. B. H., T. F.; Cheek, J.; Wojtuszewski, K.; Smith, S. R.; Trojan, M. R.; McGhan, R. M.; Kopf, A.; Kibbey, M.; Broderick, W. E. *Biochem. Biophys. Res. Commun.* **2000**, *269*, 451.
- (10) Broderick, J. B. D., R. E.; Fernandez, D. C.; Wojtuszewski, K.; Henshaw, T. F.; Johnson, M. K. *J. Am. Chem. Soc.* **1997**, *119*, 7396.
- (11) Krebs, C. H., T. F.; Cheek, J.; Huynh, B. H.; Broderick, J. B. *J. Am. Chem. Soc.* **2000**, *122*, 12497.
- (12) Henshaw, T. F. C., J.; Broderick, J. B. *J. Am. Chem. Soc.* **2000**, *122*, 8331.
- (13) Külzer, R. P., T.; Kappl, R.; Hüttermann, J.; Knappe, J. *J. Biol. Chem.* **1998**, **273**, 4897.
- (14) Emptage, M. H. K., T. A.; Kennedy, M. C.; Beinert, H.; Münck, E. *Proc. Natl. Acad. Sci. U.S.A.* **1983**, *80*, 4674.
- (15) Werst, M. M. K., M. C.; Houseman, A. L. P.; Beinert, H.; Hoffman, B. M. *Biochemistry* **1990**, *29*, 10526.

- (16) Werst, M. M. K., M. C.; Houseman, A. L. P.; Beinert, H.; Hoffman, B. M. *Biochemistry* **1990**, *29*, 10533.
- (17) Garboczi, D. N. H., J. H.; Pedersen, P. L. *J. Biol. Chem.* **1988**, *263*, 15694.
- (18) Bradford, M. Anal. Biochem. 1976, 72, 248.
- (19) Beinert, H. Meth. Enzym. 1978, 54, 435.
- (20) Beinert, H. Anal. Chem. 1983, 131, 373.
- (21) Aasa, R. V., T. J. Magn. Reson. 1975, 19, 308.
- (22) Murib, J. H. R., D. M. J. Am. Chem. Soc. 1952, 74, 339.

#### **CHAPTER III**

# SYNTHESES AND CHARACTERIZATION OF ISOTOPICALLY LABELED S-ADENOSYL-L-METHIONINES

#### III.1 Introduction

S-adenosyl-L-methionine (SAM/AdoMet) has long been regarded as a source of methyl groups for DNA methylation, biosyntheses of hormones and neurotransmitters, and regulation of signal transduction. The methylating property of SAM has been regarded as the principal reason for its existence in nature. However, a new role for SAM has been recognized in recent years. The discovery of the radical SAM superfamily of enzymes, which function by mechanisms involving free radicals as reaction inter-mediates, shows SAM serving as a free radical initiator. SAM undergoes transient cleavage to the 5'-deoxyadenosyl radical, which in turn propagates radical formation by abstracting hydrogen atoms, either from substrate molecules to form radical inter-mediates, or from glycyl residues of enzymes to activate them for radical-based biochemistry.

SAM cannot be cleaved directly into methionine and 5'-deoxyadenosyl free radical because the S-adenosyl bond is too strong (~60 kcal mol<sup>-1</sup> BDE) to be broken homolytically and spontaneously in an enzymatic site. The reaction for this process also requires the addition of an electron as shown in Figure III.1.

The source of the electron required for this process is a reduced form of an iron-sulfur cluster. The reversibility of the production of the 5'-deoxyadenosyl radical was formerly regarded as a unique property of adenosylcobalamin. However, evidence has shown that SAM could also serve as a source of this radical. <sup>3,4</sup>

Figure III.1 Reversible production of 5'-deoxyadenosyl radical from SAM.

The activation of PFL by its activating enzyme, PFL-AE, requires SAM as a co-substrate, cleaving it to methionine and 5'-deoxyadenosine (Figure III.2).<sup>4</sup> Knappe and co-workers have shown that the hydrogen atom abstracted from Gly734 of PFL is incorporated into the 5'-deoxyadenosyl product, indicating that the role of AdoMet is to produce an adenosyl radical intermediate as the immediate hydrogen atom abstractor.<sup>5</sup> Henshaw and co-workers have demonstrated that the [4Fe-4S]<sup>+</sup> is the catalytically active cluster of PFL-AE

and that it donates the electron required for reductive cleavage of SAM.<sup>6</sup> The presence of SAM has also been shown to dramatically affect the EPR signal of the [4Fe-4S]<sup>+</sup> cluster of PFL-AE, suggesting the possibility of a direct interaction between AdoMet and Fe-S cluster of PFL-AE. The mechanistic question of how the Fe-S cluster of PFL-AE interacts with SAM to generate the putative adenosyl radical, however, still remains unclear.<sup>6,7</sup>

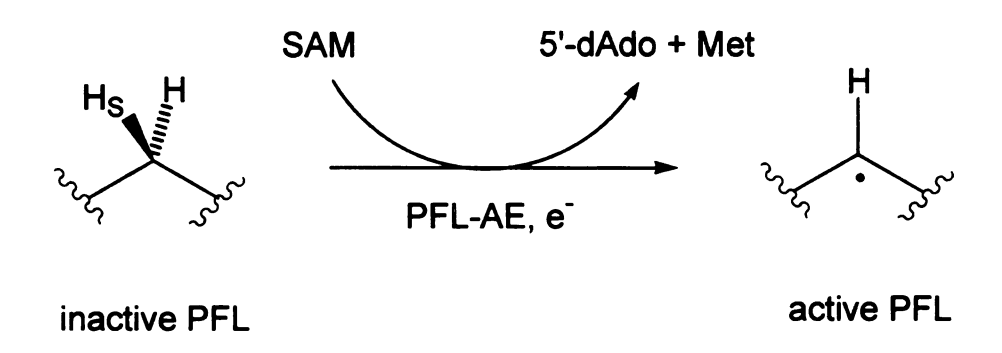


Figure III.2 Reductive cleavage of AdoMet by PFL-AE in PFL activation.

As the S-C bond is reductively cleaved during the radical generation, the sulfonium center of AdoMet is likely to be positioned close to the Fe-S cluster (Figure III.3). Using isotopically labeled AdoMets in which atoms in the sulfonium center are substituted with nuclei that have non-zero nuclear spins, the proximity of AdoMet to the cluster can be investigated. In order to probe hyperfine interactions between SAM and the cluster, the methyl group of SAM was labeled with <sup>2</sup>H and <sup>13</sup>C.

Additional labeling of the carboxy and amino groups at the methionine end of SAM were also pursued in order to investigate if the unique iron site interacts with SAM prior to the reductive cleavage of the S-C bond. The basis for this idea stems from earlier investigations with the enzyme aconitase. Aconitase catalyzes

**Figure III.3** Proposed proximity of SAM and the Fe-S cluster of PFL-AE during radical generation.

the interconversion of citrate to iso-citrate via the intermediate, cis-aconitate. The binding of the substrate on the [4Fe-4S]<sup>+</sup> cluster of active beef heart aconitase was characterized by electron-nuclear double resonance (ENDOR) measurements in the presence of substrates.<sup>8,9</sup> These studies confirmed that substrate binds to the reduced enzyme by coordination of a hydroxyl and carboxylate to the unique site iron.

The synthesis of the isotopically labeled SAM was carried out enzymatically as SAM contains a chiral sulfonium center and thus exists in two diastereo-isomeric forms, (-)- and (+)-AdoMet. (-)-AdoMet is the only methyl donor *in vivo* and can be obtained only through enzymatic synthesis. <sup>10,11</sup>

Chemical coupling reactions between adenosyl homocysteine and methyl group donating agents can also produce SAM, however, the diastereoselectivity is poor. <sup>10</sup> S-Adenosylmethionine synthetase (ATP:L-methionine S-adenosyltransferase EC2.5.1.6; AdoMet synthetase) catalyzes the formation of (-)-SAM as shown in Figure III.4. Purified from *E.coli*, it has a molecular weight of 180 kDa,

$$Mg^{2+}$$
,  $K^{+}$   $O_2C$   $O_2C$   $O_3$   $O_4$   $O_4$   $O_5$   $O_5$   $O_6$   $O_6$   $O_7$   $O_8$   $O$ 

Figure III.4 Enzymatic synthesis of S-adenosyl-L-methionine.

and the native enzyme is a tetramer of 4 identical subunits. Kinetic experiments have demonstrated that the enzymatic reaction proceeds sequentially in 4 steps:

(i) random addition of methionine and MgATP; (ii) formation of SAM and tripolyphosphate; (iii) oriented cleavage of tripolyphosphate to yield orthophosphate (Pi) and pyrophosphate (PPi); (iv) product release with

orthophosphate and pyrophosphate dissociation before SAM.<sup>12</sup> Two divalent metal ions, such as Mg<sup>2+</sup>, bind to the enzyme active site in the presence of ATP, and both are required for activity.<sup>13-15</sup> A single divalent cation, such as K<sup>+</sup>, binds in the presence of SAM, and stimulates the rate of SAM formation up to 100-fold.<sup>11</sup>

Initial preparative scale synthesis of SAM was infeasible due to product inhibition at substrate concentrations >1 mM, which may result from the formation of inactive SAM-bound-enzyme complexes.  $^{12,14,15}$  The inhibition problem was successfully overcome in incubations using 10 mM substrate in the presence of various additives, including p-toluenesulfonate (p-TsONa), and more efficiently, a high concentration of p-mercaptoethanol (p-ME), acetonitrile or urea.  $^{16}$  Pyrophosphate was also found to act as an inhibitor of SAM synthetase. Alhough it is a weaker inhibitor than SAM, it is still strong enough to show an inhibitory effect in reactions containing > 1 mM substrate. Therefore, a small amount of pyrophosphatase was added to the reaction mixture to hydrolyze pyrophosphate to orthophosphate, a weaker non-competitive inhibitor of SAM synthetase.  $^{12}$ 

#### III.2 Experimental Methods

#### III.2.1 Materials

SAM synthetase overproducing strain DM22 (pK8) was a generous gift from Dr. George D. Markham (Fox Chase Cancer Center). Methyl-D<sub>3</sub>- L-methionine, methyl- $^{13}$ C-L-methionine, and  $\alpha$ -hydrogen-D-L-methionine were

purchased from Isotech Inc. Amino-<sup>15</sup>N-L-methionine and carboxy-<sup>13</sup>C-L-methionine were purchased from CDN Isotopes. Carboxy-<sup>17</sup>O-L-methionine was synthesized from L-methionine·HCl salt in H<sub>2</sub><sup>17</sup>O. ATP, and inorganic pyrophosphatase were purchased from Sigma. These and all other chemicals were of the highest purity obtained from commercial sources.

#### III.2.2 Growth and Purification of SAM Synthetase

Expression of *E. coli* SAM synthetase

SAM synthetase overproducing strain DM22 (pK8) was stored in 50 % glycerol at -80 °C. A single colony of transformed cells was used to inoculate 50 mL LB media containing 30  $\mu$ g/mL oxytetracycline (LB/Tet). This culture was grown for 12 - 14 h to saturation and then used to inoculate 700 mL LB/Tet in each of 5 2800 mL Fernbach culture flasks. The culture was grown at 37 °C with vigorous shaking for 12 - 14 h before harvesting by centrifugation at 10,816 × g (8,000 rpm, GS3 rotor). The supernatant was decanted and the cells stored at -80 °C.

## Preparation of cell lysate for SAM synthesis

Cell paste was suspended in 100mM Tris-HCI, pH 8.0 containing 1 mM EDTA (3 – 3.5 mL/g cell). Lysozyme was added to 50  $\mu$ g/mL and the suspension was incubated at room temperature for 30 min. Phenylmethylsulfonyl fluoride (PMSF) was added to a final concentration of 0.1 mM. Cells were lysed by sonication (10 cycles of 1 min sonication with 1 min rest in between) in an ice

bath. The suspension was centrifuged at  $26,892 \times g$  (15,000 rpm, SS34) for 20 min. The supernatant was decanted and the cells stored at -80 °C until needed. Protein concentrations were determined by the method of Bradford, 17 using a kit purchased from Bio-Rad.

## Purification of SAM synthetase

Preparation of cell lysate: Cell paste was suspended in 100 mM Tris-HCl, pH 8.0 containing 10 % glycerol, 1 mM EDTA, 0.1 %  $\beta$ -ME (4 mL/g cell). PMSF was added to a final concentration of 0.1 mM, followed by lysozyme (50  $\mu$ g/mL) and trace amount of DNase and RNase (about 0.1 mg each). The lysate was incubated in ice for 1-1.5 hours, and then centrifuged at 10,816 × g (8,000 rpm, GS3) for 20 min. The supernatant was decanted and used for the next step.

Ammonium sulfate fractionation: For each 100 mL of the supernatant solution, 22 g of ammonium sulfate were added. After stirring at 4 °C for 20 min the suspension was centrifuged. The supernatant was decanted and for each 100 mL of the supernatant, 12 g of ammonium sulfate were added. After stirring at 4 °C for 20 min the precipitated protein was collected by centrifugation.

Phenyl-Sepharose chromatography: The protein was dissolved in 10 mM Tris-HCl, pH 8.0, containing 10 % glycerol, 1 mM EDTA, 0.1 %  $\beta$ -ME, and 0.75 M ammonium sulfate. The protein solution was then loaded onto a Phenyl Sepharose column (Pharmacia 16/10), which had been equilibrated with the above buffer. The column was washed with 2 volumes of the above buffer prior to running a linear gradient of 0.75 M to 0 M ammonium sulfate in 200 mL 10 mM

Tris-HCI, pH 8.0 containing 10 % glycerol, 1 mM EDTA, 0.1 %  $\beta$ -ME. Fractions containing SAM synthetase, which were eluted at the middle of the gradient (as judged by SDS-PAGE on a 12 % Tris-HCl gel), were pooled and concentrated in an Amicon concentrator with YM30 filter membranes. The purified protein was flash-frozen and stored at -80 °C.

# III.2.3 Synthesis of Carboxy-<sup>17</sup>O-L-Methionine<sup>18,19</sup>

Concentrated HCI (0.833ml) was mixed with 1.492 g L-methionine and enough MQ water was added dropwise until the solid dissolved. The water was then removed under vacuum. L-Methionine·HCI (200.0 mg) and water ( $H_2O^{17}$ , 75% enriched, 100.0  $\mu$ L) were incubated in a sealed tube for 3 days. The excess water was removed using a microdistillation set-up under vacuum. FAB-MS, calculated mass for  $C_5HO^{17}ONS = 150.12$ , found m/z M( $H^+$ ) = 151.12.

## III.2.4 Synthesis and Purification of Isotopically Labeled SAM

SAM synthesis reactions (10 mL) were carried out at room temperature with moderate stirring in 100 mM Tris-HCl, pH 8.0 containing 50 mM KCl, 26 mM MgCl<sub>2</sub>, 13 mM ATP, 1 mM EDTA, 8 % β-ME, 10 mM isotopically labeled methionine, a small amount of inorganic pyrophosphatase (about 0.25 U) and 1 mL SAM synthetase lysate (approximately 13 mg of total protein). All reagents were added in the order as listed. The reaction was monitored by thin-layer chromatography (TLC) on silica plates developed in butanol /acetic acid /water (4:1:1). The reaction was terminated by addition of 1 mL of 1 M HCl and the

precipitated protein was removed by centrifugation at  $26,892 \times g$  (15,000 rpm, SS34) for 20 min at 4 °C. The supernatant was decanted and split in half. Half of the supernatant was loaded onto a SOURCE 15S cation exchange column (Pharmacia, 8 mL), which had been charged with 1 M HCl and equilibrated with MQ H<sub>2</sub>O. The column was run with a linear gradient of 0-1 M HCl, and AdoMet eluted from 38-56 % of the gradient as a distinct peak. The other half of the supernatant was run through the same procedure. Fractions containing products were pooled, lyophilized, and stored at -80 °C until needed.

Adenosyl-methyl-D<sub>3</sub>-methionine (CD<sub>3</sub>-AdoMet) was synthesized overnight as described above with 10 mM methyl-D<sub>3</sub>-L-methionine.

Adenosyl-methyl-<sup>13</sup>C-methionine (<sup>13</sup>CH<sub>3</sub>-AdoMet) was synthesized overnight as described above with 10 mM methyl-<sup>13</sup>C-L-methionine.

Adenosyl-carboxy-<sup>13</sup>C-methionine (<sup>13</sup>COO-AdoMet) was synthesized overnight as decribed above with 10 mM carboxy-<sup>13</sup>C-L-methionine.

Adenosyl-amino-<sup>15</sup>N-methionine (<sup>15</sup>NH<sub>2</sub>-AdoMet) was synthesized overnight as described above with 10 mM amino-<sup>15</sup>N-L-methionine.

Adenosyl-carboxy-<sup>17</sup>O-methionine (CO<sup>17</sup>O-AdoMet) was synthesized overnight as described above with 10 mM carboxy-<sup>17</sup>O-L-methionine.

Adenosyl- $\alpha$ -hydrogen -<sup>2</sup>H-methionine ( $\alpha$ -<sup>2</sup>H-AdoMet) was synthesized overnight as described above with 10 mM  $\alpha$ -hydrogen -D-L-methionine.

			,
· .			

#### III.2.5 NMR Spectroscopy

NMR spectra were recorded at room temperature on a Varian Inova-300 or a VXR-300 spectrometer.

#### III.2.6 Mass Spectrometry

Mass spectral data were obtained at the Michigan State University Mass Spectrometry Facility, which is supported, in part, by a grant (DRR-00480) from the Biotechnology Research Technology Program, National Center for Research, National Institutes of Health.

#### III.3 Results and Discussions

### III.3.1 Growth and Purification of SAM Synthetase

SAM synthetase was purified from DM22(pK8) overproducing strain.

Overexpression of the protein in the *E. coli* cells was checked by SDS-PAGE on a 12 % Tris-HCl gel (Figure III.5). Typical yields were 5-8.5 g of cells per liter of bacterial culture. The cell lysate for SAM synthesis was prepared by a conjunction of enzymatic and physical lysis procedures. The purity of the crude extract was checked as well by SDS-PAGE on a 12 % Tris-HCl gel (Figure III.5). The crude extract was concentrated to approximately 13 mg/mL for AdoMet synthesis.

! !

F

,

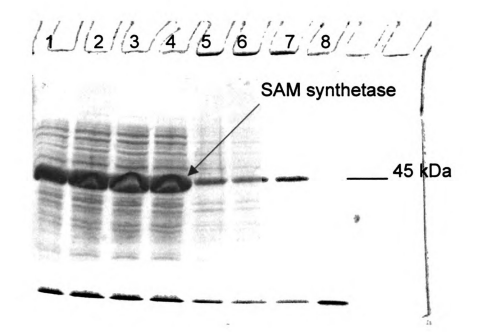


**Figure III.5** SDS-PAGE analysis of SAM synthetase. Overexpression of AdoMet synthetase in *E. coli* cells (no induction is required). Lane 8, molecular marker (kDa); Lanes 1-4, duplicate samples of whole cells; Lanes 5-7, crude extract.

AdoMet synthetase was further purified from the crude extract by ammonium sulfate fractionation and Phenyl-Sepharose chromatography.

Purified protein was > 99 % pure as judged by SDS-PAGE on a 12 % gel (Figure III.6). Yield was 16.7 mg of purified protein from 23 g cells.

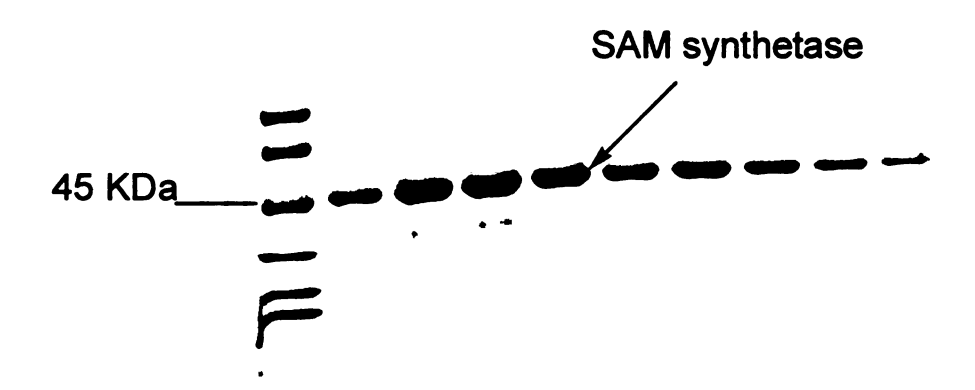


**Figure III.6** SDS-PAGE analysis of SAM synthetase fractions off the Phenyl-Sepharose column. Lane 1, molecular marker (kDa); Lanes 2-10, fractions 32-40. Fractions 33-38 were pooled.

## III.3.2 Syntheses and Purification of Isotopically Labeled SAM

Intitial SAM synthesis reactions were carried out with purified SAM synthetase, using natural abundance methionine and ATP as substrates, but pyrophosphatase was not added in the reaction mixture. The reaction was run for 5 h at ambient temperature according to the literature procedure, and the reaction progress was monitored by TLC on cellulose developed in butanol /acetic acid /water (25:4:10). 11.16 The Rf value of ATP is 0 under these condition, and due to its high polarity, SAM also has a very small Rf value, reportedly being 0.04 by descending TLC developed in butanol /acetic acid /water (5:4:1). 13 The reaction did not proceed to the formation of SAM as indicated by TLC. It was then found, in some cases, that the crude extract of SAM synthetase worked

better than the purified enzyme, as a low R<sub>f</sub> value spot was observed only on the TLC of the reaction system containing crude extract of SAM synthetase. Though the reason for the crude extract of SAM synthetase performing better than the purified enzyme is not clear, it was speculated that the pyrophosphate inhibition was partially overcome by the endogenous pyrophosphatase present in the cell lysate. Some other unknown component in the cell lysate might as well be beneficial to the performance of the enzyme. Therefore, crude extract of SAM synthetase was used for succeeding reactions. Not only does it save labor and time to purify the enzyme, which gives a rather low yield of purified enzyme, but it works very well in terms of yield and purity of the SAM synthesized. In addition to using crude extract, a small amount of inorganic pyrophosphatase was introduced into the reaction system to facilitate the hydrolysis of pyrophosphate to orthophosphate, which is a weaker non-competitive inhibitor of SAM synthetase.

The TLC for monitoring the reaction progress was improved by using butanol /acetic acid /water (4:4:1) as the mobile phase and silica plates as the stationary phase to get a better development of SAM and a clearer observation of the spots under ultraviolet light. The  $R_f$  value of the isotopic AdoMets was around 0.12-0.14. Unreacted ATP didn't develop on the plates ( $R_f$ = 0), and several faint spots were also observed from the reaction mixture, which were presumably contaminants and decomposed products. Longer reaction time (overnight instead of 5 h) was also found to help allow the reaction to go to completion. Isolation of SAM from the reaction mixture was achieved on a

Source S15 (Pharmacia) cation exchange column, after various other cation exchange columns, including Dowex-50W, Amberlite XE-64 and Mono S (HR 5/5, Pharmacia), had been earlier tried without success.

The SAM synthesis reaction is currently carried out as described in the Experimental Methods. All of the isolated AdoMets were lyophilized to yield crystalline colorless solids, presumably in the chloride salt form. The purified SAM was analyzed by  $^1$ H NMR to check its diastereoisomeric purity, as the methyl group resonances of (-)- and (+)- forms are well resolved ( $\Delta\delta \sim 0.4$  ppm). Mole ratios of approximately 94:6 for (-)- / (+)-SAM were obtained based on integrations of the two peaks in  $^1$ H NMR spectra. Since (-)-SAM is the only form enzymatically synthesized, the contamination of (+)-SAM in the purified product results from the method of isolation and the temperature at which the reaction was done, which could cause epimerization of the natural product. This was previously demonstrated by the observation of only (-)- isomer in the HPLC analysis of the enzymatic reaction mixture before isolation. $^{10}$  A virtually empirically pure (-)-AdoMet was obtained in small quantities via rapid enzymatic synthesis followed by HPLC purification.

CD<sub>3</sub>-AdoMet was synthesized overnight under similar conditions as described earlier and isolated by chromatography on a SOURCE 15S cation exchange column (Figure III.7). Yield was 38.5 mg (87.9 %) for a 10 mL of 10 mM reaction.  $^1$ H NMR (D<sub>2</sub>O):  $\delta$  8.32 (s, H2 & H8), 6.01 (d, J=3.91Hz, H1'), 4.38-4.73 (m, H3' & H2'), 3.76-3.98(m, H5', H5" & H4'), 3.52-3.62 (m, H $\alpha$ ), 3.32-3.42 (m, H $\gamma$  & H $\gamma$ '), 2.18-2.39 (m, H $\beta$  & H $\beta$ '), ppm. The  $^2$ H labeling was confirmed by

the absence of a methyl peak in the <sup>1</sup>H NMR, as well as the presence of a methyl peak in the <sup>2</sup>H NMR.

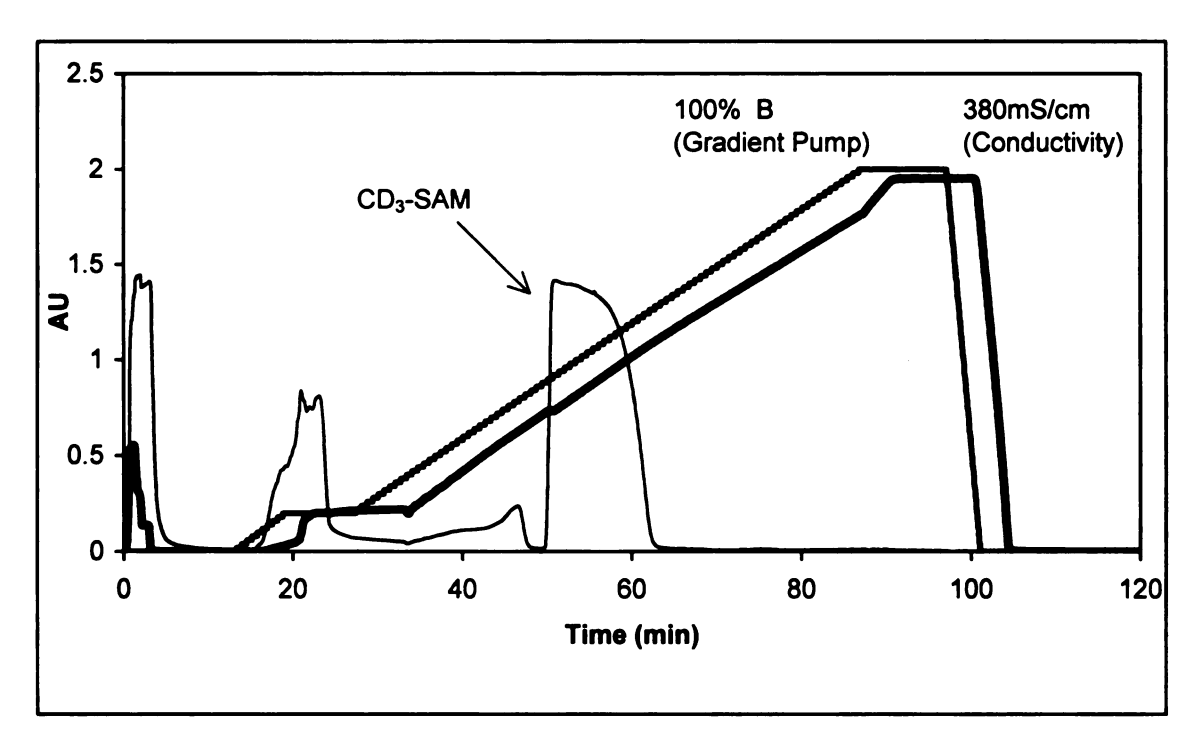


**Figure III.7** Chromatogram of isolation of CD<sub>3</sub>-AdoMet by SOURCE 15S cation exchange chromatography (Pharmacia, 8 mL), gradient from 0-1 M HCl, flow rate, 1 mL/min. CD<sub>3</sub>-SAM eluted as a distinct peak from 38 – 56 % Buffer B.

 $^{13}$ CH<sub>3</sub>-AdoMet was synthesized overnight under similar conditions as described earlier and isolated by chromatography on a SOURCE 15S cation exchange column (Figure III.8). Yield was 37.5 mg (86.0 %) for a 10 mL of 10 mM reaction.  $^1$ H NMR (300 MHz, D<sub>2</sub>O): δ 8.32 (s, H2 & H8), 6.01 (d, J=3.91, H1'), 4.38-4.71 (m, H3' & H2'), 3.77-4.01 (m, H5', H5" & H4'), 3.44-3.58 (m, Hα), 3.37-3.43 (m, Hγ & Hγ'), 2.59 & 3.08 (d, J=146.49, (+)- $^{13}$ CH3), 2.62 & 3.11 (d, J=146.49, (-)- $^{13}$ CH<sub>3</sub>), 2.20-2.35 (m, Hβ & Hβ') ppm. The  $^{13}$ C labeling was

confirmed by the distinct large splitting of the methyl peak in the <sup>1</sup>H NMR, as well as the presence of a <sup>13</sup>C peak in the <sup>13</sup>C NMR.

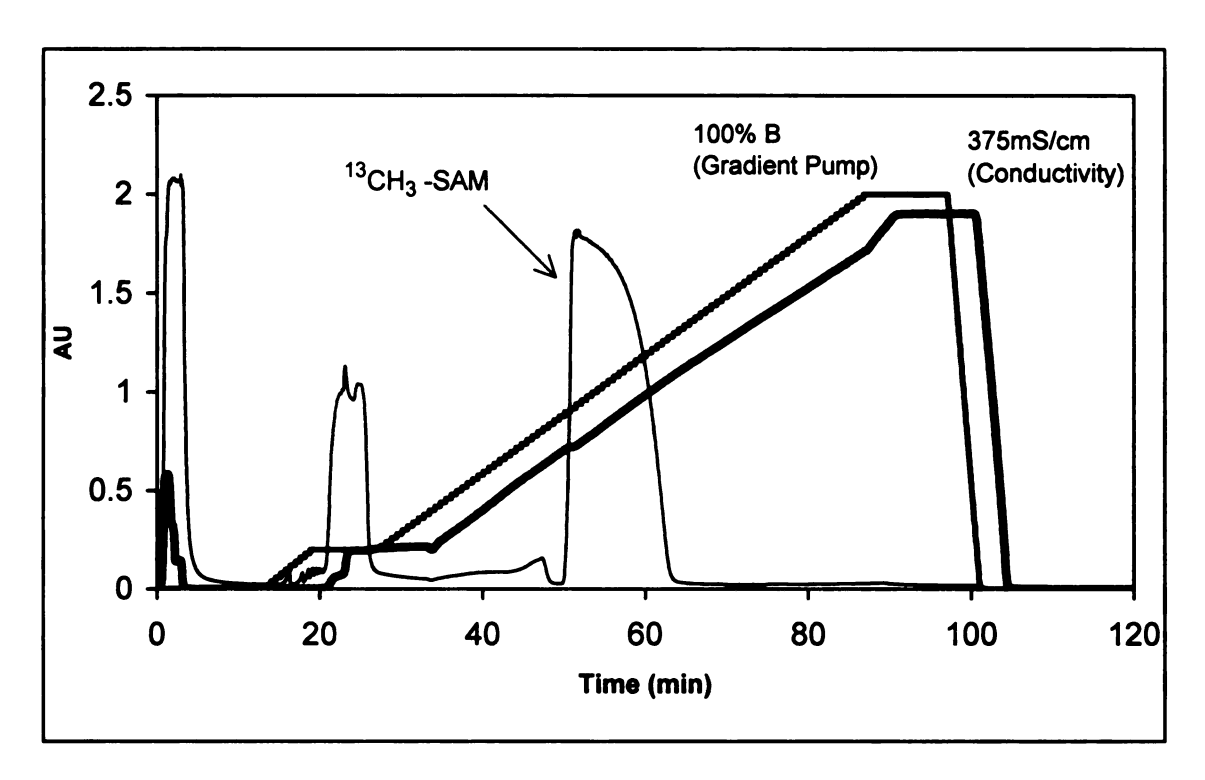


**Figure III.8** Chromatogram of isolation of <sup>13</sup>CH<sub>3</sub>-AdoMet by SOURCE 15S cation exchange chromatography (Pharmacia, 8 mL), gradient from 0-1 M HCl, flow rate, 1 mL/min. <sup>13</sup>CH<sub>3</sub>-SAM eluted as a distinct peak from 38 – 56 % Buffer B.

S-Adenosyl -<sup>15</sup>N-methionine was synthesized overnight under similar conditions as described earlier and isolated by chromatography on a SOURCE 15S cation exchange column (Figure III.9). Yield was 42.0 mg (95.9 %) for a 10 mL, 10 mM reaction. <sup>1</sup>H NMR (300 MHz, D<sub>2</sub>O):  $\delta$  8.30 (s, H2 & H8), 6.10 (d, H1'), 4.41 (m, H3' & H2'), 3.92 (t, H4'), 3.85, 3.78 (d, H5' & H5"), 3.55 (m, H $\alpha$ ), 3.39 (m, H $\gamma$  & H $\gamma$ '), 2.82 (s, CH<sub>3</sub>), 2.22 (m, H $\beta$  & H $\beta$ ') ppm.

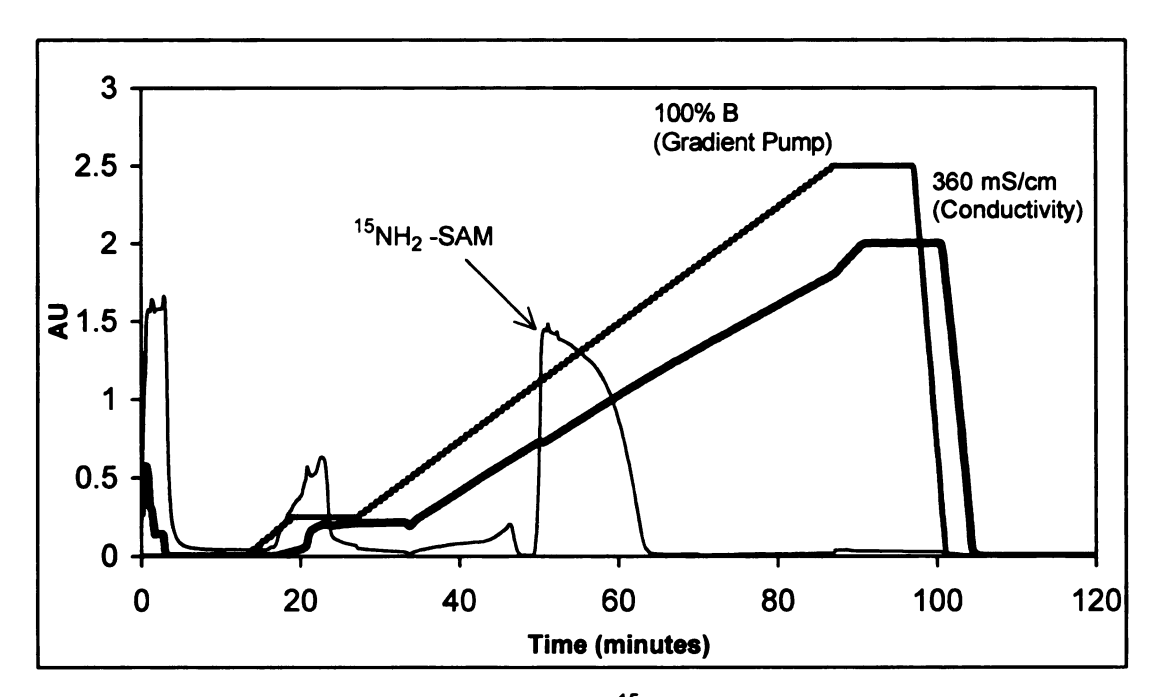


**Figure III.9** Chromatogram of isolation of <sup>15</sup>NH<sub>2</sub>-AdoMet by SOURCE 15S cation exchange chromatography (Pharmacia, 8 mL), gradient from 0-1 M HCl, flow rate, 1 mL/min. <sup>15</sup>NH<sub>2</sub>-SAM eluted as a distinct peak from 38 – 56 % Buffer B.

S-Adenosyl-carboxy-<sup>17</sup>O-methionine (CO<sup>17</sup>O-SAM) was synthesized overnight under similar conditions as for regular SAM, and isolated by chromatography on a SOURCE 15S cation exchange column (Figure III.10). Yield was 20.0 mg (45.7 %) for a 10 mL, 10 mM reaction. <sup>1</sup>H NMR (300 MHz, D<sub>2</sub>O):  $\delta$  8.30 (s, H2 & H8), 6.10 (d, H1'), 4.41 (m, H3' & H2'), 3.92 (t, H4'), 3.85, 3.78 (d, H5' & H5"), 3.55 (m, H $\alpha$ ), 3.39 (m, H $\gamma$  & H $\gamma$ '), 2.84 (s, CH<sub>3</sub>), 2.21 (m, H $\beta$  & H $\beta$ ') ppm.

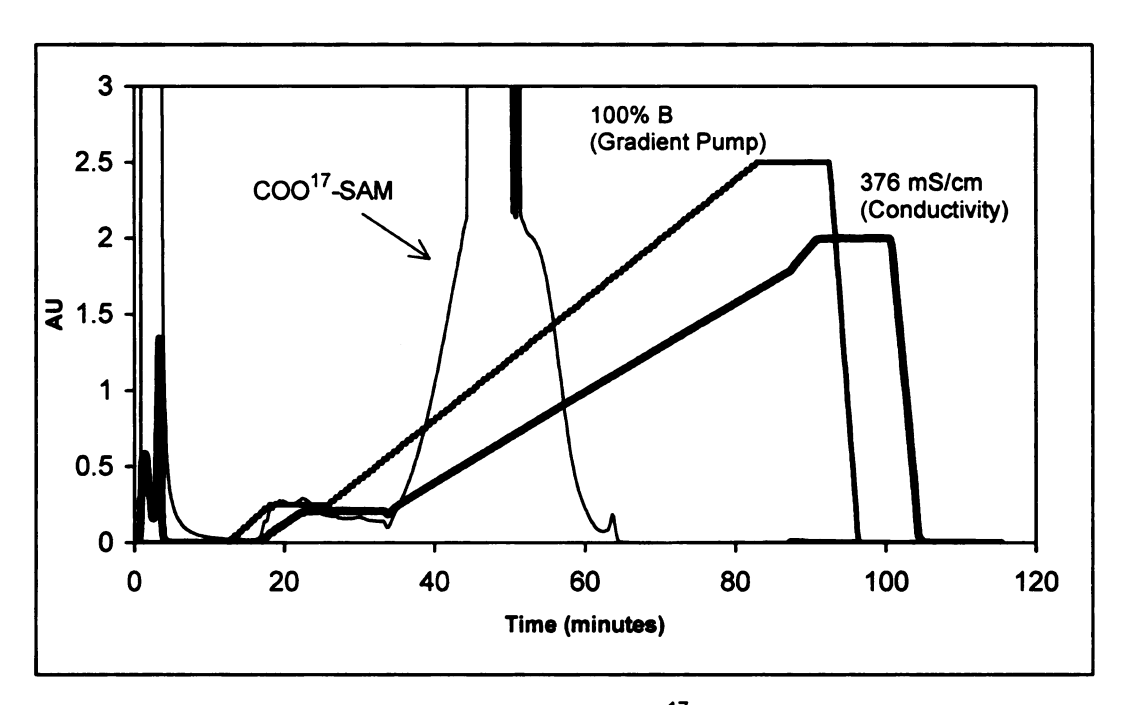


**Figure III.10** Chromatogram of isolation of COO<sup>17</sup>-AdoMet by SOURCE 15S cation exchange chromatography (Pharmacia, 8 mL), gradient from 0-1 M HCI, flow rate, 1 mL/min. COO<sup>17</sup>-SAM eluted as a distinct peak from 38 – 56 % Buffer B.

S-Adenosyl-carboxy-<sup>13</sup>C-methionine ( $^{13}$ COO-AdoMet) was synthesized overnight under similar conditions as for regular SAM, and isolated by chromatography on a SOURCE 15S cation exchange column (Figure III.11). Yield was 30.0 mg (68.5 %) for a 10 mL, 10 mM reaction.  $^{1}$ H NMR (300 MHz, D<sub>2</sub>O):  $\delta$  8.30 (s, H2 & H8), 6.10 (d, H1'), 4.41 (m, H3' & H2'), 3.92 (t, H4'), 3.85, 3.78 (d, H5' & H5"), 3.55 (m, H $\alpha$ ), 3.39 (m, H $\gamma$  & H $\gamma$ '), 2.82 (s, CH<sub>3</sub>), 2.22 (m, H $\beta$  & H $\beta$ ') ppm.

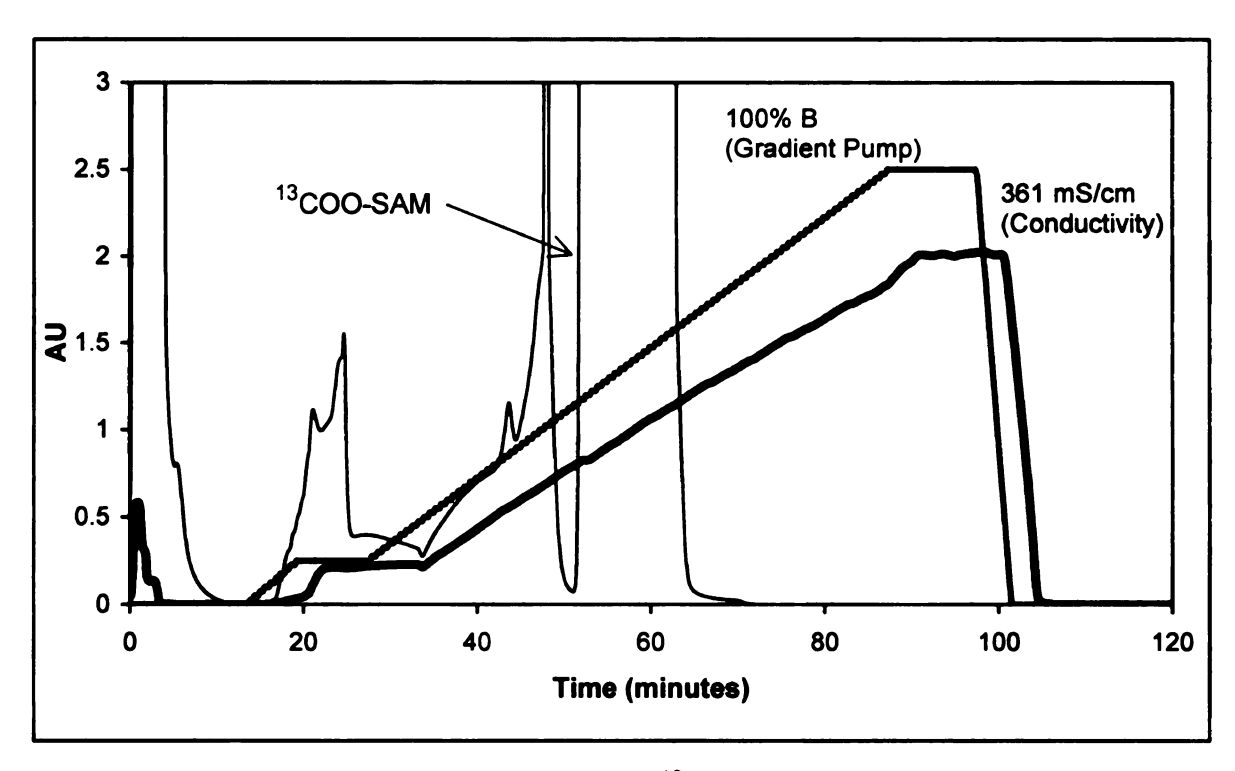


**Figure III.11** Chromatogram of isolation of <sup>13</sup>COO-AdoMet by SOURCE 15S cation exchange chromatography (Pharmacia, 8 mL), gradient from 0-1 M HCI, flow rate,1 mL/min. <sup>13</sup>COO-SAM eluted as a distinct peak from 38 –56 % Buffer B.

S-Adenosyl-2-D<sub>1</sub>-methionine ( $\alpha$ -CD-AdoMet) was synthesized overnight under similar conditions as for regular SAM, and isolated by chromatography on a SOURCE 15S cation exchange column (Figure III.12). Yield was 30.0 mg (68.5 %) for a 10 mL, 10 mM reaction. <sup>1</sup>H NMR (300 MHz, D<sub>2</sub>O):  $\delta$  8.30 (s, H2 & H8), 6.10 (d, H1'), 4.41 (m, H3' & H2'), 3.85, 3.78 (d, H5' & H5''), 3.39 (m, H $\gamma$  & H $\gamma$ '), 2.82 (s, CH<sub>3</sub>), 2.22 (m, H $\beta$  & H $\beta$ ') ppm.

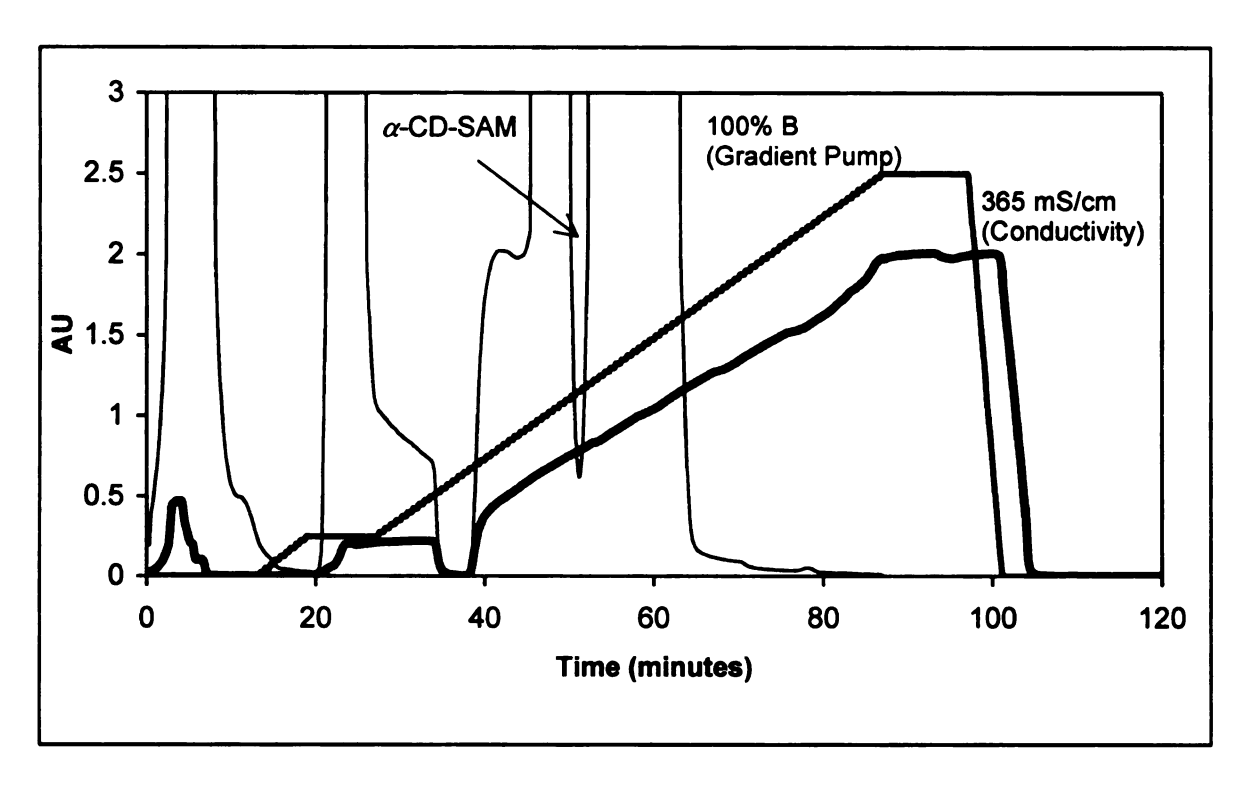


**Figure III.12** Chromatogram of isolation of  $\alpha$ -CD-AdoMet by SOURCE 15S cation exchange chromatography (Pharmacia, 8 mL), gradient from 0-1 M HCl, flow rate, 1 mL/min.  $\alpha$ -CD-SAM eluted as a distinct peak from 38 –56 % Buffer B.

### III.4 Conclusion

In conclusion, a fairly simple procedure for enzymatic synthesis of SAM on a preparative scale has been established. SAM synthetase was overexpressed and grown in E. coli cells. The enzyme was lysed by a combination of enzymatic and physical procedures, and the crude extract was used for SAM synthesis reaction without further purification. Product inhibition was overcome by addition of 8 % of  $\beta$ -ME and pyrophosphatase in the reaction mixture. A 10 mM reaction can afford over 80 % yield of SAM. SAM isolated by the method described here

has high diastereoisomeric purity, and appears to be more stable than SAM iodide salt from commercial sources. The enhanced stability of the synthesized SAM is probably due to the increased purity and the high acidity of the lyophilized product, which is eluted by HCI of around 0.5 M, may help to stabilize SAM.

This method can be easily applied to isotopically labeled substrates, as has been shown on methyl-D<sub>3</sub>-AdoMet, methyl-<sup>13</sup>C-AdoMet, amino-<sup>15</sup>N-AdoMet, carboxy-<sup>13</sup>COO-AdoMet, α-D-AdoMet and carboxy-CO<sup>17</sup>O-AdoMet, which have all been synthesized in our laboratory with some modifications of the reaction conditions according to the properties of the substrate analogues being used. Combined with other synthetic techniques, more isotopically labeled AdoMets and AdoMet analogues could be synthesized from a variety of isotopically labeled methionines and ATP, or methionine and ATP analogues. These SAM analogues will be useful as probes to study the interaction of SAM with the Fe-S cluster of PFL-AE from different perspectives.

#### III.5 References

- (1) Frey, P. Annu. Rev. Biochem. 2001, 70, 121.
- (2) Sofia, H. J. C., G.; Hetzler, B.G.; Reyes-Spindola, J.F.; Miller, N. *Nucl. Acid. R.* **2001**, *29*, 1097.
- (3) Moss, M. L. F., P.A. J. Biol. Chem. 1987, 262, 14859.
- (4) Knappe, J. N., F.A.; Blaschkowski, H.P.; Ganzler, M. *Proc. Natl. Acad. Sci. USA* **1984**, *81*, 1332.
- (5) Frey, M. R., M.; Wagner, A. F. V.; Knappe, J. *J. Biol. Chem.* **1994**, 269, 12432.
- (6) Henshaw, T. F. C., J.; Broderick, J. B. *J. Am. Chem. Soc.* **2000**, *122*, 8331.
- (7) Krebs, C. H., T. F.; Cheek, J.; Huynh, B. H.; Broderick, J. B. *J. Am. Chem. Soc.* **2000**, *122*, 12497.
- (8) Kennedy, M. C.; Werst, M.; Telser, J.; Emptage, M. H.; Beinert, H.; Hoffman, B. M. *Proc. Natl. Acad. Sci. USA* **1987**, *84*, 8854.
- (9) Werst, M.; Kennedy, M. C.; Beinert, H.; Hoffman, B. M. *Biochemistry* **1990**, *29*, 10526.
- (10) Matos, J. R. R., F. M.; Wong, C.-H. *Biotech. Appl. Biochem.* **1987**, 9, 39.
- (11) Schalk-Hihi, C. M., G. D. *Biochemistry* **1999**, *38*, 2542.
- (12) Markham, G. D. H., E. W.; Tabor, C. W.; Tabor, H. *J. Biol. Chem.* **1980**, *255*, 9082.
- (13) Cantoni, G. L. J. Biol. Chem. 1953, 204, 403.
- (14) Markham, G. D. J. Biol. Chem. 1981, 256, 1903.
- (15) Zhang, C. M., G. D.; LoBrutto, R. Biochemistry 1993, 32, 9866.
- (16) Park, J. T., J.; Roessner, C. A.; Scott, A. I. *Bioorg. Medicinal Chem.* **1996**, *4*, 2179.
- (17) Bradford, M. Anal. Biochem. 1976, 72, 248.

- (18) Emptage, M. H. K., T.A., Kennedy, M.C.; Beinert, H., Mönck, E. *Proc. Natl. Acad. Sci. USA* **1983**, *50*, 4674.
- (19) Senkus, M. B., W.G. J. Org. Chem. 1938, 2, 569.

#### **CHAPTER IV**

# INVESTIGATING THE INTERACTION OF ADOMET WITH PFL-AE USING EPR AND ENDOR SPECTROSCOPY

#### IV.1 Introduction

Iron-sulfur clusters in biological systems participate in a broad range of functions, including electron transfer, redox and nonredox catalysis, structural roles, and regulation of gene expression. A new role for Fe-S clusters has emerged in recent years as a number of enzymes have been identified that utilize Fe-S clusters and S-adenosyl-methionine (AdoMet) to generate catalytically essential radicals. This class of enzymes has been identified as the "radical S-adenosylmethionine" superfamily, with over 600 unique sequences found to date, spanning a diverse range of functions, including generation of stable protein radicals (activating enzymes for pyruvate formate-lyase for and anaerobic ribonucleotide reductase), cofactor biosynthesis (biotin 11 and lipoic acid 12.13 synthases), rearrangement reactions (lysine aminomutase), and DNA repair (spore photoproduct lyase 15). Pyruvate formate-lyase activating enzyme (PFL-AE), a representative member of this family of enzymes, generates a stable glycyl radical at G734 on pyruvate formate-lyase (PFL) via reductive cleavage of

AdoMet, converting AdoMet stoichiometrically to methionine and 5'-deoxyadenosine (5'-dAdo) as shown in Figure IV.1.<sup>6,16-18</sup> PFL utilizes the catalytically essential glycyl radical to convert pyruvate and coenzyme A (CoA) to formate and acetyl-CoA, the first committed step in anaerobic glucose metabolism in bacteria such as *Escherichia coli*.<sup>16,17</sup> Isotope labeling experiments established that the pro-S hydrogen atom abstracted from G734 in PFL is incorporated into the methyl group of the 5'-dAdo product, suggesting the presence of a 5'-dAdo radical intermediate during the activation of PFL.<sup>19</sup>

Figure IV.1 Reaction catalyzed by pyruvate formate-lyase activating enzyme.

The involvement of a 5'-dAdo radical intermediate, produced by the reductive cleavage of AdoMet, appears to be a key mechanistic feature shared by the

"radical S-adenosyl-methionine" superfamily members.<sup>3,4</sup> Elegant work by Frey and co-workers has provided direct spectroscopic evidence for an allylic analogue of the 5'-dAdo radical in lysine aminomutase.<sup>20,21</sup>

A central mechanistic question in PFL-AE, and the radical S-adenosylmethionine superfamily in general, is the role the iron-sulfur cluster plays in the reductive cleavage of AdoMet to generate the putative 5'-dAdo radical intermediate. Anaerobically purified PFL-AE contains primarily cuboidal [3Fe-4S]<sup>+</sup> clusters, with smaller quantities of [4Fe-4S]<sup>2+</sup>, [2Fe-2S]<sup>2+</sup>, and linear [3Fe-4S]<sup>+</sup> clusters. However, this mixture of clusters is converted to [4Fe-4S]<sup>2+/+</sup> clusters under reducing conditions. Such reductive cluster conversions have been observed for other members of this enzyme family, 11,23 as well as for other iron-sulfur cluster enzymes such as aconitase, 24-27 and are thought to proceed via release of Fe(II) and sulfide from the protein followed by reassembly of the [4Fe-4S] cluster. 28

It was previously demonstrated for PFL-AE that the reduced [4Fe-4S]<sup>+</sup> form of the iron-sulfur cluster is the catalytically essential and active form, serving as the source of the electron required to reductively cleave AdoMet and generate the G734 glycyl radical on PFL.<sup>29</sup> The details of this unprecedented reaction remain unanswered, including the key question of how the [4Fe-4S]<sup>+</sup> cluster interacts with AdoMet, with there being several possibilities. The [4Fe-4S]<sup>+</sup> may play a simple electron-transfer role in the reductive cleavage of AdoMet, transferring an electron to AdoMet, which then fragments to methionine and the

5'-dAdo radical. Alternatively, the [4Fe-4S] cluster may be more directly involved in the radical generation reaction, via covalent interactions with AdoMet. This may involve intermediates in which a bridging S or an Fe atom of the cluster interacts with either the sulfonium S or the 5'-adenosyl C of AdoMet, but in any case, AdoMet must bind in close proximity to the [4Fe-4S] cluster. Indirect evidence for such a close interaction of AdoMet with the [4Fe-4S] cluster of lysine aminomutase was reported by Cosper and co-workers. They demonstrated an interaction of ~2.7 Å between selenomethinione, the turnover product of Se-AdoMet, and an Fe of the [4Fe-4S] cluster by using Se X-ray absorption spectroscopy. No interaction was observed, however, between Se-AdoMet and the iron-sulfur cluster.

Iron-sulfur clusters participate in a wide range of critical biochemical reactions.<sup>2</sup> Most Fe-S clusters function in electron transfer, but an essential minority perform catalysis, such as the archetypal [4Fe-4S] cluster of aconitase, which isomerizes citrate to isocitrate. Such 4Fe catalytic clusters are distinct in having a unique Fe ion, which is not coordinated to the enzyme by a cysteinyl sulfur. The obvious role of such an Fe is a catalytic one, and indeed, the aconitase cluster isomerizes citrate/isocitrate through a mechanism in which the reactant/product is chelated to the unique cluster Fe.<sup>26,31</sup> We here demonstrate an alternate role for the unique Fe of a catalytic [4Fe-4S] cluster: the [4Fe-4S] cluster of the pyruvate formate-lyase activating enzyme (PFL-AE) "anchors" its substrate, S-adenosylmethionine (AdoMet), by a classical N/O chelate in which the unique Fe binds the amino and carboxylato groups of the methionine

fragment of AdoMet, thereby fixing the substrate geometry for subsequent reaction with the cluster.<sup>32</sup> Such coordination is supported by ENDOR work described herein, as well as by Mössbauer studies of the PFL-AE/AdoMet complex, which show that the unique iron site are dramatically perturbed in the presence of AdoMet.<sup>33</sup>

To probe these interactions of AdoMet with the [4Fe-4S] cluster of PFL-AE, we have carried out electron paramagnetic resonance (EPR) and 35 GHz pulsed electron-nuclear double resonance (ENDOR) studies of the PFL-AE-AdoMet complex with AdoMet labeled with <sup>2</sup>H and <sup>13</sup>C at the sulfonium methyl group. ENDOR observations of hyperfine interactions between the <sup>2</sup>H and <sup>13</sup>C nuclei on AdoMet and the paramagnetic  $S = \frac{1}{2} [4Fe-4S]^{+}$  cluster state of PFL-AE, would provide unequivocal direct spectroscopic evidence for a close association of AdoMet with the [4Fe-4S] cluster and information about binding geometry. 34,35 In previous work, we demonstrated the ability to reduce PFL-AE to the [4Fe-4S]<sup>+</sup> state in good vield via 5- deazariboflavin-mediated photoreduction.<sup>29</sup> In the present work, we have exploited this approach to prepare samples for ENDOR studies of AdoMet binding to the enzyme in the equilibrium geometry associated with the catalytically active paramagnetic [4Fe-4S]<sup>+</sup> state of the cluster, denoted [1+/AdoMet]. We have also studied the interactions between AdoMet and the diamagnetic [4Fe-4S]<sup>2+</sup> state via ENDOR. To do this, the [4Fe-4S]<sup>2+</sup> PFL-AE sample is first frozen in the presence of AdoMet and then *x*-irradiated at 77 K to

produce the [4Fe-4S]<sup>+</sup> valency cluster cryogenically trapped in the geometry of the 2+ state, denoted [2+/AdoMet]<sub>red</sub>. <sup>36-42</sup>

Here we also unambiguously establish the function of the unique Fe through Q-band pulsed ENDOR spectroscopic studies of the [4Fe-4S]<sup>+</sup>/AdoMet complex in which AdoMet is specifically <sup>17</sup>O-, and <sup>13</sup>C-labeled in the carboxyl group of the methionine fragment and <sup>15</sup>N labeled in the amino group. The results described here provide the first direct spectroscopic evidence for a direct interaction between AdoMet and the [4Fe-4S]<sup>+</sup> and [4Fe-4S]<sup>2+</sup> cluster states of PFL-AE. The implications of these results for the mechanism of [4Fe-4S] cluster mediated reductive cleavage of AdoMet are discussed.

#### IV.2 Experimental Methods

IV.2.1 Synthesis and Purification of CD<sub>3</sub>-AdoMet, <sup>13</sup>CH<sub>3</sub>-AdoMet, <sup>15</sup>NH<sub>2</sub>-AdoMet, <sup>13</sup>COO-AdoMet, CO<sup>17</sup>O-AdoMet, and α-D-AdoMet.
 Described in Chapter III, Section III.2.4.

# IV.2.2 [1+ / AdoMet] Sample Preparation

The as-isolated PFL-AE, in 50 mM Tris-sulfate, 200 mM NaCl, 1 mM DTT, pH 7.5, was exchanged with 50 mM Tris-HCl, 200 mM NaCl, 1 mM DTT, pH 8.5 buffer, and concentrated in an Amicon pressure cell with an YM-10 membrane in the Coy Chamber. The concentration of the protein was determined by the method of Bradford.<sup>43</sup>

The following procedures were carried out anaerobically in an inert atmosphere glove box (Mbraun) with  $O_2$  level  $\leq 3$  ppm. All buffers, solvents and bath water were deoxygenated using a vacuum/inert gas manifold before being taken into the glove box. Solid chemicals were pumped in as solids. Ice was pre-chilled with liquid nitrogen before pumping into the glove box.

PFL-AE was mixed with 20-25 % (v/v) glycerol in an eppendorf to a total volume of 200  $\mu$ L for EPR samples, or 300  $\mu$ L for parallel EPR and ENDOR samples, and pre-reduced by addition of 1 equivalent of sodium dithionite (from a freshly made 50 mM solution in 50 mM Tris buffer, pH 8.5). 5-deazariboflavin (10 mM stock solution in DMSO) was added in the dark to a final concentration of 100 μM for 400 μM or less concentrated PFL-AE, or 200 μM for PFL-AE of over 400 \( \alpha \text{M} \), and mixed well. The sample was then transferred to an EPR tube. The EPR tube was capped and inserted in a beaker tightly packed with ice-water. The sample was illuminated on ice using a 500 W halogen lamp for 1 hour with the lamp situated about 5 cm from the beaker. After illumination, the protein sample was mixed with 2 equivalents of AdoMet on ice by adding the protein to pre-measured AdoMet or isotopically labeled AdoMet solution (10 mM or 30 mM solution in 50 mM Tris buffer, pH 8.5). The sample was transferred back to the EPR tube, or split to EPR and ENDOR tubes, and flash-frozen in liquid nitrogen in the glove box.

#### IV.2.3 [2+ / AdoMet] Sample Preparation

As-isolated PFL-AE containing 0.13 % of [3Fe-4S]<sup>+</sup> (0.73  $\mu$ M spin for 560  $\mu$ M protein, as determined by EPR) was exchanged with 50 mM Tris-HCl, 200 mM NaCl, 1 mM DTT, pH 8.5 buffer, and concentrated as described in IV.2.2. In the inert atmosphere glove box, 574  $\mu$ M PFL-AE, 20 % (v/v) glycerol and 2 equivalents of CD<sub>3</sub>-AdoMet or <sup>13</sup>CH<sub>3</sub>-AdoMet were mixed on ice to make a final volume of 60  $\mu$ L. The sample was loaded into an ENDOR tube, and flash-frozen in liquid nitrogen in the glove box.

# IV.2.4 [2+/AdoMet]<sub>red</sub> Sample Preparation

[2+/AdoMet]<sub>red</sub> sample preparation was done in collaboration with Professor Brian M. Hoffman, and Dr. Charles Walsby, Department of Chemistry, Northwestern University. The [2+ / AdoMet] sample prepared as described above was  $\gamma$ -irradiated at 77 K to produce the 1+ valency cluster trapped in the geometry of the 2+ state.

# IV.2.5 EPR Spectroscopy

EPR first-derivative spectra were obtained at X-band on a Bruker ESP300E spectrometer equipped with a liquid He cryostat and a temperature controller from Oxford Instruments. Spectra were recorded at 12 K for [3Fe-4S]<sup>+</sup> and [4Fe-4S]<sup>+</sup>, and at 60 K to detect the glycyl radical. Spin quantifications were done as described previously.<sup>44</sup> The double integrals of the EPR signals were evaluated by using a computer on-line with the spectrometer. Spin

concentrations in the protein samples were determined by calibrating double integrals of the EPR spectra recorded under nonsaturating conditions (i) with a standard sample of 0.1 mM Cu(II) and 1 mM EDTA solution for the cluster signals, or (ii) with a 1.04 mM  $K_2(SO_3)_2NO$  solution for the glycyl radical signals. The concentration of the  $K_2(SO_3)_2NO$  standard was determined using the optical extinction coefficient.<sup>45</sup>

## IV.2.6 ENDOR Spectroscopy

Pulsed ENDOR spectra (35 GHz) were recorded on a spectrometer described earlier, <sup>46</sup> equipped with a helium immersion dewar, and all the measurements were carried out at approximately 2 K. Pulsed ENDOR measurements employed the three-pulse Mims ENDOR sequence ( $\pi/2-\tau-\pi/2-T-\pi/2-\tau$ -echo), where the RF was applied during the interval T.

For a nucleus (N) of spin I = 1/2 ( $^{13}$ C,  $^{1}$ H,  $^{15}$ N) interacting with a  $S = \frac{1}{2}$  paramagnetic center, the first-order ENDOR spectrum for a single molecular orientation is a doublet,

$$v_{\pm} = v_{N} \pm \frac{A}{2} \tag{1}$$

centered at  $v_N$ , the Larmor frequency, and split by A, the orientation dependent hyperfine constant, when  $v_N > A/2$ , as is true here for  $^1H$ ,  $^{13}C$ , and  $^{15}N$  nuclei. Similarly, for a deuteron,  $^2H$  (I = 1), or  $^{14}N$  (I = 1) and  $^{17}O$  (I = 5/2) where  $v_N > A/2$ , as is true here, the first-order ENDOR resonance condition can be written,

$$v_{\pm}(\pm) = v_D \pm \frac{A}{2} \pm \frac{3P}{2}$$
 (2)

where *P*, is the orientation-dependent quadrupolar splitting. This is the case with <sup>2</sup>H and <sup>17</sup>O nuclei in the present study. The full hyperfine tensor of a coupled nucleus, both principal values and orientation parameters (Euler angles) with respect to the *g*-tensor frame, is obtained by simulating the 2-D pattern of orientation-dependent ENDOR spectra recorded across the EPR envelope using the procedures and program described elsewhere.<sup>47-51</sup> The computer simulation and analysis of the frozen-solution ENDOR spectra used in the present work are described in the same references.

For a nucleus with hyperfine coupling, A, the Mims techniques have a response R that depends on the product,  $A\tau$ , according to the equation.

$$R \sim \left[1 - \cos(2\pi A \tau)\right] \tag{3}$$

This function has zeroes, corresponding to minima in the ENDOR response (hyperfine suppression holes), at  $A\tau = n$ ; n = 0, 1, 2, ..., and maxima at  $A\tau = (2n + 1)/2$ ;  $n = 0, 1, 2, ..., ^{47,48}$  The hyperfine couplings suppressed by the holes at  $A = n/\tau$ , n = 1, 2, 3, ... can be adjusted by varying  $\tau$ . However, the central, n = 0, hole at  $\nu = \nu_N$  persists regardless. This can be of significance in distinguishing a tensor that is dominated by anisotropic interactions from one that is dominated by isotropic ones. The latter would never predict ENDOR intensity near  $\nu_N$ , while the

former does so for certain orientations. By suppressing intensity near  $\nu_N$ , the n=0. Mims hole diminishes the differences between the two cases.

#### IV.3 Results and Discussion

# IV.3.1 EPR Spectroscopy

PFL-AE purified anaerobically in the presence of DTT, as is done here, contains primarily [4Fe-4S]<sup>2+</sup> clusters, with small quantities (<1% of total iron based on EPR spin quantitation) of [3Fe-4S]<sup>+</sup> clusters. Reduction of PFL-AE using photoreduced 5-deazariboflavin as described in Experimental Methods typically yields  $[4Fe-4S]^{+}$  enzyme in 300-400  $\mu$ M concentrations based on EPR spin quantitation. The presence of AdoMet produces dramatic effects on the EPR signal of the [4Fe-4S]<sup>+</sup> cluster, as shown in Figure IV.2. In the absence of AdoMet, the  $[4Fe-4S]^{+}$  cluster of PFL-AE gives a rhombic EPR signal (g = 2.02, 1.94, 1.88). However, if AdoMet is added to the reduced [4Fe-4S]<sup>+</sup>-PFL-AE, the observed EPR signal is nearly axial (g = 2.01, 1.88, 1.87). Radiolytic cryoreduction at 77 K of PFL-AE treated with AdoMet in the 2+ state produced the 1+ cluster trapped in the structure characteristic of the precursor 2+ state. The state denoted [2+/AdoMet]<sub>red</sub> has an EPR signal very similar to that of the [1+/AdoMet] state (not shown), suggesting that [2+/AdoMet] and [1+/AdoMet] have similar structures.

The X-band EPR spectra of the PFL-AE [4Fe-4S]<sup>+</sup> in the presence of CD<sub>3</sub>-AdoMet, <sup>13</sup>CH<sub>3</sub>-AdoMet, <sup>15</sup>NH<sub>2</sub>-AdoMet, <sup>13</sup>COO-AdoMet, CO<sup>17</sup>O-AdoMet

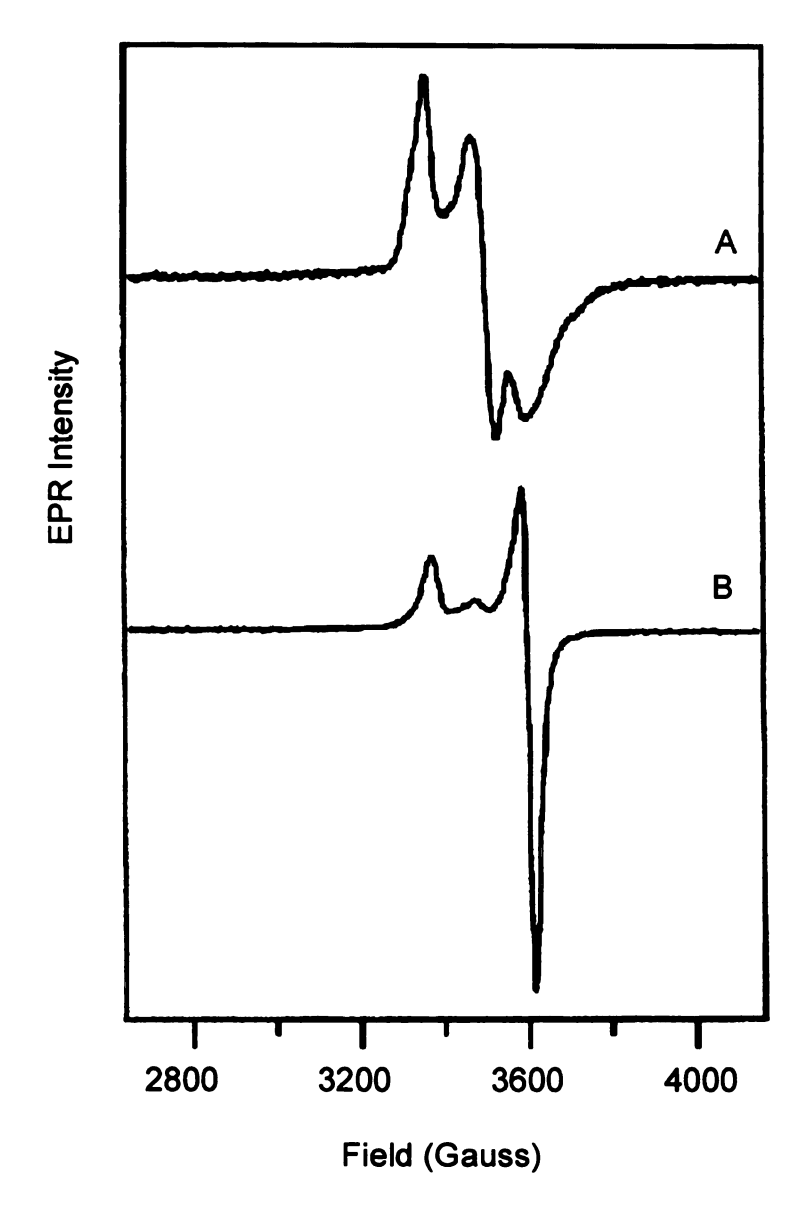


**Figure IV.2** 9.5 GHz CW EPR spectra of PFL-AE photoreduced with deazariboflavin as described in the text. (A) PFL-AE (0.7 mM) photoreduced for 1 h. The signal accounts for 197  $\mu$ M [4Fe-4S]<sup>+</sup> based on EPR spin quantitation, and has been multiplied by 3 for comparison purposes. (B) PFL-AE (0.78 mM) photoreduced for 1 h, followed by addition of two molar equivalents of AdoMet. The signal accounts for 416  $\mu$ M [4Fe-4S]<sup>+</sup> based on EPR spin quantitation. Conditions: T = 12 K, power = 20  $\mu$ W, gain = 2 x 10<sup>4</sup>, frequency = 9.483 (A) or 9.476 (B), modulation amplitude = 8.231 (A) or 9.571 (B).

and α-D-AdoMet are essentially indistinguishable from the spectra of PFL-AE [4Fe-4S]<sup>+</sup> in the presence of unlabeled AdoMet. The samples are summarized in Table IV.1 and EPR spectra are shown in Figures IV.3-IV.8.

Sample	[PFL-AE]	Fe/protein	[4Fe-4S] <sup>+</sup>	% of [4Fe-4S] <sup>+</sup> cluster	Figure #
CD <sub>3</sub> -SAM	910 μΜ	3.75	324 μ <b>M</b>	38.0	IV.3
<sup>13</sup> CH <sub>3</sub> -SAM	777 μ <b>M</b>	3.02	404 μΜ	68.9	IV.4
15NH <sub>2</sub> -SAM	567 μ <b>M</b>	3.75	224 μΜ	42.1	IV.5
<sup>13</sup> COO-SAM	750 μ <b>M</b>	3.75	141 μΜ	18.8	IV.6
CO <sup>17</sup> O-SAM	521 μ <b>M</b>	3.75	156 μ <b>M</b>	30.0	IV.7
α-D-SAM	750 μM	3.75	97.1 μΜ	12.9	IV.8

**Table IV.1** Photoreduction data of PFL-AE in the presence of isotopically labeled AdoMet.

IV.3.2 ENDOR Spectroscopic Evidence for a Close Interaction Between AdoMet and the [4Fe-4S] Cluster of PFL-AE

<sup>2</sup>H and <sup>13</sup>C ENDOR

The observed effect of AdoMet on the EPR signal of the catalytically relevant [4Fe-4S]<sup>+</sup> cluster could reflect either a close association between AdoMet and the cluster or more remote allosteric perturbations of the cluster. These

possibilities were investigated using ENDOR spectroscopy. The <sup>2</sup>H ENDOR spectra of [1+/CD<sub>3</sub>-AdoMet] and [2+/CD<sub>3</sub>-AdoMet]<sub>red</sub>, Figure IV.9, and the corresponding <sup>13</sup>C spectrum of [1+/13CH3-AdoMet] and [2+/<sup>13</sup>CH<sub>3</sub>-AdoMet]<sub>red</sub>, Figure IV.10, immediately demonstrate that the cofactor sits close to the cluster in both the 1+ and 2+ states. The <sup>2</sup>H spectra of [1+/CD<sub>3</sub>-AdoMet] taken at

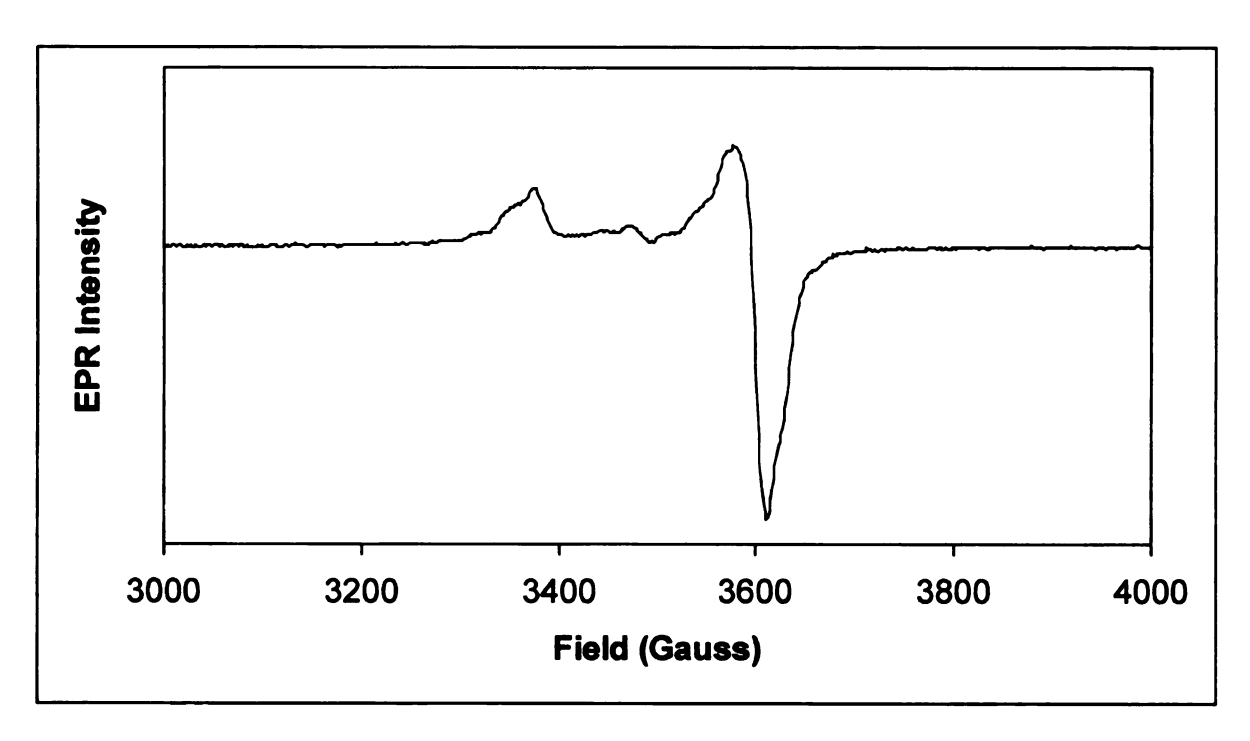


**Figure IV.3** X-band EPR spectrum of PFL-AE [4Fe-4S]<sup>+</sup> in the presence of CD<sub>3</sub>- AdoMet. The sample contained 910  $\mu$ M PFL-AE, 1 equivalent of Na<sub>2</sub>S<sub>2</sub>O<sub>4</sub>, 200  $\mu$ M 5-deazariboflavin, and 2 equivalents of CD<sub>3</sub>-AdoMet; 38.0 % reduction (based on 324  $\mu$ M spin for 910 $\mu$ M protein with 3.75 mol Fe/ mol PFL-AE); g = 2.005, 1.949, 1.883. Conditions of measurement: T = 12 K; microwave power, 20  $\mu$ W; microwave frequency, 9.47 GHz; modulation amplitude, 10.053 G; single scan.

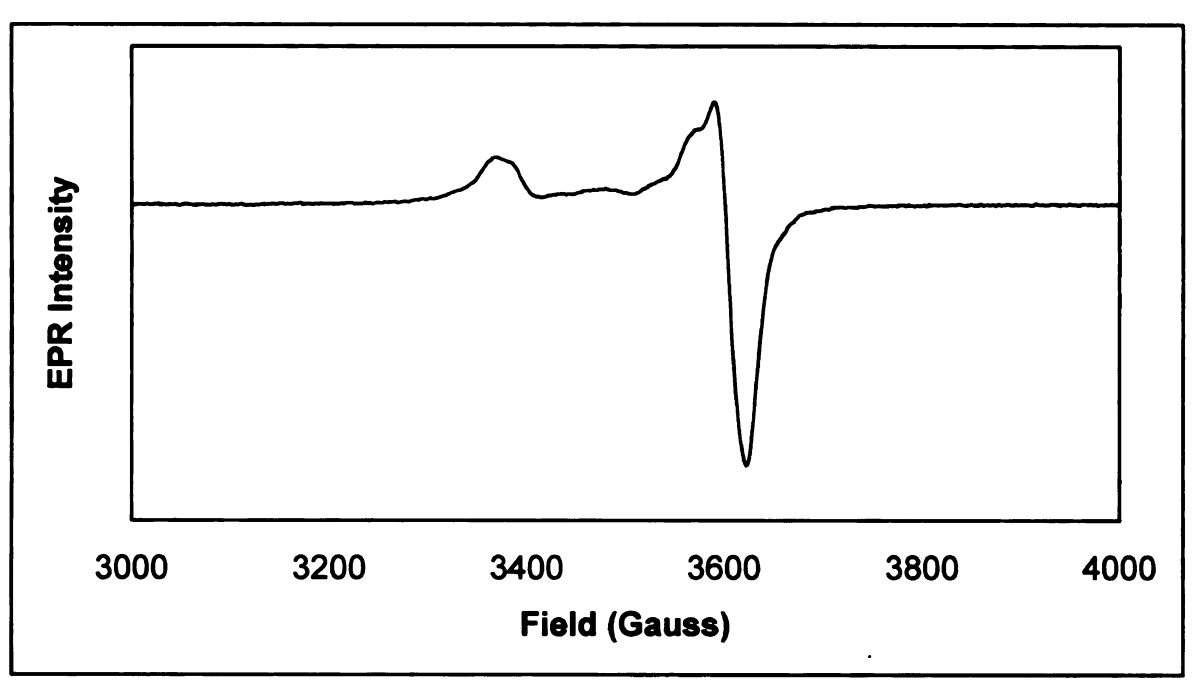


**Figure IV.4** X-band EPR spectrum of PFL-AE [4Fe-4S]<sup>+</sup> in the presence of  $^{13}$ CH<sub>3</sub>-AdoMet. The sample contained 777 μM PFL-AE, 1 equivalent of Na<sub>2</sub>S<sub>2</sub>O<sub>4</sub>, 200 μM 5-deazariboflavin, and 2 equivalents of  $^{13}$ CH<sub>3</sub>-AdoMet; 68.9 % reduction (based on 404 μM spin for 777 μM protein with 3.02 mol Fe/ mol PFL-AE); g = 2.011, 1.948, 1.880. Conditions of measurement: T = 12 K; microwave power, 20 μW; microwave frequency, 9.49 GHz; modulation amplitude, 9.571 G; single scan.

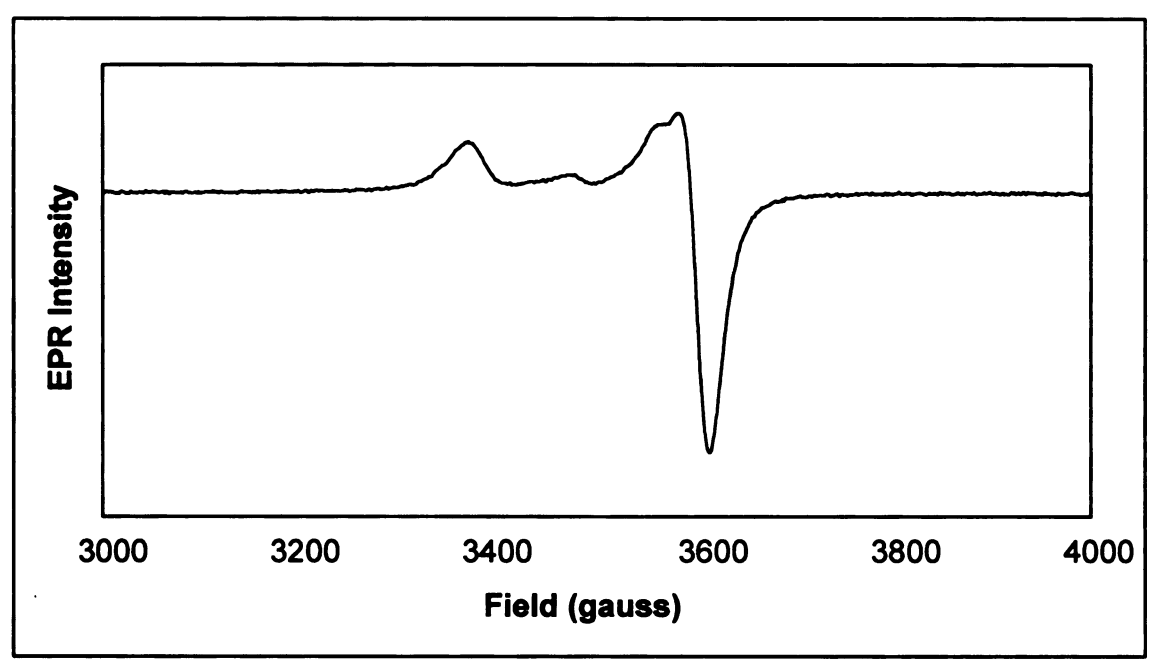


**Figure IV.5** X-band EPR spectrum of PFL-AE [4Fe-4S]<sup>+</sup> in the presence of  $^{15}$ NH<sub>2</sub>-AdoMet. The sample contained 650  $\mu$ M PFL-AE, 1 equivalent of Na<sub>2</sub>S<sub>2</sub>O<sub>4</sub>, 200  $\mu$ M 5-deazariboflavin, and 2 equivalents of  $^{15}$ NH<sub>2</sub>-AdoMet; 42.1 % reduction (based on 224  $\mu$ M spin for 567 $\mu$ M protein with 3.75 mol Fe/ mol PFL-AE); g = 2.018, 1.948, 1.883. Conditions of measurement: T = 12 K; microwave power, 20  $\mu$ W; microwave frequency, 9.49 GHz; modulation amplitude, 9.571 G; single scan.

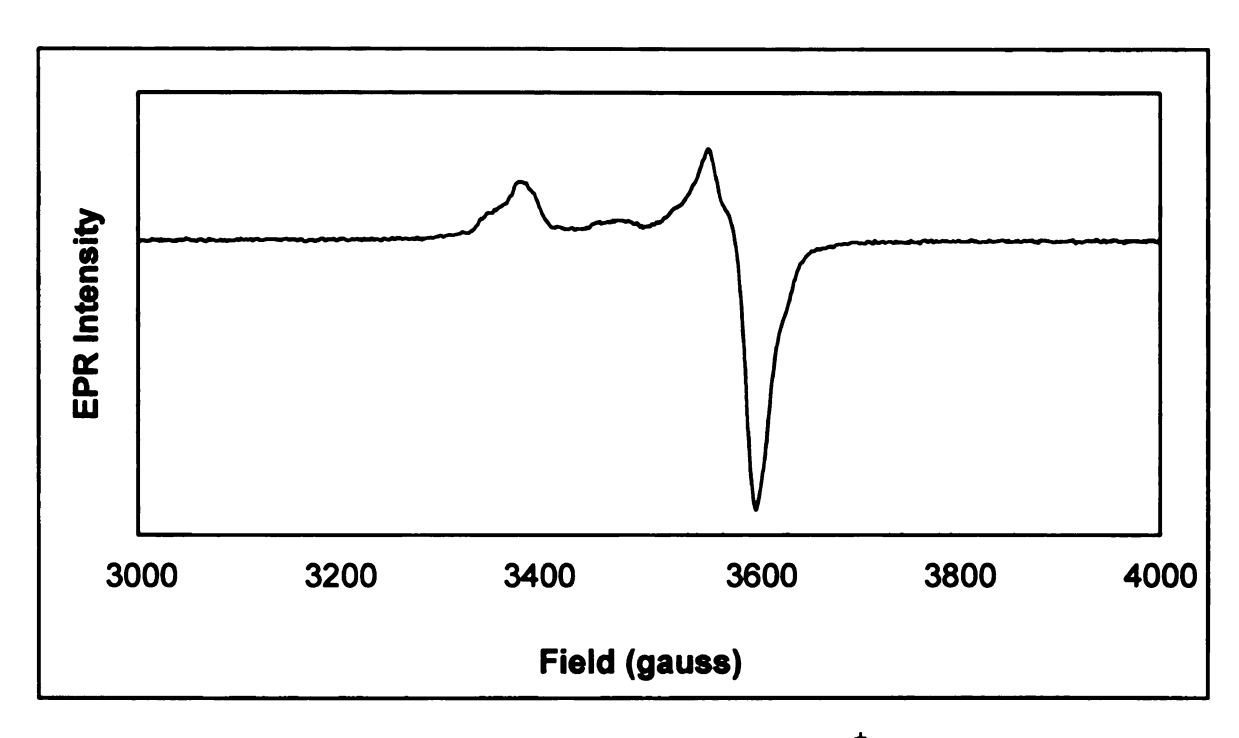


**Figure IV.6** X-band EPR spectrum of PFL-AE [4Fe-4S]<sup>+</sup> in the presence of  $^{13}$ COO-AdoMet. The sample contained 650  $\mu$ M PFL-AE, 1 equivalent of Na<sub>2</sub>S<sub>2</sub>O<sub>4</sub>, 200  $\mu$ M 5-deazariboflavin, and 2 equivalents of  $^{13}$ COO-AdoMet; 21.7 % reduction (based on 141  $\mu$ M spin for 650 $\mu$ M protein with 3.75 mol Fe/ mol PFL-AE); g = 2.01, 1.948, 1.889. Conditions of measurement: T = 12 K; microwave power, 20  $\mu$ W; microwave frequency, 9.49 GHz; modulation amplitude, 9.571 G; single scan.

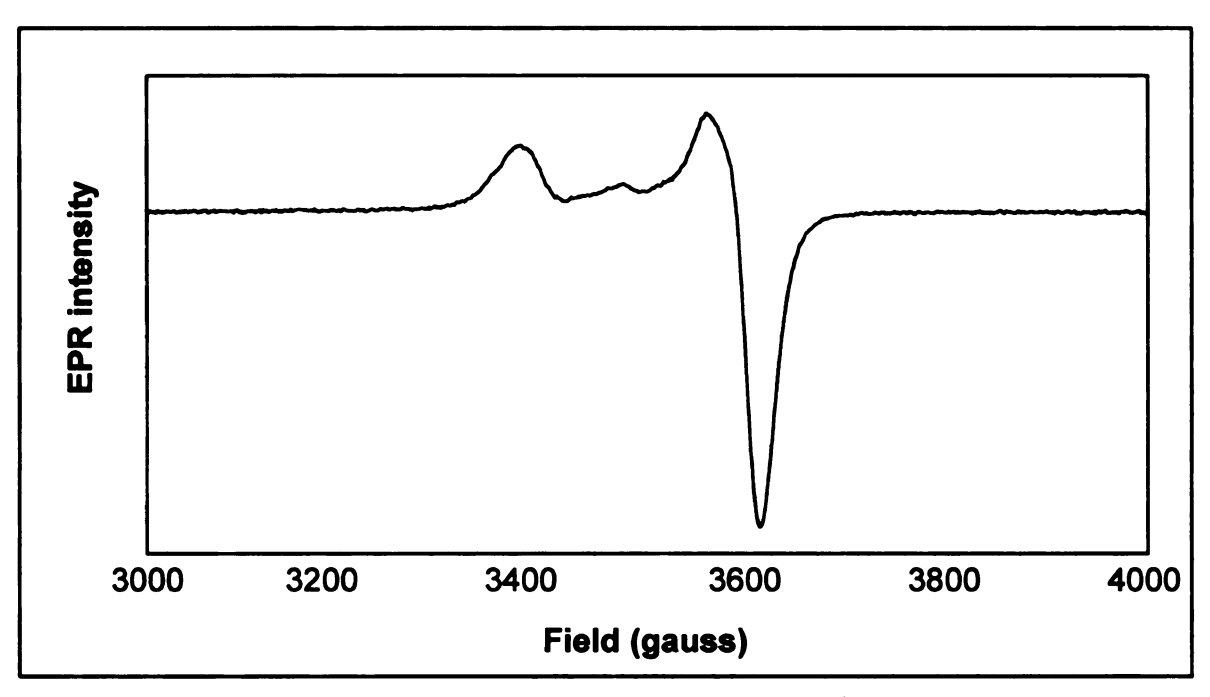


**Figure IV.7** X-band EPR spectrum of PFL-AE [4Fe-4S]<sup>+</sup> in the presence of CO<sup>17</sup>O-AdoMet. The sample contained 521  $\mu$ M PFL-AE, 1 equivalent of Na<sub>2</sub>S<sub>2</sub>O<sub>4</sub>, 200  $\mu$ M 5-deazariboflavin, and 2 equivalents of CO<sup>17</sup>O -AdoMet; 68.9 % reduction (based on 156  $\mu$ M spin for 521 $\mu$ M protein with 3.75 mol Fe/ mol PFL-AE); g = 2.01, 1.948, 1.883. Conditions of measurement: T = 12 K; microwave power, 20  $\mu$ W; microwave frequency, 9.49 GHz; modulation amplitude, 9.571 G; single scan.

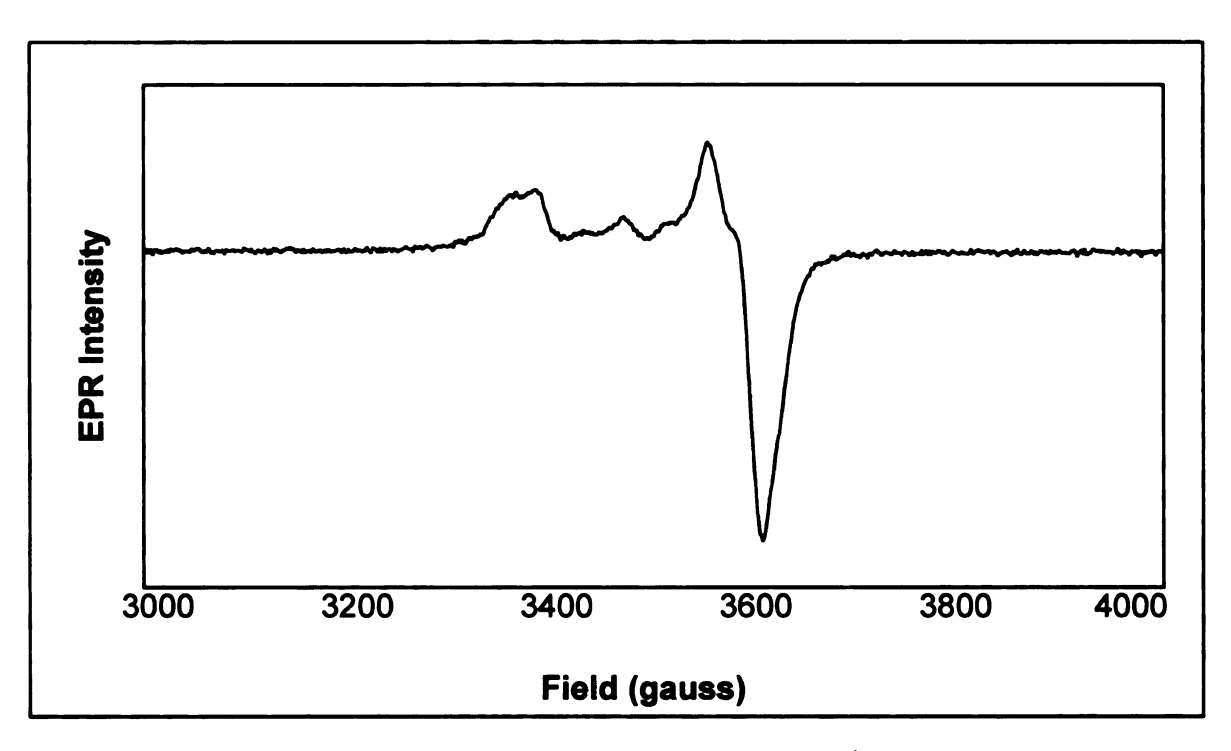


**Figure IV.8** X-band EPR spectrum of PFL-AE [4Fe-4S]<sup>†</sup> in the presence of α-D-AdoMet. The sample contained 650  $\mu$ M PFL-AE, 1 equivalent of Na<sub>2</sub>S<sub>2</sub>O<sub>4</sub>, 200  $\mu$ M 5-deazariboflavin, and 2 equivalents of α-D -AdoMet; 14.9 % reduction (based on 97.1  $\mu$ M spin for 650 $\mu$ M protein with 3.75 mol Fe/ mol PFL-AE); g = 2.01, 1.948, 1.889. Conditions of measurement: T = 12 K; microwave power, 20  $\mu$ W; microwave frequency, 9.49 GHz; modulation amplitude, 9.571 G; single scan.

**Figure IV.9** 35 GHz Mims pulsed-ENDOR spectra of PFL-AE with methyl-D<sub>3</sub>-AdoMet; (a) and (d) photoreduced sample; (b) cryoreduced sample. The spectra at  $g_{\perp}$  have been scaled to the height of the natural abundance <sup>57</sup>Fe peaks visible to higher frequency of the <sup>13</sup>C signals. Conditions: T = 2 K,  $\nu_{MW} = 34.8$  GHz, MW pulse lengths = 80 nS,  $\tau = 456$  ns, RF pulse length = 60  $\mu$ s, repetition rate = 30 Hz. Each spectrum consists of 256 points with each point an average of 240-300 transients. (c) and (e) Simulations (dashed lines) with dipolar **A** tensors. Closest <sup>2</sup>H: T = 0.6 MHz (corresponding to R = 3.1 Å for R = 1.0),  $R = 6 = 30^\circ$ ,  $R = 30^\circ$ , R =

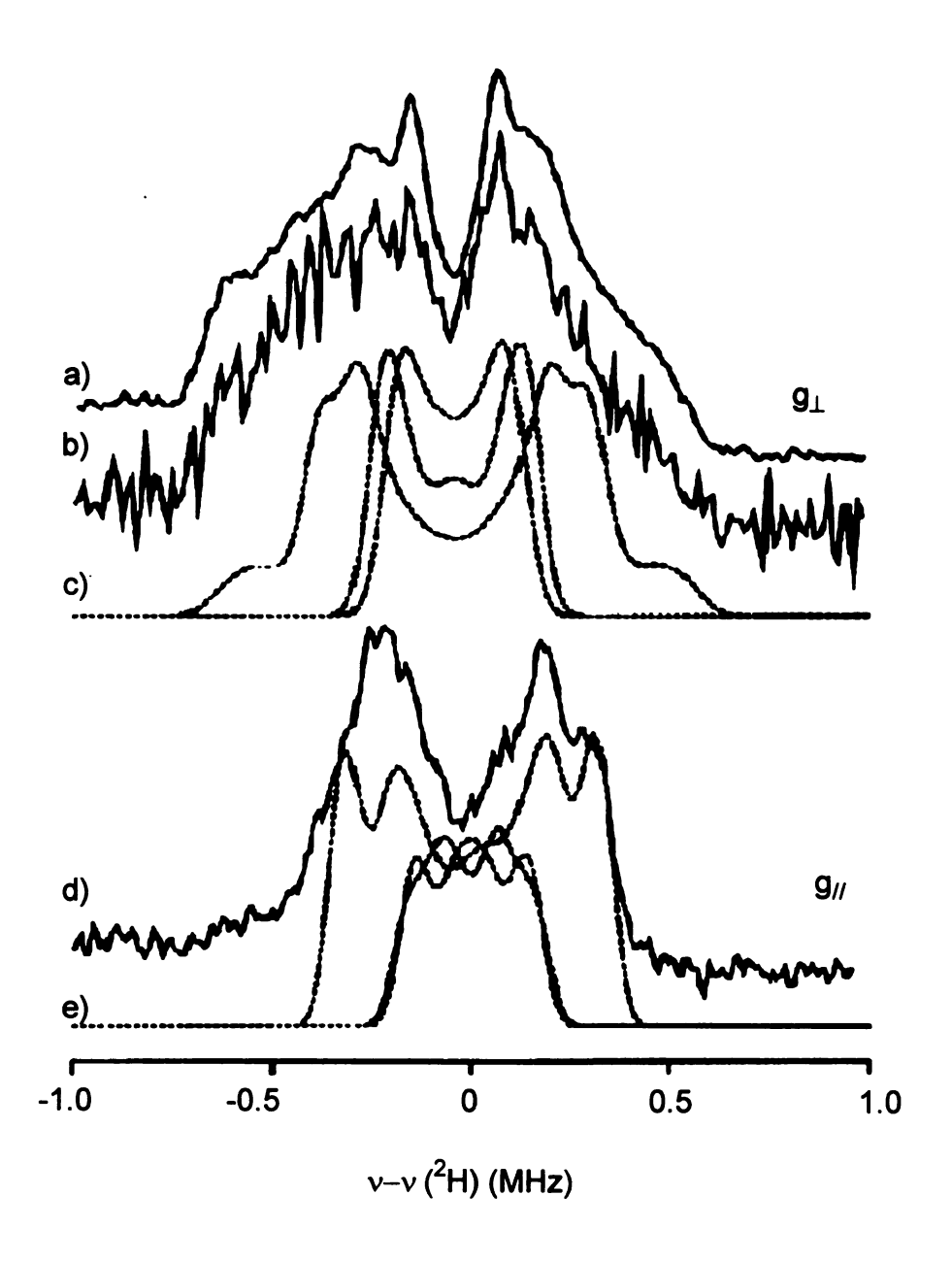
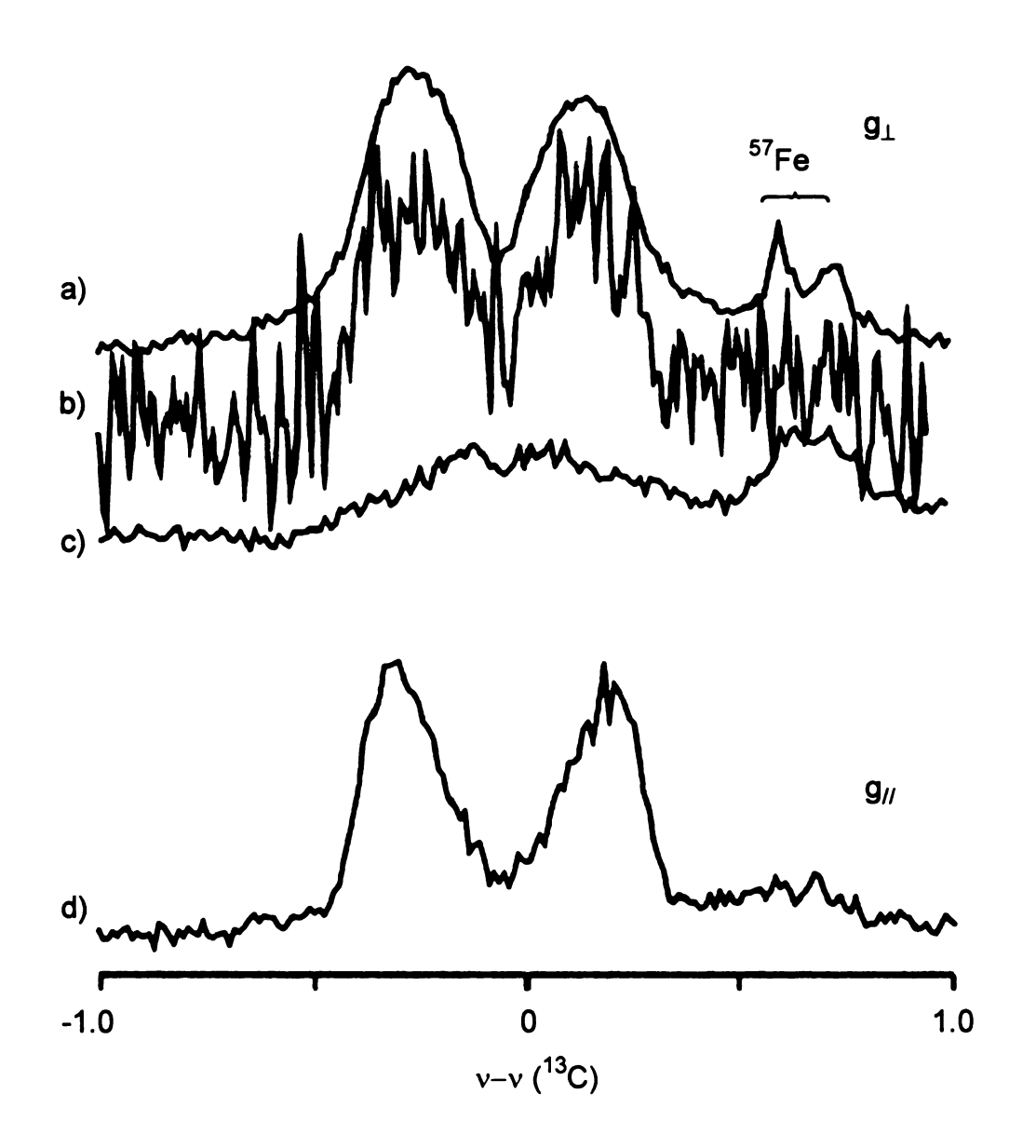


Figure IV.9



**Figure IV.10** 35 GHz Mims pulsed-ENDOR spectra of PFLAE (a) with methyl- $^{13}$ C-AdoMet, photoreduced, at  $\mathbf{g}_{\perp}$ , (b) with methyl- $^{13}$ C-AdoMet, (d) with methyl- $^{13}$ C-AdoMet, photoreduced, at  $\mathbf{g}_{\parallel}$ . Irradiated at 77 K, at  $\mathbf{g}_{\perp}$ (c) with natural abundance  $^{13}$ C-AdoMet at  $\mathbf{g}_{\parallel}$ . Experimental conditions as for Figure IV.9 except that  $\tau = 600$  nS and number of transients = 600.

g₁ and g<sub>||</sub>, Figure IV.9, both show a well-defined deuteron pattern that overlays a less-intense signal seen in the unlabeled [1+/AdoMet] sample, this ,latter is assigned to " $\Delta m = 2$ " transitions from weakly coupled <sup>14</sup>N, as seen in similar Fe-S clusters.<sup>52</sup> In the <sup>2</sup>H spectrum collected at g<sub>1</sub>, the breadth of the signal is 1.1 MHz, which, when corrected for unresolved <sup>2</sup>H quadrupole splitting of ~0.1 MHz (based on the known value for quadrupole coupling for CD<sub>3</sub>).<sup>53</sup> corresponds to a substantial <sup>1</sup>H coupling of ~6-7 MHz. For comparison, this coupling is approximately half that of water bound to a low-spin heme.<sup>54</sup> Such an interaction could not arise from an AdoMet bound at a remote site and influencing the cluster EPR spectrum by an allosteric process; at a minimum it requires the AdoMet lie adjacent to the cluster. That AdoMet binds with the same geometry to both the 1+ and 2+ clusters is confirmed by the <sup>2</sup>H ENDOR spectra of [2+/AdoMet]<sub>red</sub>, which is trapped in the geometry of [2+/AdoMet]. As illustrated in Figure IV.9, the <sup>2</sup>H spectra of [1+/CD<sub>3</sub>-AdoMet] and [2+/CD<sub>3</sub>-AdoMet]<sub>red</sub> are indistinguishable.

<sup>13</sup>C ENDOR spectra collected from [1+/<sup>13</sup>CH<sub>3</sub>-AdoMet] and [2+/<sup>13</sup>CH<sub>3</sub>-AdoMet]<sub>red</sub>, Figure IV.10, lead to identical conclusions. The two labeled samples exhibit identical hyperfine-split doublets centered at the <sup>13</sup>C Larmor frequency and arising from coupling to <sup>13</sup>C of the labeled AdoMet lying adjacent to the cluster. The spectra also show ENDOR signals from natural abundance <sup>57</sup>Fe. These are assigned to the  $\nu_+$  transition of a single iron with a coupling of A(<sup>57</sup>Fe) = 26 MHz, which is similar to that of the labile Fe site in aconitase ES (A(<sup>57</sup>Fe) = 29 MHz). The existence of this signal is useful because it provides a method for

normalizing spectra from natural abundance and <sup>13</sup>C-enriched samples, by scaling to the <sup>57</sup>Fe signal.

Field Dependence of <sup>13</sup>C ENDOR.

Details of the AdoMet binding have been obtained by analysis of the 2D patterns of 35 GHz Mims pulsed <sup>13</sup>C ENDOR spectra from [1+/<sup>13</sup>CH<sub>3</sub>-AdoMet] and <sup>2</sup>H spectra from [1+/CD<sub>3</sub>-AdoMet], each collected across the entire EPR envelope. Figure IV.11 presents the 2D set of Mims pulsed <sup>13</sup>C ENDOR spectra: at each field the spectrum is normalized to the 2-pulse electron-spin-echo (ESE) signal intensity. We note that with the value,  $\tau = 600$  ns, employed in the Mims ENDOR pulse sequence, the n = 1 "Mims suppression holes" fall sufficiently far from the <sup>13</sup>C Larmor frequency (holes at  $\Delta v$  (<sup>13</sup>C) =  $v\pm - v_C$  = ±0.833 MHz) that they do not significantly distort the observed  $^{13}$ C pattern. However the n=0"hole", centered at the <sup>13</sup>C Larmor frequency ( $\Delta v$  (<sup>13</sup>C) = 0 MHz) regardless of  $\tau$ , has a major impact on the observed signals and, as a result, it is essential to incorporate Mims suppression into the simulations. This procedure has not been thoroughly studied, and we find that the "simple" appearance of the Mims suppression holes can be altered by spin-diffusion effects. However, by simple incorporation of the Mims formula in the simulation program and by use of carefully normalized spectra, it is possible to analyze the experiments persuasively. In particular, by requiring the simulations to reproduce the relative peak intensities from field to field in the 2D pattern, as well as the frequencies, it is possible to characterize the dipolar part of the hyperfine interaction reasonably

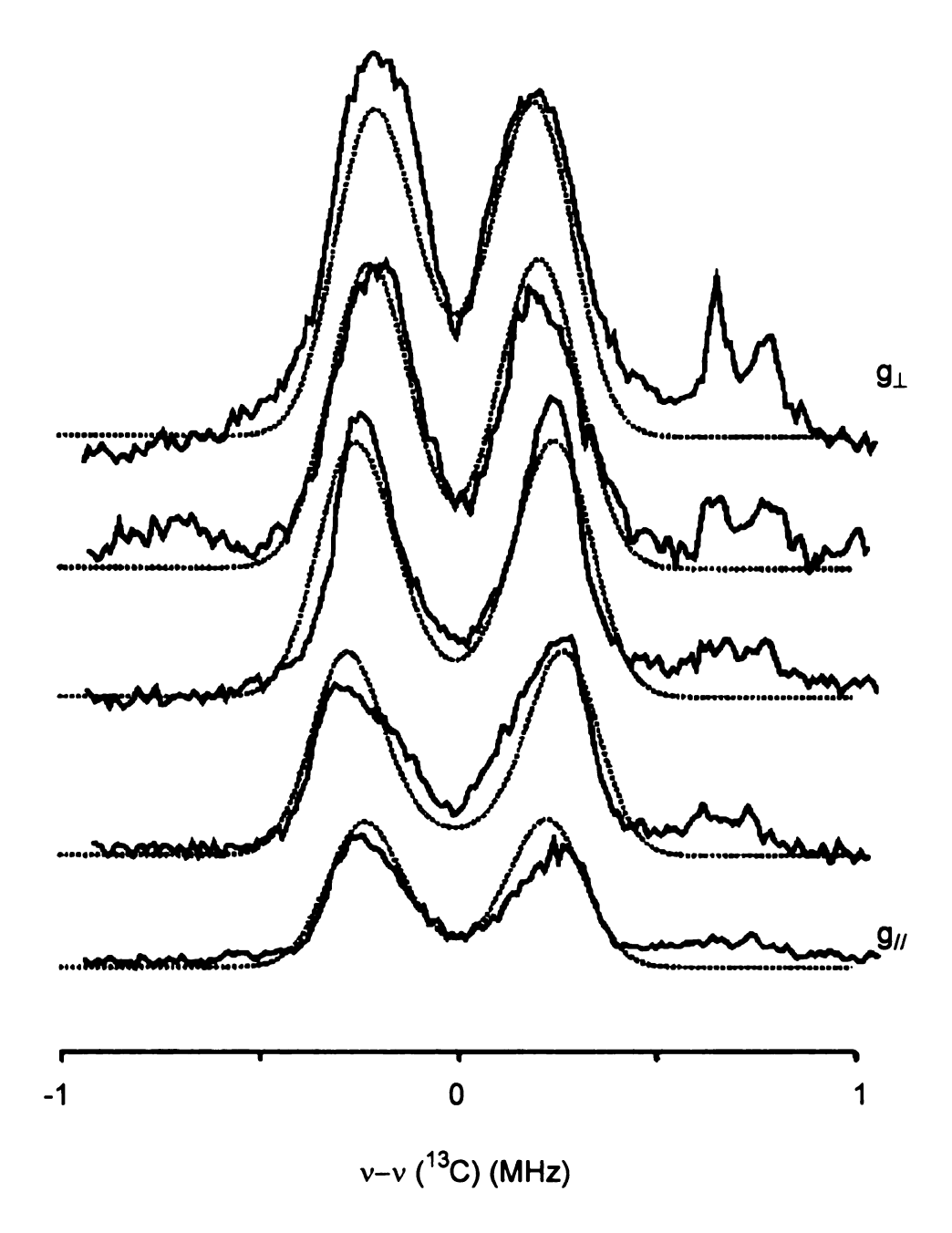


**Figure IV.11** Field dependence data with conditions as above (full line) and **simulation** (dashed line). Simulation parameters:  $\mathbf{A} = [-0.6, 0.4, -0.5]$ ,  $\alpha = \beta = 30^{\circ}$ ,  $\gamma = 0^{\circ}$ ; EPR line width = 170 MHz, ENDOR line width = 0.2 MHz;  $\tau = 600$  ns, **Mims** suppression effects included.

well; the attention to intensities is particularly important at fields and for orientations where the hyperfine coupling approaches zero and may change sign. As shown in Figure IV.11, through systematic efforts we obtained excellent simulations of the peak positions and intensities with a  $^{13}$ C hyperfine tensor that has principal values,  $\mathbf{A}(^{13}\text{C}) = [-0.6(1), +0.4(1.5), -0.5(1)]$  MHz and Euler angles relative to the g-tensor frame of  $\theta = 30^{\circ}$ ,  $\psi = 30^{\circ}$ . We note that although  $A_1$  and  $A_3$  do not appear to differ within error, the errors are correlated. To reproduce the curvature of the outer edges of the 2D plot,  $A_1$  must be ~0.1 MHz larger than  $A_3$ , and thus  $\mathbf{A}(^{13}\text{C})$  is constrained to be nonaxial.

The  $^{13}$ C tensor can be decomposed into the sum of an isotropic part,  $\mathbf{a}_{\mathrm{iso}}(^{13}\mathrm{C}) = -0.23$  MHz, and two, mutually perpendicular, dipolar tensors,  $\mathbf{T}(^{13}\mathrm{C}) = [-0.33, +0.66, -0.33] = [-7\mathrm{C}, 27\mathrm{C}, -7\mathrm{C}]$  MHz, and  $\mathbf{t}(^{13}\mathrm{C})$  ) [-0.03, -0.03, +0.06] = (-) [-t, -t, 2t] MHz. The former we assign to the through space dipolar interaction between the  $^{13}\mathrm{C}$  and spin of the cluster; the latter we assign to the "local" interaction with the spin on the  $^{13}\mathrm{C}$  itself whose presence is disclosed by the isotropic term. The hyperfine tensor, thus, can be decomposed into the "nonlocal" dipolar interaction with the cluster and a "local" term that arises from spin density on the  $^{13}\mathrm{C}$ ,  $\mathbf{A}(^{13}\mathrm{C})_{\mathrm{loc}} = -[\mid \mathbf{a}_{\mathrm{iso}}-(^{13}\mathrm{C})\mid \mathbf{1}+\mathbf{t}(^{13}\mathrm{C})]$ . The presence of spin density at the methyl group of AdoMet, as manifest in this local term, requires that AdoMet lie in contact with the cluster, weakly interacting with it through an incipient bond/antibond. The opposite signs of the through-space and local contributions suggests that the spin on the methyl carbon is not directly delocalized from the

cluster but involves spin polarization through an intervening atom, presumably the sulfonium sulfur of AdoMet.

The nonlocal through-space coupling tensor, T, contains information about the geometry of AdoMet binding. The dipole interaction between the cluster and nucleus j of AdoMet, here the <sup>13</sup>C of the labeled methyl, can be written as,

$$H_{HF} = \hat{S} \cdot \sum_{i} T_{j} \cdot \hat{I}_{j}$$

where

$$T_{j} = g_{e} \beta_{e} g_{N}^{j} \beta_{N} \sum_{i=1}^{4} \frac{K_{i}}{r_{ij}^{3}} t_{ij} \approx \frac{g_{e} \beta_{e} g_{N}^{j} \beta_{N}}{r_{kj}^{3}} K_{k} t_{kj} \equiv T_{j} t_{kj}$$

$$\tag{4}$$

Here  $K_i$  is the spin-projection coefficient for  $Fe_i$  of the spin coupled S=1/2 cluster, the  $Fe_i$ -Nuc<sub>j</sub> distance is  $r_{ij}$ , and  $\mathbf{t}_{kj}$  is the dimensionless through-space electron-nuclear dipolar matrix. Calculations indicate that only the dipole coupling to the nearest iron ion, k, need be considered to a first approximation, as indicated in equation 4, and hence the dipole coupling to nucleus j is characterized by the parameter,  $T_j \equiv g\beta g_N^j \beta_N K_k r_{jk}^3$ .

The determination of  $r_{C-k}$  from the parameter  $T_C$  for the <sup>13</sup>C -methyl requires knowledge of  $K_k$ . Mössbauer spectroscopic studies of [1+(AdoMet)] in progress do not yet provide the  $K_i$  for the four Fe ions, and therefore we consider the known spin coefficients of the 1+ cluster of substrate-bound aconitase (ES), which also has a labile, noncysteine cluster ligand; these are |K| = 0.86, 1.57, 1.60, and 1.78.<sup>55</sup> When interpreting the <sup>13</sup>C dipolar interaction constant,  $T_C = 0.33$ 

MHz, in this way, the point-dipole-calculated distance between the methyl  $^{13}$ C and Fe<sub>k</sub> of the cluster then would take one of four rather well-defined distances, depending on which value of K is associated with Fe<sub>k</sub>; these are listed in Table IV.2. The range of possible values for  $r_{C-k}$  given the uncertainties in the simulations and including the full range for the values of K then spans the range  $\sim$ 4-5 Å (Table IV.2).

К	r( <sup>2</sup> H-Fe <sub>n</sub> ) - 10% uncertainty in T	r( <sup>13</sup> C-Fe <sub>n</sub> ) - range in T from simulation
1.78	3.8 ± 0.1	5.0 ± 0.6
1.60	3.7 ± 0.1	4.9 ± 0.6
1.57	3.6 ± 0.1	4.9 ± 0.6
0.86	3.0 ± 0.1	4.0 ± 0.6

**Table IV.2** T values derived from the dipolar interpretation of the <sup>2</sup>H ENDOR data.

Field Dependence of 2H ENDOR.

The  $^2$ H and  $^{13}$ C ENDOR data have been tested for self-consistency by analysis of the 2D set of 2H Mims pulsed ENDOR spectra collected for [1+/CD<sub>3</sub>-AdoMet]. Figure IV.9 includes the spectra at both  $\mathbf{g}_{\perp}$  and  $\mathbf{g}_{\parallel}$ ; the intervening

spectra (not included) show that the breadth of the pattern decreases monotonically from  $\textbf{g}_{\perp}$  to  $\textbf{g}_{\parallel}.$  The deuteron spectrum is not highly resolved but the hyperfine splitting at  $\mathbf{g}_{\perp}$  is roughly twice that of the splitting at  $\mathbf{g}_{||}$ . For a CD<sub>3</sub> moiety, the maximum  $^{2}$ H quadrupole coupling is only  $P \sim 0.1 \text{ MHz}^{53}$  and for a  $^{2}$ H spectrum as broad as that shown in Figure V.9, the shape is dominated by the hyperfine interaction to the three deuterons (i = 1-3). The spectra are compatible with a surprisingly simple model in which the AdoMet is bound alongside the cluster and the outer features of the CD<sub>3</sub> ENDOR response are governed by the through-space dipolar interaction between the closest methyl deuteron and the spin density on a single Fe ion of the cluster; the inner part of the pattern is filled in by intensity from the other two methyl-group deuterons. The outer features of the field-dependent <sup>2</sup>H pattern can be modeled by the interaction of one deuteron with a single iron  $Fe_k$  where the C-D1 bond points at  $Fe_k$  with the dipole coupling parameter,  $T_D = g\beta g\beta_v K_n/r_{D-k}^3 = 0.60$  MHz. The calculated point-dipole distance between the closest methyl deuteron and the  $Fe_k$  of the cluster again take one of four rather narrowly defined distances that span the range ~3.0-3.8 A. Contributions from the more remote deuterons were calculated under the constraint of this location for D1 and tetrahedral geometry around the methyl carbon, along with simple assumptions as to the orientation of the AdoMet; it also depends somewhat on the choice of  $K_k$ . As shown by the calculated spectra in Figure IV.9, the data can be represented by summing the contributions from the three methyl deuterons calculated in this fashion. The parameters used for the calculations are given in the legend to Figure IV.9.

While the analysis for the <sup>13</sup>C is robust, the analysis for the deuterons is not unique, however. This is because the behavior of the D1 pattern cannot be well modeled at small couplings due to unavoidable uncertainties about the contributions from the D2, D3 signals, and the effects of the n = 0 "Mims hole". Thus, the spectra can be fit with an alternate model for D1 in which an isotropic coupling makes a significant contribution to the <sup>2</sup>H observed pattern. While such simulations themselves are not unique, a representative simulation that describes the outer spectral features utilized a tensor, A = [0.3, 0.3, 1.0] MHz, corresponding to an isotropic coupling a = 0.53 MHz and an anisotropic contribution of the form [-0.23, -0.23, 0.47] MHz. In this model, the lack of resolution in the small coupling region of the <sup>2</sup>H spectra again is attributed to the presence of signals from the other two deuterons which, although chemically equivalent, would have different isotropic couplings. The isotropic coupling to deuteron j likely varies as  $\cos^2 \theta_i$ , where  $\theta_i$  is the dihedral angle between the  $\pi$ orbital on S that acquires spin from the cluster and the  $C-D_i$  bond.<sup>56</sup> For example, if D1 has the maximum possible coupling ( $\theta$ = 0), the other two will have 4-fold smaller values ( $\theta = \pm 2\pi/3$ ,  $\cos^2 \theta = 1/4$ ), thus contributing intensity near the center of the spectrum as required by experiment.

In principle, one might hope to distinguish between the two models by examining the modulation depth of the  $^2$ H ESEEM time-domain trace at X-band frequencies. However, attempts to do this were not successful. While the quality of the simulations based on the two models is similar, there are some grounds for preferring one of them. As shown in Table IV.1, the values of  $T_C$  and of  $T_D$ 

derived from the dipolar interpretation of the  $^2$ H data yield a model where the C-D1 bond (bond length of  $\sim 1$  Å) points toward Fe<sub>k</sub>. The "isotropic" model of the  $^2$ H 2D pattern yields a correspondingly diminished  $T_D$  that corresponds to a value of  $r(^2$ H-Fe<sub>k</sub>) that, however, is comparable to that of  $r(C-Fe_k)$ . Thus, we favor the purely dipole model as the better approximation. However, the  $r(D1-Fe_k)$  predicted from the value of  $T_D$  derived from the model with substantial isotropic  $^2$ H coupling are close to those for  $r(^{13}C-Fe_k)$ ; for example, for the covalent model, choosing the K values in descending order produces distances of 4.5, 4.4, 4.3, and 3.5 Å, all of which are within the range of the distances deduced for  $r(^{13}C-Fe_k)$ .

IV.3.3 Coordination of S-Adenosylmethionine to the Unique Iron Site Interaction with the Catalytically Essential Reduced State.

The catalytically essential  $[4Fe-4S]^+$  (S = 1/2) cluster of PFL-AE is EPR-active, as shown above, and this allowed us to use electron-nuclear double resonance (ENDOR) spectroscopy to define the interaction of SAM with the [4Fe-4S] cluster of PFL-AE, which, in turn, provides important insights into the mechanism of radical generation.  $^{32,57}$  To investigate the possibility of coordination of SAM to the unique site of the [4Fe-4S] cluster of PFL-AE, we prepared isotopically labeled S-adenosylmethionine in order to probe the coupling between the paramagnetic iron sulfur cluster and specific nuclei on SAM. The amino and carboxylate moieties of SAM were the most likely

candidates for coordination to the unique iron site, so SAM was synthesized with <sup>17</sup>O at the carboxylate oxygen, with <sup>13</sup>C at the carboxylate carbon, and with <sup>15</sup>N at the amine nitrogen.<sup>57</sup> Each labeled SAM was added to photoreduced [4Fe-4S]<sup>+</sup>-PFL-AE, and the solutions were frozen for ENDOR measurements. The observation of ENDOR signals for all three nuclei (Figure IV.12) demonstrated for the first time that SAM forms a classical five-membered chelate ring with the unique iron of the [4Fe-4S] cluster of PFL-AE. The <sup>17</sup>O (12.2 MHz) and <sup>13</sup>C (0.71 MHz) couplings observed in the PFL-AE/SAM complex are very similar to those found for aconitase with carboxylate-labeled citrate/isocitrate.<sup>26,31</sup> The strong couplings support direct coordination of a carboxylate oxygen of SAM to the unique iron in PFL-AE, as was also seen in the aconitase enzyme-substrate complex. The <sup>15</sup>N coupling (5.8 MHz) is comparable to those observed for <sup>15</sup>N ligands in other enzyme systems (15N-histidine bound to the Rieske [2Fe-2S] cluster<sup>58</sup> and <sup>15</sup>N-ACC (ACC = 1-aminocyclopropane-1-carboxylic acid) coordinated to the non-heme iron of ACC oxidase)<sup>59</sup> and again is consistent with direct coordination.

Field-Dependence of the <sup>13</sup>C, <sup>17</sup>O, and <sup>15</sup>N ENDOR Data

<sup>2</sup>D field-frequency plots of ENDOR spectra collected across the EPR envelope were obtained from photoreduced [4Fe-4S]<sup>+</sup>-PFL-AE in the presence of (i) carboxyl-<sup>13</sup>C- SAM (ii) carboxyl-<sup>17</sup>O-SAM, and (iii) amino-<sup>15</sup>N-SAM. Simulation of the 2D patterns allowed determination of the details of the coordination of the methionine fragment of SAM to the unique iron of the [4Fe-4S] cluster. We

**Figure IV.12.** 35-GHz pulsed ENDOR spectra of PFL-AE with (a)  $^{17}$ O and (b)  $^{13}$ C carboxylato-labeled and (c)  $^{15}$ N-amino-labeled AdoMet compared with data from an unlabeled sample, at  $g_{\perp}$ Conditions: T = 2 K. (a)  $^{17}$ O labeled, Davies ENDOR.  $\nu_{MW} = 34.9$  MHz; microwave pulse lengths = 80, 40, 80 ns; RF pulse length ) 60 ms. Number of averaged transients at each point:  $^{17}$ O, 288; unlabeled, 200. (b)  $^{13}$ C-labeled, Mims ENDOR.  $\nu_{MW} = 34.8$  MHz, microwave pulse lengths = 80 ns,  $\tau$  = 552 ns, RF pulse length = 60 ms. Number of averaged transients:  $^{13}$ C-labeled, 144; unlabeled, 600. (c)  $^{15}$ N-labeled, Davies ENDOR.  $\nu_{MW} = 34.9$  MHz; microwave pulse lengths = 80, 40, 80 ns; RF pulse length = 60 ms. Number of average transients:  $^{15}$ N-labeled, 80; unlabeled, 624.

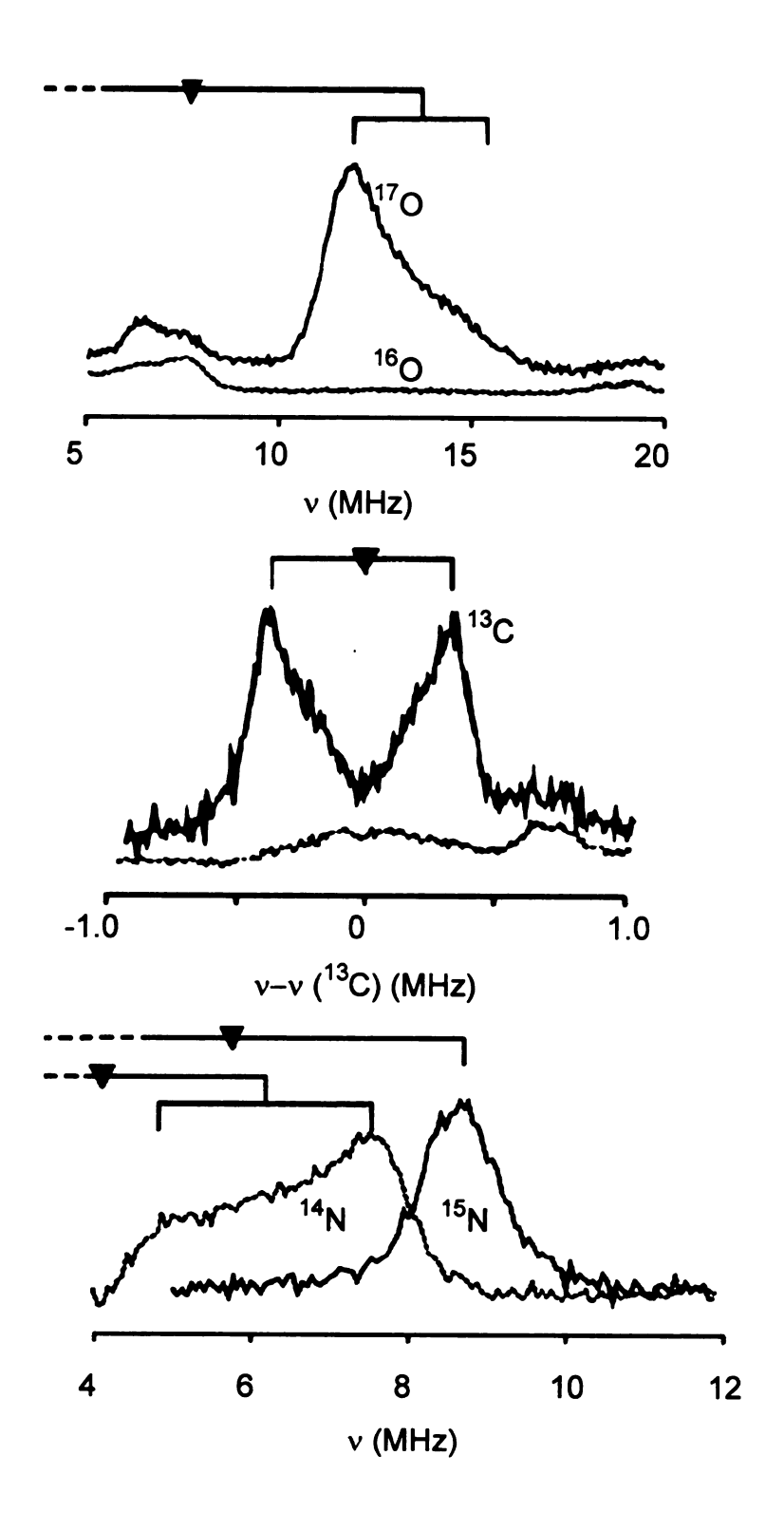
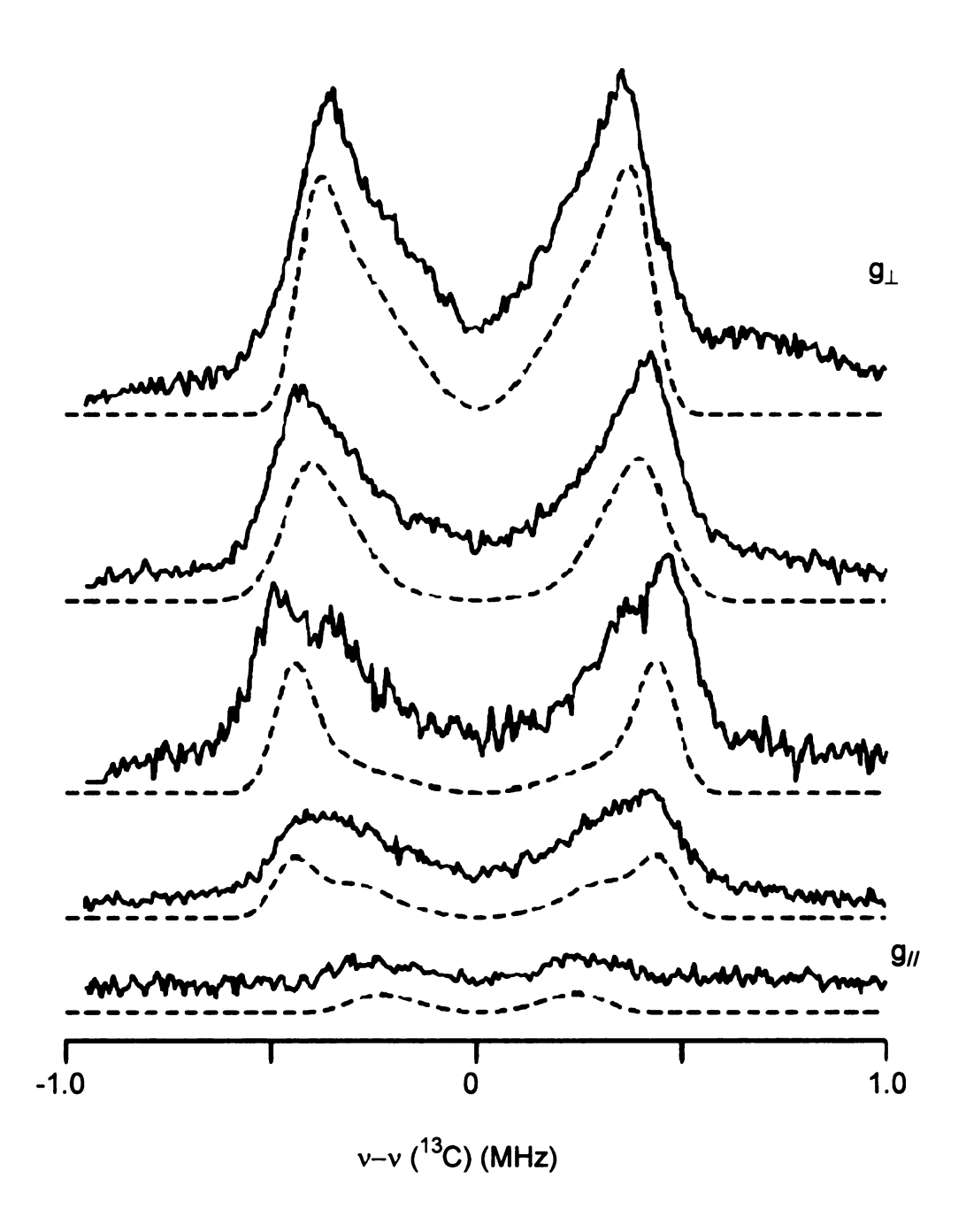


Figure IV.12

reported previously that large <sup>17</sup>O and <sup>15</sup>N couplings observed in the presence of (ii) and (iii) indicate direct coordination of SAM to the unique iron via a fivemembered-ring chelate.<sup>57</sup> Analysis of the field dependence of these interactions as well as the carboxyl-13C interaction allows a full analysis of the geometry and bonding of SAM to the 4Fe-4S cluster. (i) Carboxyl-<sup>13</sup>C-SAM. Figure IV.13 presents the 2-D Mims pulsed <sup>13</sup>C ENDOR patterns for [4Fe-4S]<sup>+</sup>-PFL-AE (reduced photolytically) with carboxyl-<sup>13</sup>C-SAM. The signal intensities have been normalized to the height of the electron spin-echo to enable analysis of the effect of signal suppression from the Mims pulse sequence used in these experiments. As explained in the Experimental Methods although Mims pulsed ENDOR spectroscopy is the best method for measuring small couplings, there is a suppression "hole" with zero ENDOR intensity at the Larmor frequency (in this case,  $\Delta v$  (<sup>13</sup>C) = 0 MHz), corresponding to A = 0. This masks the difference between isotropic hyperfine interactions, which do not produce spectral intensity near A = 0, and dipolar interactions, which do so for certain orientations. The isotropic interaction and local contributions to the anisotropic interaction are useful for determining bonding and delocalization, while the nonlocal dipolar interactions between an electron spin and a nucleus not involved in spin delocalization can be used to determine the electron-nuclear distance and the orientation of the nucleus within the g-tensor coordinate frame. Using a procedure similar to that applied in the analysis of the <sup>13</sup>C ENDOR spectra from [4Fe-4S]<sup>+</sup>-PFLAE with <sup>13</sup>CH<sub>3</sub>-SAM, <sup>32</sup> we simulated both the spectral shapes and the intensities to obtain the  $^{13}$ C hyperfine tensor:  $A(^{13}$ C) = [-1.1, 0.95, 0.82] MHz



**Figure IV.13.** Field dependence data (s) and simulations (---) from 35-GHz Mims pulsed ENDOR of PFL-AE with carboxy-<sup>13</sup>C-SAM, with conditions as in Figure IV.12. Simulation parameters: **A** = [1.1, -0.95, -0.82],  $\alpha$  = 30,  $\beta$ =  $\gamma$  = 90, EPR line width = 120 MHz, ENDOR line width = 0.1 MHz,  $\tau$  = 562 ns. Mims suppression effects are included.

and Euler angles, relative to the *g*-tensor frame, of  $\theta$ = 30°, and  $\varphi$  = 0°. The <sup>13</sup>C tensor can be decomposed into the sum of an isotropic component,  $a_{iso}(^{13}C)$  = 0.22 MHz, and two mutually perpendicular dipolar tensors,  $T(^{13}C)$  = [-2T, T, T] = [-1.28, 0.64, 0.64] MHz and  $t(^{13}C)$  = [t, -2t, t] = [-0.04, 0.09, -0.04] MHz. The first of these is assigned to the through-space dipolar interaction between the cluster spin and the <sup>13</sup>C nucleus. The latter is derived from a local interaction with electron spin density on the carbon atom itself with the <sup>13</sup>C nucleus. This anisotropic term is correlated with the isotropic coupling as the spin on carbon is in an sp<sub>n</sub> hybrid, with the p-orbital contribution giving the former and the s-orbital contribution the latter. From  $T(^{13}C)$ , we can approximate  $r(Fe(unique)-^{13}C)$  by neglecting any interaction with spins on other atoms of the cluster, assuming a point-dipole- point-dipole interaction, and taking n = 3, which gives

$$T = g\beta g_N \beta_N K \frac{\left(\frac{3}{4}\right)}{r(Fe^{-13}C)^3}$$
 (5)

where the constant terms have their usual meaning and K is the spin projection coefficient for the unique Fe of the spin coupled S = 1/2 cluster. Although the values of K for PFL-AE are not known, it is reasonable to use the known coefficients of substrate-bound aconitase (ES), which also has a labile, noncysteine cluster ligand: K = 1.57. This gives Fe(unique)- $^{13}$ C) = 3.3 ± 0.1 Å.

There is as yet no crystal structure of PFL-AE, but there are reports of crystal structures from three other members of the radical-SAM superfamily.

These are (i) coproporphyrinogen III oxidase (HemN). 60 (ii) biotin synthase (BioB), 61 (iii) the ligand binding protein MoaA. 62 Comparison of the structures of these three proteins reveals that the geometry of SAM binding is similar in each case. The distance from the unique Fe to the carboxyl carbon of bound SAM is in the range of 2.92-3.15 Å. Considering the crudeness of the ENDOR estimate, it is in quite satisfactory agreement. (ii) Carboxyl-17O-SAM, and (iii) Amino-15N-SAM. Figures IV.14 and IV.15 present 2D field-frequency ENDOR patterns for these two nuclei, along with simulations of these patterns calculated with programs ENDORSIM for <sup>15</sup>N<sup>63</sup> and GENDOR for <sup>17</sup>O.<sup>64</sup> As shown, the patterns are well reproduced by simulations that use tensors with significant isotropic components  $(a_{iso}(^{15}N) = 6.4 \text{ MHz}, a_{iso}(^{17}O) = 10.7 \text{ MHz})$ , as expected for direct coordination to an Fe of the reduced Fe-S cluster. Taking into account the couplings expected for unit spin in the 2s orbitals of a <sup>15</sup>N and <sup>13</sup>C, these correspond to comparable low spin densities, ~1% for sp<sub>3</sub> orbitals. However, the <sup>15</sup>N dipolar tensor is highly rhombic, whereas the dipolar component of the hyperfine interaction with <sup>17</sup>O is nearly axial, an indication of the expected difference in hybridization of the two atoms.

### IV.4 Conclusion

PFL-AE has been shown to utilize the [4Fe-4S]<sup>+</sup> state of the cluster to catalyze the reductive cleavage of AdoMet and subsequent generation of the glycyl radical of PFL.<sup>29</sup> During this catalytic turnover, the [4Fe-4S]<sup>+</sup> cluster is oxidized to [4Fe-4S]<sup>2+</sup>, thereby indicating that the cluster is the source of the

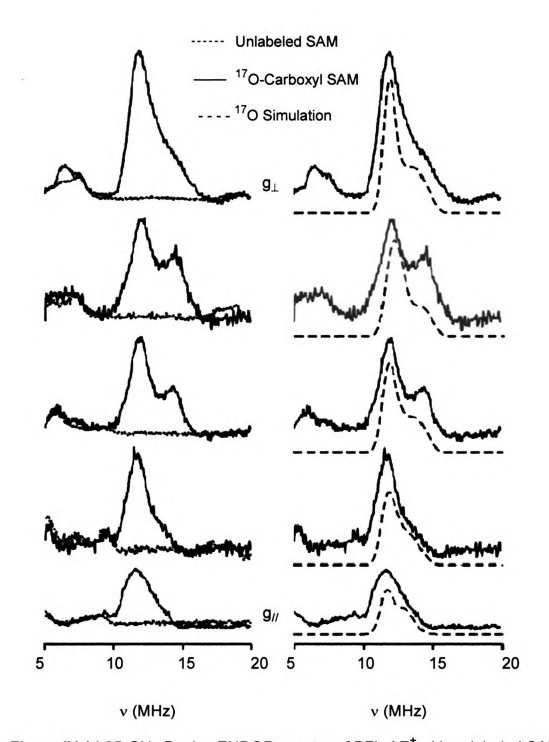


**Figure IV.14** 35-GHz Davies ENDOR spectra of PFL-AE\* with unlabeled SAM and with  $^{17}\text{O-carboxyl}$  SAM. Left: Comparison of ENDOR from  $^{17}\text{O-labeled}$  and unlabeled SAM. Right:  $^{17}\text{O}$  ENDOR and simulations. Experimental conditions: T=2 K; Davies pulse sequence; microwave pulse lengths = 80, 40, 80 ns; repetition rate = 100 Hz; RF pulse length = 60 ms.  $^{17}\text{O}$  Simulation parameters: Program GENDOR, **A** = [8.6, 14.4, 8.2],  $\alpha$  = 30,  $\beta$  =  $\gamma$  = 0, **P** = [-0.05. 0.1, -0.05],  $\alpha$  = 30,  $\beta$  =  $\gamma$  = 0, ENDOR line width = 0.5 MHz, EPR line width = 100 MHz.

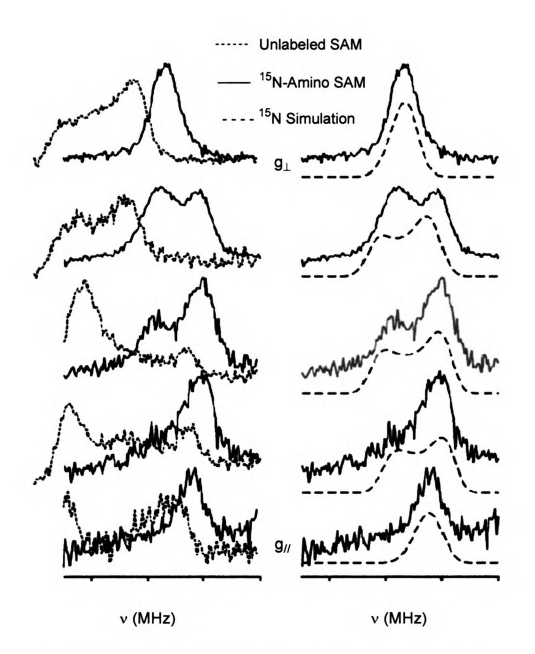


**Figure IV.15.** 35-GHz Davies ENDOR of PFL-AE<sup>+</sup> with unlabeled SAM and with  $^{15}$ N-amino SAM. Left: Comparison of  $^{14}$ N and  $^{15}$ N ENDOR. Right:  $^{15}$ N ENDOR and simulations. Experimental conditions: T=2 K; Davies pulse sequence; microwave pulse lengths = 80, 40, 80 ns; repetition rate = 100 Hz; RF pulse length = 60 ms.  $^{15}$ N Simulation parameters: Program ENDORSIM, **A** = [9.7, 6, 3.5],  $\alpha$  = 0,  $\beta$  = 30,  $\gamma$  = 0, ENDOR line width = 0.8 MHz. EPR line width = 300 MHz.

electron necessary for reductive cleavage of AdoMet. Taken at face value, these results might suggest that the iron sulfur cluster in PFL-AE is serving a simple electron-transfer role, much like the iron-sulfur clusters found in numerous electron-transfer proteins. Indeed, such a role has been proposed for the iron-sulfur cluster in the related anaerobic ribonucleotide reductase activating enzyme. However, it is also possible that the redox chemistry is occurring not by remote electron transfer, but through covalent chemistry between the cluster and AdoMet. As a first step toward probing the details of the mechanism of radical generation by PFL-AE, we have investigated the interaction between AdoMet and the iron-sulfur cluster of PFL-AE. Significantly, it is possible to probe the interaction of AdoMet with the catalytically active [4Fe-4S]<sup>+</sup> of PFL-AE, because PFL-AE/[4Fe-4S]<sup>+</sup> does not reductively cleave AdoMet in the absence of PFL 29.66

Initial evidence that AdoMet might be closely associated with the cluster was provided by EPR spectroscopy in Figure IV.2: the presence of AdoMet produces a clear effect on the EPR signal of the [4Fe-4S]<sup>+</sup> state of PFL-AE, causing the distinctly rhombic signal to become nearly axial. Such a dramatic change in the EPR signal of the cluster would be consistent with AdoMet coordinating to an iron of the cluster or otherwise closely associating with the cluster. A change in signal such as that observed in Figure IV.2, however, also could be explained if AdoMet binds at a remote site and causes changes in the cluster through allosteric interactions. The EPR spectrum of the [2+/AdoMet]<sub>red</sub> is

identical to that of [1+/AdoMet], indicating that the AdoMet binds in the same fashion to both 1+ and 2+ states.

To determine the nature of AdoMet binding to the 2+ and 1+ states of PFL-AE, we have carried out <sup>2</sup>H and <sup>13</sup>C ENDOR studies of specifically labeled AdoMets bound to the enzyme. Since the catalytic turnover of AdoMet involves chemistry occurring at the sulfonium center, we reasoned that atoms in the vicinity of the sulfonium are most likely to be located close to the cluster, and thus AdoMet labeled at the sulfonium methyl was used in this study. The observation of substantial <sup>2</sup>H and <sup>13</sup>C hyperfine couplings from labeled AdoMet bound to the 1+ cluster of PFL-AE clearly demonstrates that AdoMet binds adjacent to the 4Fe cluster as shown in Figure IV.9 and Figure IV.10. Moreover. the observation of identical spectra from the 1+ and cryoreduced 2+ enzyme further shows that the position of AdoMet relative to the Fe-S cluster in PFL-AE is identical in the oxidized and reduced states. Modeling of the dipolar interactions between the cluster and the methyl-13C and -2H of AdoMet shows that the methyl group of AdoMet is quite close to one of the irons of the cluster, as close as ~3.0 Å for the methyl proton and no more than ~4-5 Å for the methyl carbon, with the calculated value dependent on the identity of the nearby Fe. Most intriguinaly, the existence of an isotropic contribution to the <sup>13</sup>C tensor requires that there be overlap between orbitals on the cluster and on AdoMet, namely, that there are incipient covalent interactions between AdoMet and the cluster. The most plausible interpretation is that this interaction is of a dative character, between a

negatively charged sulfide of the cluster and the positively charged sulfur of AdoMet, as shown in Figure IV.16.<sup>32</sup>

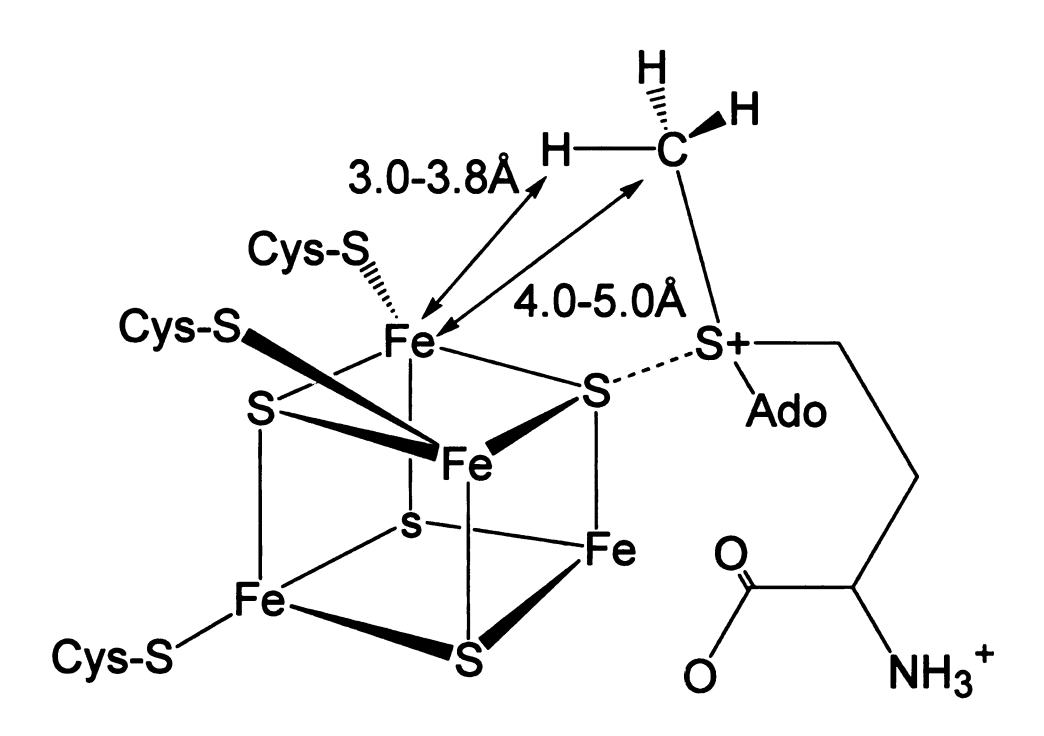


Figure IV.16 Model for the Interaction of AdoMet with the [4Fe-4S] of PFL-AE

An alternative model for the interaction of AdoMet with the cluster would involve a direct coordination of the sulfonium of AdoMet to an iron of the cluster. This would be analogous to the recent proposal by Cosper and co-workers for lysine aminomutase, in which the sulfonium of AdoMet is poised near (but not coordinated to) the unique iron site of the cluster, and where the Met formed by reductive cleavage coordinates to the unique site.<sup>30</sup> We disfavor this model for PFL-AE primarily for two reasons. First, we see no evidence for a nearby iron in Xe-XAS spectra of PFL-AE[4Fe-4S]<sup>+</sup>/SeSAM or PFL-AE[4Fe-4S]<sup>2+</sup>/SeSAM.<sup>67</sup>

Se-AdoMet has been proposed to be an effective probe in studying the interaction of the sulfonium center of AdoMet with the Fe-S cluster of PFL-AE. Se-AdoMet, the substrate analogue, and selenomethionine (Se-Met), the cleaved product analogue, along with the [4Fe-4S] clusters of PFL-AE at different oxidation states were used to mimic the enzyme-substrate (ES) and enzymeproduct (EP) complexes, and to follow the course of the cleavage reaction by a variety of spectroscopic methods, including EPR, XAS, ENDOR and ESEEM. However, none of the samples prepared of PFL-AE in the presence of Se-AdoMet displayed a Se-Fe interaction in Se K-edge XAS. Incubation of the [4Fe-4S]<sup>2+</sup> cluster of PFL-AE with Se-Met, Se-Met / 5'-dAdo, and Se-Met / 5'-dAdo / PFL yielded Se-edge and FT spectra that were similar to that of Se-Met alone. The spectrum of [4Fe-4S]<sup>2+</sup> of PFL-AE with Se-AdoMet was similar to that of Se-AdoMet alone. This observation that the selenium compounds maintained their initial structures was expected though, since the [4Fe-4S]<sup>2+</sup> cluster is not the catalytically relevant cluster, and therefore should not react with AdoMet. The samples prepared with the pre-reduced cluster of PFL-AE showed very little enzymatic turnover in the presence of Se-AdoMet upon the addition of PFL. This could be attributed to reaction of the PFL-AE [4Fe-4S] with Se-AdoMet prior to mixing with PFL. No Se-Fe interaction was observed in this sample, indicating that Se-Met does not coordinate to the cluster after turnover. <sup>67</sup>

Second, Noodleman and Case have shown by using DFT methods that most of the increased electron density associated with going from a 2+ to a 1+ cluster resides on the sulfide and cysteinal sulfurs, with very little being

associated with the irons of the cluster.<sup>68</sup> The significantly larger electron density and partial negative charge at the sulfurs of the cluster, corresponding to partial positive charge at the irons, suggests that the positively charged sulfonium would prefer to interact with a sulfide. The electron density changes at sulfur proposed by Noodleman and Case also point to the likelihood of sulfur-based, rather than iron-based, redox chemistry in iron-sulfur clusters. 68 The ENDOR results presented here do not preclude the possibility of an Fe-sulfonium interaction in PFL-AE such as proposed in LAM. However, it should be noted that in LAM, AdoMet functions as a reversibly cleaved cofactor, while in PFL-AE, AdoMet acts as a substrate that undergoes irreversible C-S bond cleavage. Any apparent differences in the mode of interaction of AdoMet with the cluster in PFL-AE and LAM may simply reflect the differences in the roles of AdoMet. If, as we are proposing here, the sulfonium of AdoMet interacts with a sulfur, not an iron of the cluster, then what is the role for the unique (noncysteine-coordinated) iron site that appears to be conserved among these enzymes?

Partly on the basis of electrostatics and partly on the precedent with aconitase, <sup>24-26</sup> we proposed that the methionine carboxylate of AdoMet coordinates to the unique iron, displacing whatever ligand is present in the absence of AdoMet. Additional results reported here from our ENDOR investigation indicated that the methionine end of AdoMet forms a five-membered-ring chelate to the unique Fe of the [4Fe-4S] cluster of PFL-AE, with the amino nitrogen and one carboxylate oxygen as ligands to this Fe. This is reminiscent of the amino acid ACC chelating the non-heme Fe of ACCO,

although this is the first example of such coordination on an iron-sulfur cluster. This interaction "anchors" the nonreacting end of AdoMet, thereby positioning the substrate in the proper configuration for the subsequent radical chemistry with the cluster at the reactive end of AdoMet as shown in Figure IV.17. As discussed above, this active configuration likely involves a close interaction of the AdoMet sulfonium and a  $\mu$ -3 bridging sulfide of the cluster, an interaction that may provide a pathway for inner-sphere electron transfer from the cluster to the

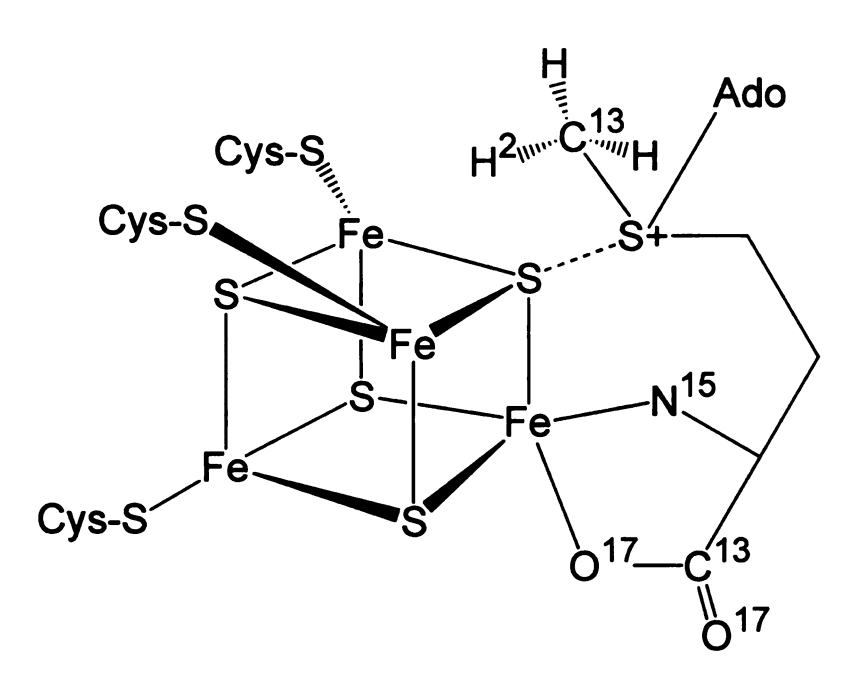


**Figure IV.17** AdoMet forms a classical N/O chelate with the unique iron site of the [4Fe-4S] cluster of PFL-AE.

AdoMet. The site-differentiated [4Fe-4S] cluster of PFL-AE appears to be conserved throughout the Fe-S/AdoMet family, as all members have the same three cysteine (CX<sub>3</sub>CX<sub>2</sub>C) cluster binding motif.

Taken together, the spectroscopic results presented herein provide significant insight into the mechanism by which PFLAE, and more generally, all of the radical-SAM enzymes, initiate radical catalysis using an iron-sulfur cluster and S-adenosylmethionine as shown in Figure IV.18. As illustrated through EPR-detected single-turnover experiments, PFL-AE utilizes a reduced [4Fe-4S]<sup>+</sup>

**Figure IV.18** Proposed mechanism for iron-sulfur cluster and SAM-mediated radical generation catalyzed by PFL-AE.

cluster in catalysis, and this cluster is the source of the electron required for reductive cleavage of SAM and subsequent generation of the glycyl radical in PFL. Mössbauer spectroscopy was used to identify a unique iron site in the [4Fe-4S] cluster of PFL-AE, and ENDOR spectroscopy showed that SAM coordinates to this unique iron via a classic five-member amino acid chelate ring in both the oxidized [4Fe-4S]<sup>2+</sup> and reduced [4Fe-4S]<sup>+</sup> states. ENDOR spectroscopy also demonstrated the close proximity of the sulfonium moiety to the cluster in both oxidation states.

The proposed mechanism outlined in Figure IV.18 shows SAM binding to the oxidized [4Fe-4S]<sup>2+</sup> cluster of PFL-AE via coordination of the unique site, which puts the sulfonium in orbital overlap with one of the  $\mu$ 3-bridging sulfides of the [4Fe-4S]<sup>2+</sup> cluster. One-electron reduction (mediated by reduced flavodoxin in vivo) provides the reduced [4Fe-4S]<sup>+</sup> cluster complexed to SAM. This [4Fe-4S1<sup>+</sup>-SAM complex is stable in the absence of the substrate PFL; however, in the presence of PFL, inner-sphere electron transfer from the [4Fe-4S]<sup>+</sup> cluster to the sulfonium of SAM initiates homolytic S-C(5') bond cleavage. The resulting methionine is left bound to the unique site of the oxidized [4Fe-4S]<sup>2+</sup> cluster, while the adenosyl radical intermediate abstracts the pro-S H from G734 of PFL. The catalytic cycle is completed upon displacement of methionine and 5'deoxyadenosine with an S- adenosylmethionine cosubstrate. It is of interest to note that recent synthetic models of the radical-SAM enzymes based on sitedifferentiated [4Fe-4S] clusters have provided evidence for reductive cleavage of sulfonium moieties by reduced [4Fe-4S] clusters, although a stable synthetic cluster-sulfonium complex has not yet been reported.<sup>69,70</sup>

The past 10 years have seen an explosion in interest in the enzymes now known to comprise the radical-SAM superfamily. These enzymes catalyze a diverse set of reactions, all of which are initiated by H atom abstraction. The evidence for adenosyl radical intermediates in some of these reactions led toearly speculation of similarities to B12-catalyzed radical reactions, the classic example of adenosylradical- mediated reactions in biology. However, the evidence to date points to novel chemistry utilized by the radical- SAM enzymes to generate adenosyl radical intermediates. This chemistry has at its core the use of a site-differentiated [4Fe-4S] cluster to coordinate and activate S-adenosylmethionine for reductive cleavage. Although many questions remain regarding the detailed mechanisms of these fascinating enzymes, it is clear that these ubiquitous enzymes are revealing new insights into the chemistry of iron-sulfur clusters.

### IV.5 References

- (1) Beinert, H. H., R. H.; Münck, E. Science 1997, 277, 653.
- (2) Beinert, H. J. Biol. Inorg. Chem. 2000, 5, 2.
- (3) Cheek, J. B., J. B. J. Biol. Inorg. Chem. 2001, 6, 209.
- (4) Frey, P. A. Annu. ReV. Biochem. 2001, 70, 121.
- (5) Sofia, H. J. C., G.; Hetzler, B. G.; Reyes-Spindola, J. F.; Miller, N. E. *Nucl. Acids Res.* **2001**, *29*, 1097.
- (6) Broderick, J. B. D., R. E.; Fernandez, D. C.; Wojtuszewski, K.; Henshaw, T. F.; Johnson, M. K. *J. Am. Chem. Soc.* **1997**, *119*, 7396.
- (7) Külzer, R. P., T.; Kappl, R.; Hu"ttermann, J.; Knappe, J. *J. Biol. Chem.* **1998**, *273*, 4897.
- (8) Ollagnier, S. M., E.; Schmidt, P. P.; Eliasson, R.; Gaillard, J.; Deronzier, C.; Bergman, T.; Gra¨slund, A.; Reichard, P.; Fontecave, M. J. Biol. Chem. 1997, 272, 24216.
- (9) Sanyal, I. C., G.; Flint, D. H. Biochemistry 1994, 33, 3625.
- (10) Guianvarc'h, D. F., D.; Bui, B. T. S.; Nunzi, F.; Marquet, A. *Biochem. Biophys. Res. Commun.* **1997**, *236*, 402.
- (11) Duin, E. C. L., M. E.; Crouse, B. R.; Allen, R. M.; Sanyal, I.; Flint, D. H.; Johnson, M. K. *Biochemistry* **1997**, *36*, 11811.
- (12) Busby, R. W. S., J. P. M.; Yu, D. S.; Babcock, G. T.; Marletta, M.A. *J. Am. Chem. Soc.* **1999**, *121*, 4706.
- (13) Miller, J. R. B., R. W.; Jordan, S. W.; Cheek, J.; Henshaw, T. F.; Ashley, G. W.; Broderick, J. B.; Cronan, J. E., Jr.; Marletta, M. A. *Biochemistry* **2000**, *39*, 15166.
- (14) Lieder, K. B., S.; Ruzicka, F. J.; Beinert, H.; Reed, G. H.; Frey, P.A. *Biochemistry* **1998**, *37*, 2578.
- (15) Rebeil, R. S., Y.; Chooback, L.; Pedraza-Reyes, M.; Kinsland, C.; Begley, T. P.; Nicholson, W. L. *J. Bacteriol.* **1998**, *180*, 4879.

- (16) Knappe, J. E., S.; Frey, M.; Wagner, A. F. V. *Biochem. Soc. Trans.* **1993**, *21*, 731.
- (17) Wong, K. K. K., J. W.; Sigel, S. a., Ed.; Marcel Dekker: New York, 1994; Vol. 30, p 361.
- (18) Broderick, J. B. H., T. F.; Cheek, J.; Wojtuszewski, K.; Trojan, M.R.; McGhan, R.; Smith, S. R.; Kopf, A.; Kibbey, M.; Broderick, W. E. *Biochem. Biophys. Res. Commun.* **2000**, *269*, 451.
- (19) Frey, M. R., M.; Wagner, A. F. V.; Knappe, J. *J. Biol. Chem.* **1994**, *269*, 12432.
- (20) Magnusson, O. T. R., G. H.; Frey, P. A. *J. Am. Chem. Soc.* **1999**, 121, 9764.
- (21) Magnusson, O. T. R., G. H.; Frey, P. A. *Biochemistry* **2001**, *40*, 7773.
- (22) Krebs, C. H., T. F.; Cheek, J.; Huynh, B.-H.; Broderick, J. B. *J. Am. Chem. Soc.* **2000**, *122*, 12497.
- (23) Ollagnier, S. M., C.; Mulliez, E.; Gaillard, J.; Schuenemann, V.; Trautwein, A.; Mattioli, T.; Lutz, M.; Fontecave, M. *J. Am. Chem. Soc.* **1999**, *121*, 6344.
- (24) Kent, T. A. D., J. L.; Kennedy, M. C.; Huynh, B. H.; Emptage, M.H.; Beinert, H.; Münck, E. *Proc. Natl. Acad. Sci. U.S.A.* **1982**, *79*, 1096.
- (25) Emptage, M. H. K., T. A.; Kennedy, M. C.; Beinert, H.; Munck, E. *Proc. Natl. Acad. Sci. U.S.A.* **1983**, *80*, 4674.
- (26) Werst, M. M. K., M. C.; Beinert, H.; Hoffman, B. M. *Biochemistry* **1990**, *29*, 10526.
- (27) Werst, M. M. K., M. C.; Houseman, A. L.; Beinert, H.; Hoffman, B. M. *Biochemistry* **1990**, *29*, 10533.
- (28) Ugulava, N. B. G., B. R.; Jarrett, J. T. *Biochemistry* **2000**, *39*, 5206.
- (29) Henshaw, T. F. C., J.; Broderick, J. B. *J. Am. Chem. Soc.* **2000**, 122, 8331.
- (30) Cosper, N. J. B., S. J.; Ruzicka, F.; Frey, P. A.; Scott, R. A. *Biochemistry* **2000**, *39*, 15668.

- (31) Kennedy, M. C. W., M.; Telser, J.; Emptage, M. H.; Beinhert, H.; Hoffman, B. M. *Proc. Natl. Acad. Sci. U.S.A.* **1987**, *84*, 8854.
- (32) Walsby, C. J. H., W.; Broderick, W. E.; Cheek, J.; Ortillo, D.; Broderick, J. B.; Hoffman, B. M. *J. Am. Chem. Soc.* **2002**, *124*, 3143.
- (33) Krebs, C. B., W. E.; Henshaw, T. F.; Broderick, J. B.; Huynh, B.H. *J. Am. Chem. Soc.* **2002**, *124*, 912.
- (34) Lee, H.-I. D., A. F.; Fann, Y.-C.; Lakner, F. J.; Hager, L. P.; Hoffman, B. M. J. Am. Chem. Soc. 1997, 119, 4059.
- (35) Tierney, D. L. M., P.; Doan, P. E.; Masters, B. S. S.; Hoffman, B.M. *J. Am. Chem. Soc.* **1998**, *120*, 2983.
- (36) Symons, M. C. R. P., R. L. Proc. R. Soc. London B 1978, 201, 285.
- (37) Davydov, R. M. *Biofizika* **1980**, *25*, 203.
- (38) Kappl, R. H.-B., M.; Hüttermann, J.; Bartlett, N.; Symons, M. C. *R. Biochim. Biophys. Acta* **1985**, 827, 327.
- (39) Leibl, W. N., W.; Hüttermann, J. *Biochim. Biophys. Acta* **1986**, *870*, 20.
- (40) Davydov, R. K., R.; Hutterman, R.; Peterson, J. *FEBS Lett.* **1991**, 295, 113.
- (41) Davydov, R. K., S.; Graslund, A.; Ehrenberg, A. *J. Am. Chem. Soc.* **1994**, *116*, 11120.
- (42) Davydov, R. V., A. M.; Komar-Panicucci, S.; Hoffman, B. M.; Lippard, S. J. *Biochemistry* **1999**, *38*, 4188.
- (43) Bradford, M. Anal. Biochem. 1976, 72, 248.
- (44) Aasa, R. V., T. J. Magn. Reson. 1975, 19, 308.
- (45) Murib, J. H. R., D. M. J. Am. Chem. Soc. 1952, 74, 339.
- (46) Davoust, C. E. D., P. E.; Hoffman, B. M. *J. Magne. Reson.* **1996**, 119, 38.
- (47) Mims, W. B. *In Electron Spin-Echoes*; Plenum Press: New York, 1972.

- (48) Mims, W. B. *Proc. R. Soc. London B* **1965**, 283, 452.
- (49) Hoffman, B. M. M., J.; Venters, R. A. *J. Magn. Reson.* **1984**, *59*, 110.
- (50) Hoffman, B. M. V., R. A.; Martinsen, J. J. Magn. Reson. **1985**, *62*, 537.
- (51) Hoffman, B. M. Acc. Chem. Res. 1991, 24, 164.
- (52) Houseman, A. L. P. O., B. H.; Kennedy, M. C.; Fan, C.; Werst, M. M.; Beinert, H.; Markley, J. L.; Hoffman, B. M. *Biochemistry* 1992, 31, 2073.
- (53) Ragle, J. L. M., M.; Presz, D.; Minott, G. *J. Magn. Reson.* **1975**, *20*, 195.
- (54) Fann, Y.-C. G., N. C.; Osmulski, P. A.; Hager, L. P.; Sligar, S. G.; Hoffman, B. M. *J. Am. Chem. Soc.* **1994**, *116*, 5989.
- (55) Telser, J. H., H.; Lee, H.-I.; Adams, M. W. W.; Hoffman, B. M. *J. Am. Chem. Soc.* **1998**, *120*, 861.
- (56) Werst, M. M. D., C. E.; Hoffman, B. M. *J. Am. Chem. Soc.* **1991**, *113*, 1533.
- (57) Walsby, C. J. O., D.; Broderick, W. E.; Broderick, J. B.; Hoffman, B. M. J. Am. Chem. Soc. 2002, 124, 11270.
- (58) Gurbiel, R. J. D., P. E.; Gassner, G. T.; Macke, T. J.; Case, D. A.; Ohnishi, T.; Fee, J. A.; Ballou, D. P.; Hoffman, B. M. *Biochemistry* **1996**, *35*, 7834.
- (59) Rocklin, A. M. T., D. L.; Kofman, V.; Brunhuber, N. M. W.; Hoffman, B. M.; Christoffersen, R. E.; Reich, N. O.; Lipscomb, J.D.; Que, L., Jr. Proc. Natl. Acad. Sci. U.S.A. 1999, 96, 7905.
- (60) Layer, G.; Moser, J.; Heinz, D. W.; Jahn, D.; Schubert, W.-D. *EMBO J.* **2003**, *22*, 6214.
- (61) Berkovitch, F.; Nicolet, Y.; Wan, J. T.; Jarrett, J. T.; Drennan, C. L. *Science* **2004**, *303*, 76.
- (62) Hänzelmann, P.; Schindelin, H. *Proc. Natl. Acad. Sci. U.S.A.* **2004**, *101*. 12870.

- (63) Smoukov, S. K.; Davydov, R. M.; Doan, P. E.; Sturgeon, B.; Kung, I. Y.; Hoffman, B. M.; Kurtz, D. M., Jr. *Biochemistry* **2003**, *42*, 6201.
- (64) Hoffman, B. M. D., V. J.; Doan, P. E.; Gurbiel, R. J.; Houseman, A. L. P.; Telser, J.; Berliner, L. J., Reuben, J., Ed.; Plenum Press: New York, 1993; Vol. 13,, pp 151-218.
- (65) Padovani, D. T., F.; Trautwein, A. X.; Mulliez, E.; Fontecave, M. Biochemistry 2001, 40, 6713.
- (66) Knappe, J. N., F., A.; Blaschkowski, H. P.; Gänzler, M. *Proc. Natl. Acad. Sci. U.S.A.* **1984**, *81*, 1332.
- (67) Cosper, M. M. C., N.J.; Hong, W.; Shokes, J.E.; Broderick, W.E.; Broderick, J.B.; Johnson, M.K.; Scott, R.A. *Prot. Sci.* **2003**, *12*, 1573.
- (68) Noodleman, L. C., D. A. Adv. Inorg. Chem. 1992, 38, 423.
- (69) Daley, C. J. A. H., R. H. *Inorg. Chem.* **2001**, *40*, 2785. (70) Daley, C. J. A. H., R. H. *J. Inorg. Biochem.* **2003**, *97*, 287.

### **CHAPTER V**

# SYNTHESES AND CHARACTERIZATION OF S-ADENOSYL-L-METHIONINE ANALOGS

### V. 1 Introduction

S-adenosylmethionine synthase (adenosine 5'-triphosphate:L-methionine S-adenosyltransferase, EC 2.5.1.6) catalyzes the reaction shown in Figure V.1.

$$O_2C$$
 $O_2C$ 
 $O_2C$ 
 $O_2C$ 
 $O_3C$ 
 $O_3C$ 

**Figure V.1** Synthesis of S-adenosyl-L-methionine as catalyzed by SAM synthetase.

The product, *S*-adenosylmethionine is the primary methyl group donor in intermediary metabolism and is utilized by methyltransferases for the methylation of RNA, DNA, histones, proteins, polysacharrides, steroids, and numerous other metabolites; methylation can occur on carbon, oxygen, sulfur, and nitrogen. A number of metabolic functions including chemotaxis, restriction-modification of DNA, amino acid modification, and neurotransmitter biosynthesis depend upon *S*-adenosylmethionine.<sup>1</sup>

The concentration of *S*-adenosylmethionine, and hence, the level of methylation activity is controlled primarily by *S*-adenosylmethionine synthetase and by *S*-adenosyl-homocysteine hydrolase, which degrades *S*-adenosylhomocysteine, a potent product inhibitor of most *S*-adenosylmethionine utilizing enzymes to homocysteine and adenosine.<sup>2</sup>

Analogues of methionine, *S*-adenosylhomocysteine, and *S*-adenosylmethionine have been studied as possible substrates and inhibitors of the enzymes involved in *S*-adenosylmethionine metabolism.<sup>3</sup> For example, ethionine and *S*-triflouromethyl- homocysteine have been found as inhibitors of rat liver *S*-adenosylmethionine synthetase and the ethyl and propyl analogues of *S*-adenosylmethionine are substrates for some methyl transferases.<sup>3-5</sup> Interest on *S*-adenosylmethionine synthetase has prompted the study of potential new inhibitors, including those shown in Figure V.2.<sup>6</sup>

Examination of the five analogues as potential inhibitors of *E. coli*S-adenosylmethionine synthetase showed that the vinyl and allyl derivatives

(I and II) of methionine act as substrates and that the disulfide derivatives (III and IV) act as competitive inhibitors with respect to methionine. The *S*-cyano derivative is neither a substrate nor inhibitor.<sup>6</sup>

The vinyl and allyl analogues of methionine are of interest herein due to their potential as precursors for the formation of vinyl and allyl analogues of SAM. The activation of PFL by its activating enzyme, pyruvate formate-lyase activating enzyme (PFL-AE), requires SAM as a co-substrate. SAM undergoes a transient cleavage to form methionine and the putative 5'-deoxyadenosyl radical, which

I: 
$${}^{+}H_{3}N$$
 $COO^{-}$ 

II:  ${}^{+}H_{3}N$ 
 $COO^{-}$ 

III:  ${}^{+}H_{3}N$ 
 $COO^{-}$ 

V:  ${}^{+}H_{3}N$ 
 $S$ 
 $CH_{3}$ 
 $COO^{-}$ 

V:  ${}^{+}H_{3}N$ 
 $S$ 
 $S$ 
 $CH_{3}$ 
 $COO^{-}$ 

**Figure V.2** Methionine analogues: (I) S-vinylhomocysteine, (II) S-allylhomocysteine, (III) S-(methanethio)cysteine, (IV) S-(methanethio)homocysteine, and (V) S-cyanohomocysteine.

then abtracts a hydrogen from the glycine 734 residue in PFL to form the glycyl radical and 5'-deoxyadenosine.<sup>7,8</sup> The source of the electron for this reductive cleavage is the reduced state of the [4Fe-4S]<sup>+</sup> cluster in PFL-AE.<sup>9</sup> However, direct observation of SAM or 5'-deoxyadenosyl radicals has not been achieved; analogues of SAM may make it possible to trap the AdoMet-based radical before it undergoes homolytic cleavage.

An allylic analogue of the 5'-deoxyadenosyl radical has also been characterized as an intermediate in the reaction of lysine 2,3-aminomutase (LAM). A member of the radical SAM superfamily, LAM catalyzes the interconversion of L- $\alpha$ -lysine and L- $\beta$ -lysine. The reaction proceeds through a 1,2-amino group shift and requires the cleavage of an unactivated C-H bond. The

enzyme also mediates hydrogen transfers between substrate, product and coenzyme, which makes the reaction closely resemble those catalyzed by adenosylcobalamin. However, LAM utilizes SAM and not adenosylcobalamin as the hydrogen carrier. However, LAM utilizes SAM and not adenosylcobalamin

The [4Fe-4S] clusters of LAM play an important role in the reaction. Upon binding of SAM, the cluster can be reduced from the +2 oxidation state to the 1+ oxidation state. The [4Fe-4S] cluster donates one electron to SAM, resulting in the cleavage of the coenzyme to produce the 5'deoxyadenosyl radical and methionine in which the latter remains coordinated to the cluster during the catalytic cycle. Replacement of SAM by anSAM (3',4'-anhydro-S-adenosyl-L-methionine) as a coenzyme for LAM results in the formation of a radical stabilized by allylic delocalization during the reductive cleavage as shown in Figure V.3. 10

Figure V.3 Allylic delocalization of anSAM during reductive cleavage.

The allylic surrogate of the more reactive 5'-deoxyadenosyl radical generated by the anSAM has been characterized by EPR spectroscopy using isotopic labeling and spectral simulations. <sup>10</sup> The 5'-deoxyadenosyl radical is widely believed to be the radical initiator in adenosylcobalamin-dependent reactions and in certain reactions that utilize SAM. <sup>15</sup> The intermediacy of the putative 5'-deoxyadenosyl radical has been questioned due to the fact that it had never been observed spectroscopically. <sup>16</sup> However, the introduction of the 3'-4' unsaturation into the ribosyl moiety of the SAM coenzyme provided sufficient stabilization to allow EPR observation and characterization of the analogue of the adenosyl radical. <sup>10</sup>

# V.2 Experimental Methods

### V.2.1 Materials

The adenosine kinase plasmid was a generous gift from Dr. Perry A. Frey (University of Wisconsin-Madison). DL-Homocysteine and L-homocystine were obtained from Sigma. All other chemicals were of the highest purity and obtained from commercial sources.

# V.2.2 NMR Spectroscopy

NMR spectra were recorded at room temperature on a VXR-300 spectrometer.

### V.2.3 Radiochemical Assay of Adenosine Kinase<sup>17</sup>

Purified AdoK (grown in the lab from a pet-24b vector with the cDNA and transformed into BL21(DE3) competent cells) was obtained by loading the AdoK cell lysate onto a DE 52 anion exchange column. Standard radiochemical assay was prepared in a final volume of 200  $\mu$ L with the following components: 180.6  $\mu$ L TRIS malate (pH 7) buffer, 2.5  $\mu$ L ATP (100 mM), 2.5  $\mu$ L MgCl<sub>2</sub> (100 mM), 2.6  $\mu$ L U-<sup>14</sup>C Adenosine (50  $\mu$ Ci/mL), 2.0  $\mu$ L BSA (1.19 mg/mL), and 10.0  $\mu$ L AdoK. The reaction mix was incubated for 10 min at 37°C and heated to 100°C for 1 min. Aliquots of 30  $\mu$ L were transferred to DE-81 discs (Whatman) and the discs were washed several times with 2 mM ammonium formate (pH 7) and placed in scintillation vials for counting. One unit of activity was defined as a  $\mu$ mol of used substrate per minute.

# V.2.4 Synthesis of S-Vinylhomocysteine 18,19

DL-Homocystine (5.0 g) was dissolved in liquid ammonia and sodium was added in small portions until the reaction was complete as evidenced by the persistence of a blue color of the solution for 10 minutes. The blue color was dispelled by the addition of a minimal amount of ammonium iodide. The ammonia was evaporated under a stream of nitrogen and the gray-white residue was dried under reduced pressure for several hours at room temperature. Dry dimethylsulfoxide (60.0 ml) was added and the slurry of DL-homocysteine sodium thiolate was bubbled with acetylene at room temperature under subdued light for 60 minutes. If the solution darkened or thickened, the reaction was

terminated early. The reaction mixture was cooled on ice and was carefully neutralized with 0.5N HCL. The mixture was left at 4°C for several hours and the crystalline product was removed by filtration and washed successively with cold water, methanol, acetone and ether. It was dried under reduced pressure. The average theoretical yield based on homocystine was 60-65%. <sup>18</sup> <sup>1</sup>H NMR (300 MHz, DMSO): <sup>19</sup>  $\delta$  6.29 (1H), 5.15 (2H), 3.70 (t, 1H), 2.75 (t, 2H), 1.95 (m, 2H) ppm.

# V.2.5 Synthesis of S-Allylhomocysteine<sup>6,20</sup>

DL-Homocysteine thiolactone (0.765 g, 5.0 mmol) was added to a solution of sodium methoxide (27.0 g, 11.7 mmol sodium metal in 21.0 ml methanol) at 0°C and the solution was stirred for 30 minutes. Allyl chloride (5.0 mmol) was then added over a period of 5 minutes. The resulting mixture was stirred for 1.25 hours. The reaction mixture was filtered and the filtrate was concentrated to a volume of 2 ml by evaporation under reduced pressure. NaOH (30.0 ml, 1N) was added and the resulting solution was refluxed for 1.25 hours. The pH was lowered to 5 by adding concentrated HCl and the volume was reduced to about 5ml. The resulting suspension was filtered and the precipitate was dissolved in hot water (4.0 ml) and filtered. Absolute ethanol (16.0 ml) was added to the filtrate and was cooled at -20°C for two days. Crystalline S-allyl-DL-homocysteine was obtained by vacuum filtration. (0.56g, 62.8 % yield); <sup>1</sup>H NMR (300 MHz, D<sub>2</sub>O/DCl): δ 5.89 (m, 1H), 5.27 (m, 2H), 2.76 (t, 2H), 2.33 (m, 2H) ppm.

V.2.6 Synthesis of 3',4'- Anhydroadenosine Triphosphate (anATP)

Synthesis of 2'3'-O-methoxyethylideneadenosine<sup>21</sup>

Adenosine (3.0 g, 0.011mol) was suspended in dry dioxane (75.0 ml). Trimethyl orthoacetate (4.12 g, 0.034 mol) and trichloroacetic acid (4.87 g, 0.030 mol) were added and the mixture was heated to 50°C for 20 minutes. The clear solution was neutralized with 120 ml of 5% aqueous NaHCO<sub>3</sub> solution. The volume was reduced to about 100 ml under reduced pressure and was extracted with CHCl<sub>3</sub> (3x100 ml). The combined organic phase was dried with MgSO<sub>4</sub>, filtered and evaporated to give a white solid. (3.57, 98.0%)

Reaction of 2'3'-O-Methoxyethylideneadenosine with Sodium Iodide and Pivalyl Chloride in Pyridine<sup>22</sup>

Unpurified 2'3'-O-Methoxyethylidene-adenosine (1.29 g, 0.004 mol) was dissolved in 40 ml pyridine. Nal (11.98g, 0.08mol) was added and the solution was vigorously stirred and was heated to reflux. Pivalyl chloride (4.79 ml, 0.04 mol) was added and the reaction was stirred at reflux for 10 minutes. The solution was allowed to cool for 20 minutes and 10 ml of methanol was added and stirred for 3 hours. The red solution was poured into 200 ml of H<sub>2</sub>O containing NaHCO<sub>3</sub> (10.0 g) and NaS<sub>2</sub>O<sub>3</sub> (1.00 g). The resulting yellow solution was extracted with ether (3x200 ml) and the organic phase was washed with water (1x200 ml). The wash was back-extracted with ether (1x100 ml) and the combined organic phase was evaporated to give a gum. Co-evaporation using toluene and 98% ethanol (50.0 ml, 1:1) gave a yellow-brown solid. The crude

product obtained (2.17 g) is ~37% 6-N-pivalamido-9-(3-iodo-3-deoxy-2-O-[4,4-dimetyl-3-pivaloxypent-2-enoyl]-5-O-pivalyl- $\beta$ -D-xylofuranosyl)purine and ~16% 6-N-pivalylamido-9-(3-deoxy-5-O-pivalyl-2-O-[4,4-dimethyl-3-pivaloxypent-2-enoyl]- $\beta$ -D-glycero-pent-3-enofuranosyl)purine.

Synthesis of 6-N-Pivalamido-9-(3-deoxy-5-O-pivalyl-2-O-[4,4-dimethyl-3-pivaloxypent-2-enoyl]-β-D-glycero-pent-3-enofuranosyl)purine<sup>22</sup>

The crude product from the reaction of 2'3'-O-methoxyethylidene-adenosine with sodium iodide and pivalyl chloride in pyridine (1.89 g) and AgOAc (2.07 g, 0.012 mol) were stirred in 75.0 ml of pyridine at 5°C for 3 days. The resulting dark solution was poured into 150 ml of 5% NaHCO<sub>3</sub>. The mixture was extracted with ether (3x200 ml) and the combined organic phase was washed with water (1x100 ml) and evaporated. The crude product was passed through a silica column and eluted with ethyl acetate to obtain the pure product. (1.42g, 45.2%yield);  $^1$ H NMR (300 MHz, CDCl<sub>3</sub>):  $\delta$  8.78 (s, 1H), 8.66 (s, 1H), 8.08 (s, 1H), 6.62 (d, 1H), 6.08 (m, 1H), 5.74 (s, 1H), 5.43 (s, 1H), 4.73 (s, 1H), 1.44 (s, 9H), 1.30 (s, 9H), 1.22 (s, 9H) ppm.

Synthesis of 9-(3-Deoxy-β-D-glycero-pent-3-enofuranosyl)adenine (anAdo)<sup>22</sup>
6-N-Pivalamido-9-(3-deoxy-5-O-pivalyl-2-O-[4,4-dimethyl-3-pivaloxypent-2-enoyl]-β-D-glycero-pent-3-enofuranosyl)purine (0.57 g ) and NaOMe (0.22 g of Na metal in 9.00 ml of methanol) was stirred at room temperature overnight. The reaction mixture was evaporated to dryness and was dissolved in 54.20 ml of

H<sub>2</sub>O-95% ethanol (4:1) and filtered through Celite. The filtrate was concentrated and the pure product was obtained after allowing it to precipitate from the solution. (0.06g, 30.0% yield); <sup>1</sup>H NMR (300 MHz, CDCl<sub>3</sub>): δ 8.24 (s, 1H), 8.20 (s, 1H), 6.31 (d, 1H), 5.75 (d, 1H), 5.27 (t, 1H), 5.27 (m, 2H), 4.07 (d, 2H) ppm.

Synthesis of 3',4'-Anhydroadenosine Triphosphate (anATP)<sup>10</sup>

The preparation of anATP was prepared in a single reaction mixture by the action of three different kinases. The 50.0 ml reaction contained 2.75 mM anAdo dissolved in PIPES buffer pH = 7 (48.0 ml), 10 mM MgCl<sub>2</sub> (101.65 mg), 0.25mM ATP (6.89 mg), 20 mM P-creatine (255.0 mg), Adenosine Kinase  $(12.0U, 200.0 \mu L)$ , Adenylate Kinase  $(2000U, 324.0 \mu L)$ , and Creatine Kinase (2000U, 6.45 mg). The reaction was incubated at room temperature and an addition 100  $\mu$ L of AdoK was added after 1.0 hour. The reaction progress was monitored by anion-exchange HPLC (Hypersil SAX, 5µ, 125x4.0mm) using a 100 mM NaH<sub>2</sub>PO<sub>4</sub> as a buffer with gradient from 0-1.0 M NaCl in 27 minutes. The reaction was stopped after 18.0 hours. The reaction mixture was applied to a DEAE-Sephadex-A-25 column (Pharmacia) with a linear gradient from 0-0.5 M NH<sub>4</sub>HCO<sub>3</sub> followed by 100 ml of 0.5 M NH<sub>4</sub>HCO<sub>3</sub>. The pooled anATP fractions were evaporated in vacuo. (67.41g, 99%);  $^{1}H$  NMR (300 MHz,  $D_{2}O$ ):  $\delta$  8.17 (s, H-2 or H-8), 8.13 (s, H-2 or H-8), 6.42 (s, 1H), 5.54 (s, 1H), 5.15 (s, 1H), 4.57 (d, 2H) ppm.

### V.2.7 Synthesis of SAM Analogues

Synthesis of Adenosyl-S-allyl-DL-homocysteine (allyl SAM)

Allyl SAM synthesis reaction (10 mL) was carried out at room temperature with moderate stirring in 100 mM Tris-HCl, pH 8.0 containing 50 mM KCl, 26 mM MgCl<sub>2</sub>, 13 mM ATP, 1 mM EDTA, 8 % β-ME, 20 mM S-allylhomocysteine, inorganic pyrophosphatase (5  $\mu$ L) and 1 mL SAM synthetase lysate (approximately 13 mg of total protein). All reagents were added in the order as listed. The reaction was monitored by thin-layer chromatography (TLC) on silica plates developed in butanol /acetic acid /water (4:1:1). The reaction was terminated by addition of 1 mL of 1 M HCl and precipitated protein was removed by centrifugation at 26,892× g (15,000 rpm, SS34) for 20 min at 4 °C. The supernatant was decanted and split in half. Half of the supernatant was loaded onto a SOURCE 15S cation exchange column (Pharmacia, 8 mL), which had been charged with 1 M HCl and equilibrated with MQ H<sub>2</sub>O. The column was run with a linear gradient of 0-1 M HCl, and AdoMet eluted as a distinct peak from 38 - 56 % Buffer B. The other half of the supernatant was run through the same procedure. Fractions containing products were pooled, lyophilized, and stored at -80 °C until needed. (4 mg, 10.0%); <sup>1</sup>H NMR (300 MHz, D<sub>2</sub>O): δ 8.27, 8.21 (s, adenine H-2 and H-8), 6.04 (d, 1H), 5.02 (m, 2H), 4.70 (s, 1H), 4.41 (m, 2H), 3.78 (t, 1H), 3.70(t, 2H) 3.67, 3.62 (d, 2H), 3.53, 3.27 (m, 2H), 2.92 (d, 2H), 2.82 (s, 3H), 1.58 (m, 2H) ppm.

### Synthesis of anSAM

Anhydro *S*-adenosyl-L-methionine (anSAM) was carried out at room temperature overnight as described above with 10 mM anhydro ATP and 13 mM methionine. (4 mg, 7.6%);  $^{1}$ H NMR (500 MHz, D<sub>2</sub>O):  $\delta$  8.20, 8.17 (s, adenine H-2 and H-8), 6.48 (d, 1H), 5.88 (s, 1H), 5.49 (s, 1H), 4.39 (q, 2H), 3.72 (t, 3H), 3.52 (m, 1H), 3.40 (s, 1H), 2.96 (s, 3H), 2.29 (q, 2H) ppm.

### V.3 Results and Discussion

### V.3.1 Radiochemical Assay of Adenosine Kinase

The results from the assay showed that only 23 % of the radiolabeled adenosine had been converted to radiolabled ATP. Despite its low activity, the purified AdoK lysate was used to test the phosphorylation of adenosine to optimize the efficiency of the enzymatic phosphorylation reaction. Following the protocol described in the experimental procedures, it was seen that despite the observed activity of the AdoK enzyme, it was not able to phosphorylate the adenosine to create ATP.

# V.3.1 Synthesis of S-Vinylhomocysteine

The synthesis of the vinyl analogue is outlined in Figure IV.4.

DL-homocystine was dissolved in liquid ammonia while making sure that the reaction set-up was anaerobic by keeping a constant flow of N<sub>2</sub> gas. Sodium metal was added in small pieces to regulate the vigorous reaction. This was continued until a persistent dark blue solution was observed. NH<sub>4</sub>I was added

Figure V.4 Reaction mechanism for the synthesis of S-vinylhomocysteine.

until all the blue color of the reaction mix disappeared. Care was observed to avoid excess addition of the NH<sub>4</sub>I salt. The crude product was allowed to dry by running a continuous flow of N<sub>2</sub> gas in the reaction mix. After two hours, the crude product was further dried under reduced pressure overnight taking care not to expose it to air. Dry dimethylsulfoxide was added to the vacuum dried DL-homocysteine sodium thiolate. Removal of water and dissolved gasses in DMSO was necessary to prevent the regeneration of homocystine. Acetylene was bubbled into the slurry for about 90 minutes, and the reaction was quenched by cooling the reaction mixture on ice and neutralizing it with 5 M HCI. The desired product was allowed to grow from the reaction mix in the cold box at 4°C. The white precipitate was collected the next day and washed with cold water,

methanol, acetone and ether. <sup>1</sup>H NMR of the purified product showed that the chemical shifts correspond to the starting material, homocystine.

# V.3.2 Synthesis of S-Allylhomocysteine

The synthesis of *S*-allyl-homocysteine as shown in Figure V.5 was a modification of the procedure of Kolenbrander and of Kim and co-workers.<sup>6,20</sup>

Na metal was added to the methanol in an ice bath and was stirred for 5 minutes before the DL-homocysteine thiolactone was added. A milky white suspension was formed and was stirred for 30 minutes. The filtrate was collected and reduced in volume to approximately 2 mL using a rotary evaporator. The concentrated filtrate was then refluxed after the addition of 1M NaOH.

Figure V.5 Reaction mechanism for the synthesis of S-allylhomocysteine.

After 90 minutes, the volume of the reaction mix was again reduced to about 5 mL using the rotary evaporator. The crude product, which was a white suspension, was cooled on ice and the pH was adjusted to pH 4 with concentrated HCL. Initial work on the purification of the crude product involved filtering the suspension and removing the solvent from the filtrate under reduced pressure. Ethanol was then added to dissolve the desired product and the filtrate was concentrated and cooled to obtain the crystalline S-allylhomocysteine. However, the recrystallization process takes several days to form the desired product and the yields were very poor (20-25%). An alternative method was employed where the crude product was washed with cold deionized water to remove the water soluble impurities and the undissolved white precipitate was dried under vacuum. The percent yield increased to 68% using this method of purification. <sup>1</sup>H NMR in DCI/D<sub>2</sub>O showed the expected chemical shifts to be upfield by around 2 ppm. This was resolved by limiting the amount of the DCL added to the NMR sample.

V.3.3 Synthesis of 3',4'-Anhydroadenosine Triphosphate (anATP)

Synthesis of 2'3'-O-Methoxyethylideneadenosine

The reaction for the protection of the hydroxy groups of adenosine is shown in Figure V.6. The white suspension formed after mixing adenosine, trimethyl orthoacetate, and tricholoacetic acid in dioxane becomes clear upon heating to 50°C in a water bath. After stirring for 20 minutes, 5% NaHCO<sub>3</sub> was added to neutralize the excess trichloroacetic acid. The volume was then reduced

to about 100 mL using the rotary evaporator. The desired product was then extracted with chloroform. The organic layer was dried by the addition of anhydrous MgSO<sub>4</sub>, filtered and the solvent removed under vacuum overnight to yield a white solid.

Figure V.6 Reaction scheme for the protection of adenosine.

Reaction of 2'3'-O-Methoxyethylideneadenosine with Sodium Iodide and Pivalyl Chloride in Pyridine

The protected adenosine, 2'3'-O-methoxyethylideneadenosine, and Nal were dissolved in pyridine. To protect the light sensitive Nal, the reaction flask was covered in aluminum foil. The reaction mixture was heated to reflux and pivalyl chloride was added dropwise to regulate the vigorous reaction. The red solution that was formed was allowed to reflux for about 4-10 minutes more to maximize the production of the desired products. It has been shown that the

reflux time of the reaction mixture affects the % yield of the desired products A and B as shown in the reaction scheme in Figure V.7 with the corresponding percent yields presented in Table V.1.<sup>22</sup> After cooling for 20 minutes, MetOH

**Figure V.7** Reaction of 2'3'-O-methoxyethylideneadenosine with sodium iodide and pivalyl chloride in pyridine.

% Yield	2 min	4 min	6 min	8 min	10 min
Α	2.4	4	8.8	13	16
В	41	44	38	31	29
С	16	15	15	13	15

Table V.1 Percent yield of pivalyl reaction products at various reflux times.<sup>22</sup>

was added and was stirred for 3 and ½ hours. An aqueous solution of NaHCO<sub>3</sub> and Na<sub>2</sub>S<sub>2</sub>O<sub>3</sub> was added before extracting the desired products with diethyl ether. The pooled organic layer was washed with water, dried with anhydrous MgSO<sub>4</sub>, filtered and the solvent removed using the rotary evaporator. The crude product was further dried under vacuum overnight to yield a yellow orange solid. The <sup>1</sup>H NMR spectrum was not obtained, as the crude product does not require purification prior to the next step of the synthesis. Of the three products formed in this reaction step, only products B and C will react with AgOAc as shown in Figure V.8 to form the protected 2' and 3'-deoxyadenosine. Product A will remain unreacted and will not interfere in the reaction.

Synthesis of 6-N-Pivalamido-9-(3-deoxy-5-O-pivalyl-2-O-[4,4-dimethyl-3-pivaloxypent-2-enoyl]-β-D-glycero-pent-3-enofuranosyl)purine

The crude product from the above reaction was redissolved in pyridine and AgOAc was added and stirred overnight at 10°C. The reaction flask was covered in aluminum foil to protect the light sensitive AgOAc from being reduced. An aqueous solution of 5% NaHCO<sub>3</sub> was added before extracting the desired

**Figure V.8** Reaction with AgOAc of the crude product from the 2'3'-O- methoxyethylideneadenosine reaction with with sodium iodide and pivalyl chloride.

product with diethyl ether. The pooled organic phase was dried with anhydrous MgSO<sub>4</sub>, filtered, and the solvent removed using the rotary evaporator. The yellow residue formed was further dried under vacuum overnight. Purification of the crude product was done via column chromatography by passing the product mixture through a column packed with silica gel (200 mesh) and equilibrated with ethyl acetate. Thin layer chromatography of the fractions collected showed that product A elutes with an  $R_f$  value of 0.85. The 2'-deoxy product elutes with an  $R_f$  value of 0.72.

Synthesis of 9-(3-Deoxy-β-D-glycero-pent-3-enofuranosyl)adenine (anAdo)

The deprotection reaction, as described by the reaction scheme in Figure V.9, was carried out by dissolving the protected 3'-deoxyadenosine in NaOMe. The yellow solution was stirred overnight and evaporated to dryness by keeping a constant flow of  $N_2$  gas over the reaction mix. The yellow paste formed was further dried under vacuum and was redissolved in  $H_2O$ -95% EtOH (4:1) and filtered through Celite. The filtrate was reduced to about 100mL using the rotary evaporator and cooled to 4°C to induce precipitation. The precipitate collected was a dark tan in color.

Figure V.9 Deprotection of 3'-deoxyadenosine in NaOMe.

Synthesis of 3',4'-Anhydroadenosine Triphosphate (anATP)

The enzymatic phosphorylation of 3'-deoxyadenosine was carried out following the procedures outlined by Frey and co-workers. <sup>10</sup> Using three kinases and an enzymatic amount of ATP to initiate the formation of the anATP, a small-

scale reaction was carried out as a trial run to optimize the conditions for the large-scale enzymatic phosphorylation reaction. The 1 mL reaction mix consisted of the following components: 10 mM MgCl<sub>2</sub> (10 μL - 1M stock), 0.25 mM ATP (9.7 μL -25.7 mM stock), 20 mM Phosphocreatine (5.0 mg), 0.6U Adenosine Kinase (10 μL), 40U Adenylate Kinase (6.5 μL), 40U Creatine Kinase (12.9 μL), 30 mM anAdenosine (794 μL), 25 mM PIPES pH=7 buffer (157 μL). To monitor the course of the reaction, a 25 μL aliquot of the reaction mix was collected at certain time intervals and loaded into a Spehrisorb S5 SAX column (Pharmacia) with a linear gradient of 0-100% 100 mM NaH<sub>2</sub>PO<sub>4</sub>/1 M NaCl pH = 3 to check the completion of the reaction. To determine the elution time of the starting material, a 25 μL sample of anAdo in 25 mM PIPES pH=7 buffer was loaded onto the column (Figure V.10). Baseline separation methods obtained between AMP, ADP and ATP showed that AMP elutes at 4-5 minutes, ADP elutes at 10-11 min and ATP elutes at 14-16 minutes.

The first sample aliquot of the enzymatic phosphorylation reaction was taken 6 hours after the reaction was initiated. The chromatogram shows two absorbance peaks due to two sample injections (Figure V.11). The first sample injected was thought to be insufficient to detect the formation of the anATP, so a second 25  $\mu$ L aliquot was loaded into the column about 2 minutes after the first injection. Other sample aliquots taken were 15 (Figure V.12), 24 (Figure V.13), and 42 (Figure V.14) hours after the start of the reaction. From the absorbance peaks of the anATP produced, it can be observed that the reaction

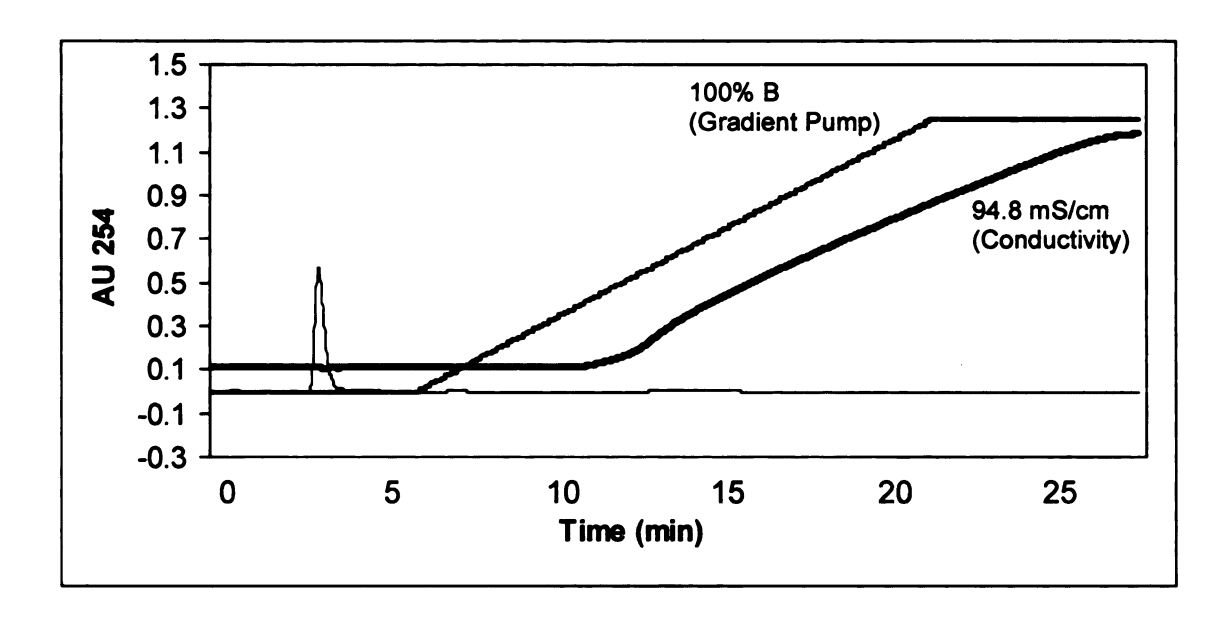


**Figure V.10** Elution time of anAdo loaded into a Spherisorb S5 SAX column. The buffer used was 100 mM NaH<sub>2</sub>PO<sub>4</sub> pH = 3.0 for pump A and 100 mM NaH<sub>2</sub>PO<sub>4</sub>/1 M NaCl pH = 3.0 for pump B. AnAdo eluted as a distinct peak at 3-4 minutes and 0% buffer B.

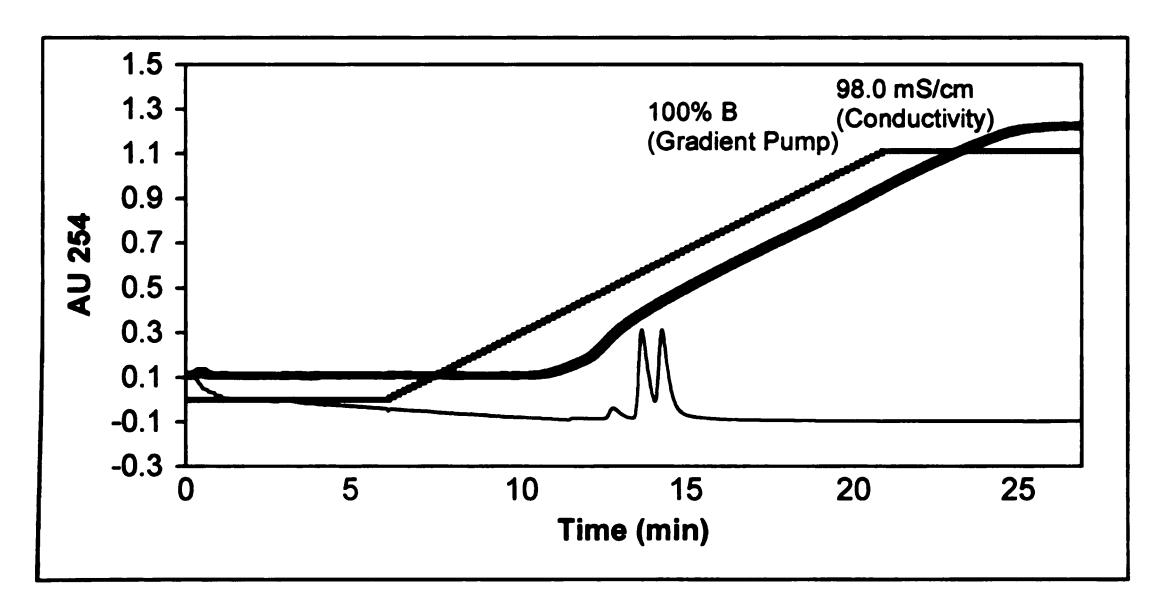


**Figure V.11** Elution time of anATP (6 hours) loaded into a Spherisorb S5 SAX column. The buffer used was 100 mM NaH<sub>2</sub>PO<sub>4</sub> pH = 3.0 for pump A and 100 mM NaH<sub>2</sub>PO<sub>4</sub>/1 M NaCl pH = 3.0 for pump B. AnATP eluted as a distinct peak at 13-14 minutes and 29-37% buffer B.

was complete at around 18 hours, which was the period of reaction time reported by Frey and co-workers, as the size of the anATP peak actually decreases as the reaction time was increased.

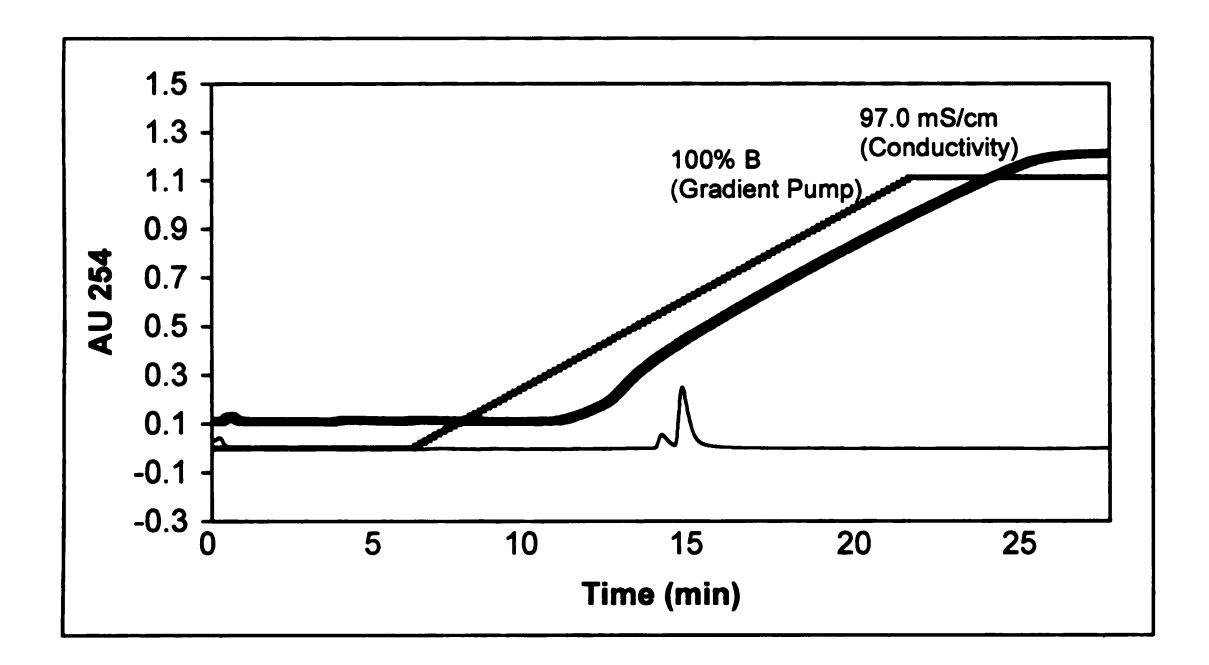


**Figure V.12** Elution time of anATP (15 hours) loaded into a Spherisorb S5 SAX column. The buffer used was 100 mM NaH<sub>2</sub>PO<sub>4</sub> pH = 3.0 for pump A and 100 mM NaH<sub>2</sub>PO<sub>4</sub>/1 M NaCl pH = 3.0 for pump B. AnATP eluted as a distinct peak at 13-14 minutes and 28-40% buffer B.

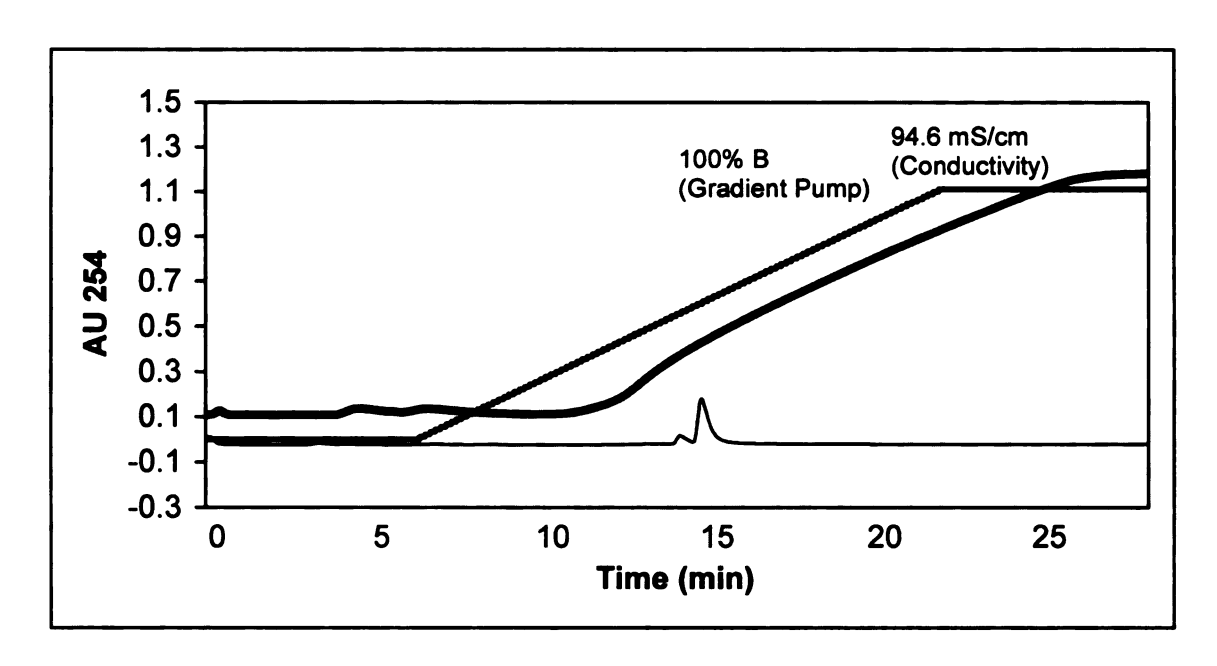


**Figure V.13** Elution time of anATP (24 hours) loaded into a Spherisorb S5 SAX column. The buffer used was 100 mM NaH<sub>2</sub>PO<sub>4</sub> pH = 3.0 for pump A and 100 mM NaH<sub>2</sub>PO<sub>4</sub>/1 M NaCl pH = 3.0 for pump B. AnATP eluted as a distinct peak at 13-14 minutes and 29-38% buffer B.

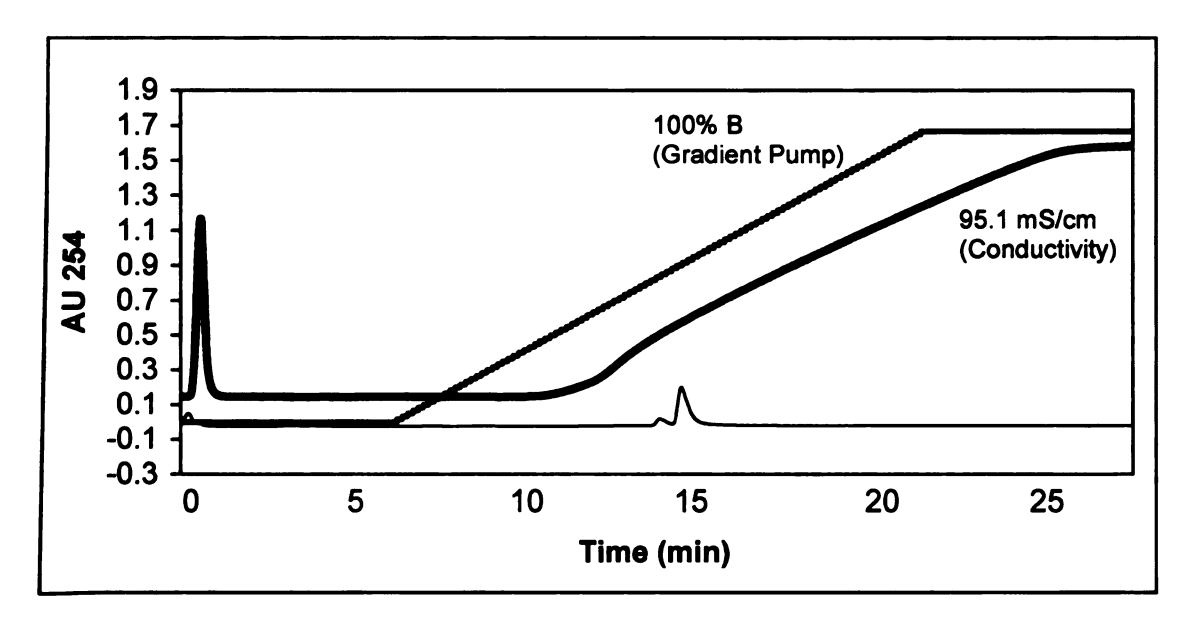


**Figure V.14** Elution time of anATP (42 hours) loaded into a Spherisorb S5 SAX column. The buffer used was 100 mM NaH<sub>2</sub>PO<sub>4</sub> pH = 3.0 for pump A and 100 mM NaH<sub>2</sub>PO<sub>4</sub>/1 M NaCl pH = 3.0 for pump B. AnATP eluted as a distinct peak at 13-14 minutes and 29-38% buffer B.

The large-scale enzymatic phosphorylation of anAdo was then carried out and had the following components in the reaction mix: 101.7 mg MgCl<sub>2</sub>, 6.89 mg ATP, 255 mg phospho-creatine, 200 uL adenosine kinase, 324 uL adenvlate kinase, 6.45 mg creatine kinase, and 2.75 mM anadenosine in 25 mM PIPES buffer pH=7 with a final volume of 50 mL. The reaction was allowed to run for 18 hours and the reaction mix was loaded onto a DEAE-Sephadex A-25 column (Pharmacia) that had been equilibrated with 10 mM NH₄HCO₃ at 4°C. The nucleotide was eluted with a linear gradient of 0-0.5 M NH<sub>4</sub>HCO<sub>3</sub>. The column eluate was collected beginning at 375 mL of column flowthrough and 2mL fractions were monitored at 260 nm. After 32 fractions were collected, 1 mL fractions were collected until an additional 18 fractions were obtained. The fractions with the highest absorbance values at 260 nm (fractions 71-78) as shown in Figure V.15 were pooled and lyophilized under vacuum to a white solid. The concentration of the anATP was determined spectrophotometrically as follows. A 5 mg sample was dissolved in 25 mM PIPES buffer pH 7, and the absorbance reading was taken at 260 nm. Using the value of 14000 mol<sup>-1</sup> cm<sup>-1</sup> for the molar extinction coefficient, it was determined that about 74 mg of anATP was produced. This value is equivalent to a % yield exceeding a 100%, but the product obtained is a mixture of regular ATP and the desired anATP. The presence of regular ATP in the final phosphorylation product is due to the catalytic amount of ATP used to initiate the phosphorylation reaction and correction for this in the crude product results to 67.41g of anATP. Further

purification of the crude mixture to separate the two products was not done to maximize the amount of anATP for the enzymatic synthesis of anSAM.

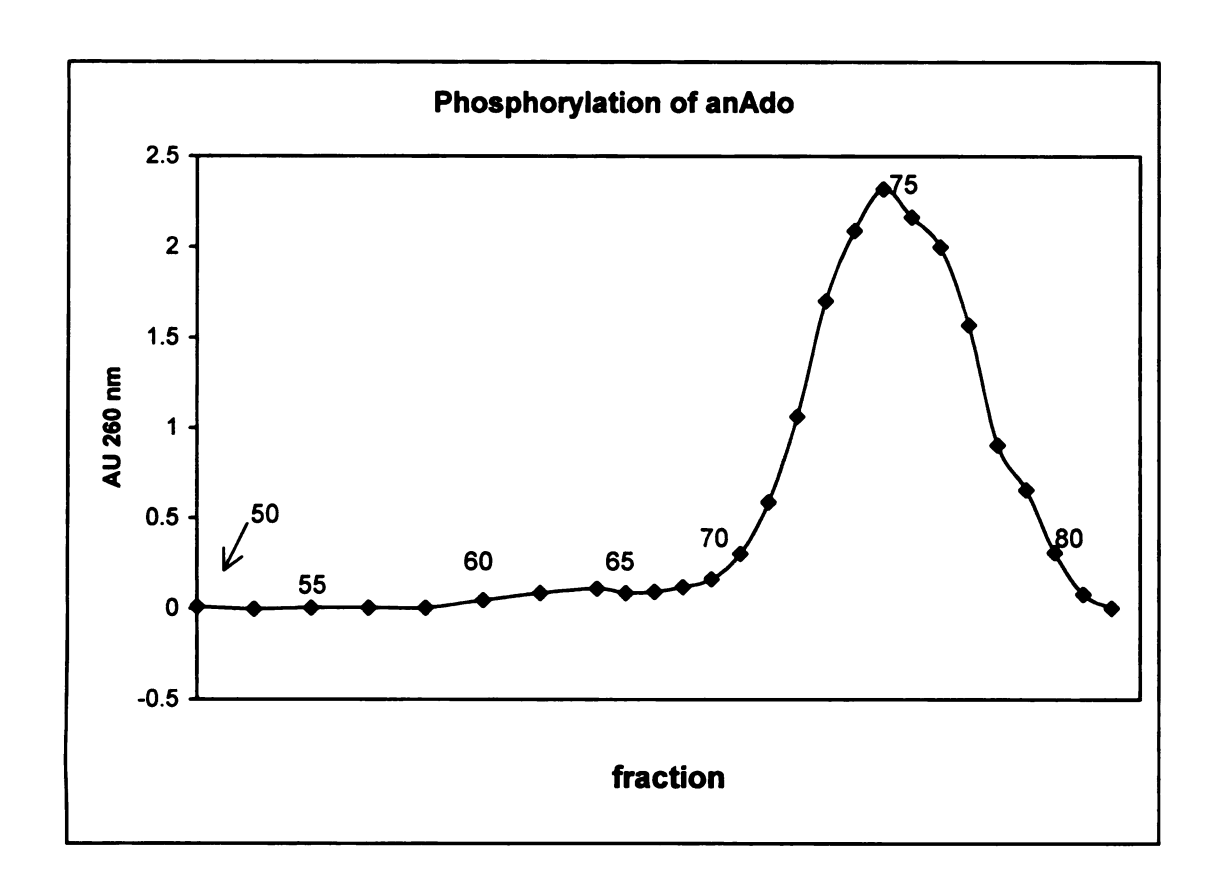


Figure V. 15 Absorbance readings of the anATP fractions collected.

# V.3.4 Synthesis of SAM Analogues

# Synthesis of S-allylSAM

The enzymatic synthesis of allyISAM as shown in the reaction scheme in Figure V.16 was carried out at room temperature following the procedures outlined by Park and co-workers.<sup>4</sup> The reaction mix had the following components: 37.0 mg KCl, 22.0 mg S-allyl-L-homocysteine, 18  $\mu$ L 0.5M EDTA,

2 1/2 1/2

52.7 mg MgCl<sub>2</sub>, 0.8 mL 8% β-ME, 5 μL inorganic pyrophosphatase, 1 mL SAM synthetase, 8.2 mL 100 mM TRIS·HCl pH =8 and 74 mg ATP. The S-allyl-homocysteine was dissolved in the buffer by gently heating it in a water bath. The rest of the components were added and stirred overnight and quenched with 1

Figure V.16 Enzymatic synthesis of adenosyl-S-allyl-L-homocysteine

mL of 1M HCI. The reaction mix was spun at 18,000 rpm for 30 minutes and loaded onto a SOURCE 15S cation exchange column (Pharmacia, 8 mL), which had been charged with 1 M HCl and equilibrated with MQ  $H_2O$ . The column was run with a linear gradient of 0-1 M HCl, and AdoMet eluted from 38-56% of the gradient as a distinct peak as shown if Figure V.17. The other half of the supernatant was run through the same procedure. Fractions containing products were pooled, lyophilized, and stored at -80 °C until needed.

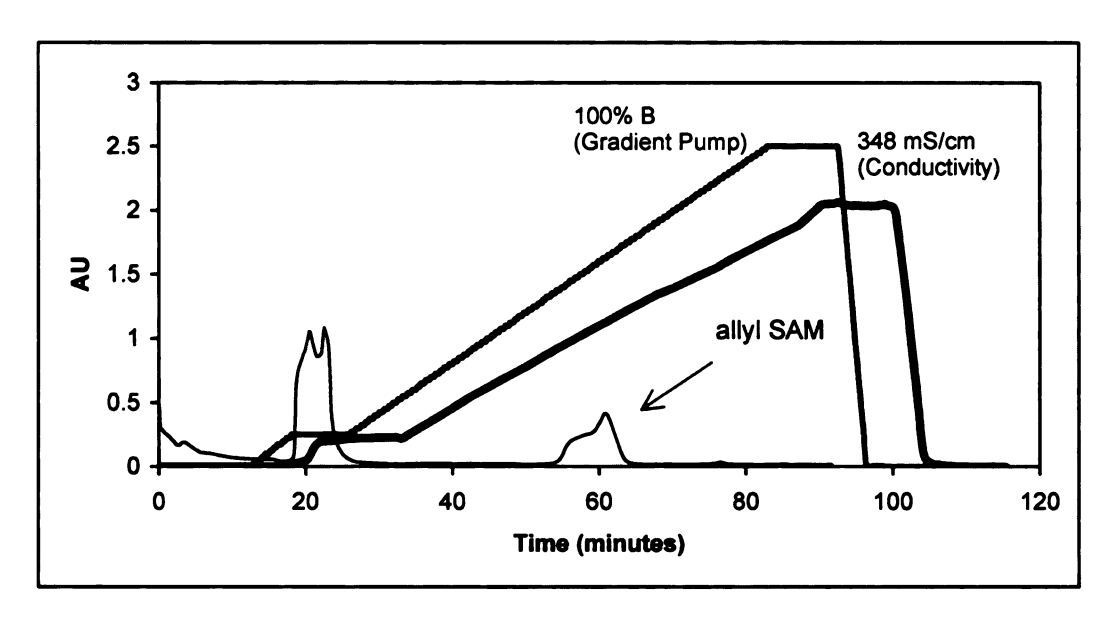


Figure V. 17 Chromatogram of isolation of allyISAM by SOURCE 15S cation exchange chromatography (Pharmacia, 8 mL), gradient from 0-1 M HCl, flow rate = 1 mL/min. AllyISAM eluted as a distinct peak from 38 – 56 % buffer B.

# Synthesis of anSAM

The enzymatic synthesis of anSAM as shown in Figure V.18 was carried out using the procedure described by Park and co-workers and had the following components in the reaction mix: 37.9 mg KCl, 26.6 mg L-methionine, 18  $\mu$ L 0.5 M EDTA, 52.7 mg MgCl<sub>2</sub>, 0.8 mL 8%  $\beta$ -ME, 5  $\mu$ L inorganic pyrophosphatase, 1 mL SAM synthetase, 8.2 mL 100 mM TRIS·HCl pH =8 and 74 mg crude anATP. The reaction mix was stirred overnight and 1 mL of 1 M HCl was added to quench the reaction. The white suspension formed was spun in centrifuge at 18,000 rpm for 30 minutes and loaded onto a SOURCE 15S cation exchange column (Pharmacia, 8 mL), which had been charged with 1 M HCl and equilibrated

Figure V.18 Enzymatic synthesis of 3', 4'-anhydro-S-adenosyl-L-methionine.

with MQ H<sub>2</sub>O. The column was run with a linear gradient of 0-1 M HCl, and AdoMet eluted as a distinct peak from 38 – 56 % of the gradient as shown in Figure V.19. The other half of the supernatant was run through the same procedure. Fractions containing products were pooled, lyophilized, and stored at –80 °C until needed. <sup>1</sup>H NMR (500 MHz, D<sub>2</sub>O): δ 8.20, 8.17 (s, adenine H-2 and H-8), 6.48 (d, 1H), 5.88 (s, 1H), 5.49 (s, 1H), 4.39 (q, 2H), 3.72 (t, 3H), 3.52 (m, 1H), 3.40 (s, 1H), 2.96 (s, 3H), 2.29 (q, 2H) ppm.

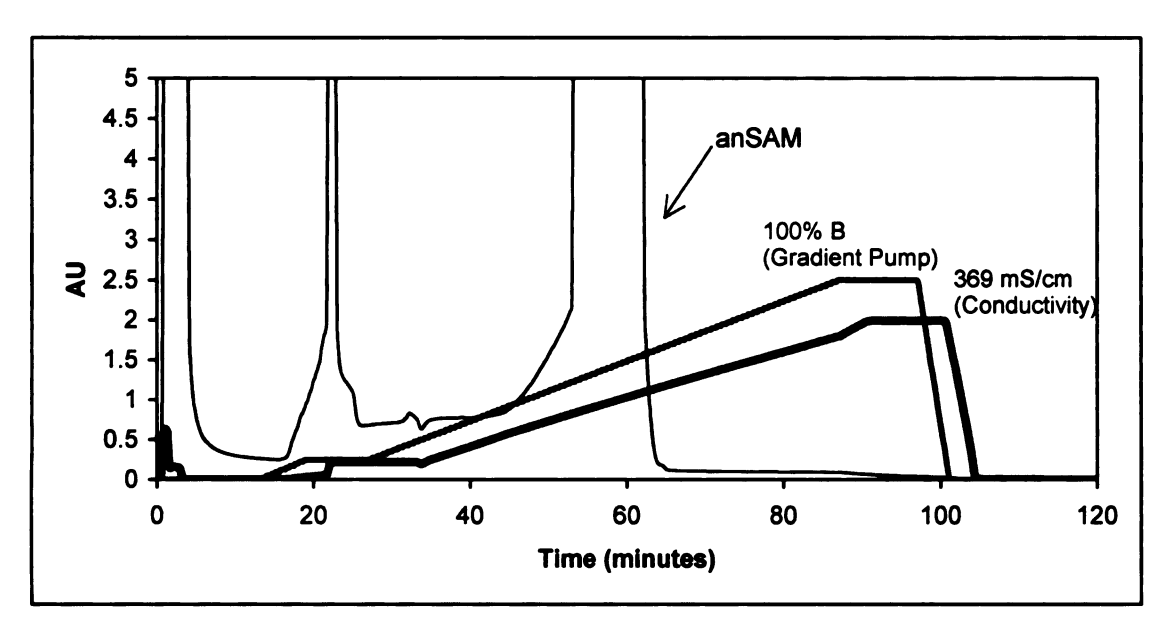


**Figure V.19** Chromatogram of isolation of anSAM by SOURCE 15S cation exchange chromatography (Pharmacia, 8 mL), gradient from 0-1 M HCl, flow rate = 1 mL/min. AnSAM eluted as a distinct peak from 38 – 56 % buffer B.

#### V.4 Conclusion

The synthesis of the SAM analogues was carried out by using the procedures outlined for the enzymatic synthesis of SAM. By using S-allyl-homocysteine, an analog of methionine, the allyl analogue of SAM was purified and characterized. The efficiency of the reaction is not very high but a significant amount of the SAM analog was generated. The S-vinylhomocysteine was not successfully synthesized following the procedures outlined in the experimental methods. Reduction of the disulfide bond results in a very reactive DL-homocysteine sodium thiolate, which is prone to oxidation to regenerate the DL-homocystine. A more efficient way of making this analogue without using liquid ammonia and the addition of sodium metal has not been reported as of this time.

The synthesis of the anSAM analogue on the other hand, requires the multi-step synthesis of anAdo, followed by the enzymatic phosphorylation to generate anATP. The enzymatic phosphorylation of anAdo requires the action of three kinases and an enzymatic amount of ATP. However, the kinases needed especially adenosine kinase (AdoK) are not readily available and to synthesize a significant amount of anSAM for EPR and ENDOR analysis, it will be prohibitive to employ such a method. Repeated attempts to synthesize ATP using the purified AdoK resulted to very little amount of ATP formed. In addition, purified AdoK showed very little activity and was ineffective in the overall enzymatic phosphorylation procedure.

In an attempt to find an alternative method in synthesizing anATP, a synthetic route seems to be the answer to solving this dilemna. Kraybill and coworkers have reported the synthesis of ATP analogues which can be used by mutant protein kinases.<sup>23</sup> The phosphorylation they employed involves suspending the nucleoside in trimethyl phosphate under argon at 0°C. Phosphorous oxychloride was added until a homogeneous mixture was obtained. Tert-butylpyrophosphoric acid dissolved in DMSO was then poured into the reaction and after 1 minute, the mixture was neutralized with triethylammonium bicarbonate. The volatile materials were then evaporated and the resulting white solid dissolved in water and purified by HPLC. This method has not yet been employed in the phosphorylation of anAdo and efforts are underway to determine the efficiency of this procedure.

The importance in the syntheses of these AdoMet analogues lies in the fact that investigating the interaction of S-adenosyl-L-methionine and the Fe-S cluster of PFL-AE will give us insight into the mechanism by which the 5'-deoxyadenosyl radical is generated. Due to its transient existence, spectroscopic methods have not been able to detect this important intermediate. However, the use of SAM analogues might be the key in the first step in understanding the mechanism by which the 5'-deoxyadenosyl radical is formed.

#### V.5 References

- (1) Udsin, E. B., R.T.; Creveling, C.R., Ed. *Biochemisty of S-Adenosylmethionine and Related Compounds*; Macmillan and Co.: London, 1982.
- (2) Salvatore, F. B., E.; Zappia, V.; Williams-Ashman, H.; Schlenk, F., Ed. *The Biochemistry of Adenosylmethionine*; Columbia Univ. Press: New York, 1977.
- (3) Cox, R. S., R.C. Arch. Biochem. Biophys. 1969, 129, 615.
- (4) Parks, L. W. J. Biol. Chem. 1958, 232, 169.
- (5) Schlenk, F. D., J.L. *Biochem. Biophys. Acta* **1975**, 385, 312.
- (6) Kim, H. J. B., T.J.; Nathin, S.J.; McMullen, H.F.; Hansen, D.E. *Anal. Biochem.* **1992**, *207*, 68.
- (7) Knappe, J. N., F.A.; Blaschkoski, H.P.; Ganzler, M. *Proc. Natl. Acad. Sci. USA* **1984**, *81*, 1332.
- (8) Knappe, J. S., T. *Biochem. Biophys. Res. Commun.* **1976**, *71*, 1110.
- (9) Henshaw, T. F. C., J.; Broderick, J. B. *J. Am. Chem. Soc.* **2000**, *122*, 8331.
- (10) Magnusson, O. T. R., G.H.; Frey, P.A. *Biochemistry* **2001**, *40*, 7773.
- (11) Frey, P. A. B., S. Adv. Free Radical Chem. 1999, 2, 1.
- (12) Abeles, R. H. D., D.H. Acc. Chem. Res. 1976, 9, 114.
- (13) Lieder, K. W. B., S.; Ruzicka, F.J.; Beinart, H.; Reed, G.H.; Frey, P.A. *Biochemistry* **1998**, *37*, 2578.
- (14) Cosper, N. J. B., S.J.; Ruzicka, F. Frey, P.A.; Scott, R.A. *Biochemistry* **2000**, *39*, 15668.
- (15) Banerjee, R., Ed. *Chemistry and Biochemistry of B*<sub>12</sub>; Wiley-Interscience: New York, 1999.
- (16) Licht, S. B., S.; Stubbe, J. *Biochemistry* **1999**, *38*, 1221.

- (17) Spychala, J. D., N.S.; Takabayashi, K.; Datta, M.; Fox, I.H.; Gribbin, T.; Mitchell, B.S. *Proc. Natl. Acad. Sci. USA* **1996**, *93*, 1232.
- (18) Leopold, W. R. M., J.A.; Miller, E.C. Cancer Res. 1982, 42, 4364.
- (19) Leopold, W. R. M., J.A.; Miller, E.C. *Biochem. Biophys. Res. Commun.* **1979**, *88*, 395.
- (20) Kolenbrander, H. M. Canadian. J. Chem. 1969, 47, 3271.
- (21) Robins, M. J. M., R.; Jones, R.A.; Fouron, Y. *J. Am. Chem. Soc.* **1976**, *98*, 8204.
- (22) Robins, M. J. J., R.A.; Mengel, R. *J. Am. Chem. Soc.* **1976**, *98*, 8213.
- (23) Kraybill, B. C. E., L.L.; Blethrow, J.D.; Morgan, D.O.; Shokat, K.M. *J. Am. Chem. Soc.* **2002**, *124*, 12118.

#### **CHAPTER VI**

# MECHANISTIC INVESTIGATION OF ADOMET ANALOGS

#### VI.1 Introduction

Electron paramagnetic resonance (EPR) spectroscopy has been central to the developing understanding of the radical-SAM enzymes. It was EPR spectroscopy that first demonstrated the presence of a stable glycyl radical in pyruvate formate lyase. 1,2 and EPR has now been used to identify glycyl radicals in other enzymes, including the anaerobic ribonucleotide reductase<sup>3</sup> and benzylsuccinate synthase.4 that are substrates of radical-SAM activating enzymes. EPR spectroscopy has also played a key role in identifying iron-sulfur clusters in radical-SAM enzymes and, together with Mössbauer spectroscopy, in characterizing cluster types and oxidation states and identifying the catalytically active cluster. 3,5-17 Electron-nuclear double resonance (ENDOR) spectroscopy. which probes coupling between electronic and nuclear spins. 18 was used to provide the first evidence for the close proximity of SAM to the iron-sulfur cluster, as well as for direct coordination of the unique iron site of the iron-sulfur cluster by SAM. 19,20 This unprecedented structural motif, with the amino and carboxylate moieties of SAM coordinating the unique iron site of a [4Fe-4S] cluster, appears to be a key element of radical-SAM enzyme function, as it has now appeared in

crystal structures of three diverse members of the radical-SAM superfamily.<sup>21-23</sup> In addition to this novel coordination mode, ENDOR spectroscopy provided evidence for direct orbital overlap between the sulfonium of SAM and the iron-sulfur cluster, a feature of the SAM-cluster interaction that is not apparent in the X-ray crystal structures but is indisputable based on the ENDOR data.<sup>19</sup> EPR and ENDOR spectroscopies have clearly been central to the development of understanding of the radical-SAM enzymes, and have more than once been the basis for radical new ways of thinking about these fascinating enzymes.

Pyruvate formate-lyase (PFL), an enzyme involved in anaerobic glucose metabolism in *Escherichia coli* and other facultative anaerobes, has the distinction of being the first enzyme ever identified to contain a stable and catalytically essential glycyl radical.<sup>1,2,24</sup> This remarkable discovery was made using electron paramagnetic resonance (EPR) spectroscopy in combination with isotopic labeling, together with analysis of the products of oxygenolytic cleavage of the radical-containing protein. The identification of a catalytically essential glycyl radical in pyruvate formate-lyase raised three key questions: (1) What is the mechanism by which a glycyl radical mediates the C-C bond cleavage reaction of converting pyruvate to formate, (2) what is responsible for the unusual stability of the glycyl radical, and (3) how is the glycyl radical generated? The first question has been the subject of active investigation for nearly 30 years, and yet uncertainty remains regarding the precise role of the glycyl radical in catalysis.<sup>25</sup>

Early work on PFL-AE was performed on enzyme purified under aerobic conditions and,<sup>26</sup> in some cases, on enzyme that had been completely denatured

prior to purification and subsequently refolded.<sup>27</sup> Because PFL-AE is active in anaerobic bacteria and because it contained an as-yet unidentified metal center. in order to identify the enzyme with its functionally relevant metal center, we would have to purify the protein without denaturation and without exposure to oxygen. Our early attempts to purify the protein in this manner involved simply using Ar-purged buffers on our protein purification columns and collecting protein fractions in a glovebag. This methodology allowed PFL-AE to be eluted from the column as a dark red-brown fraction; however, the color would rapidly fade if the fractions were not quickly frozen or transferred to more strictly anaerobic conditions. Once procedures were in place to isolate protein containing this chromophore, spectroscopic studies were initiated. UV-visible spectra revealed a chromophore with broad, overlapping transitions, characteristic of an iron-sulfur cluster, although the type of cluster was not immediately obvious from the spectra. Iron and sulfide analyses confirmed this preliminary finding, as they showed approximately equivalent amounts of iron and sulfide in the protein.<sup>25</sup> Using resonance Raman spectroscopy, we were able to further define the metal center as a mixture of [2Fe-2S]<sup>2+</sup> and [4Fe-4S]<sup>2+</sup> clusters in the isolated enzyme, with only [4Fe-4S]<sup>2+</sup> clusters remaining after reduction by dithionite.<sup>6</sup> EPR spectra of both of these states showed no signal, as expected for diamagnetic [2Fe-2S]<sup>2+</sup> and [4Fe-4S]<sup>2+</sup> clusters; however, if the protein was reduced in the presence of S-adenosylmethionine, a nearly axial signal (g = 2.013, 1.889, 1.878) characteristic of a [4Fe-4S]<sup>+</sup> cluster was observed. These results suggested not only that S-adenosylmethionine affected the ability to reduce to the [4Fe-4S]<sup>+</sup>

state, but that the [4Fe-4S]<sup>+</sup> state might be the catalytically active state, as it was the state present under reducing conditions in the presence of the cosubstrate S-adenosylmethionine.<sup>25</sup>

Further modifications of our expression and purification conditions, which yielded more-soluble PFL-AE with a higher iron-sulfur cluster content, also slightly modified the cluster composition and behavior. EPR and resonance Raman spectroscopies now revealed the presence of a [3Fe-4S]<sup>+</sup> cluster (g = 2.01, 1.94) in the isolated enzyme that accounted for approximately two-thirds of the total iron in the sample.<sup>8</sup> The form of the remaining iron was identified using Mössbauer spectroscopy after the protein had been labeled with <sup>57</sup>Fe.

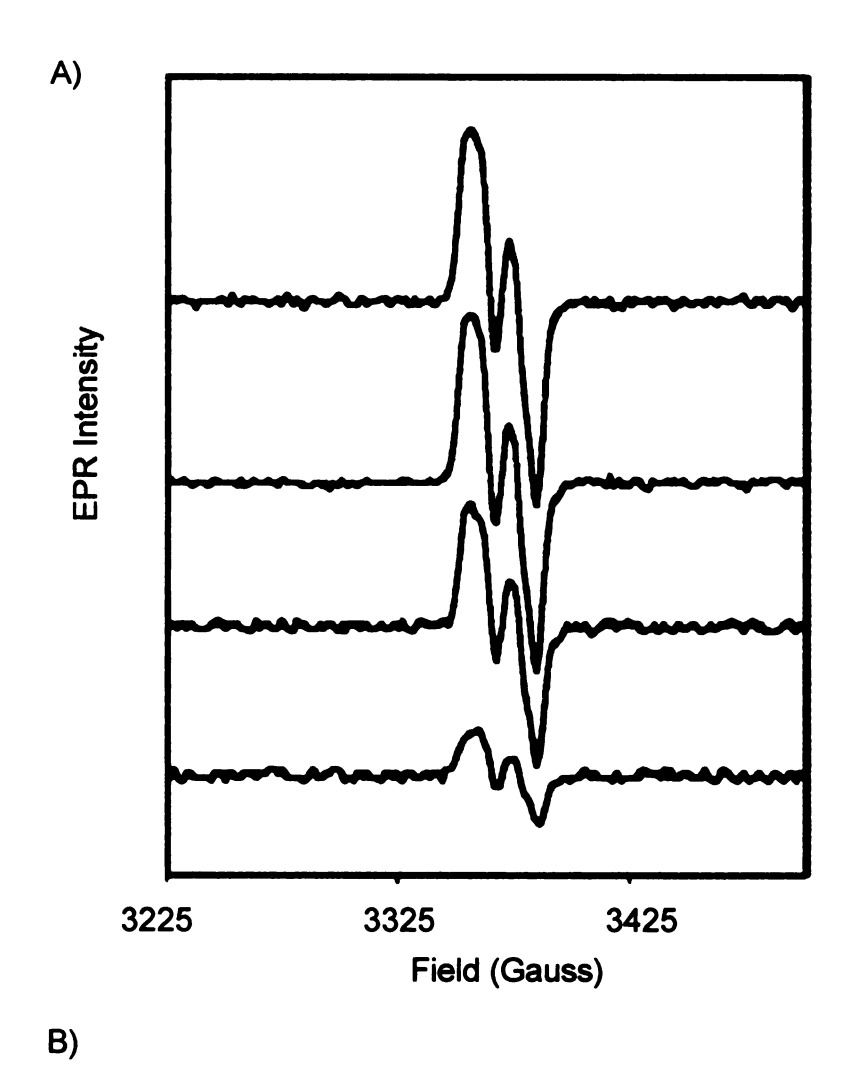
Mössbauer spectra confirmed that approximately 67% of the iron was present in the form of a cuboidal [3Fe-4S]<sup>+</sup> cluster ( $\delta$ = 0.28 mm/s,  $\Delta E_Q$  = 0.60 mm/s), while the remaining 33% of the iron was found as a mixture of [2Fe-2S]<sup>2+</sup> ( $\delta$ = 0.29,  $\Delta E_Q$  = 0.58), [4Fe-4S]<sup>2+</sup> ( $\delta$ = 0.45,  $\Delta E_Q$  = 1.15), and linear [3Fe-4S]<sup>+</sup> clusters. Addition of dithionite to this protein sample containing four different types of clusters resulted in a protein sample containing only [4Fe-4S]<sup>2+/+</sup> clusters.<sup>9</sup>

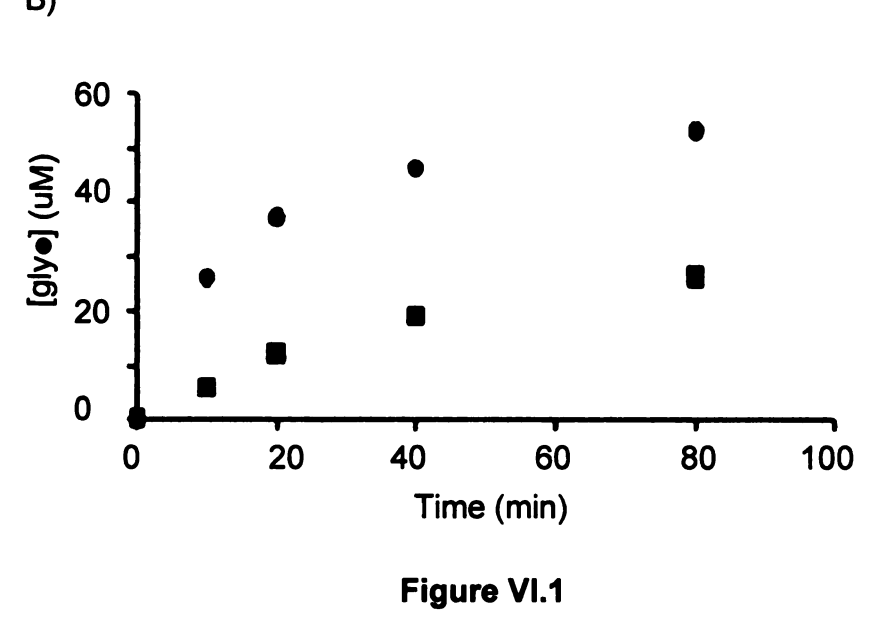
Despite the unusual mixture of clusters present in purified PFL-AE, the enzyme was found to be catalytically active in the typical assay mixture, which includes PFL, PFL-AE, S-adenosylmethionine, and 5-deazariboflavin as a photoreductant.<sup>6,8</sup> The published assay for PFL-AE activity involves incubation of PFL-AE, PFL, S-adenosylmethionine, 5-deazariboflavin, and buffer components in the presence of an intense halogen lamp.<sup>26-28</sup> At varying time intervals, an

aliquot of the mixture is removed and added to a cuvette containing pyruvate and CoA (the PFL substrates) as well as malic dehydrogenase, citrate synthase, and NAD, which are required for coupling PFL turnover to the spectroscopically detectable reduction of NAD+ to NADH. PFL activity is thus measured indirectly via the coupling assay, and the amount of active PFL for that time point is then inferred, which allows for the calculation of the rate of PFL activation. All manipulations must be done under strict anaerobic conditions because of the extreme air sensitivity of the glycyl radical, and so, in addition to being an indirect assay of PFL-AE activity, it is guite cumbersome and prone to experimental error. Because of the difficulty of the published assay and our questions as to its reliability, we developed a simple and direct assay for PFL-AE activity that involves monitoring production of the PFL glycyl radical as a function of time by EPR spectroscopy as shown in Figure VI.1. This assay provides a direct (although still discontinuous) measure of the rate of production active PFL by PFL-AE. Using this assay method, we were able to obtain a specific activity for PFL-AE of 98000 pmol min<sup>-1</sup> mg<sup>-1</sup>, significantly higher than has been previously reported.<sup>7,27</sup> Removal of the cluster by oxidation and chelation of the iron, followed by gel filtration, resulted in complete loss of PFL-AE activity, demonstrating that the cluster was essential for the catalytic reaction.<sup>25</sup>

The studies described above clearly demonstrated, for the first time, the strict dependence of PFL-AE catalytic activity on the presence of the iron-sulfur cluster. Our observation of four different clusters in purified PFL-AE, however,

Figure VI.1 Assay of PFL-AE activity using EPR spectroscopy. (A) EPR spectra recorded at 10, 20, 40, and 80 min (bottom to top) during PFL activation. (B) Plots of the glycyl radical spin quantitation as a function of time for PFL-AE at 6.25 ug/mL (•) and 25 ug/mL (•); higher concentrations of AE provide a higher rate of activation, as expected. EPR parameters: *T*, 60 K; microwave power, 20 μW; microwave frequency, 9.48 GHz; modulation amplitude, 5.054 G.



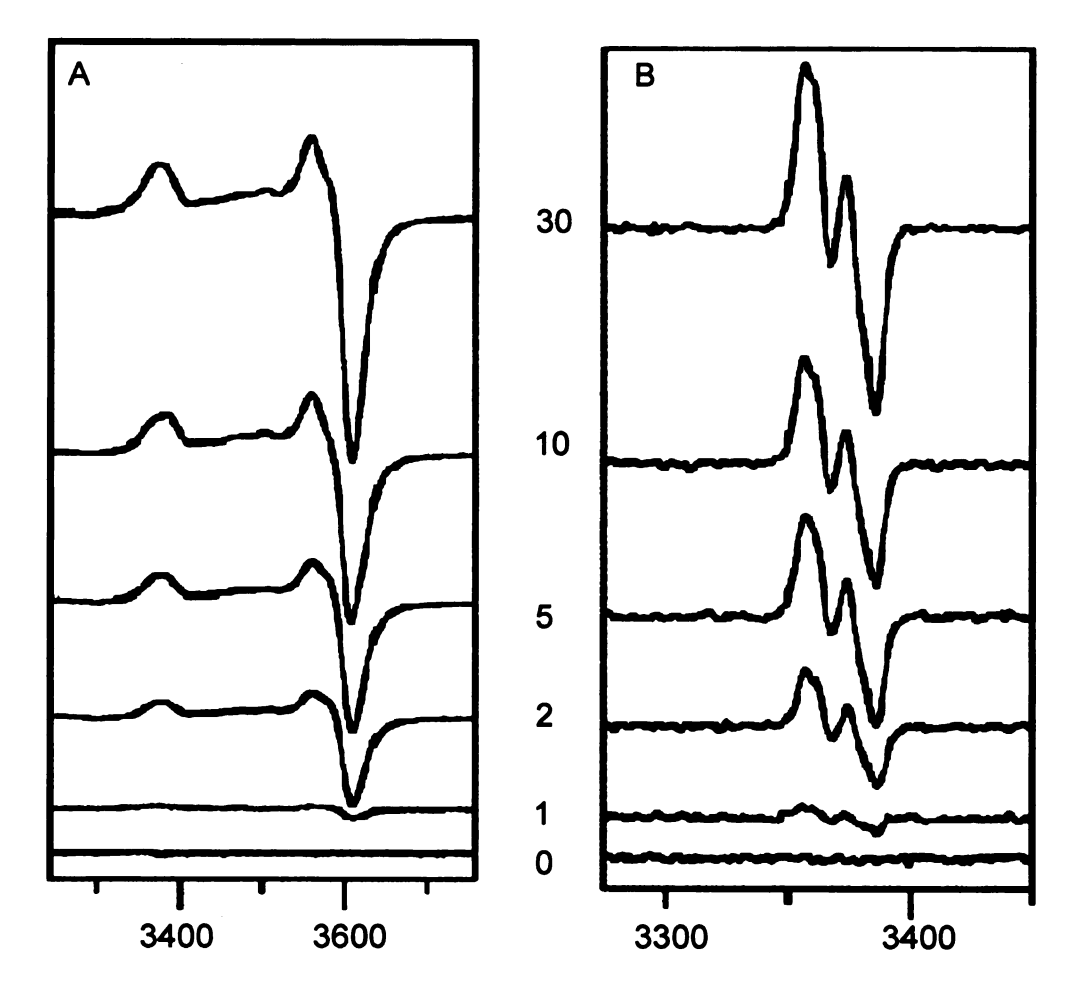


raised an obvious question: Which cluster form was responsible for the catalytically required generation of the glycyl radical of PFL? Because a reductant was required during the activation of PFL and because, in the presence of the reductant dithionite, only [4Fe-4S]<sup>2+/+</sup> clusters are observed in PFL-AE,<sup>9</sup> it was reasonable to propose that [4Fe-4S] clusters were involved in the catalytic activity of PFL-AE. However, direct evidence for the active cluster form was elusive, as reductant was required for PFL activation but reductant also caused cluster transformations.<sup>25</sup>

To examine this issue more clearly, we used 5-deazariboflavin-mediated photoreduction of PFL-AE to achieve single-turnover conditions. 17 The advantage of photoreduction is that it can be used to reduce the PFL-AE iron-sulfur cluster to a specified state, and then excess reductant can be easily removed by simply placing samples in the dark. This then allows monitoring of the reactivity of specific cluster states of PFL-AE, without interference from reductants that might cause cluster interconversions. Furthermore, changes in cluster state due to enzymatic turnover could be monitored. The results of these experiments are shown in Figure VI.2.<sup>17</sup> The starting state for the protein prior to photoreduction is the diamagnetic [4Fe-4S]<sup>2+</sup> state in these experiments, and with increasing time of photoreduction, increasing amounts of  $[4Fe-4S]^{+}$  cluster (g = 2.01, 1.89, 1.88) are observed by EPR spectroscopy, as seen in Figure VI.2, panel A. These EPR spectra of PFL-AE are recorded in the presence of S-adenosylmethionine, which is not reductively cleaved by PFL-AE in the absence of PFL. At each time point of photoreduction, the PFL-AE + S-adenosylmethionine sample was divided: half of

the sample was used directly for EPR analysis, and the other half was mixed with an equimolar amount of PFL before being frozen for EPR analysis. EPR spectra of the samples containing PFL are shown in Figure VI.2, panel B. It is clear from these spectra that the [4Fe-4S]<sup>2+</sup> state of PFL-AE is unable to generate the glycyl radical on PFL in the absence of exogenous reductant; however, as the amount of [4Fe-4S]<sup>+</sup> cluster on PFL-AE increases, the amount of glycyl radical produced on PFL also increases. EPR spin quantitation reveals a 1:1 correspondence between the amount of [4Fe-4S] on PFL-AE and the amount of glycyl radical generated on PFL (Figure VI.2, panel C). 17 Also apparent from these spectra is the disappearance of the [4Fe-4S] + EPR signal concomitant with appearance of the glycyl radical EPR signal (the glycyl radical EPR spectra shown were recorded at 60 K, a temperature at which the [4Fe- 4S] signal is not observed; however, when recorded at 12 K, the samples included in panel B of Figure VI.2 showed no evidence for a [4Fe-4S] + EPR signal). Taken together, these results provide strong evidence that the [4Fe-4S] \* state of PFL-AE is the catalytically active state and that this reduced cluster provides the electron necessary for reductive cleavage of S-adenosylmethionine and subsequent abstraction of a H atom from G734 of PFL as shown in Figure VI.3. Thus, one [4Fe-4S]<sup>+</sup>-PFL-AE generates one PFL-Gly· and, in the process, is oxidized to [4Fe-4S]<sup>2+</sup>-PFL-AE.<sup>17</sup>

Figure VI.2 EPR-detected single-turnover experiments to define the catalytically active iron-sulfur cluster in PFL-AE. (A) EPR spectra of samples containing PFL-AE, SAM, and 5-deazariboflavin as a function of illumination (reduction) time in minutes. (B) EPR spectra of samples as in A to which PFL has been added prior to freezing for EPR. (C) EPR spin quantitation of the [4Fe-4S]<sup>+</sup> and glycyl radical signals shows a 1:1 correspondence.



Field (Gauss)

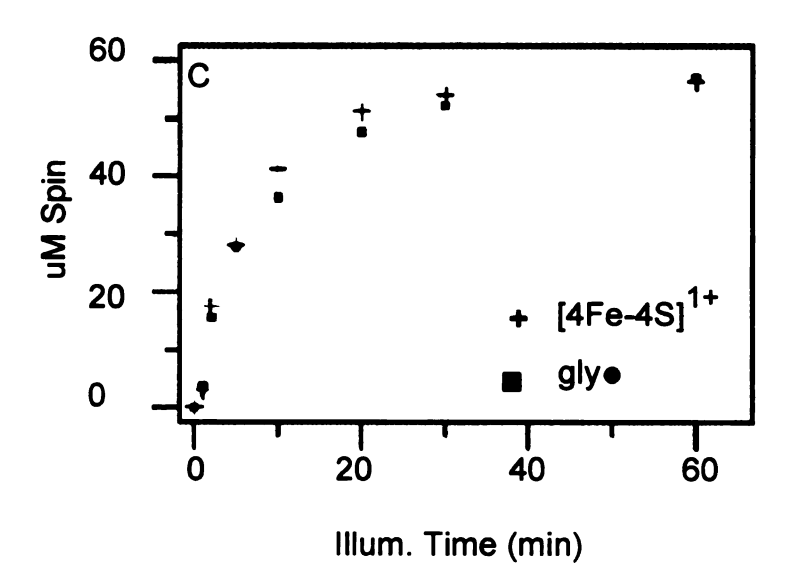


Figure VI.2

Figure VI.3 Reaction catalyzed by pyruvate formate-lyase activating enzyme.

On the basis of these observations, we propose a mechanism, outlined in Figure VI.4, in which SAM binds to the oxidized  $[4Fe-4S]^{2+}$  cluster of PFL-AE via coordination of the unique site, which puts the sulfonium in orbital overlap with one of the  $\mu_3$ -bridging sulfides of the  $[4Fe-4S]^{2+}$  cluster. One-electron reduction (mediated by reduced flavodoxin *in vivo*) provides the reduced  $[4Fe-4S]^{+}$  cluster complexed to SAM. This  $[4Fe-4S]^{+}$ -SAM complex is stable in the absence of the substrate PFL; however, in the presence of PFL, inner-sphere electron transfer from the  $[4Fe-4S]^{+}$  cluster to the sulfonium of SAM initiates homolytic S-C(5')

bond cleavage. The resulting methionine is left bound to the unique site of the oxidized [4Fe-4S]<sup>2+</sup> cluster, while the adenosyl radical intermediate abstracts the pro-S H from G734 of PFL. The catalytic cycle is completed upon displacement of methionine and 5'-deoxyadenosine with an S-adenosylmethionine cosubstrate.<sup>25</sup> It is of interest to note that recent synthetic models of the radical-SAM enzymes based on site-differentiated [4Fe-4S] clusters have provided evidence for reductive cleavage of sulfonium moieties by reduced [4Fe-4S] clusters, although a stable synthetic cluster-sulfonium complex has not yet been reported.<sup>29,30</sup>

In order to probe this proposed mechanism, we employed S-adenosyl-methionine analogues to verify the formation of the proposed reduced [4Fe-4S]<sup>†</sup> cluster complexed to SAM prior to the homolytic cleavage of the S-C(5') bond and the activation of PFL. S-allyl-AdoMet, an S-adenosylmethionine analog with an allyl side-chain instead of the methyl group in regular SAM was used to activate PFL. Our hypothesis was that the presence of the allylic side-chain might help stabilize any radical species formed during the activation and might thereby prevent the homolytic cleavage of SAM; such stabilization would allow us to detect the SAM radical via EPR spectroscopy. Another good analogue to employ is the 3'-anhydroAdoMet where an allylic stabilization on the ribosyl group can be obtained after the homolytic cleavage of the S-C(5') bond. This allylic radical can be detected by EPR spectroscopy as shown by the work done by Frey and co-workers with this AdoMet analog and lysine 2,3-aminomutase enzyme, also a member of the radical SAM superfamily.<sup>31</sup>

**Figure VI.4** Proposed mechanism for iron-sulfur cluster and SAM-mediated radical generation catalyzed by PFL-AE.

## VI.2 Experimental Methods

### VI.2.1 Materials

PFL and PFL-AE were grown and purified as described in Chapter II. Allyl-AdoMet and 3'-anhydro-AdoMet were synthesized as described in Chapter IV. 5-deazariboflavin was synthesized as described by the methods below. All other chemicals were of the highest purity and obtained from commercial sources.

## VI.2.2 NMR Spectroscopy

NMR spectra were recorded at room temperature on a VXR-300 spectrometer.

# VI.2.3 Mass Spectrometry

Mass spectral data were obtained at the Michigan State University Mass Spectrometry Facility, which is supported, in part, by a grant (DRR-00480) from the Biotechnology Research Technology Program, National Center for Research, National Institutes of Health.

## VI.2.4 Synthesis of 5-Deazariboflavin

Synthesis of 6-[N-(D-ribityl)-3,4-xylidino]uracil<sup>6,32</sup>

A mixture of 1.175 g (7.9 mmol) of 6-chlorouracil, 6.125 g (24 mmmol) of N-D-ribityl-3,4-xylidine, 31 mL of water, and 15 mL of ethanol was stirred under reflux for 17.5 hours. The mixture was then cooled on ice, which resulted in crystal formation. Sodium hydroxide (0.72g) was added and the mixture was stirred for three more hours. The solid formed was removed by filtration while washing with cold water. The filtrate and washings obtained were adjusted to pH 3.01 by the addition of concentrated hydrochloric acid and concentrated using the rotary evaporator. The crude product was extracted with boiling methanol leaving the sodium chloride undissolved. The filtrate and methanol washings were dried using the rotary evaporator until a residual gum is formed. It was recrystallized in 15 mL of water and placed in a 4°C cold box overnight. A cream-

colored solid was obtained and dried under vacuum. (1.54 g, 53.6% Yield):  $^{1}$ H NMR (300 MHz, DMSO-d<sub>6</sub>):  $\delta$  10.37 (s, 1H), 10.04 (s, 1H), 6.87-7.30 (m, 3H), 3.82-3.58 (m, 4H), 3.54-3.11 (m, 8H), 2.2 (s, 6H) ppm.

Synthesis of 6-[N-2',3',4',5'-tetra-O-acetyl-(D-ribityl)-3,4-xylidinoluracil<sup>33</sup>

A mixture of 1.54 g of 6-[N-(D-ribityl)-3,4-xylidino]uracil (4.74 mmol) and 12.5 mL acetic anhydride was stirred vigorously for 15 minutes on ice. Over a period of 30 minutes, 0.5 mL perchloric acid was added drop-wise to the cold and stirring mixture. It was then stirred at 20°C in a water bath for 165 minutes.

Methanol (4 mL) was added drop-wise to the solution and cooled to 0°C with ice. The solution was concentrated and the residue formed was dissolved in 15 mL chloroform. It was washed with saturated aqueous sodium bicarbonate and water and dried over anhydrous MgSO<sub>4</sub>. The solvent was removed using a rotary evaporator and the yellow residue was crystallized from chloroform/petroleum ether. The yellow solid formed was dried under vacuum. (1.5 g, 79.2% yield): <sup>1</sup>H NMR (300 MHz, MeOH-d<sub>4</sub>): δ 7.25 (s, 1H), 7.10 (s, 1H), 6.95 (d, 1H), 5.30 (m, 2H), 5.15 (s, 1H), 4.8 (s, 1H), 3.73-4.38 (m, 4H), 2.3 (s, 6H), 2.15 (s, 4H), 2.00 (s, 4H), 1.85 (s, 4H) ppm.

Synthesis of 2',3',4',5'-tetra-O-acetyl-5-deazariboflavin<sup>34</sup>

A mixture of crushed 1.54g of 6-[N-2',3',4',5'-tetra-O-acetyl-(D-ribityl)-3,4-xylidino]uracil (2.87 mmol) and 4 mL of DMF was treated with 0.40 mL POCl<sub>3</sub>.

The mixture was allowed to stand for 30 minutes until a red solution was formed.

The reaction was then stirred for 15 minutes at 100°C. The reaction mixtures was poured on crushed ice (approximately 100 mL), stirred and then crushed. The pH of the suspension was adjusted to pH 6 using ammonium hydroxide and stirred for 30 minutes. The product was filtered and washed with 250 mL water and ether:methanol (2:1) and dried under vacuum to obtain the yellow solid. (1.40g, 88.0%):  $^{1}$ H NMR (300 MHz, DMSO-d<sub>6</sub>):  $\delta$  8.75 (s, 1H), 7.75 (s, 2H), 4.38-5.90 (m, 7H), 2.40 (s, 3H), 2.30 (s, 3H), 2.20, (s, 3H), 2.10 (s, 3H), 2.00 (s, 3H), 1.50 (s, 3H) ppm.

# Synthesis of 5-deazariboflavin<sup>33</sup>

A mixture of 1.40g of 2',3',4',5'-tetra-O-acetyl-5-deazariboflavin and 13.54 mL or 1M HCl saturated in 99.98% methanol was stirred for 18 hours at room temperature. The reaction mixture was dried using the rotary evaporator to yield a yellow residue. The crude product was then treated with water, cooled with ice, and filtered and washed with cold water. The yellow product was further washed with ether:methanol (2:1) and dried under vacuum. (0.75 g, 65.6 % yield)  $^{1}$ H NMR (300 MHz, DMSOd<sub>6</sub>)  $\delta$ : 11.1 (s, 1H), 8.8 (s, 1H), 8.8 (s, 1H), 7.9 (s, 2H), 7.8 (s, 2H), 3.1-5.2 (m, 11H), 2.4 (s, 6H), 2.3 (s, 6H) ppm. FAB-MS, calculated mass for  $C_{18}H_{21}N_3O_6 = 375.38$ , found m/z = 376.00.

## VI.2.5 Single Turnover Experiment with PFL-AE and Allyl-AdoMet

PFL-AE was purified as described previously<sup>8</sup> except that 1 mM DTT was included in all buffers. Samples were prepared in an anaerobic chamber at 0°C

using 1321  $\mu$ M PFL-AE (3.70 Fe/monomer) in 100 mM TRIS pH 8.0 diluted to 200  $\mu$ M using 50 mM Tris (pH 8.0). 5-Deazariboflavin was added in the dark to a final concentration of 100  $\mu$ M. The samples were illuminated by a 500 W halogen lamp for the indicated times (1,2,5,10,30 and 60 minutes), followed by addition of allyl-AdoMet to 2 mM. In the dark, each sample was split into two sets, and to one an equimolar amount of PFL solution (final concentration of 200  $\mu$ M PFL) was added. Samples were stored frozen in the dark until EPR spectra were recorded

## VI.2.6 EPR Spectroscopy

EPR first-derivative spectra were obtained at X-band on a Bruker ESP300E spectrometer equipped with a liquid He cryostat and a temperature controller from Oxford Instruments. Spectra were recorded at 12 K for [3Fe-4S]<sup>†</sup> and [4Fe-4S]<sup>†</sup>, and at 60 K to detect glycyl radical. Spin quantifications were done as described previously. The double integrals of the EPR signals were evaluated by using a computer on-line with the spectrometer. Spin concentrations in the protein samples were determined by calibrating double integrals of the EPR spectra recorded under nonsaturating conditions (i) with a standard sample of 0.1 mM Cu(II) and 1 mM EDTA solution for the cluster signals, or (ii) with a 1.04 mM K<sub>2</sub>(SO<sub>3</sub>)<sub>2</sub>NO solution for the glycyl radical signals. The concentration of the K<sub>2</sub>(SO<sub>3</sub>)<sub>2</sub>NO standard was determined using the optical extinction coefficient.

### VI.3 Results and Discussion

### VI.3.1 Synthesis of 5-Deazariboflavin

Synthesis of 6-[N-(D-ribityl)-3,4-xylidino]uracil

The synthesis of 6-[N-(D-ribityl)-3,4-xylidino]uracil was obtained following the reaction shown in Figure VI.5. N-D-ribityl-3,4-xylidine and 6-chlorouracil was refluxed for 17.5 hours in water and ethanol and a light brown solution was

$$H_3C$$
 $H_3C$ 
 $H_3C$ 

**Figure VI.5** Reaction mechanism for the synthesis of 6-[N-(D-ribityl)-3,4-xylidino] uracil.

formed. Cooling this clear solution resulted in the formation of tan-colored fine needles. After the addition of sodium hydroxide, more tan-colored precipitate formed and the mixture was further cooled on ice and stirred for 3 more hours.

The tan-colored solid obtained was virtually pure N-D-ribityl-3,4-xylidine based on its <sup>1</sup>H NMR. The desired product was obtained from the filtrate by removing the solvent using the rotary evaporator and redissolving the crude product in boiling methanol. The resulting yellow solution was adjusted to pH 3.10 and the solvent was removed by using the rotary evaporator to yield a cream-colored gum. Recrystallization of the product was performed by dissolving the residual gum in a minimal amount of water added drop-wise. The yellow-colored solution was stored in the cold box at 5°C for about three days to allow the crystals to crash out from the solution. The 6-[N-(D-ribityl)-3,4-xylidino] uracil was filtered out using a frit funnel and was dried under vacuum. A second batch of product was obtained by reducing the volume of the filtrate after the first batch of precipitate was collected and storing this yellow solution in the cold box at 5°C for an additional 3 days.

Synthesis of 6-[N-2',3',4',5'-tetra-O-acetyl-(D-ribityl)-3,4-xylidino]uracil

The cream colored 6-[N-(D-ribityl)-3,4-xylidino]uracil was reacted with acetic anhydride as shown in Figure VI.6 to form 6-[N-2',3',4',5'-tetra-O-acetyl-(D-ribityl)-3,4-xylidino]uracil. Perchloric acid was added drop-wise to the bright yellow solution to regulate the vigorous reaction. The reaction mixture was stirred for 165 minutes at which point, the reaction have reached completion. Methanol was added to quench the excess acetic anhydride and the crude product, which was an orange/brown residue, turns yellow upon dissolution in chloroform. To recrystallize the desired product, the yellow residue obtained after washing the

chloroform solution and removing the solvent in vacuum, was redissolved in a minimal amount of chloroform and petroleum ether was added drop-wise until the solution became cloudy. Care was taken not to add excess petroleum ether as it

$$H_3C$$
 $H_3C$ 
 $H_3C$ 

**Figure VI.6** Reaction mechanism for the synthesis of 6-[N-2',3',4',5'-tetra-O-acetyl-(D-ribityl)-3,4-xylidino]uracil.

would result in an oily residue and prevent the crystallization process. The yellow suspension was allowed to stand in the cold box at 5°C overnight to allow the maximum amount of 6-[N-2',3',4',5'-tetra-O-acetyl-(D-ribityl)-3,4-xylidino]uracil to form. A yellow solid was obtained and it was dried under vacuum after filtration.

Synthesis of 2',3',4',5'-tetra-O-acetyl-5-deazariboflavin

Crushed 6-[N-2',3',4',5'-tetra-O-acetyl-(D-ribityl)-3,4-xylidino]-uracil was dissolved in dry DMF to yield a bright yellow solution. Upon the addition of POCl<sub>3</sub>, the reaction mixture turned from yellow to orange. Continued stirring for 30 minutes resulted in a deep red solution upon which the mixture was heated to 100°C in an oil bath for 15 minutes. Crushed ice was added to quench the

reaction and a cream suspension was formed. The pH was adjusted to 6 and the product was filtered using a frit funnel covered with aluminum foil. The cyclisation reaction as shown in Figure VI.7 is light- sensitive so the reaction flask and the 2',3',4',5'-tetra-O-acetyl-5-deazariboflavin obtained was covered with aluminum foil the whole time.

**Figure VI.7** Reaction mechanism for the synthesis of 2',3',4',5'-tetra-O-acetyl-5-deazariboflavin.

### Synthesis of 5-deazariboflavin

5-Deazariboflavin was obtained by deacetylating the light-sensitive 2',3',4',5'-tetra-O-acetyl-5-deazariboflavin in the presence of 99.8% methanol and a solution of 1M HCl in ether as shown in Figure VI.8. The reaction flask was kept wrapped in aluminum foil to keep the product formed from photoreducing. Care was taken to keep the product away from light and the synthesized 5-deazariboflavin was stored in a -20°C freezer until needed.

$$H_3C$$
 $H_3C$ 
 $H_3C$ 

Figure VI.8 Reaction mechanism of the synthesis of 5-deazariboflavin.

# VI.3.2 Single Turnover Experiment with PFL-AE and Allyl-AdoMet

Single turnover conditions for PFL-AE can be achieved by limiting the amount of reductant. The clean conversion to [4Fe-4S]<sup>+</sup> provided by photoreduction has allowed us to carry out single turnover experiments for glycyl radical production, since removing illumination eliminates the exogenous reductant. PFL-AE was photoreduced for various times, after which a 10-fold excess of allyl-AdoMet was added and the sample was wrapped in aluminum foil to prevent further reduction. Each sample was then split into two halves and equimolar PFL was added to one-half in the dark. EPR spectra were recorded to detect formation of [4Fe-4S]<sup>+</sup>, the glycyl radical or some kind of EPR-active species that is allyl-AdoMet based in these samples. Figures VI.9 (a-f) show the 12 K EPR spectra of PFL-AE/allyl-AdoMet after photoreduction for 0, 1, 2, 5, 10, and 30 min. Quantitation of these EPR signals results in 68.3, 72.8, 108.7, 118.8, 117.3, and 123.2 

µM spins, respectively. The nearly axial EPR signals shown in Figure VI.9 (a-f) are characteristic of a [4Fe-4S]<sup>+</sup> cluster, and are essentially

identical to the EPR signal previously reported for photoreduced PFL-AE in the presence of AdoMet. After 60 min of illumination, 85% of the cluster in PFL-AE is in the reduced [4Fe-4S]<sup>1+</sup> state. Saturation of cluster reduction is indicated by the illumination time course shown in Figure VI.10.

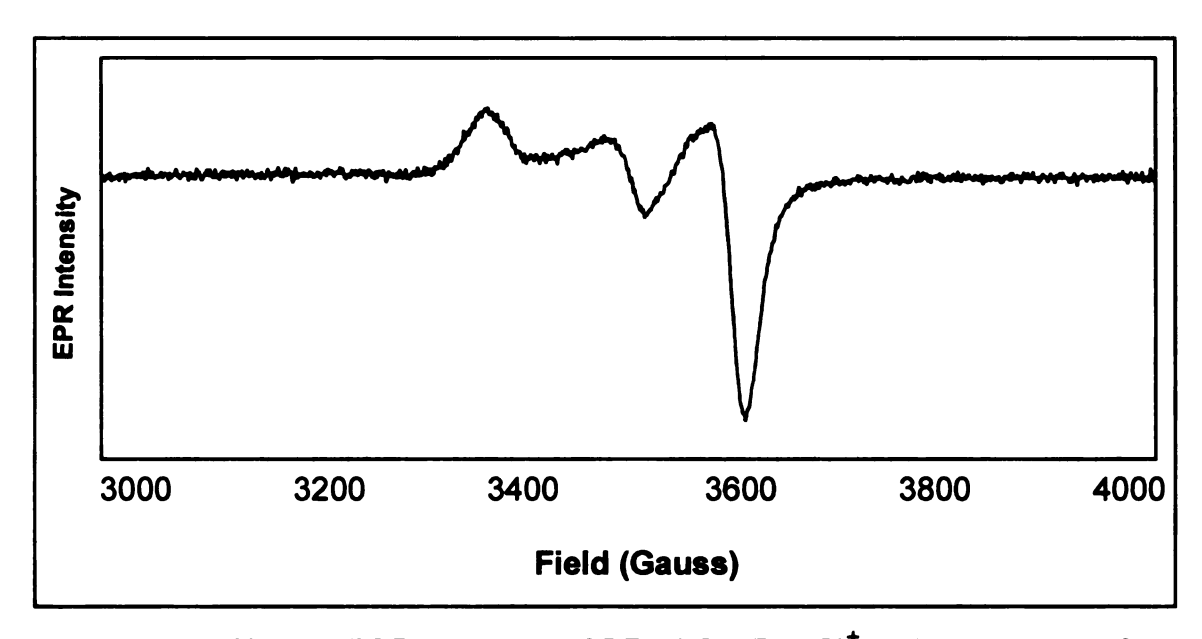


**Figure VI.9.a** X-band EPR spectrum of PFL-AE [4Fe-4S]<sup>+</sup> in the presence of allyl-AdoMet after 1 minute of illumination. The sample contained 200 μM PFL-AE, 1 equivalent of Na<sub>2</sub>S<sub>2</sub>O<sub>4</sub>, 100 μM 5-deazariboflavin, and 2 equivalents of allyl-AdoMet; 9.23 % reduction (based on 68.3 μM spin for 200 μM protein with 3.70 mol Fe/ mol PFL-AE); g = 2.011, 1.948, 1.880. Conditions of measurement: T = 12 K; microwave power, 20 μW; microwave frequency, 9.49 GHz; modulation amplitude, 10.084 G; single scan.

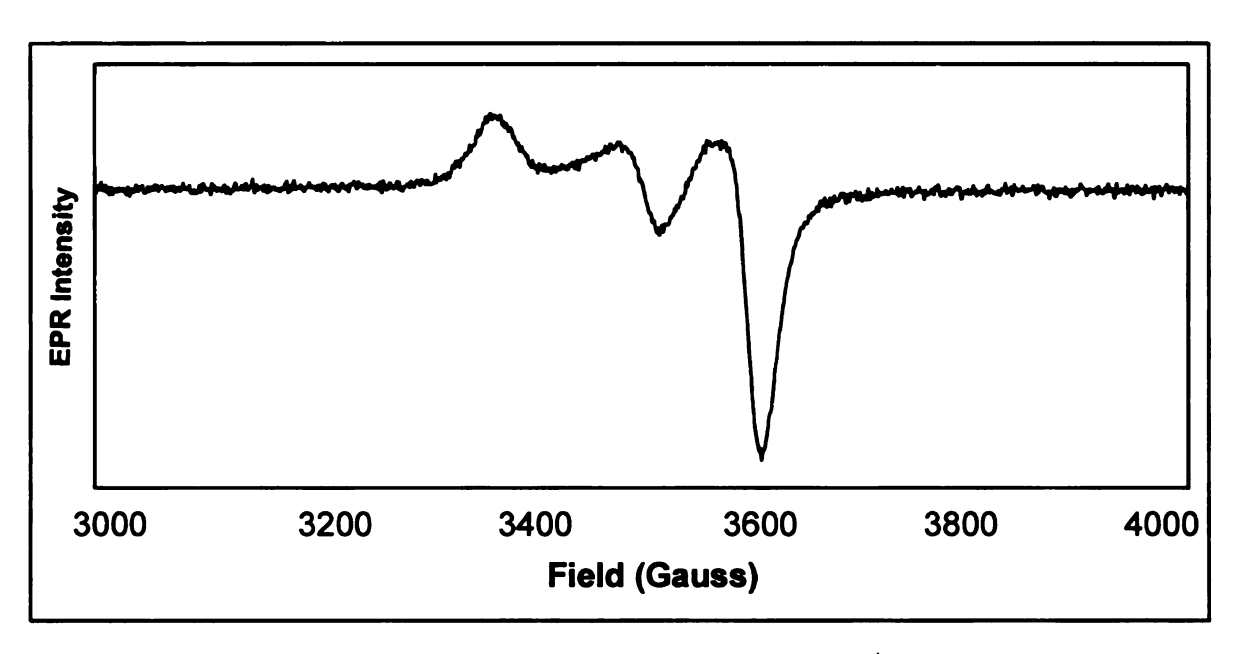


**Figure VI.9.b** X-band EPR spectrum of PFL-AE [4Fe-4S]<sup>+</sup> in the presence of allyl-AdoMet after 2 minutes of illumination. The sample contained 200  $\mu$ M PFL-AE, 1 equivalent of Na<sub>2</sub>S<sub>2</sub>O<sub>4</sub>, 100  $\mu$ M 5-deazariboflavin, and 2 equivalents of allyl-AdoMet; 9.84 % reduction (based on 72.8  $\mu$ M spin for 200 $\mu$ M protein with 3.70 mol Fe/ mol PFL-AE); g = 2.011, 1.948, 1.880. Conditions of measurement: T = 12 K; microwave power, 20  $\mu$ W; microwave frequency, 9.49 GHz; modulation amplitude, 10.084 G; single scan.

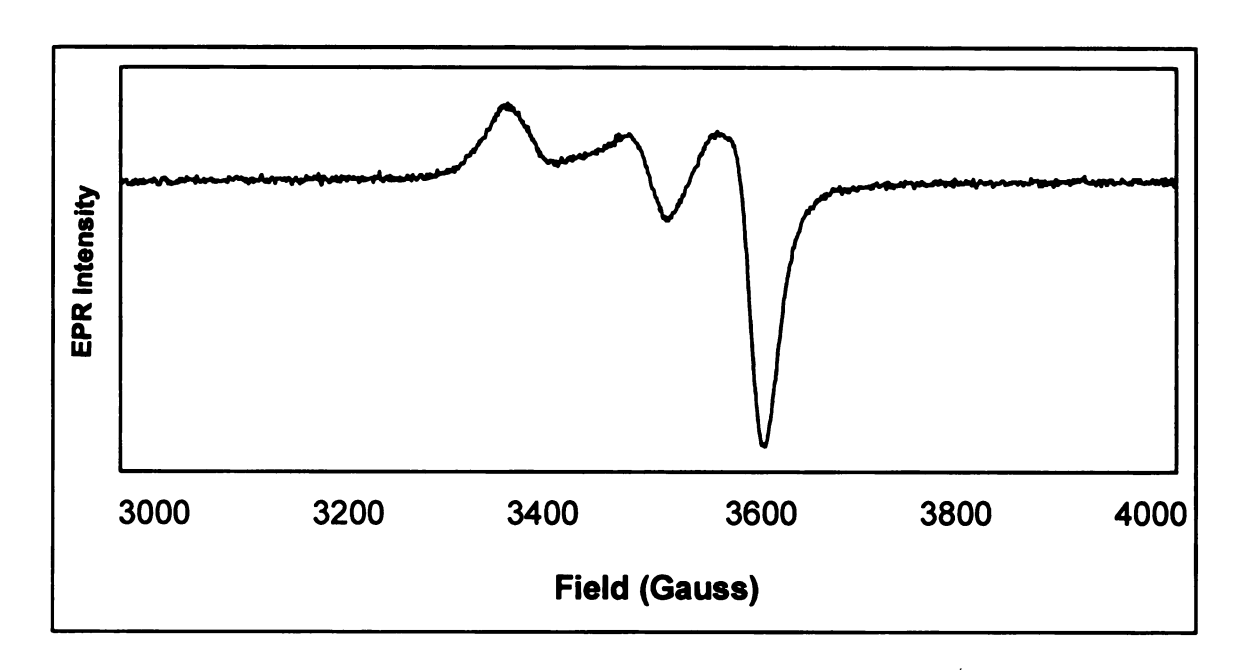


**Figure VI.9.c** X-band EPR spectrum of PFL-AE [4Fe-4S]<sup>+</sup> in the presence of allyl-AdoMet after 5 minutes of illumination. The sample contained 200  $\mu$ M PFL-AE, 1 equivalent of Na<sub>2</sub>S<sub>2</sub>O<sub>4</sub>, 100  $\mu$ M 5-deazariboflavin, and 2 equivalents of allyl-AdoMet; 14.7 % reduction (based on 108.7  $\mu$ M spin for 200 $\mu$ M protein with 3.70 mol Fe/ mol PFL-AE); g = 2.011, 1.948, 1.880. Conditions of measurement: T = 12 K; microwave power, 20  $\mu$ W; microwave frequency, 9.49 GHz; modulation amplitude, 10.084 G; single scan.

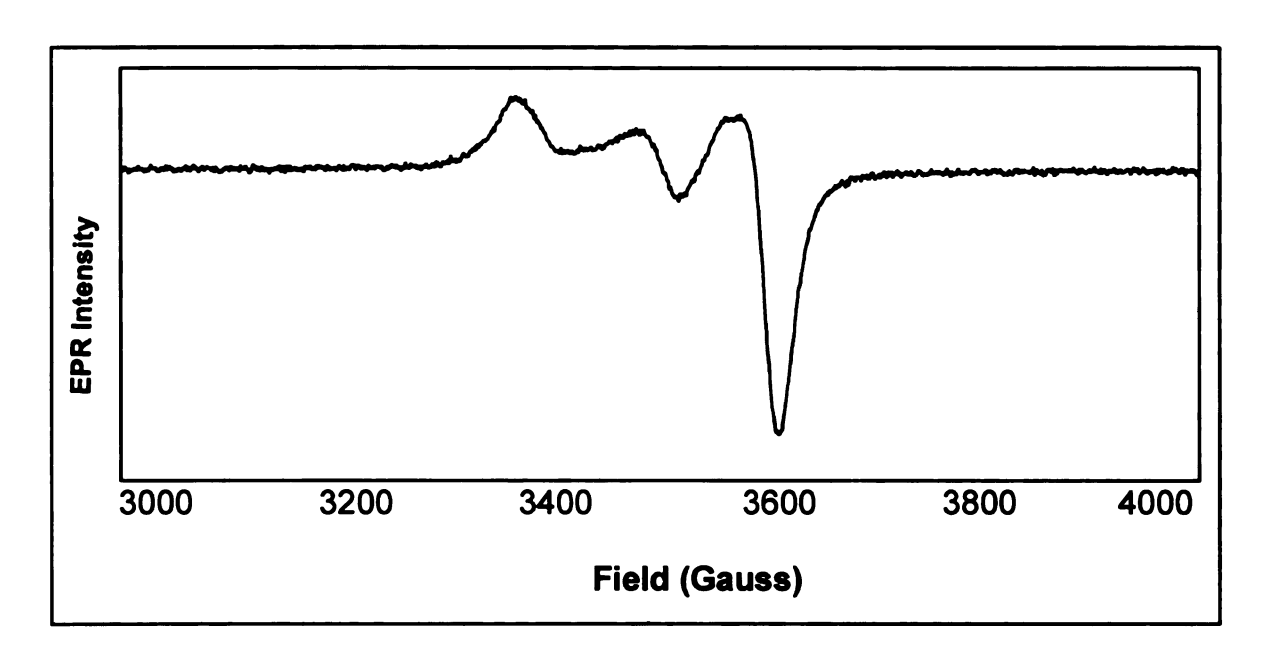


**Figure VI.9.d** X-band EPR spectrum of PFL-AE [4Fe-4S]<sup>+</sup> in the presence of allyl-AdoMet after 10 minutes of illumination. The sample contained 200  $\mu$ M PFL-AE, 1 equivalent of Na<sub>2</sub>S<sub>2</sub>O<sub>4</sub>, 100  $\mu$ M 5-deazariboflavin, and 2 equivalents of allyl-AdoMet; 16.1 % reduction (based on 118.8  $\mu$ M spin for 200 $\mu$ M protein with 3.70 mol Fe/ mol PFL-AE); g = 2.011, 1.948, 1.880. Conditions of measurement: T = 12 K; microwave power, 20  $\mu$ W; microwave frequency, 9.49 GHz; modulation amplitude, 10.084 G; single scan.

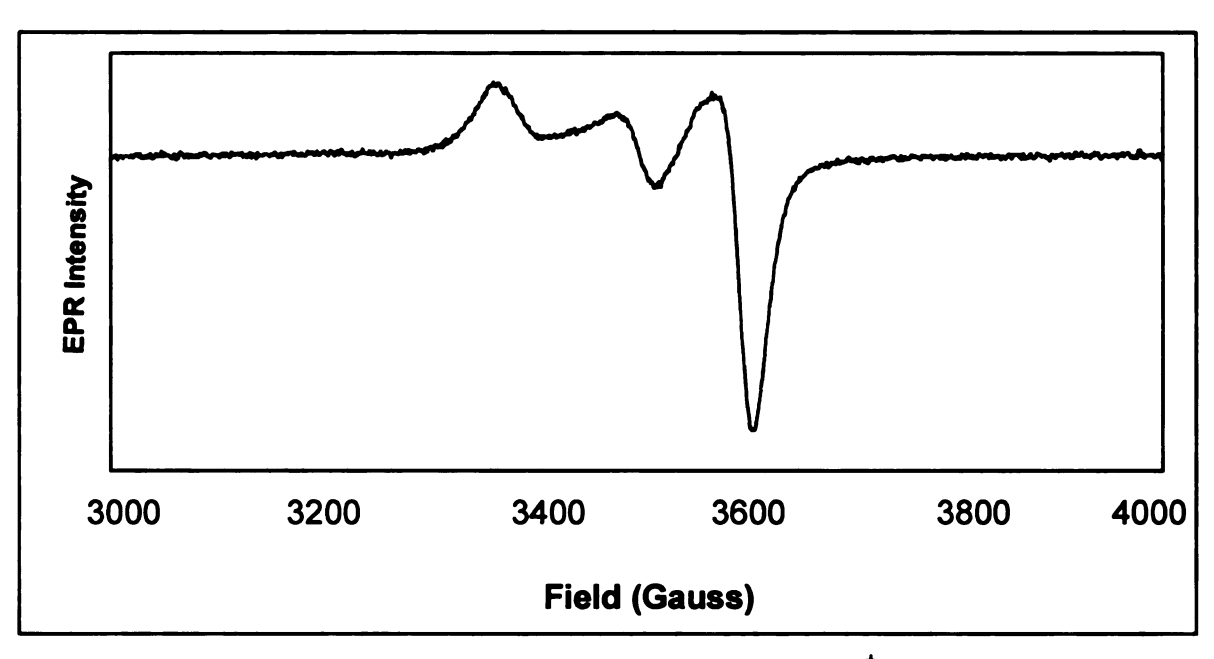


**Figure VI.9.e** X-band EPR spectrum of PFL-AE [4Fe-4S] <sup>+</sup> in the presence of allyl-AdoMet after 30 minutes of illumination. The sample contained 200  $\mu$ M PFL-AE, 1 equivalent of Na<sub>2</sub>S<sub>2</sub>O<sub>4</sub>, 100  $\mu$ M 5-deazariboflavin, and 2 equivalents of allyl-AdoMet; 15.9 % reduction (based on 117.3  $\mu$ M spin for 200 $\mu$ M protein with 3.70 mol Fe/ mol PFL-AE); g = 2.011, 1.948, 1.880. Conditions of measurement: T = 12 K; microwave power, 20  $\mu$ W; microwave frequency, 9.49 GHz; modulation amplitude, 10.084 G; single scan.

4	

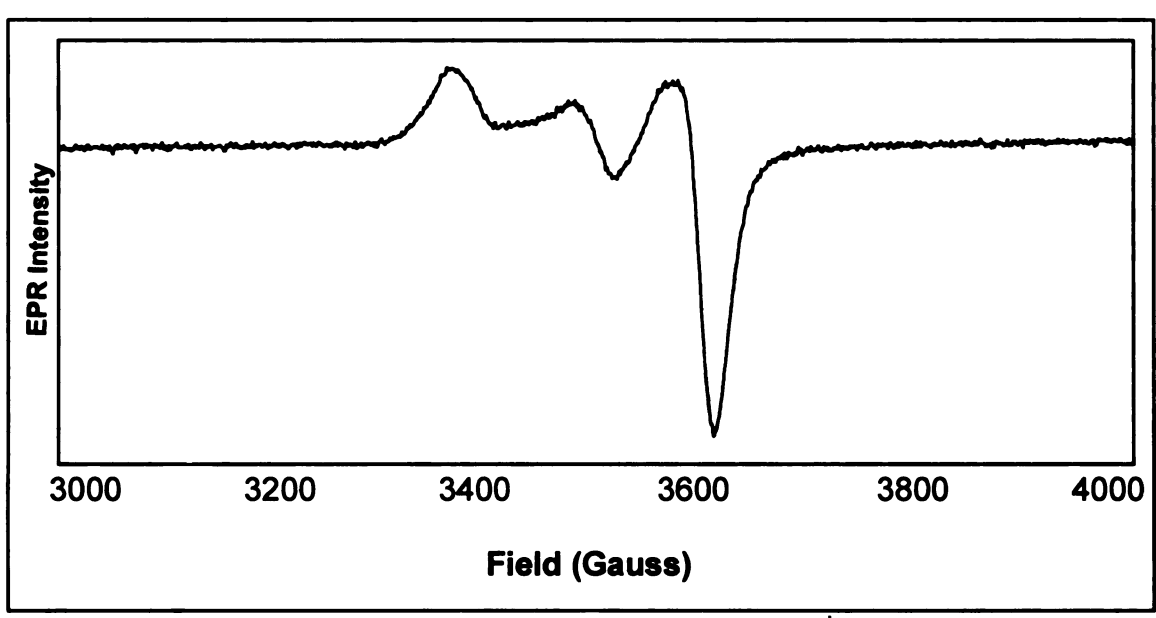


**Figure VI.9.f** X-band EPR spectrum of PFL-AE [4Fe-4S] <sup>†</sup> in the presence of allyl-AdoMet after 60 minutes of illumination. The sample contained 200  $\mu$ M PFL-AE, 1 equivalent of Na<sub>2</sub>S<sub>2</sub>O<sub>4</sub>, 100  $\mu$ M 5-deazariboflavin, and 2 equivalents of allyl-AdoMet; 16.6 % reduction (based on 123.3  $\mu$ M spin for 200 $\mu$ M protein with 3.70 mol Fe/ mol PFL-AE); g = 2.011, 1.948, 1.880. Conditions of measurement: T = 12 K; microwave power, 20  $\mu$ W; microwave frequency, 9.49 GHz; modulation amplitude, 10.084 G; single scan.

EPR spectra (12 K) for samples with PFL added are shown in Figure VI.11 (a-f). An EPR signal characteristic of the PFL-AE [3Fe-4S]<sup>1+</sup> radical was observed and spin quantitation of the EPR signals at each time point correspond to 18.1, 11.35, 9.6, 3.7, 10.98 and 6.26  $\mu$ M for 1, 2, 5, 10, and 30 min illumination, respectively.

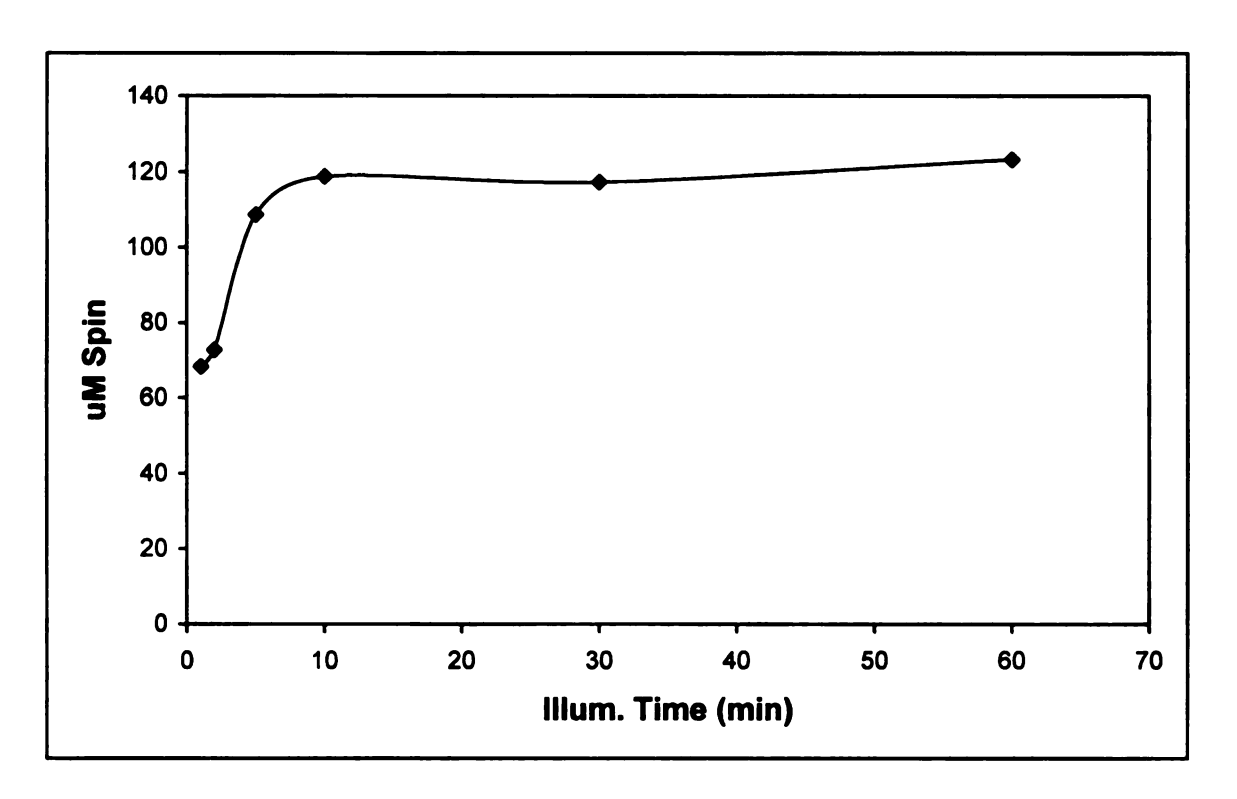


**Figure VI.10** Spin quantitation of the EPR spectra shown in Figure VI.9 (a-f) [4Fe-4S]<sup>+</sup> as a function of illumination time.

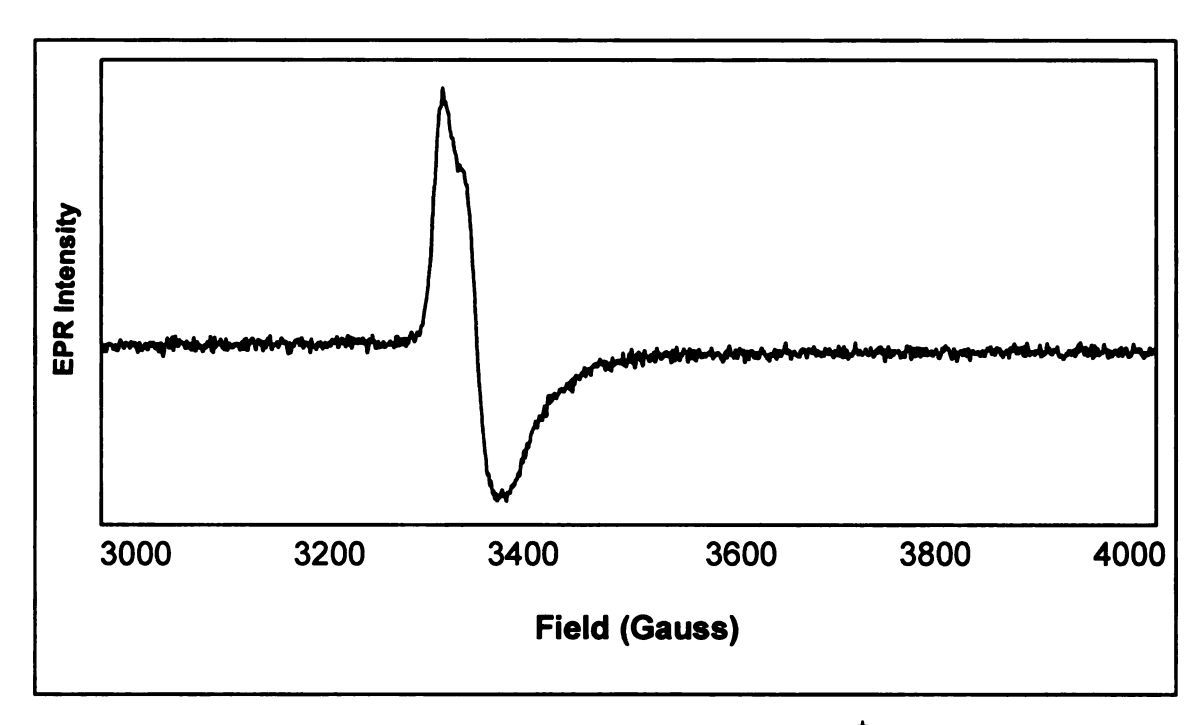


**Figure VI.11.a** X-band EPR spectrum of PFL-AE [3Fe-4S]<sup>+</sup> in the presence of allyl-AdoMet after 1 minute of illumination. The sample contained 200  $\mu$ M PFL-AE, 200  $\mu$ M PFL, 1 equivalent of Na<sub>2</sub>S<sub>2</sub>O<sub>4</sub>, 100  $\mu$ M 5-deazariboflavin, and 2 equivalents of allyl-AdoMet; 2.45 % (based on 18.1  $\mu$ M spin for 200 $\mu$ M protein with 3.70 mol Fe/ mol PFL-AE); g = 2.017. Conditions of measurement: T = 12 K; microwave power, 20  $\mu$ W; microwave frequency, 9.49 GHz; modulation amplitude, 10.084 G; single scan.

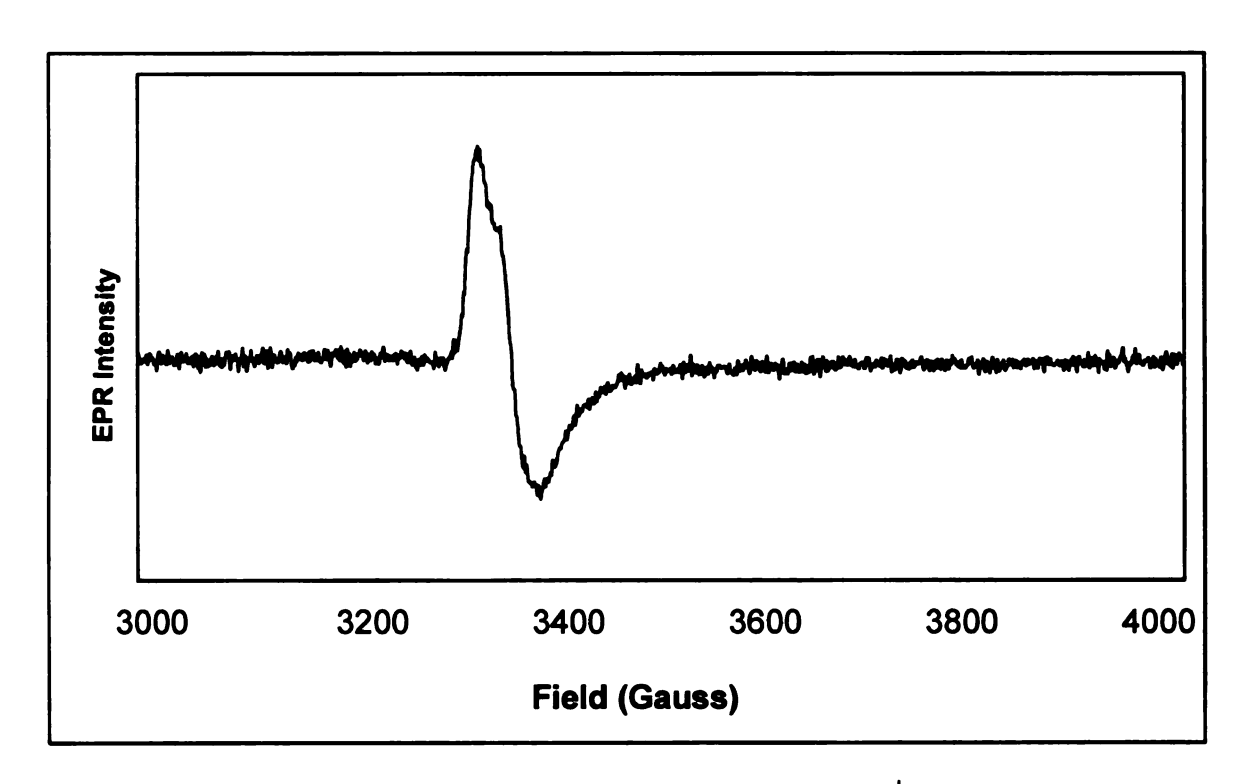


**Figure VI.11.b** X-band EPR spectrum of PFL-AE [3Fe-4S]<sup>+</sup> in the presence of allyl-AdoMet after 2 minutes of illumination. The sample contained 200  $\mu$ M PFL-AE, 200  $\mu$ M PFL, 1 equivalent of Na<sub>2</sub>S<sub>2</sub>O<sub>4</sub>, 100  $\mu$ M 5-deazariboflavin, and 2 equivalents of allyl-AdoMet; 1.53 % (based on 11.4  $\mu$ M spin for 200 $\mu$ M protein with 3.70 mol Fe/ mol PFL-AE); g = 2.017. Conditions of measurement: T = 12 K; microwave power, 20  $\mu$ W; microwave frequency, 9.49 GHz; modulation amplitude, 10.084 G; single scan.

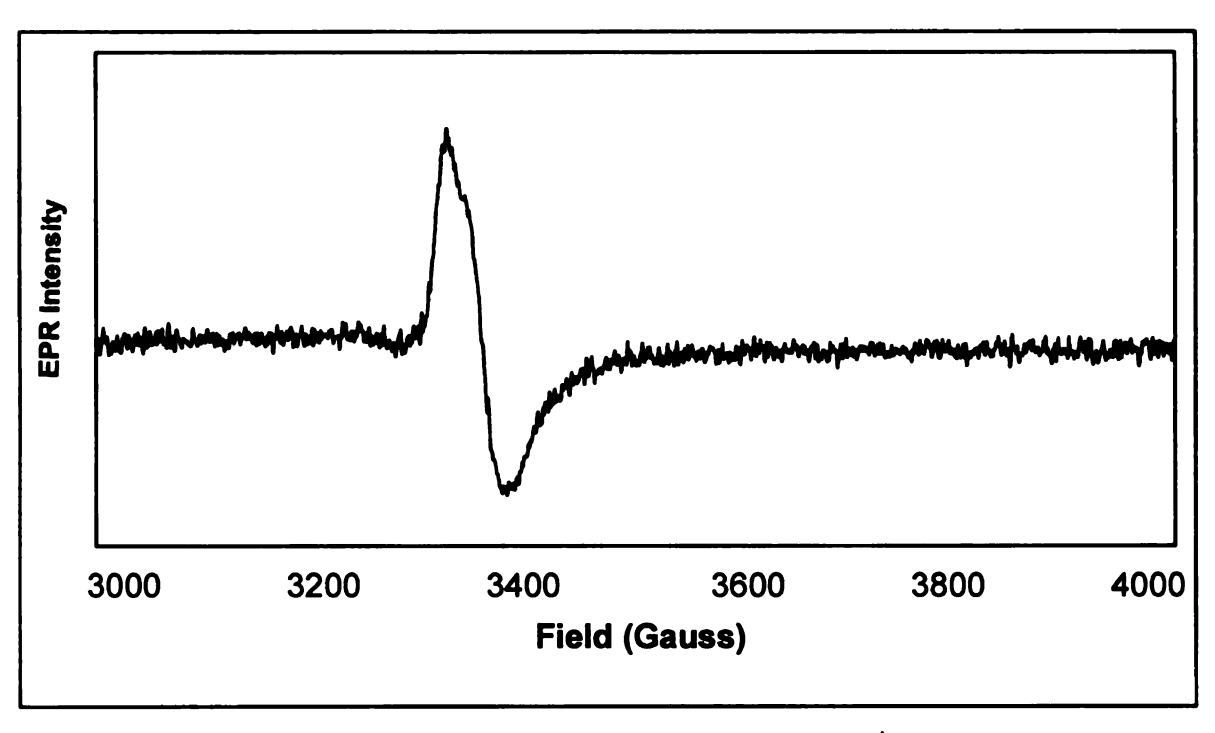


**Figure VI.11.c** X-band EPR spectrum of PFL-AE [3Fe-4S]<sup>+</sup> in the presence of allyl-AdoMet after 5 minutes of illumination. The sample contained 200 μM PFL-AE, 200 μM PFL, 1 equivalent of Na<sub>2</sub>S<sub>2</sub>O<sub>4</sub>, 100 μM 5-deazariboflavin, and 2 equivalents of allyl-AdoMet; 1.30 % (based on 9.6 μM spin for 200 μM protein with 3.70 mol Fe/ mol PFL-AE); g = 2.017. Conditions of measurement: T = 12 K; microwave power, 20 μW; microwave frequency, 9.49 GHz; modulation amplitude, 10.084 G; single scan.

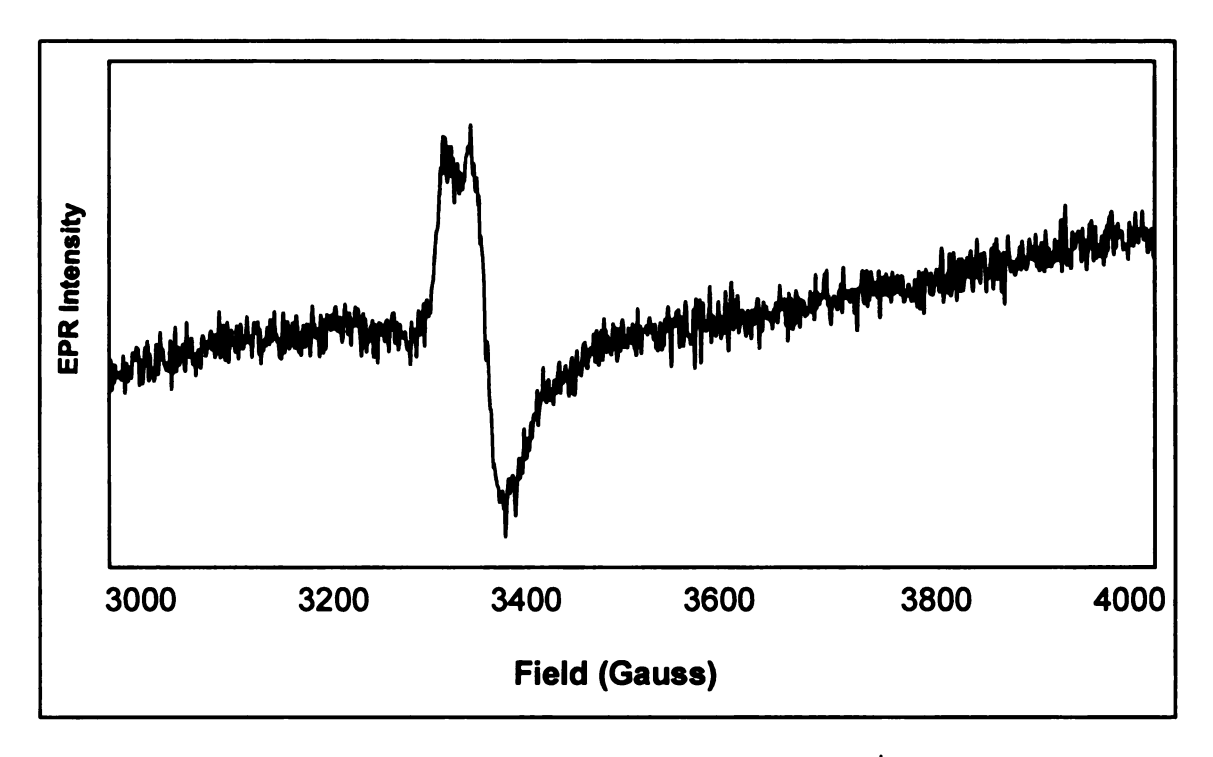


**Figure VI.11.d** X-band EPR spectrum of PFL-AE [3Fe-4S] <sup>+</sup> in the presence of allyl-AdoMet after 10 minutes of illumination. The sample contained 200  $\mu$ M PFL-AE, 200  $\mu$ M PFL, 1 equivalent of Na<sub>2</sub>S<sub>2</sub>O<sub>4</sub>, 100  $\mu$ M 5-deazariboflavin, and 2 equivalents of allyl-AdoMet; 0.50 % (based on 3.7  $\mu$ M spin for 200 $\mu$ M protein with 3.70 mol Fe/ mol PFL-AE); g = 2.017. Conditions of measurement: T = 12 K; microwave power, 20  $\mu$ W; microwave frequency, 9.49 GHz; modulation amplitude, 10.084 G; single scan.

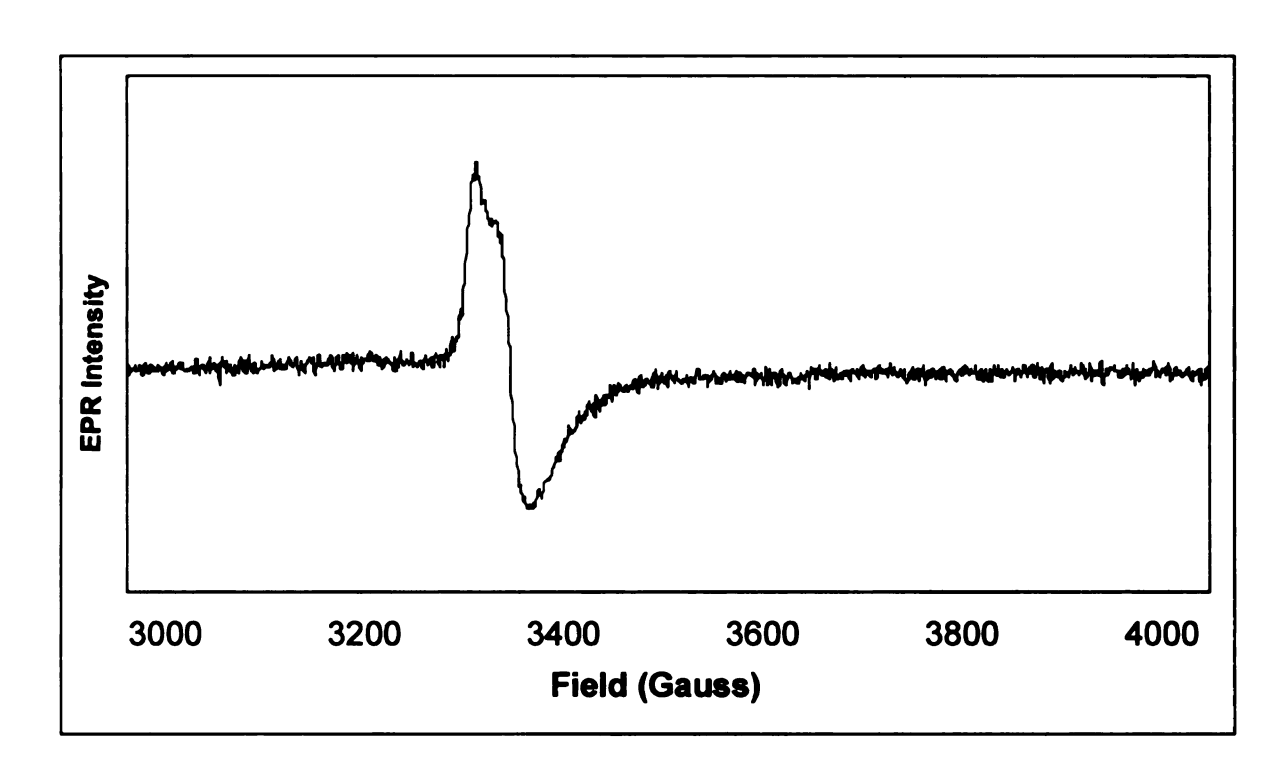


**Figure VI.11.e** X-band EPR spectrum of PFL-AE [3Fe-4S]<sup>+</sup> in the presence of allyl-AdoMet after 30 minutes illumination. The sample contained 200  $\mu$ M PFL-AE, 200  $\mu$ M PFL, 1 equivalent of Na<sub>2</sub>S<sub>2</sub>O<sub>4</sub>, 100  $\mu$ M 5-deazariboflavin, and 2 equivalents of allyl-AdoMet; 1.48 % (based on 11.0  $\mu$ M spin for 200 $\mu$ M protein with 3.70 mol Fe/ mol PFL-AE); g = 2.017. Conditions of measurement: T = 12 K; microwave power, 20  $\mu$ W; microwave frequency, 9.49 GHz; modulation amplitude, 10.084 G; single scan.

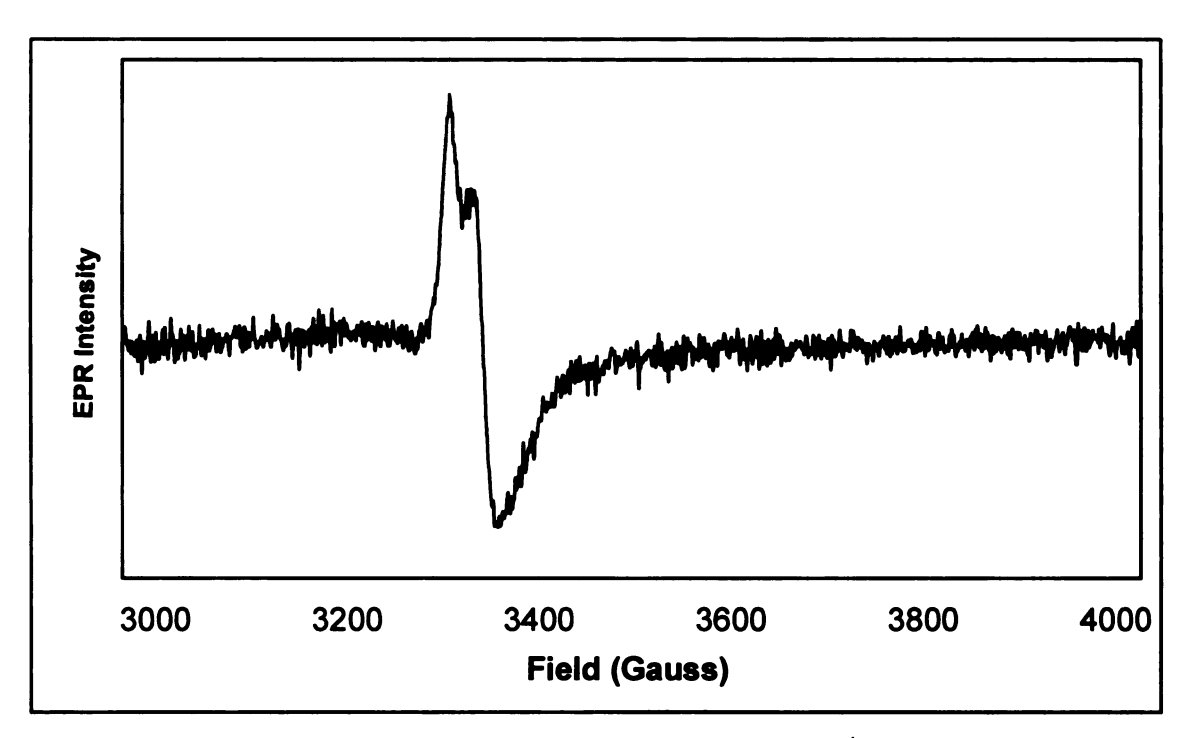


**Figure VI.11.f** X-band EPR spectrum of PFL-AE [3Fe-4S]<sup>+</sup> in the presence of allyl-AdoMet after 60 minutes of illumination. The sample contained 200  $\mu$ M PFL-AE, 200  $\mu$ M PFL, 1 equivalent of Na<sub>2</sub>S<sub>2</sub>O<sub>4</sub>, 100  $\mu$ M 5-deazariboflavin, and 2 equivalents of allyl-AdoMet; 0.85 % (based on 6.26  $\mu$ M spin for 200 $\mu$ M protein with 3.70 mol Fe/ mol PFL-AE); g = 2.017. Conditions of measurement: T = 12 K; microwave power, 20  $\mu$ W; microwave frequency, 9.49 GHz; modulation amplitude, 10.084 G; single scan.

The formation of the nearly axial EPR spectrum at 12 K upon the addition of allyl-AdoMet to PFL-AE showed that there was a similar interaction between regular AdoMet and PFL-AE and the allyl-AdoMet with PFL-AE. However, the AdoMet analogue was not able to activate PFL as proven by the EPR spectrum at 60K, which did not show the generation of the glycyl radical (data not shown). The EPR signal observed at 12 K for the EPR samples with PFL might be due to the presence of residual [3Fe-4S]<sup>1+</sup> clusters present. The EPR spectrum of the asisolated PFL-AE shows a 97.9  $\mu$ M concentration of the [3Fe-4S]<sup>1+</sup> cluster as shown in Figure VI.12.

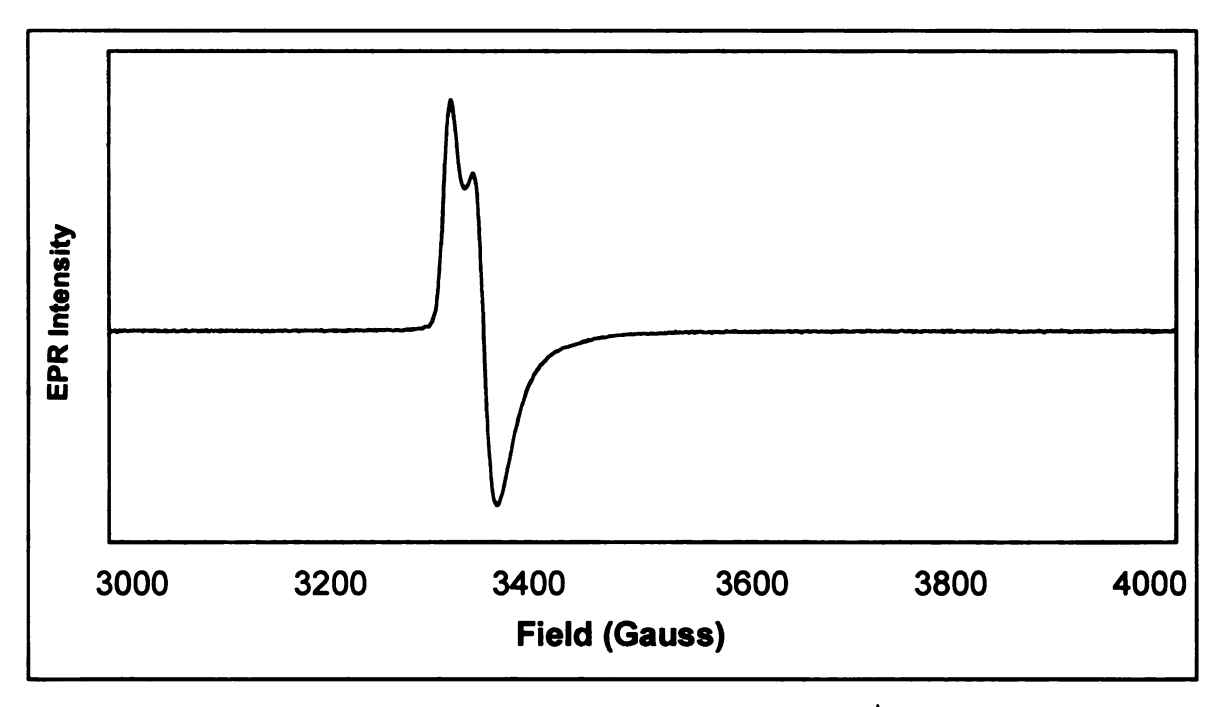


**Figure VI.12** X-band EPR spectrum of PFL-AE [3Fe-4S]<sup>+</sup> of as-isolated protein (based on 97.9  $\mu$ M spin for 1321  $\mu$ M protein with 3.70 mol Fe/ mol PFL-AE); g = 2.017. Conditions of measurement: T = 12 K; microwave power, 20  $\mu$ W; microwave frequency, 9.49 GHz; modulation amplitude, 10.084 G; single scan.

#### VI.4 Conclusion

The involvement of adenosyl radical intermediates in both the Fe-S/AdoMet and adenosylcobalamin-dependent enzymes raises intriguing mechanistic questions regarding the role of iron-sulfur clusters in radical generation. The data presented here support the conclusion that the allyl-AdoMet, an S-adenosylmethionine analogue, interacts with the reduced [4Fe-4S]<sup>+</sup> cluster of PFL-AE. A nearly axial EPR spectrum was obtained very similar to what was observed for regular AdoMet and PFL-AE. However, addition of an equimolar amount of PFL does not result in the expected activation of PFL. which would involve the formation of the glycyl 734 radical. The EPR spectrum at 12K corresponding to the presence of the [4Fe-4S] to cluster disappears and is replaced by what appears to be residual [3Fe-4S]<sup>+</sup>. At 60K, no signal is observed, which means that there was no PFL-based radical formed. Since the typical [4Fe-4S]<sup>+</sup>/AdoMet signal was initially observed, we can conclude that there is interaction between the reduced cluster of PFL-AE and the ally-AdoMet. However, since no glycyl radical is generated, allyl-AdoMet acts either as an inhibitor to the activation process or that it has a very low efficiency for activation, such that the electron from the reduced cluster gets guenched along the process.

To monitor the formation of an Ado-based radical subsequent to homolytic cleavage, the 3'-anhydroAdoMet analogue is a useful probe. Not only will it allow the homolytic cleavage of the S-C(5') bond but it will also form the stable anhydro allylic counterpart of the transient deoxyadenosyl radical species; this should be detectable by EPR spectroscopy. Work is currently underway to synthesize the

3'-anhydro-AdoMet analogue. At present, the 3'-anhydro adenosine has been successfully synthesized and new methods of phosphorylating the 3'-anAdo are being explored to maximize the efficiency of the phosphorylation step to generate anATP. The enzymatic method has been employed but the yields obtained were very low for both the phosphorylation step as well as the enzymatic synthesis of 3'-anhydroAdoMet. An alternative method of phosphorylation step has been reported by Kraybill and co-workers where the yields for the phosphorylation of different nucleosides range from 10-50%.

While the EPR experiment presented have shown that allyl-AdoMet interacts with the [4Fe-4S]<sup>+</sup> cluster of PFL-AE, it has not provided evidence that the proposed catalytic mechanism is the route by which PFL-AE works in activating PFL. However, additional work with the 3'-anhydroAdoMet analogue will give us a better insight into the mechanism by which PFL-AE, as well as the rest of members of the radical SAM superfamily of enzymes works.

### VI.5 References

- (1) Knappe, J. N., F. A.; Blaschkowski, H. P.; Gänzler, M. *Proc. Natl. Acad. Sci. USA* **1984**, *81*, 1332.
- (2) Wagner, A. F. V. F., M.; Neugebauer, F. A.; Schäfer, W.; Knappe, *Proc. Natl. Acad. Sci. USA* **1992**, *89*, 996.
- (3) Mulliez, E. F., M.; Gaillard, J.; Reichard, P. *J. Biol. Chem.* **1993**, *268*, 2296.
- (4) Krieger, C. J. R., W.; Albracht, S. P. J.; Spormann, A. M. *J. Biol. Chem.* **2001**, *276*, 12924.
- (5) Petrovich, R. M. R., F. J.; Reed, G. H.; Frey, P. A. *J. Biol. Chem.* **1991**, *266*, 7656.
- (6) Broderick, J. B. D., R. E.; Fernandez, D. C.; Wojtuszewski, K.; Henshaw, T. F.; Johnson, M. K. *J. Am. Chem. Soc.* **1997**, *119*, 7396.
- (7) Külzer, R. P., T.; Kappl, R.; Hüttermann, J.; Knappe, J. *J. Biol. Chem.* **1998**, *273*, 4897.
- (8) Broderick, J. B. H., T. F.; Cheek, J.; Wojtuszewski, K.; Trojan, M. R.; McGhan, R.; Smith, S. R.; Kopf, A.; Kibbey, M.; Broderick, W. E. *Biochem. Biophys. Res. Commun.* **2000**, *269*, 451.
- (9) Krebs, C. H., T. F.; Cheek, J.; Huynh, B.-H.; Broderick, J. B. *J. Am. Chem. Soc.* **2000**, *122*, 12497.
- (10) Petrovich, R. M. R., F. J.; Reed, G. H.; Frey, P. A. *Biochemistry* **1992**, *31*, 10774.
- (11) Lieder, K. B., S.; Ruzicka, F. J.; Beinert, H.; Reed, G. H.; Frey, P. A. *Biochemistry* **1998**, *37*, 2578.
- (12) Liu, A. G., A. J. Biol. Chem. 2000, 275, 12367.
- (13) Ollagnier, S. M., C.; Mulliez, E.; Gaillard, J.; Schuenemann, V.; Trautwein, A.; Mattioli, T.; Lutz, M.; Fontecave, M. *J. Am. Chem. Soc.* **1999**, *121*, 6344.
- (14) Tamarit, J. M., E.; Meier, C.; Trautwein, A.; Fontecave, M. *J. Biol. Chem.* **1999**, *274*, 31291.

- (15) Ollagnier, S. M., E.; Schmidt, P. P.; Eliasson, R.; Gaillard, J.; Deronzier, C.; Bergman, T.; Gra"slund, A.; Reichard, P.; Fontecave, M. J. Biol. Chem. 1997, 272, 24216.
- (16) Ollagnier, S. M., E.; Gaillard, J.; Eliasson, R.; Fontecave, M.; Reichard, P. *J. Biol. Chem.* **1996**, *271*, 9410.
- (17) Henshaw, T. F. C., J.; Broderick, J. B. *J. Am. Chem. Soc.* **2000**, *122*, 8331.
- (18) Hoffman, B. M. Acc. Chem. Res. 2003, 36,, 522.
- (19) Walsby, C. J. H., W.; Broderick, W. E.; Cheek, J.; Ortillo, D.; Broderick, J. B.; Hoffman, B. M. *J. Am. Chem. Soc.* **2002**, *124*, 3143.
- (20) Walsby, C. J. O., D.; Broderick, W. E.; Broderick, J. B.; Hoffman, B. M. J. Am. Chem. Soc. 2002, 124, 11270.
- (21) Layer, G. M., J.; Heinz, D. W.; Jahn, D.; Schubert, W.-D. *EMBO J.* **2003**, *22*, 6214.
- (22) Berkovitch, F. N., Y.; Wan, J. T.; Jarrett, J. T.; Drennan, C. L. *Science* **2004**, *303*, 76.
- (23) Hänzelmann, P. S., H. *Proc. Natl. Acad. Sci. U.S.A.* **2004**, *101*, 12870.
- (24) Unkrig, V. N., F. A.; Knappe, J. Eur. J. Biochem. 1989, 184, 723.
- (25) Walsby, C. J. O., D.; Yang, J.; Nnyepi, M.R.; Broderick, W.E.; Hoffman, B.M.; Broderick, J.B. *Inorg. Chem.* **2005**, *44*, 727.
- (26) Conradt, H. H.-B., M.; Hohmann, H.-P.; Blaschkowski, H. P.; Knappe, J. *Arch. Biochem. Biophys.* **1984**, *228*, 133.
- (27) Wong, K. K. M., B. W.; Lewisch, S. A.; Baxter, M. K.; Ridky, T. W.; Ulissi-DeMario, L.; Kozarich, J. W. *Biochemistry* **1993**, 32, 14102.
- (28) Brush, E. J. L., K. A.; Kozarich, J. W. *Biochemistry* **1988**, *27*, 2217.
- (29) Daley, C. J. A. H., R. H. Inorg. Chem. 2001, 40, 2785.
- (30) Daley, C. J. A. H., R. H. J. Inorg. Biochem. 2003, 97, 287.
- (31) Magnusson, O. T. R., G.H.; Frey, P.A. J. Am. Chem. Soc. 2001, 40,

7773.

- (32) Ashton, W. T. B., R.D.; Tolman, R.L. *Heterocyclic Chem.* **1978**, *15*, 489.
- (33) Smit, P. S., G.A.; Vander Plas, H.C. *Recl. Trav. Chim. Pays-Bays.* **1986**, *105*, 538.
- (34) Yoneda, F. Meth. Enzy. 1980, 66, 267.

#### **CHAPTER VII**

#### **CONCLUSIONS**

The recent discovery of the radical SAM superfamily provided evidence for the importance of radical-based catalysis in a number of well studied but previously unresolved biochemical pathways. With over 600 members, these radical SAM proteins catalyze a myriad of reactions, which include methylations, isomerization, ring formations, sulfur insertion, anaerobic oxidations, and protein radical formation. Evidence exists that these proteins generate a radical species by reductive cleavage of S-adenosylmethionine (SAM/AdoMet) through an unusual Fe-S center. Pyruvate formate-lyase-activating enzyme (PFL-AE) from *E. coli*, a member of this superfamily, is a 28 kDa monomeric protein that activates the enzyme pyruvate formate-lyase (PFL). Upon abstraction of the pro-S hydrogen from the Gly734 residue in the presence of its co-substrate AdoMet, the catalytically active glycyl radical is generated.<sup>2,3</sup>

A key mechanistic question regarding this family is the role of the [4Fe-4S] cluster. In particular, the clusters of these enzymes have a "unique" iron site that is not coordinated to the enzyme by a cysteinal sulfur. Whether this unique Fe had a specific catalytic function in PFL-AE as such a unique site does in aconitase, was a major outstanding question in the field. In the work described in this thesis, electron paramagnetic spectroscopy (EPR) and 35 GHz electron-

nuclear double resonance spectroscopy (ENDOR) was used to define the role of the cluster in PFL-AE. The experiments disclosed that the cluster plays at least a dual role: 1) the unique Fe anchors the AdoMet cofactor by chelating the amino and carboxy groups of methionine; and 2) electron transfer from the cluster initiates homolytic cleavage of the S-C5' bond of Adomet.<sup>4</sup>

<sup>2</sup>H and <sup>13</sup>C pulsed ENDOR spectroscopy was performed on [4Fe-4S]<sup>+</sup>-PFL-AE with bound AdoMet that had been labeled at the methyl position with either <sup>2</sup>H and <sup>13</sup>C. The substancial <sup>2</sup>H and <sup>13</sup>C hyperfine from the labels clearly demonstrated that AdoMet binds adjacent to the 4Fe cluster. The cofactor was shown to bind in the same geometry to both the 1+ and 2+ states of the cluster through cryoreduction of the frozen [4Fe-4S]<sup>2+</sup>/AdoMet complex to form the EPRactive reduced (1+) state which was trapped in the structure of the oxidized (2+) state.<sup>5</sup> Modeling of the through-space electron-nuclear dipolar interaction between the cluster electron spin and the methyl -13C and <sup>2</sup>H of AdoMet, as derived from orientation-selective, 2-D ENDOR datasets, showed that the shortest distance between an AdoMet methyl proton and an iron cluster is  $\sim$ 3.7(2) Å, with a distance of  $\sim$  4.9(6) Å from the methyl carbon to this iron as shown in Figure VII.1. Close analysis disclosed an intriguing discovery of a through-bond (local), isotropic contribution to the <sup>13</sup>C interaction, which requires overlap between orbitals on the cluster and on AdoMet. The most plausible origin is a dative interaction of the positively charged sulfide of the cluster (Figure VII.1), rather than with the unique Fe of the cluster. These results led to a proposed reaction mechanism in which inner-sphere electron transfer from the

cluster to AdoMet via the sulfide-sulfonium interaction causes cleavage of the sulfonium-adenosyl bond.<sup>5,6</sup>

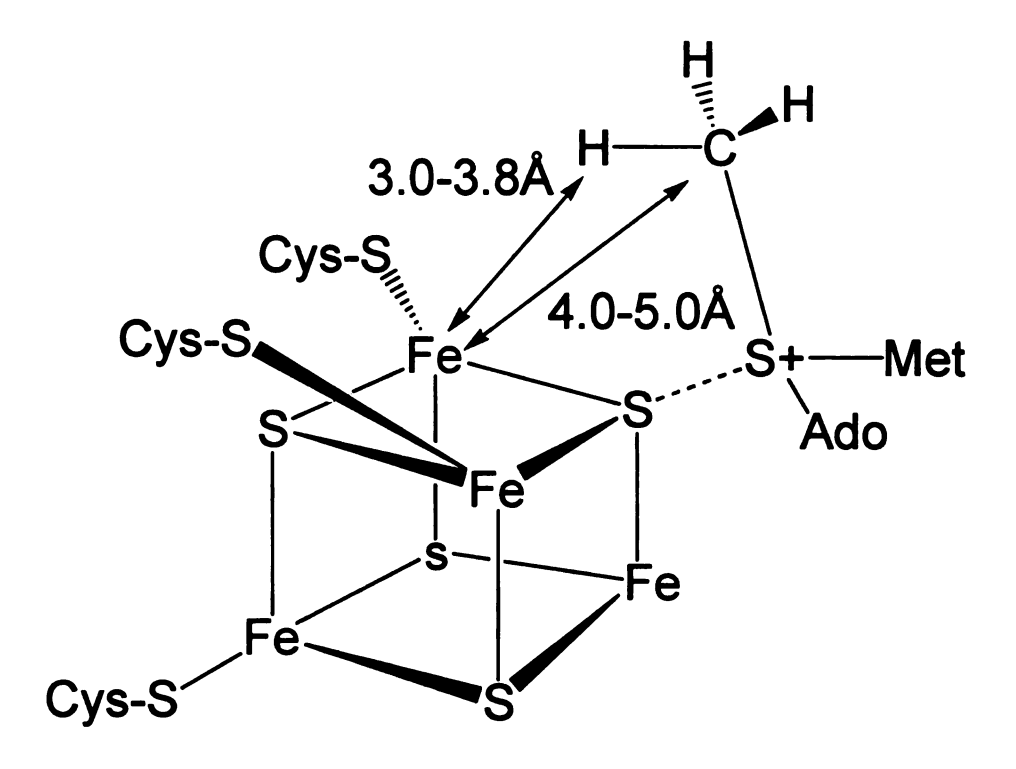


**Figure VII.1** Interaction of AdoMet With the [4Fe-4S] cluster of PFL-AE, as deduced from <sup>2</sup>H and <sup>13</sup>C pulsed Q-band ENDOR spectroscopy.

The results of the initial ENDOR investigations were significant and interesting, however they offered no role for the unique cluster iron. Because every enzyme in the Fe-S/AdoMet family appears to have a unique iron, it seemed important to determine its function. To examine the coordination sphere of the unique Fe, we performed additional 35 GHz pulsed ENDOR spectroscopic studies of [1+/AdoMet] labeled with <sup>17</sup>O/<sup>13</sup>C in the carboxyl group of the methionine fragment, and with <sup>15</sup>N in the amino group. ENDOR signals revealed that both the carboxylato and amino groups of methionine are coordinated to the

unique iron of the [4Fe-4S] cluster in a classical five-membered-ring N/O chelate. This interaction anchors the methionine end of AdoMet, thereby presumably fixing the geometry of the sulfonium linkage for subsequent radical chemistry as shown in Figure VII.2.<sup>6,7</sup>

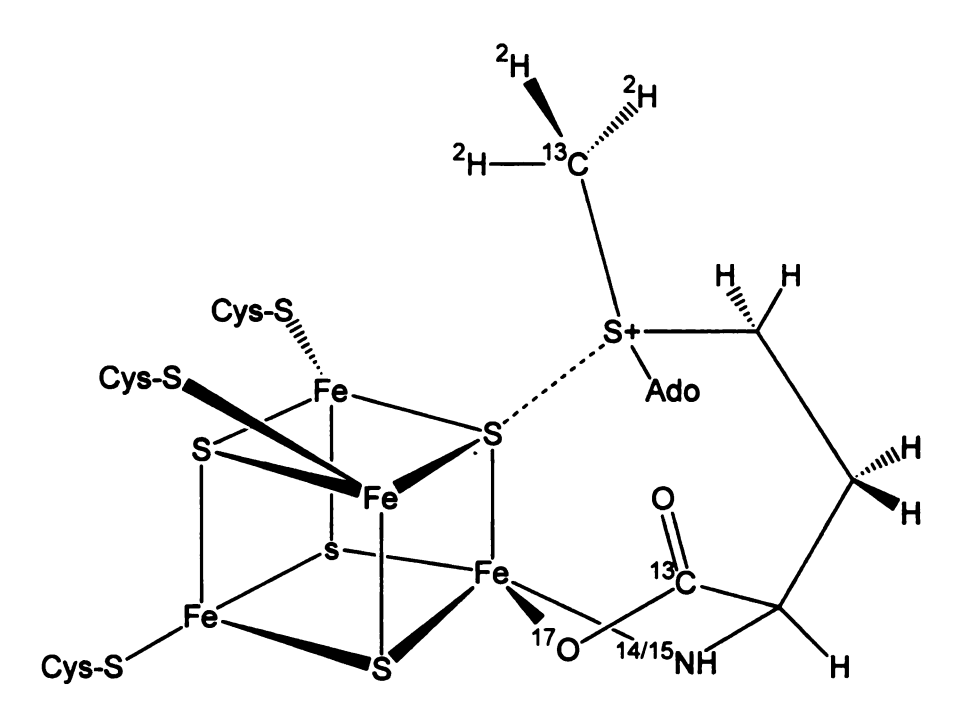


**Figure VII.2** Representation of the proposed interactions of AdoMet with the [4Fe-4S] cluster of PFL-AE, as derived from ENDOR spectroscopy of the atoms <sup>2</sup>H, <sup>13</sup>C, <sup>14/15</sup>N, and <sup>17</sup>O.

Given the evidence provided by our ENDOR spectroscopic investigations of the interaction of AdoMet with the [4Fe-4S] cluster of PFL-AE, we decided to take the investigation one step further by using analogues of AdoMet to probe the formation of the elusive 5'-deoxyadenosyl radical species, a transient intermediate that has never been detected spectroscopically. The 5'-dAdo radical

is believed to be formed during the activation of PFL by PFL-AE and by other radical SAM enzymes during catalysis. The available evidence suggests that the reduced [4Fe-4S] cluster of PFL-AE donates an electron to initiate the reductive cleavage of AdoMet at the S-C (5') bond. The transient 5'-deoxy-adenosyl radical formed then abstracts the pro-S hydrogen atom at the Gly734 residue of PFL to form the catalytically active glycyl radical. The idea of using analogues of AdoMet was to exert some control over the homolytic cleavage resulting in the formation of a more stable counterpart of the 5'-deoxyadenosyl radical that is more susceptible to spectroscopic investigations.

Three analogues of AdoMet were considered as suitable candidates for the investigation. The allyl-AdoMet and the vinyl-AdoMet analogues were synthesized from ATP and the appropriate methionine analog based on previously reported procedures for the preparative-scale enzymatic synthesis of AdoMet. Unfortunately, the synthesis of S-vinyl homocysteine has not been successful in generating a reasonable amount of this methionine analogue needed for the next step in the synthesis. On the other hand, the synthesis of S-allyl homocysteine has resulted in a yield of 54% while the enzymatic synthesis of allyl-AdoMet gives a respectable yield of ~10%. EPR spectroscopic investigations of the Allyl-AdoMet with the reduced [4Fe-4S] of PFL-AE shows the expected interaction of the Allyl-AdoMet- [4Fe-4S] \* complex resulting in a nearly axial EPR spectrum. However, addition of an equimolar amount of PFL to the mix does not result in the formation of the glycyl radical of PFL or any radical species that can be detected by EPR. The axial EPR spectrum also disappears

which suggests that the electron transfer from the reduced [4Fe-4S] cluster of PFL-AE may have taken place but was quenched, perhaps by the solvent, such that the dAdo radical needed to generate the PFL glycyl radical was not generated.

The third analogue is the 3'-anhydroAdoMet, which was employed by Frey and co-workers as a co-factor of the enzyme lysine 2,3-aminomutase (LAM), another member of the radical SAM superfamily. 12 Upon the reductive cleavage of this AdoMet analogue, the radical formed is stabilized by the allylic delocalization on the ribosyl group, affording a radical species that is EPR detectable. Synthesis of this analogue has been achieved but the yield was too low to allow us to use this analogue for EPR and ENDOR spectroscopic investigations. Modifications in the synthesis of this analogue is being undertaken to increase the yield and to allow us to determine if this analogue will work as a co-substrate for PFL-AE.

Additional work has been done as well to determine the strength of the interaction of AdoMet with both the as–isolated and photoreduced PFL-AE. This was done using equilibrium dialysis experiments where a tritiated AdoMet was equilibrated between a protein solution and the running buffer used to purify the protein in question. Scintillation counts obtained for both the buffer and the protein end of the dialysis set-up will allow us to calculate for the rate of dissociation of AdoMet from PFL-AE. The results so far have been promising but more experiments are needed to obtain a more reliable  $K_d$  value from the experiment.

#### References

- (1) Sofia, H. J. C., G.; Hetzler, B.G.; Reyes-Spindola, J.F.; Miller, N.E. *Nuc. Acids Res.* **2001**, *29*, 1097.
- (2) Kulzer, R. P., T.; Kappl, R.; Huttermann, J.; Knappe, J. *J. Biol. Chem.* **1998**, *273*, 4897.
- (3) Frey, P. A. Annu. Rev. Biochem. 2001, 70, 121.
- (4) Hoffman, B. M. Acc. Chem. Res. 2003, 36, 522.
- (5) Walsby, C. H., W.; Broderick, W.E.; Cheek, J.; Ortillo, D.; Broderick, J.B.; Hoffman, B.M. *J. Am. Chem. Soc.* **2002**, *124*, 3143.
- (6) Walsby, C. J. O., D.; Yang, Jian, Nnyepi, M.R.; Broderick, W.E.; Hoffman, B.M.; Broderick, J.B. *Inorg. Chem.* **2005**, *44*, 727.
- (7) Walsby, C. J. O., D.; Broderick, W.E.; Broderick, J.B.; Hoffman, B.M. *J. Am. Chem. Soc.* **2002**, *124*, 11270.
- (8) Cheek, J. B., J.B. Arch. Biochem. Biophys. 2005, 433, 288.
- (9) Park, J. T., J.; Roessner, C.A.; Scott, I. *Bioorg. Medicinal Chem.* **1996**, *4*, 2179.
- (10) Kim, H. J. B., T.J.; Nathin, S.J.; McMullen, H.F.; Hansen, D.E. *Anal. Biochem.* **1992**, *207*, 68.
- (11) Kolenbrander, H. M. Can. J. Chem. 1969, 47, 3271.
- (12) Magnusson, O. T. R., G.H.; Frey, P.A. *J. Am. Chem. Soc.* **2001**, *40*, 7773.